



Wissenschaftszentrum Weihenstephan
für Ernährung, Landnutzung und Umwelt

Lehrstuhl für Lebensmittelverfahrenstechnik und Molkereitechnologie

Improving the nutritional quality of dairy powders – analyzing and modeling lysine loss during spray drying as influenced by drying kinetics, thermal stress, physical state and molecular mobility

Iris Schmitz-Schug

Vollständiger Abdruck der von der Fakultät Wissenschaftszentrum Weihenstephan für Ernährung, Landnutzung und Umwelt der Technischen Universität München zur Erlangung des akademischen Grades eines

Doktor-Ingenieurs

genehmigten Dissertation.

Vorsitzende(r): Univ.-Prof. Dr. K.-H. Engel

Prüfer der Dissertation: 1. Univ.-Prof. Dr. U. M. Kulozik

2. Univ.-Prof. Dr. U. A. Peuker

(Technische Universität Bergakademie Freiberg)

3. Univ.-Prof. Dr. P. Först

Die Dissertation wurde am 18.09.2013 bei der Technischen Universität München eingereicht und durch die Fakultät Wissenschaftszentrum Weihenstephan für Ernährung, Landnutzung und Umwelt am 09.12.2013 angenommen.

Bibliografische Information der Deutschen Nationalbibliothek

Die Deutsche Nationalbibliothek verzeichnet diese Publikation in der Deutschen Nationalbibliografie; detaillierte bibliografische Daten sind im Internet über <http://dnb.d-nb.de> abrufbar.

ISBN 978-3-8439-1888-6

© Verlag Dr. Hut, München 2014
Sternstr. 18, 80538 München
Tel.: 089/66060798
www.dr.hut-verlag.de

Die Informationen in diesem Buch wurden mit großer Sorgfalt erarbeitet. Dennoch können Fehler nicht vollständig ausgeschlossen werden. Verlag, Autoren und ggf. Übersetzer übernehmen keine juristische Verantwortung oder irgendeine Haftung für eventuell verbliebene fehlerhafte Angaben und deren Folgen.

Alle Rechte, auch die des auszugsweisen Nachdrucks, der Vervielfältigung und Verbreitung in besonderen Verfahren wie fotomechanischer Nachdruck, Fotokopie, Mikrokopie, elektronische Datenaufzeichnung einschließlich Speicherung und Übertragung auf weitere Datenträger sowie Übersetzung in andere Sprachen, behält sich der Autor vor.

1. Auflage 2014

Acknowledgements

This PhD thesis was carried out during my time as a research assistant at the Chair for Food Process Engineering and Dairy Technology of Technische Universität München from October 2008 to September 2012. I would like to take this opportunity to thank all those who supported me during this time and who contributed to the success of this work. I am deeply grateful for these people that enabled me to build and mature my character into whom I am today.

I wish to express my deepest thanks to my supervisor Prof. Dr.-Ing. Ulrich Kulozik for his guidance and professional expertise. I am very grateful for excellent research facilities, his confidence and the freedom to pursue this project with own ideas, helpful discussions and unrestricted support in all concerns.

I would like to thank Prof. Dr.-Ing. Urs Peuker and Prof. Dr.-Ing. Petra Först for examining this PhD thesis as well as Prof. Dr. Karl-Heinz Engel for taking over the chair of the examination board.

Special thanks go to Prof. Dr.-Ing Petra Först for her guidance and support during my PhD. I greatly enjoyed the scientific freedom she granted me, still watching carefully the steps leading to the final success. I always appreciated hearing her point of view. I am very grateful for her sound advice and the many insightful discussions of the research.

I am very grateful to Dr. Alessandro Gianfrancesco and Dr.-Ing. Gerhard Niederreiter from Nestlé, who cooperated in this project, for the fruitful discussions and the possibility to carry out experiments at their facilities.

Many thanks go to Carina Gerhard who excellently carried out huge parts of the experimental work. I really appreciated our collaboration, her pleasant character and many helpful technical discussions. I would also like to acknowledge Cornelia Strixner for the assistance with the spray-drying experiments. Furthermore I would like to convey my gratitude to Sabine Grabbe for her many efforts to get the software and hardware for the simulations running as well as for her immediate and supreme help with any computer problems. I am very grateful to Sabine Becker and Friederike Schöpflin for their excellent help with problems of a non-scientific nature. I would similarly like to extend my thanks to Christian Ederer, Franz Fraunhofer and Erich Schneider for their technical support.

I would like to give special thanks to my office colleagues Rita Schaupp and José Toro for the great atmosphere as well as for the steady scientific and life discussions. We shared together many of the joys, frustrations, sweet and bitter things of our everyday life experiences.

I would like to thank all further institute members, both past and present, for a wonderful time at the institute and for the cordial working environment.

I would like to express my gratitude to the students who contributed to this project during their internships, student research projects, Bachelor's theses, Master's theses, Diploma theses or as student assistants: Franziska Bauer, Mariachiara Di Crescenzo, Sabrina Engelbrecht, Helene Kling, Sebastian Krauß, Sabrina Leda, Simone Mittermaier, Magdalena Rechenmacher, Sonja Terszowski, Barbara Treml, Isabel Ußmüller, Katharina Voigt, Judith Voit and Sven Wiesner.

Finally I am especially grateful to my family for always supporting and loving me as who I am. Without them, I do not know where I would be in my life. Their love, encouragement, support, humor, and wisdom contributed greatly to the success of this thesis. Danke!

Zusammenfassung

Sensitive Inhaltsstoffe von Lebensmitteln, Pharma- oder Bioprodukten können durch ungeeignete Prozessbedingungen geschädigt werden. Jedoch können durch die Kopplung der Produkteigenschaften mit den Prozesscharakteristiken Produktionsprozesse hinsichtlich der Qualität der sensitiven Inhaltsstoffe optimiert werden. Hierzu ist es im Falle von Lebensmitteln erforderlich, eine Brücke zwischen der Lebensmitteltechnologie und der Verfahrenstechnik zu schlagen. Der Fokus dieser Arbeit lag auf der essentiellen Aminosäure Lysin in einer Modellmilchrezeptur, deren Zusammensetzung von der typischen Zusammensetzung von Säuglingsmilch abgeleitet war. Lysin ist ein wichtiger Nährstoff, der während der Verarbeitung z.B. durch die Maillardreaktion blockiert werden kann. Bei der Herstellung von Milchpulvern ist die Sprühtrocknung bekanntermaßen der kritische Produktionsschritt bzgl. des Lysinverlustes. Sowohl der Wasserentzug als auch die hohen Temperaturen während der Sprühtrocknung können zu Lysinverlusten führen.

Im Bereich der Lebensmitteltechnologie stellen Reaktionskinetik und Stabilitätskonzepte wichtige Instrumente zur Optimierung von Produktionsprozessen im Hinblick auf die ernährungsphysiologische Qualität dar. Bislang wurde die Stabilität von Milchpulvern vor allem anhand von Stabilitätskonzepten beurteilt, die auf der Wasseraktivität und dem physikalischen Zustand beruhen. Diese Konzepte können die Stabilität von Lebensmitteln jedoch häufig nur zum Teil erklären. Aus diesem Grund war es ein Ziel dieser Arbeit, diese etablierten Stabilitätskonzepte um die molekulare Mobilität zu ergänzen. Zur Bestimmung des physikalischen Zustandes wurden der Glasübergang und die Kristallisation der Laktose mittels dynamischer Differenzkalorimetrie gemessen. Die Laktosekristallisationsverzögerung war abhängig von der Glasübergangstemperatur und konnte mittels der Williams-Landel-Ferry-Gleichung modelliert werden. Dagegen konnte die Kinetik der Laktosekristallisation nicht mit der Avrami-Gleichung beschrieben werden, was die Bildung verschiedener Kristallformen andeutet. Die molekulare Mobilität, gemessen mittels niedrigauflösender ^1H NMR, stellte sich als schnelles und einfach durchzuführendes Messverfahren zur Charakterisierung von Milchpulvern heraus. Die transversale Relaxationszeit stieg oberhalb der Glasübergangstemperatur stark an und stieg auch im kristallinen Zustand weiter an. Allerdings beeinflussten die Kristallisationsbedingungen die transversale Relaxationszeit im kristallinen Zustand, was in Übereinstimmung mit den Beobachtungen zur Laktosekristallisationskinetik die Bildung verschiedener Kristallformen andeutet. Des Weiteren führte die Kristallisation zu einem sprunghaften Anstieg des zweiten Moments. Dies zeigt, dass die niedrigauflösende ^1H NMR auch zur Analyse der Kristallstruktur eingesetzt werden kann. Das Ausmaß des Lysinverlustes in drei verschiedenen Milchrezepturen nach einer thermischen Behandlung konnte unter Einbeziehung des physikalischen Zustandes und der molekularen Mobilität erklärt werden. Demnach lässt sich schlussfolgern, dass sowohl der physikalische Zustand als auch die molekulare Mobilität entscheidend für die chemische Stabilität von Milchpulvern verantwortlich sind. Diese Ergebnisse zu den Stabilitätscharakteristiken der Modellmilchrezeptur lieferten eine fundierte Grundlage zur Analyse der Reaktionskinetik des Lysinverlustes.

Der Einfluss des Wasserentzugs auf den Lysinverlust wurde mittels Vakuumtrocknung bei moderaten Temperaturen und bei Zeitmaßstäben, die es erlaubten die Schädigungskinetik aufzunehmen, ermittelt. Der Gehalt an verfügbarem Lysin sank während des Wasserentzugs. Sowohl die Trocknungsrate als auch die thermischen Bedingungen während der Trocknung

hatten einen signifikanten Einfluss auf den Lysinverlust bei Wassergehalten über 10 %. Ein starker Anstieg des Lysinverlustes wurde bei Wassergehalten unterhalb von 10 % beobachtet, wenn thermische Beanspruchungen zum Tragen kamen. Folglich scheinen Lysinverluste während der Trocknung durch die Dynamik des Wasserentzugs hervorgerufen zu werden.

Thermisch induzierte Lysinverluste wurden bei hohen Konzentrationen, d.h. im trockenen Zustand, und bei Bedingungen, die für die Sprühtrocknung relevant sind, untersucht. Die Lysinverluste stiegen signifikant mit steigender Temperatur und längeren Erhitzungszeiten. Die Geschwindigkeit des Lysinverlustes war hoch während der ersten Erhitzungsminuten, wobei es sich um den für die Sprühtrocknung relevanten Zeitabschnitt handelt. Danach verlangsamte sich die Geschwindigkeit des Lysinverlustes für alle Wasseraktivitäten und Temperaturen. Die Wasseraktivität hatte ebenfalls einen signifikanten Einfluss auf den Lysinverlust. Der Lysinverlust erreichte nach einer Erhitzungszeit von 30 min ein Maximum von 81 % bei einer Wasseraktivität von 0,17 und einer Temperatur von 90 °C. Der Wasseraktivitätsbereich des maximalen Lysinverlustes war bei niedrigeren Temperaturen zu höheren Wasseraktivitäten verschoben. Dieser Effekt konnte dem physikalischen Zustand zugeschrieben werden, wobei sich der gummiartige (rubbery) Zustand als der reaktivste Zustand hinsichtlich des Lysinverlustes herausstellte.

Alle genannten Ergebnisse berücksichtigend konnte gezeigt werden, dass der Lysinverlust mit einer Reaktion pseudo-zweiter Ordnung modelliert werden kann. Die Reaktionsgeschwindigkeitskonstanten stiegen mit steigender Temperatur an. Bei einer Temperatur von 90 °C wurde die höchste Reaktionsgeschwindigkeitskonstante bei einer Wasseraktivität von 0,23 ermittelt. Bei niedrigeren Temperaturen verschob sich dieses Maximum zu höheren Wasseraktivitäten. Die Temperaturabhängigkeit der Reaktionsgeschwindigkeitskonstante konnte in der Nähe der Glasübergangstemperatur und im rubbery-Zustand mittels der Williams-Landel-Ferry-Gleichung (WLF) beschrieben werden. Die Glasübergangstemperatur wurde mit Hilfe der Gordon & Taylor-Gleichung berechnet. Bei höheren Temperaturen und Wassergehalten wurde eine Arrheniusabhängigkeit ermittelt. Die Aktivierungsenergie E_A und der präexponentielle Faktor k_0^* der Arrheniusgleichung wurden als Funktion des Wassergehaltes ausgedrückt. Somit war es möglich, den Lysinverlust in Abhängigkeit der Temperatur, des Wassergehaltes und des physikalischen Zustandes bei für die Sprühtrocknung typischen Bedingungen zu modellieren.

Das Reaktionskinetikmodell stellte einen wesentlichen Baustein des Modells für den Lysinverlust während der Sprühtrocknung dar. Zur weiteren Ausarbeitung dieses Modells wurden die erwähnten Konzepte der Lebensmitteltechnologie im Folgenden mit Ansätzen der Verfahrenstechnik verknüpft. Der Einfluss der Sprühtrocknungsbedingungen auf den Lysinverlust sowie die Trocknungskinetik der Modellmilchrezeptur wurden ermittelt und der Sprühtrocknungsprozess mittels numerischer Strömungsmechanik (computational fluid dynamics, CFD) simuliert.

Das Ausmaß des Lysinverlustes während der Sprühtrocknung konnte durch die richtige Wahl der Sprühtrocknungsbedingungen kontrolliert werden, d. h. indem die Lufteintrittstemperatur und das Luft-Flüssigkeitsverhältnis angepasst wurden. Abhängig von den Sprühtrocknungsbedingungen im Labor- und Pilotmaßstab wurde ein Lysinverlust von 0 – 10,4 ± 2,9 % bestimmt. Die Verweilzeit der Partikel, die im Sprühturm im Pilotmaßstab mit kurzer Bauform länger als im Sprühturm im Labormaßstab mit langer Bauform war, stellte einen Hauptein-

flussfaktor auf den Lysinverlust dar. Der Median der Partikelverweilzeit lag bei 6 s für den Laborsprühtrockner und bei 17 s für den Pilotsprühtrockner. Es zeigte sich, dass das Trocknungsluft-Flüssigkeitsverhältnis ein geeigneter Parameter ist, um verschiedene Trocknerbauarten zu vergleichen. Das Ausmaß des Lysinverlustes während der Lagerung der sprühtrockneten Pulver konnten durch niedrige Lagertemperaturen und niedrige Pulverwassergehalte begrenzt werden.

Die Trocknungskinetik der Modellmilchrezeptur wurde mittels der Trocknung von liegenden Tropfen und dünnen Filmen in einem konvektiven Trocknungskanal untersucht. Der erste Trocknungsabschnitt mit konstanter Trocknungsrate konnte vom zweiten Trocknungsabschnitt mit fallender Trocknungsrate abgegrenzt werden. Es stellte sich heraus, dass die Dünnschichttrocknung reproduzierbarere und verlässlichere Ergebnisse lieferte als die Tropfentrocknung. Die Trocknungskinetik wurde mittels der Methode der charakteristischen Trocknungsratenkurve (characteristic drying-rate curve, CDRC) und dem Reaktionstechnikansatz (reaction-engineering approach, REA) modelliert. Mit dem Reaktionstechnikansatz, welcher erfolgreich in die numerische Strömungssimulation der Sprühtrocknung eingebaut werden konnte, ließen sich genauere Voraussagen zum Trocknungsverlauf machen.

Um die Partikeleigenschaften im Laufe der Verweilzeit zu bestimmen, wurde ein dreidimensionales numerisches Strömungssimulationsmodell der Sprühtrocknung aufgestellt. Das war erforderlich, da die Sprühtrocknung als Black Box angesehen werden muss, d.h. eine repräsentative Probennahme in verschiedenen Prozessstadien ist nicht durchführbar. Das Modell wurde mit den experimentellen Ergebnissen aus dem Pilotmaßstab validiert, wobei eine sehr gute Übereinstimmung zwischen den Versuchs- und Simulationsergebnissen erzielt wurde. Das Reaktionskinetikmodell wurde mit den Partikeleigenschaften entlang der Partikelbahnen gekoppelt, um ein Vorhersageinstrument für den Lysinverlust zu erhalten. Dadurch wurde die entscheidende Rolle der Partikelverweilzeit offensichtlich, was sich auch bereits in den Versuchen angedeutet hatte. Die anschließende Optimierungsstudie offenbarte potentielle Verbesserungsstrategien für den Sprühtrocknungsprozess. In diesem Zusammenhang sollten die Trocknergeometrie, das Luftströmungsprofil und die Tropfenzerstäubung grundlegend überdacht werden.

Zusammenfassend lässt sich festhalten, dass durch die Kopplung der Reaktionskinetik des Lysinverlustes mit der Trocknungskinetik und der numerischen Strömungssimulation der Sprühtrocknung ein vielversprechendes Instrument entwickelt wurde, um die Qualität sprühtrockneter Milchprodukte zu verbessern. Aufwendige Trial-and-Error-Versuche werden dadurch überflüssig. Des Weiteren kann der vorgeschlagene Ansatz leicht auf andere Sprühtrocknungsanwendungen übertragen werden, z. B. auf die gezielte Bildung von Mikrokapseln oder zur Erhöhung der Überlebensrate von Mikroorganismen. Der Erfolg dieses Projektes kann seinem interdisziplinären Ansatz zugeschrieben werden, der an der Schnittstelle zwischen der Lebensmitteltechnologie und der klassischen Verfahrenstechnik angesiedelt ist.

Summary

Sensitive ingredients of food, pharmaceutical products or biological products can be damaged due to inappropriate processing conditions. Production processes can be optimized with regard to the quality of the sensitive ingredients by coupling product properties with process characteristics. In the case of food products, this requires linking food technology and process engineering. This study was focused on the essential amino acid lysine in a model dairy-formulation whose composition was derived from the typical composition of infant formulae. Lysine is an important nutrient which can be blocked by the Maillard reaction during drying processes. In the production of dairy powders, spray drying is known to be the critical processing step concerning lysine loss. Both dehydration and elevated temperatures can induce lysine losses during spray drying.

In the field of food technology, reaction kinetics and stability concepts represent valuable tools to optimize production processes with regard to nutritional quality. So far, the stability concepts based on water activity or on the glass-transition temperature have mainly been used to predict the stability of dairy powders. However, these concepts often only partly predict the stability of food products. Therefore, one aim of this study was to complement the established stability concepts by the molecular mobility as measured by low resolution ^1H NMR. Glass transition and crystallization of lactose were measured by differential scanning calorimetry. The delay of lactose crystallization was a function of the glass transition temperature and could be modeled by the Williams-Landel-Ferry equation. Lactose crystallization kinetics could not be modeled by the Avrami equation which indicates the formation of different crystal forms. The molecular mobility measured by low resolution ^1H NMR proved to be a fast and easy method for the characterization of dairy powders. The transversal relaxation time showed a sharp increase above the glass transition temperature and increased further in the crystalline state. However, the crystallization conditions affected the transversal relaxation time in the crystalline state, which indicated the formation of different crystal forms in accordance with the observations of the lactose-crystallization kinetics. Furthermore, crystallization led to a step increase of the second moment. Hence, low resolution ^1H NMR could also be used to analyze the crystalline structure. The extent of lysine loss in three different dairy formulations after a thermal treatment could be explained by taking into account the physical state together with the molecular mobility. Thus, it can be concluded that both the physical state and the molecular mobility are decisive for the chemical stability of dairy powders. These results on the stability characteristics of the model dairy-formulation provide a sound basis for the analysis of the reaction kinetics of lysine loss.

The impact of dehydration on the loss of available lysine was assessed using vacuum dehydration at moderate temperatures at time scales that allow recording the degradation kinetics. The content of available lysine decreased during dehydration. The drying rate as well as the thermal conditions during drying had no significant impact on the loss of available lysine above a water content of 10%. A sharp increase in lysine loss was observed at water contents below 10% when thermal stresses become important. In conclusion, the dynamics during water removal seem to provoke lysine loss during drying.

Thermally-induced lysine losses were studied in high-concentration systems, i.e., in the dry state, and in conditions that are relevant for spray drying. Lysine losses increased significantly

with increasing temperatures and at prolonged heating times. The rate of lysine loss due to heating was fast during the first few minutes, which is the most relevant time scale for the spray-drying process. Then the rate of lysine loss slowed down for all water activities and temperatures. The water activity had a significant impact on lysine loss, as well. A maximum of 81% in lysine loss was observed at a water activity of 0.17 at 90°C after a heating time of 30 min. The water activity range of maximum lysine loss was shifted to higher water activities for lower temperatures. This effect could be linked to the physical state of lactose. The rubbery state emerged to be most reactive with regard to lysine loss.

Combining these results, it was shown that lysine loss can be modeled with pseudo-second order reaction kinetics. The reaction-rate constants increased with increasing temperatures. At 90°C, the highest reaction-rate constant was found at a water activity of 0.23. This maximum was shifted to higher water activities for lower temperatures. The temperature dependence of the reaction-rate constants could be modeled using the Williams-Landel-Ferry (WLF) equation in the vicinity of the glass-transition temperature and in the rubbery state. The glass-transition temperature was calculated with the Gordon & Taylor equation. At higher temperatures and water contents, Arrhenius-type behavior was determined. The activation energy E_A and the pre-exponential factor k_0^* of the Arrhenius equation were expressed as a function of the water content. Thus, lysine losses were modeled as a function of temperature, water content and physical state under conditions that are typical of spray drying.

This reaction kinetics model was used to build a model which describes the lysine loss due to spray drying. To achieve this, the mentioned concepts of food technology were combined with concepts of process engineering. The impact of the spray-drying conditions was assessed, the drying kinetics of the model dairy-formulation was determined and the spray-drying process was simulated by computational fluid dynamics.

The extent of lysine loss could be controlled by the correct choice of spray drying conditions, i.e., by adjusting the air-inlet temperature and the air-to-liquid ratio. Depending on the spray drying conditions, $10.4 \pm 2.9\%$ lysine loss down to no lysine loss was determined after spray drying on a laboratory and pilot scale. A major impact on lysine loss could be attributed to the particle residence-time, which was shown to be longer for the short-form pilot-scale spray dryer than for the tall-form laboratory scale spray dryer. The median particle residence-time was 6 s in the laboratory-scale dryer and 17 s in the pilot-scale dryer. The air-to-liquid ratio of the spray dryer proved to be a good parameter to compare different types of spray dryers. The extent of lysine loss during the storage of the spray-dried powders was independent of the extent of lysine loss during spray drying. Lysine loss during storage could be reduced by low storage temperatures and low water contents of the powder.

Sessile-droplet and thin-film drying in a convective drying channel were applied to study the drying kinetics of the model dairy-formulation. The constant-rate and falling-rate drying stages could be distinguished. Thin-film drying turned out to provide more reproducible and reliable results. Consequently, thin-film drying should be preferred to sessile droplet drying. The drying kinetics was modeled with the characteristic drying-rate curve and the reaction-engineering approach. Better predictions were obtained by the reaction-engineering approach, which was successfully implemented in the computational fluid-dynamics (CFD) simulation of spray drying.

A 3D CFD model of spray drying was set up to determine the particle properties along their residence time. This is necessary because the spray dryer must be considered as a black box, i.e., it is hardly possible to take representative samples at different process stages. The model was validated with the experimental results of spray drying on a pilot scale. An excellent accordance between the experiments and the simulation was obtained. The reaction kinetics model was coupled with the particle properties along the particle tracks to create a predictive tool for the lysine loss. Thus, as it was hypothesized from the spray-drying experiments, the importance of the particle residence-time was highlighted. The following optimization study revealed potential strategies to ameliorate the spray drying process. In this context, the dryer geometry, air flow pattern and droplet atomization should be reconsidered carefully.

To sum up, coupling reaction kinetics of lysine loss that take into account the physical state of lactose, i.e., glassy, rubbery or crystalline, with drying kinetics and computational fluid dynamics of spray drying proved to be a promising tool to enhance the quality of spray-dried dairy products without the need of many trial-and-error experiments. The proposed approach can be transferred to other spray drying applications, e.g. for the targeted formation of microcapsules or to enhance the survival of microorganisms. The success of this project can be attributed to its interdisciplinary approach which builds a bridge between food technology and process engineering.

Table of contents

Acknowledgements	III
Zusammenfassung	V
Summary	IX
Table of contents	XIII
List of symbols and abbreviations	XVII
1 Introduction	21
2 Theoretical background	23
2.1 Importance and loss of available lysine	23
2.1.1 Impact of temperature on lysine loss	24
2.1.2 Role of water activity	25
2.1.3 Importance of the dairy powder composition	25
2.1.4 Effect of the processing conditions	26
2.2 Physical state, molecular mobility and stability concepts	27
2.2.1 Glass-transition concept, crystallization and physical state	27
2.2.2 Molecular mobility	29
2.3 Spray drying	32
2.4 Drying kinetics	35
2.4.1 Experimental methods to determine the drying kinetics	35
2.4.2 Modeling approaches to describe drying kinetics	38
2.5 Computational fluid dynamics	41
3 Objective	45
4 Material and methods	47
4.1 Composition and preparation of the model dairy-formulation	47
4.2 Freeze drying	48
4.3 Thermal treatment	48

4.4	Vacuum dehydration	49
4.5	Spray drying on a laboratory and pilot scale	50
4.5.1	Spray drying on a laboratory scale	50
4.5.2	Spray drying on a pilot scale	51
4.5.3	Scale up of the spray-drying process	51
4.5.4	Residence-time distribution of the particles	52
4.6	Thin-film drying and droplet drying	53
4.6.1	Experimental set up of the drying channel	53
4.6.2	Modeling drying kinetics	55
4.7	Analytical methods	58
4.7.1	Available lysine	58
4.7.2	Contact angle	59
4.7.3	Density	59
4.7.4	Glass-transition temperature and crystallization of lactose	61
4.7.5	Interfacial tension	62
4.7.6	Molecular mobility	63
4.7.7	Particle size	64
4.7.8	Solubility	64
4.7.9	Spray characteristics of the pneumatic nozzle	65
4.7.10	Viscosity	65
4.7.11	Water content and water activity	65
4.7.12	Water sorption and desorption isotherm	66
4.8	Statistical analysis	66
5	Results and discussion	69
5.1	Characterization of the model dairy-formulation	69
5.1.1	Material characteristics of the model dairy-formulation concentrate	69

5.1.2	Sorption behavior and physical state	72
5.1.3	Molecular mobility	78
5.1.4	Impact of the protein and lactose content on the physical state of lactose... ..	83
5.2	Thermally-induced lysine loss	85
5.2.1	Impact of the heating conditions	85
5.2.2	Role of physical state.....	87
5.2.3	Role of the molecular mobility.....	89
5.2.4	Reaction mechanism of lysine loss.....	89
5.2.5	Modeling reaction kinetics of lysine loss	90
5.2.6	Influence of the matrix composition.....	101
5.3	Dehydration-induced lysine loss.....	105
5.3.1	Characterization of the dehydration kinetics	105
5.3.2	Impact of the dehydration conditions on lysine loss	109
5.3.3	Impact of the lactose and protein content.....	111
5.4	Spray drying.....	113
5.4.1	Process performance, powder characteristics and scale up	113
5.4.2	Residence-time distribution of the particles	123
5.4.3	Lysine loss	125
5.5	Drying kinetics.....	130
5.5.1	Thin film and droplet drying	131
5.5.2	Characteristic drying-rate curve	133
5.5.3	Reaction-engineering approach	135
5.5.4	Evaluation of the drying-kinetics models.....	137
6	Modeling lysine loss during spray drying.....	141
6.1	Description of the computational fluid-dynamics model of spray drying	141
6.2	Analysis of the simulation results and validation of the model.....	146

6.3	Optimization of the spray-drying process with regard to lysine loss.....	152
6.3.1	Modification of the air profile by a secondary air inlet.....	152
6.3.2	Variation of the spray-dryer geometry	154
7	Conclusion.....	157
8	References	161

List of symbols and abbreviations

a	model coefficient /-	d_{10}	diameter of the 10% percentile /m
a_0	offset value/-	$d_{3,2}$	Sauter mean diameter /m
a_w	water activity /-	d_{50}	median diameter /m
a^*	red/green value /-	d_{90}	diameter of the 90% percentile/m
A_p	product-surface area /m ²	db_T	bottom diameter /m
AIC_c	corrected Akaike criterion /-	D	diameter /m
ALR_{nozzle}	air to liquid ratio of the nozzle	D_v	vapor-air diffusivity /m ² .s ⁻¹
ALR_{dryer}	air to liquid ratio of the dryer	E_A	activation energy /J.mol ⁻¹
b	model coefficient /-	E_{A0}	plateau value of the activation energy/J.mol ⁻¹
b_1	constant /s ⁻¹	ER	evidence ratio /-
b^*	yellow/blue value /-	f	frequency /-
B_0	external magnetic field /T	f_L	proton fraction of the mobile component /-
B_1	oscillating magnetic field /T	f_s	proton fraction of the immobile component /-
BIC	Bayesian information criterion /-	F	cumulative residence-time distribution /-
c	model coefficient /-	g	acceleration of gravity /m.s ⁻²
c_p	specific heat capacity /J.(kg.K) ⁻¹	h	heat-transfer coefficient /W.(m ² .K) ⁻¹
$c_{p,air}$	specific heat capacity of air /J.(kg.K) ⁻¹	h_F	film thickness /m
$c_{p,w}$	specific heat capacity of water vapor /J.(kg.K) ⁻¹	h_m	mass-transfer coefficient /m.s ⁻¹
c_s	solid concentration of the concentrate /kg.kg ⁻¹	h_T	height /m
C	concentration /kg.kg ⁻¹	k	reaction-rate constant /min ⁻¹
C'	constant of the GAB model /-	k_{Av}	rate constant of the Avrami equation /s ^{-n_{Av}}
C_1	constant of the WLF model /-	k_{Tg}	reaction-rate constant at the glass-transition temperature /min ⁻¹
C_2	constant of the WLF model /K	k_0^*	preexponential factor /min ⁻¹
$C_{1,r}$	relative constant of the WLF model /-	k_1^*	constant /min ⁻¹
$C_{2,r}$	relative constant of the WLF model /K	k_2^*	constant /min ⁻¹
C_0	initial concentration /kg.kg ⁻¹ , (mol NH ₂). (g dry matter) ⁻¹	K	constant of the Gordon & Taylor equation /-
C_{E1}	constant /% db	K'	constant of the GAB model /-
C_{E2}	constant /% db	L	likelihood function /-
C_k	constant /% db	L^*	lightness /-
C_t	concentration at time t / (mol NH ₂). (g dry matter) ⁻¹	m	mass /kg
C_∞	equilibrium concentration /kg.kg ⁻¹	m_p	product mass /kg
C^*	color-saturation index (chroma)/-	m_s	mass of solids /kg
d_d	droplet diameter /m	m_w	mass of water /kg
d_p	particle diameter /m	M_2	second moment /s ⁻²
d_s	equal-volume sphere diameter /m		

\dot{m}	mass-flow rate /kg.s ⁻¹	T_{in}	inlet-air temperature /°C, K
n_{Av}	Avrami index /-	T_m	mean temperature /°C, K
n	sample size /-	T_{out}	outlet-air temperature /°C, K
N	drying rate /kg.s ⁻¹	T_p	product temperature /°C, K
N_{max}	maximum drying rate /kg.s ⁻¹	T_r	reference temperature /°C, K
p	number of parameters /-	T_s	surface temperature /°C, K
P_{AIC}	probability that one model is more likely than another one	T_{wb}	wet-bulb temperature /°C, K
Q_3	cumulative particle-size distribution /-	T_{∞}	temperature with infinite crystallization delay /°C, K
R	radius /m	T^*	reference temperature /K
r_v	latent heat of vaporization /J.kg ⁻¹	v	velocity /m.s ⁻¹
R^2	coefficient of determination /-	v_{mr}	mixing-rate velocity /m.s ⁻¹
R_g	specific gas constant /J.(kg.K) ⁻¹	V	volume /m ³
Re	Reynolds number /-	V_{crit}	critical volume /m ³
RH	relative humidity /%	\dot{V}	volume-flow rate /m ³ .s ⁻¹
RH_{out}	relative humidity of the outlet air /%	w_1	weight fraction of the dry matter /kg.kg ⁻¹
RH_s	relative humidity at the surface /-	w_2	weight fraction of water /kg.kg ⁻¹
RH_b	relative humidity of the bulk gas /-	x	particle size /m
s^2	experimental variance /-	x	water content of the air (db) /kg.kg ⁻¹ , %
S	surface /m ²	X	water content (db) /kg.kg ⁻¹ , %
Sc	Schmidt number /-	X_0	initial water content (db) /kg.kg ⁻¹ , %
Sh	Sherwood number /-	X_0	water content of the peak maximum (db) /kg.kg ⁻¹ , %
SS_{lof}	lack-of-fit mean squares /-	X_{cr}	critical water content (db) /kg.kg ⁻¹ , %
SS_{pe}	pure error mean squares /-	X_e	equilibrium water content (db) /kg.kg ⁻¹ , %
SS_r	residual some of squares /-	X_m	monolayer water content (db) /kg.kg ⁻¹ , %
U	intensity of the NMR signal /-	X^*	water content (wb) /kg.kg ⁻¹ , %
\underline{t}	time /s		
\bar{t}	mean residence time /s		
T	temperature /°C, K		
T_1	longitudinal relaxation time /s		
T_2	transversal relaxation time /s		
$T_{2,1}$	transversal relaxation time of the immobile component /s		
$T_{2,2}$	transversal relaxation time of the mobile component /s		
T_b	bulk-gas temperature /°C, K		
T_e	equilibrium temperature /°C, K		
T_g	glass-transition temperature /°C, K		
T_{g1}	glass-transition temperature of the dry matter /°C, K		
T_{g2}	glass-transition temperature of water /°C, K		

α	crystallinity /-	CDRC	characteristic drying-rate curve
Δ	difference /-	CFD	computational fluid dynamics
ΔE_v	apparent activation energy /J.mol ⁻¹	CPMG	Carr-Purcell-Meiboom-Gill
$\Delta E_{v,e}$	equilibrium apparent activation energy /J.mol ⁻¹	db	dry basis
η	contact angle /°	FID	free induction decay
η	dynamic viscosity /Pa.s	GAB	Guggenheim-Anderson-de Boer
η_w	dynamic viscosity of water vapor /Pa.s	HPLC	high performance liquid chroma- tography
φ	dimensionless water content /-	NMR	nuclear magnetic resonance
μ	magnetic moment /A.m ²	RANS	Reynolds-averaged Navier Stokes
ν_G	kinematic viscosity of the gas /m ² .s ⁻¹	REA	reaction-engineering approach
λ_{air}	thermal conductivity of air /W.(m.K) ⁻¹	rf	radio frequency
λ_w	thermal conductivity of water vapor /W.(m.K) ⁻¹	wb	wet basis
ρ	density /kg.m ³		
ρ_d	density of the concentrate /kg.m ³		
ρ_s	density of the dry matter /kg.m ³		
$\rho_{v,b}$	bulk vapor concentration /kg.m ⁻³		
$\rho_{v,s}$	vapor concentration at the sam- ple-gas interface /kg.m ⁻³		
$\rho_{v,sat}$	saturated vapor concentration /kg.m ⁻³		
ρ_w	density of water /kg.m ³		
σ	interfacial tension /N.m ⁻¹		
τ	crystallization delay /s		
τ_{10}	10% percentile of the residence- time distribution /s		
τ_{50}	median residence time /s		
τ_{90}	90% percentile of the residence- time distribution /s		
τ_i	impulse spacing time /s		
τ_{Tg}	crystallization delay at the glass- transition temperature /s		
τ_{Tr}	crystallization delay at the refer- ence temperature /s		
ξ	characteristic drying rate /-		

1 Introduction

Spray drying is widely used in the food, pharmaceutical and chemical industries to produce powdered products. The advantage of spray drying is that huge quantities can be dried fast, cost-efficient and with less thermal stress than in the case of other drying methods. Generally, spray drying is known to be a gentle drying process. However, sensitive ingredients may be damaged during spray drying, e.g. starter cultures, probiotics, enzymes, proteins, active pharmaceutical ingredients or essential nutrients like the essential amino acid lysine. This is a major concern because these sensitive ingredients are often essential for the quality of the final product. However, research on spray drying has so far mainly focused on conventional aspects of process engineering.

In any production process, sensitive ingredients, e.g. nutrients, can be preserved and their degradation minimized if the circumstances are identified which lead to product deteriorations. Once these mechanisms are understood, the product characteristics as well as the processing and storage conditions can be optimized with regard to the product quality. For instance, desired functional properties of β -lactoglobulin can be created when the heating conditions are chosen in a targeted way using a reaction kinetics model for its denaturation (Tolkach and Kulozik 2007). Ghandi et al. (2012) could differentiate between the impact of dehydration and thermal stresses on the survival rate of spray-dried dairy-fermentation bacteria when they determined the inactivation kinetics during convective drying and isothermal heating. Foerst and Kulozik (2012) deduced optimization strategies for low-temperature vacuum drying of probiotic bacteria from their inactivation model. This shows that the destruction of sensitive ingredients can be controlled during processing. To achieve this, detailed reaction kinetics of the loss reactions has to be established, the influencing factors have to be identified and this knowledge has then to be linked to the processing conditions.

In dairy formulations, valuable ingredients comprise vitamins such as vitamin B₁, proteins such as β -lactoglobulin, polyunsaturated fatty acids (PUFA) as docosahexaenoic (DHA) or arachidonic acid and available lysine. Available lysine is an essential amino acid, i.e., an important nutrient which is decisive for the nutritional value. Lysine is only available to the human metabolism if its ϵ -amino group is free. In dairy products, this amino group is mainly blocked by the early Maillard reaction with the reducing sugar lactose. This loss of available lysine occurs already at rather gentle conditions in highly concentrated systems, e.g. during spray drying and storage of dairy powders. Thus, it is a good indicator for the chemical stability of powdered dairy products. The kinetics of lysine loss in liquid milk is well known (Fink and Kessler 1986a, Horak and Kessler 1981). It is used to choose optimized temperature-time conditions for the heat treatment of liquid milk. Thus, lysine losses are minimized and it is possible to produce UHT milk with a lysine loss of less than 3%, while for autoclave sterilization losses can reach 30-40%. However, these correlations are not known for conditions relevant to spray drying.

Powdered dairy formulations are usually produced by spray drying a concentrate. Before spray drying, the ingredients of the concentrate are reconstituted and mixed, heat-treated for microbial safety and concentrated by evaporation in the following. Spray drying causes lysine losses of up to 20% and was identified to be the critical production step concerning lysine loss in dairy formulations. This can be explained by the fact that the rate of lysine loss is higher in

the dry state, i.e., at high concentrations, than in the liquid state. During spray drying, the product temperature is rising while the product is being dehydrated, i.e., the concentration of the reactants increases. Thus, the drying kinetics, the temperature level and the particle flow pattern inside the spray dryer, which determines the particle residence time distribution, might affect the extent of lysine loss. However, there is only very limited knowledge of whether major losses occur due to thermal or dehydration stresses. To evaluate and understand how it comes to lysine loss during spray drying, the spray-drying process must be analysed in detail. This requires on the one hand a profound knowledge of the drying kinetics and particle properties during spray drying. On the other hand, the consolidated analysis of the reaction kinetics of lysine loss is indispensable.

The aim of this study is to evaluate in a fundamental way the impact of the spray drying conditions on lysine loss in a model dairy formulation. The reaction kinetics of lysine loss will be established combining the product properties with the processing characteristics. Thus a bridge will be built between process engineering and food technology. Important aspects of food technology will be addressed like molecular mobility, physical state, matrix composition and reaction kinetics of thermally and dehydration-induced lysine loss. To the same degree, spray drying will be studied from a processing engineer's point of view. This will include drying kinetics, residence time distribution of the particles in the spray dryer, scale up of the spray drying process and computational fluid dynamics of spray drying. The acquired knowledge will be summarized in a comprehensive model which describes lysine loss during spray drying. Thanks to the modular concept and the fundamental investigations of this study, this model can easily be adapted to other processing applications, product types and target compounds or product properties. Examples include the targeted formation of microcapsules during spray drying or enhancing the survival rate of microorganisms.

2 Theoretical background

2.1 Importance and loss of available lysine¹

Lysine is an essential amino acid which is often the limiting factor regarding the nutritional value of food. Lysine is a ketogenic amino acid, i.e., its metabolic products are required for the biosynthesis of ketone bodies and fatty acids (Elmadfa and Leitzmann 1990). The main role of lysine in the human metabolism is the protein synthesis especially in the liver (Tomé and Bos 2007). Lysine deficiency or surplus negatively affects the growth, DNA content of the brain and the urea synthesis in immature infants (Stein 2003). In general, the overall digestion behavior is adapted if a deficiency of essential amino acids prevails (Kondoh and Torii 2011). The deficiency of essential amino acids is symptomized by a reduced appetite, low weight gain and nervousness. Lysine requirement of infants is $64 \text{ mg} \cdot (\text{kg} \cdot \text{d})^{-1}$ and of adults $30 \text{ mg} \cdot (\text{kg} \cdot \text{d})^{-1}$ (FAO/WHO/UNO 2007). However, lysine can only be metabolised in the human body if it has a free reactive ϵ -amino group, referred to as “available” lysine (Meade et al. 2005, Moughan and Rutherfurd 2008). The loss of available lysine leads to a loss of the protein quality, i.e., nutritional value, and to a decrease in the digestibility (van Boekel 1998). Dairy powders, which are for example intended for enteral formulas or infant food, are particularly vulnerable to the loss of available lysine due to their lysine rich proteins, their high reducing sugar (lactose) content, the high temperatures applied during manufacturing and the long storage times (Chavez-Servin et al. 2008, Ferrer et al. 2003b, Pereyra Gonzales et al. 2003).

There are several pathways which can lead to the loss of lysine, for instance reactions with polyunsaturated fatty acids upon oxidation, development of isopeptides, formation of lysinolalanine, reactions with oxidized phenols, acylation, racemisation, etc. (Meade et al. 2005, Moughan and Rutherfurd 2008, van Boekel 1998). The main cause for lysine degradation is, however, the Maillard reaction of lysine residues with lactose. During the early stages of the Maillard reaction, the lactose forms a Schiff’s base with the ϵ -amino group of lysine, which leads to the formation of the Amadori compound lactuloselysine via the Amadori rearrangement (Belitz et al. 2001). The Maillard reaction is influenced by various factors, e.g. temperature, water activity, lysine-lactose ratio, physical state and pH (Meade et al. 2005, Moughan and Rutherfurd 2008). Due to its importance, the physical state will be dealt with together with the molecular mobility in a separate chapter (see chapter 2.2).

¹ Partly published in: Schmitz I, Gianfrancesco A, Kulozik U, Foerst P (2011) Kinetics of lysine loss in an infant formula model system at conditions applicable to spray drying. *Drying Technology* 29(16):1876-1883; Schmitz-Schug I, Foerst P, Kulozik U (2013) Impact of the spray drying conditions and residence time distribution on lysine loss in spray dried infant formula. *Dairy Science & Technology* 93(4):443-462; Schmitz-Schug I, Gianfrancesco A, Foerst P, Kulozik U (2013) Impact of dehydration on lysine loss in a model dairy formulation. *Drying Technology* 31(13-14):1477-1484; Schmitz-Schug I, Gianfrancesco A, Kulozik U, Foerst P (2013) Physical state, molecular mobility and chemical stability of powdered dairy formulations. *Food Research International* 53(1):268-277; Schmitz-Schug I, Kulozik U, Foerst P (2014) Reaction kinetics of lysine loss in a model dairy formulation as related to the physical state. *Food and Bioprocess Technology* 7:877-886

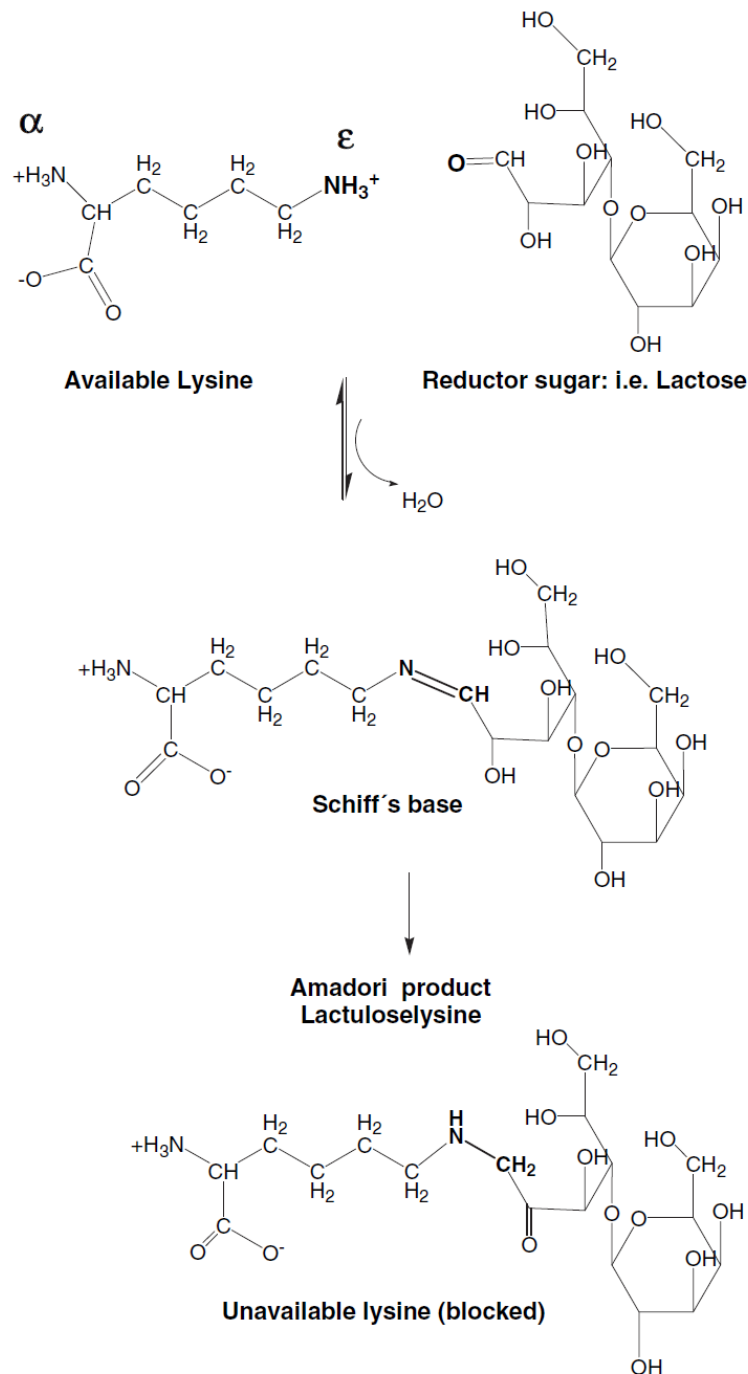


Fig. 2.1 Early stage of the Maillard reaction in dairy products (Chavez-Servin et al. 2008)

2.1.1 Impact of temperature on lysine loss

In general, lysine losses are higher at prolonged heating times and when higher temperatures are applied because this accelerates the Maillard reaction (Ferrer et al. 2003b, Fink and Kessler 1986b, Horak and Kessler 1981, Malec et al. 2002, Morales et al. 1995, Roux et al. 2009, Rufian-Henares et al. 2002, Rutherford and Moughan 2008). Thomsen et al. (2012), for example, observed that the average lactosylation of β -lactoglobulin increased at higher water

activities and when higher temperatures were applied. During the storage of dairy powders, lysine loss increased with increasing temperature (Chavez-Servin et al. 2008, Guerra-Hernandez et al. 2002, Pereyra Gonzales et al. 2010, van Mil and Jans 1991). Several authors reported that no or only slight loss of available lysine could be detected in powdered infant formulas or whole-milk powder stored at 20 or 25°C for 3 to 24 months (Chavez-Servin et al. 2008, van Mil and Jans 1991, Guerra-Hernandez et al. 2002). When the same powders were stored at higher temperatures (35-55°C) significant losses occurred, indicating the temperature effect. Pereyra Gonzales et al. (2010) observed during the storage of dairy powders that the rate constants of lysine loss decreased near the glass-transition temperature of lactose due to the low molecular mobility. In their case, neither crystallization of lactose had an impact on the rate constants of lysine loss, nor water activity on the temperature dependence of the rate constants. Chavez-Servin et al. (2008) showed that lysine was mainly blocked during the manufacture of formulas rather than during the storage because the increasing hydroxymethylfurfural values observed throughout the storage did not correlate with the lysine loss.

2.1.2 Role of water activity

As for water activity, a maximum of lysine loss is usually found in a certain water activity range. Above this critical water activity, the reactants are too diluted, below it the concentration of reactants is so high that diffusion becomes limiting (van Boekel 2001). Depending on the matrix, reported maximum rates for the Maillard reaction in dairy powders are in the water activity range of 0.2-0.8 (Ge Pan and Melton 2007, Labuza and Saltmarch 1981, Malec et al. 2002, Morgan et al. 1999, Vuataz 1988). When a model system composed of lactose and casein was stored at 37, 50 and 60°C, water activity most notably influenced the rate constants for available lysine loss at mild temperatures (Malec et al. 2002). A study of a carbohydrate-based food-model system, which contained L-lysine and D-xylose as reactants, showed that higher water contents decreased the temperature dependence of the Maillard reaction at product temperatures (40-90°C) representative of spray-drying conditions (Miao and Roos 2004).

2.1.3 Importance of the dairy powder composition

In the literature, almost no data is available on the impact of the lactose-protein ratio and of the whey protein-casein ratio on the loss of available lysine. Generally, losses in infant formula are higher than in cow's milk which can be ascribed, amongst other factors, to the modified whey protein-casein ratio and to the high lactose content (Finot et al. 1981, Rutherfurd and Moughan 2005). It was found that in commercial spray-dried infant formulas lysine was significantly more degraded if the whey protein-casein ratio was adjusted, i.e., if they were enriched with whey, than if it was similar to cow's milk (Birlouez-Aragon et al. 2004). This can be explained by the preferential carbonylation of whey protein compared to casein in milk powders (Fenaille et al. 2005). In contrast, other studies report that higher levels of whey protein did not considerably increase levels of blocked lysine in commercial infant formulas (Evangelisti et al. 1994). Replacing parts of lactose by maltodextrin resulted in lower lysine losses. At low dry matter concentrations, i.e., in the liquid state, model systems of whey protein and lactose showed higher losses upon heating than casein-lactose systems (Morales et al.

1995, Rufian-Henares et al. 2006). In comparison, lysine losses were lower in raw whole milk than in the model systems, which was explained by protein-protein interactions which reduced the accessibility of lysine residues (Morales et al. 1995). Morgan et al. (2005) observed higher lysine-loss rates at higher lactose-protein ratios in whey-protein concentrates, which is in accordance with the results of Burin et al. (2000) for the colour formation in whey products. Ferrer et al. (2000) found no significant impact of the lactose content and protein composition during the processing but during the storage of adapted and follow-up infant formulas. In summary, results found in the literature are contradictory, which makes it difficult to draw any reliable conclusion, especially on the impact of the whey protein-casein ratio.

2.1.4 Effect of the processing conditions

The extent of lysine loss during the processing of food products depends on the processing conditions. Charissou et al. (2007) studied lysine loss in model cookies caused by baking and determined a mean lysine loss of 60-70%. They concluded that the lysine loss during the baking of cookies could be minimized when high baking temperatures were used in combination with short baking times. Ilo and Berghofer (2003) linked the rate of amino acid loss during extrusion cooking of sweetcorn grits to the intensity of the shear stress. Losses of available lysine during drying of spaghetti could be reduced by decreasing the temperature level or by decreasing the exposure time to high temperatures (Dexter et al. 1984). In the production of powdered dairy products, high losses of available lysine occur particularly during spray drying (Ferrer et al. 2000, Finot 1983, Guyomarc'h et al. 2000, Holsinger et al. 1973). Lysine losses of 5-35% after spray drying of dairy powders are reported in the literature (Contreras-Calderon et al. 2009, Ferrer et al. 2000, Finot 1983). Higher temperatures during the spray drying of skim-milk powder caused a higher degree of lactosylation, i.e., of lysine loss. The outlet temperature of the drying air had a bigger impact than the inlet temperature of the drying air (Guyomarc'h et al. 2000). In order to control the destruction of sensitive ingredients, detailed reaction kinetics of the loss reactions have to be established and the influencing factors have to be identified. This knowledge can then be linked to the processing conditions and the process can be optimized with regard to sensitive ingredients of the product. The kinetics of lysine loss in liquid milk is well known. It can be used to minimize lysine losses during the heat treatment of liquid milk by choosing optimized temperature-time conditions (Fink and Kessler, 1986; Horak and Kessler, 1981). Thus, it is possible to produce UHT milk with a lysine loss of less than 3%, while for autoclave sterilization losses can reach 30-40%. However, these causal connections have not yet been studied at conditions relevant to spray drying.

To sum up, the data available so far has been obtained from storage studies or simple model systems. However, there is still a lack of knowledge about the reaction kinetics of lysine loss in the dry state at elevated temperatures and for short time scales as well as for more complex systems. Furthermore, the impact of dehydration on lysine loss has so far not been determined. Once this kinetics is known, it can be linked to the processing conditions and the process can be optimized with regard to lysine loss.

2.2 Physical state, molecular mobility and stability concepts²

Several concepts exist to characterize the chemical and biological stabilities of food products. The water activity concept is based on the idea that the chemical or biological stability is a function of water activity and that a food product is most stable at its monolayer water content (Rahman 2010). A stability map (Fig. 2.2) can be drawn with bacterial growth, yeast growth, non-enzymatic browning reactions, etc. as a function of water activity (Roos 2002, Rahman 2009). However, water activity alone cannot explain stability in many cases but has to be coupled with other stability concepts. For instance, Bell et al. (1998) have shown for a model-food system that the rate of glycine loss and non-enzymatic browning is not only determined by water activity but also to a large extent by the physical state. The physical state is taken into account by the glass-transition concept. Stability concepts which consider the molecular mobility are useful to explain e.g. the kinetics of bimolecular reactions.

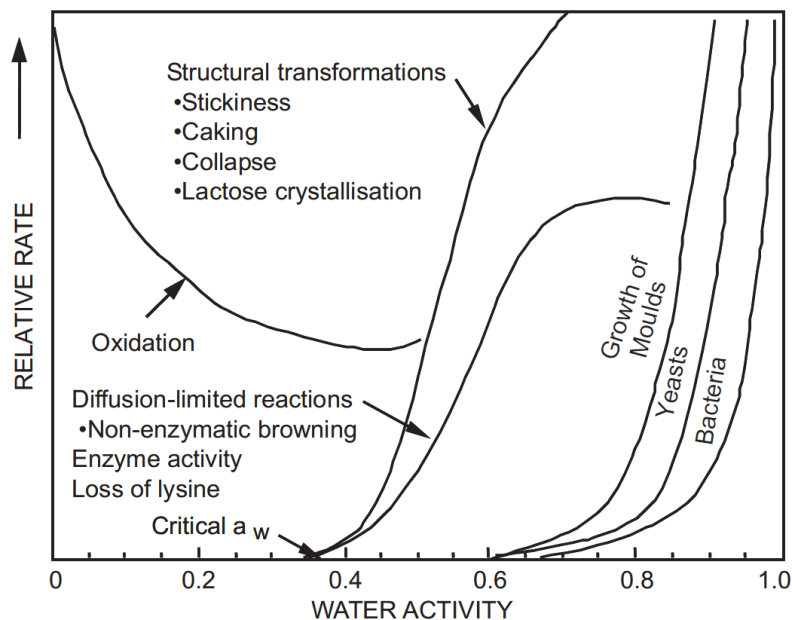


Fig. 2.2 Stability map of food products based on the water activity concept (Roos 2002)

2.2.1 Glass-transition concept, crystallization and physical state

The glass-transition concept takes the glass-transition temperature as a reference temperature for the stability (Champion et al. 2000, Rahman 2010, Roos 1995, Roos 2010). The glass-transition temperature characterizes the transition from the glassy state to the rubbery state. Glass transition is a second-order phase transition leading to significant changes of the mechanical and physical properties. In the glassy state below the glass-transition temperature the viscosity reaches high values of $>10^{12}$ Pa.s (Roos 1995). Consequently, the mobility is limited to short-range rotational molecular motions and vibrations. Thus, the rate of diffusion-

² Partly published in: Schmitz I, Gianfrancesco A, Kulozik U, Foerst P (2011) Kinetics of lysine loss in an infant formula model system at conditions applicable to spray drying. *Drying Technology* 29(16):1876-1883; Schmitz-Schug I, Gianfrancesco A, Kulozik U, Foerst P (2013) Physical state, molecular mobility and chemical stability of powdered dairy formulations. *Food Research International* 53(1):268-277

controlled reactions is normally slow which results in good stability. Above the glass-transition temperature the system is in the rubbery state which is characterized by a higher mobility than in the glassy state, allowing long-range coordinated molecular motion. Both states are known as amorphous states, i.e., states without an ordered molecular structure. However, these states are unstable. Increasing the temperature or the water content will result in the crystallization of the system after a certain time known as crystallization delay (Vuataz 2002). The crystalline state is characterized by an increased mobility compared to the glassy state and by an ordered crystalline structure (Roos 1995). This concept can be used to establish state diagrams, as it was for example done by Vuataz (2002) for milk. These can be used as a tool to predict the stability or to optimize processing. As for drying, milk powder can be either in the amorphous or in the crystalline state after drying. The glassy state will only be attained if the water is removed sufficiently fast to avoid the formation of crystalline structures. This is the case for spray drying if the drying parameters are chosen adequately (Langrish 2008, Roos 2010). Glassy powders can also be produced by freeze drying given the correct freezing and sublimation conditions. In contrast, slow drying processes create crystalline powders. Examples include many vacuum-drying applications or spray drying and fluidized-bed drying under high-humidity conditions or high air-inlet temperatures (Chiou et al. 2008, Langrish 2008, Yazdanpanah and Langrish 2011).

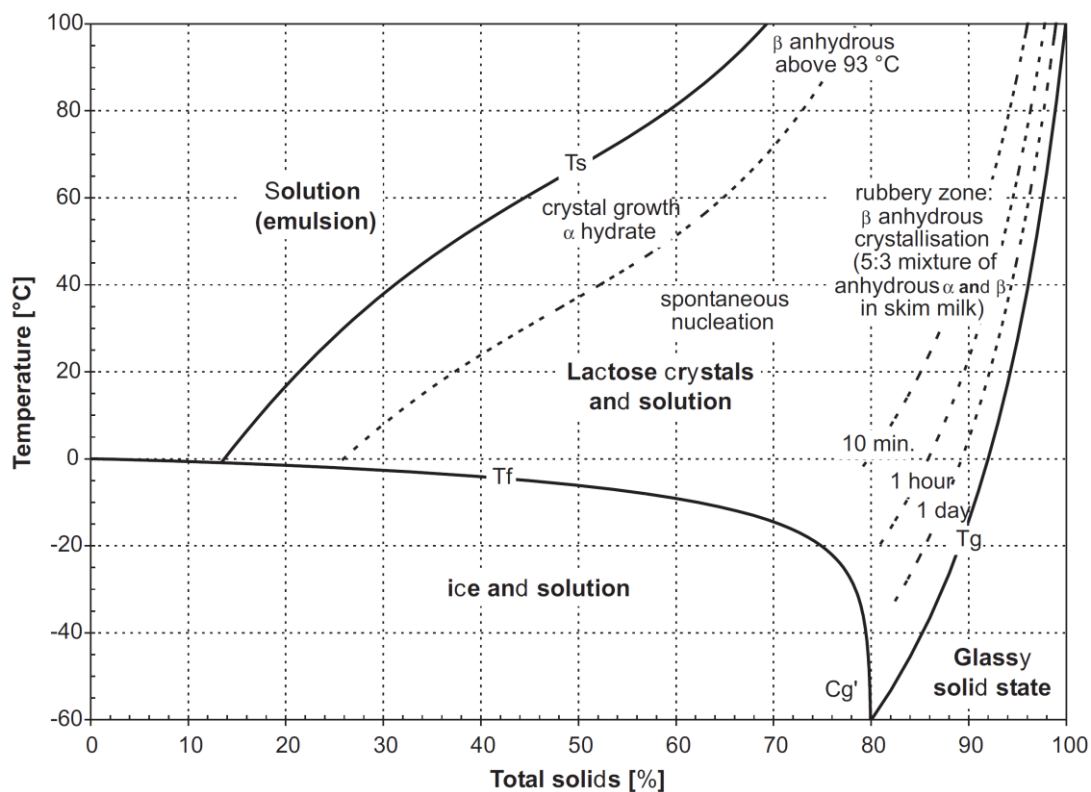


Fig. 2.3 State diagram of milk (Vuataz 2002)

In amorphous dairy-powder particles, fat globules and proteins are surrounded by a continuous phase of amorphous lactose and other low molecular-weight components (Walstra et al. 2006, Thomsen et al. 2005c). Lactose in dairy powders may on the one hand exist in different physical states, namely glassy, rubbery or crystalline, and is thus host to the other compo-

nents. On the other hand, lactose is a reactant of the Maillard reaction which is considered to be the major cause for the loss of available lysine (cf. chapter 2.1). It has been shown for skim-milk powders and food-model systems that the rate of lysine loss and non-enzymatic browning is low in the glassy state and near the glass-transition temperature (Karmas et al. 1992, Pereyra Gonzales et al. 2010). Crystallization of lactose in dairy powders is retarded by the presence of proteins compared to pure lactose powders (Haque and Roos 2004, Jouppila and Roos 1994, Morgan et al. 2005). The crystallization delay, i.e., the induction time until lactose starts to crystallize under given conditions, is dependent on the lactose-protein ratio as well as on the type of protein. When lactose crystallizes, on the one hand bound water is liberated, leading to an increase in water activity and to the initiation of deteriorative chemical reactions, e.g. the Maillard reaction (Roos 2002, Thomsen et al. 2005a, Walstra et al. 2006). On the other hand, crystallized lactose is not any longer available for reactions with proteins, which can limit the reaction rate. It was shown that lactose crystallization is strongly coupled with browning (Miao and Roos 2005, Thomsen et al. 2005a, 2005b) as lactose crystallization triggers the development of late-stage Maillard reaction products. The influence of the physical state on lysine loss is ambiguous in the literature. According to Thomsen et al. (2005a), the formation of furosine, an indicator of the early Maillard reaction, is not triggered by lactose crystallization in whole-milk powder. This is in accordance with findings by Morgan et al. (2005) and Pereyra Gonzales et al. (2010) concerning lysine loss in skim-milk powder. In contrast, Huss (1970) concluded that lysine loss in skim-milk powder was accelerated while lactose was crystallizing and afterwards, in the crystalline state, the rate of lysine loss was lower again. Similarly, Vuataz (1988) determined a small deceleration of the lysine-loss rate in crystalline skim-milk powders compared to amorphous skim-milk powder. To sum up, the glass-transition temperature is a useful reference to estimate the stability of dairy powders with regard to lysine loss. However, the contradictory results concerning the crystalline state highlight that the glass-transition concept alone is not sufficient to predict the stability regarding lysine loss.

This deficiency of the glass-transition concept is not limited to lysine loss. The glass-transition concept often fails to predict the stability of sensitive products. For instance, Aschenbrenner et al. (2012) concluded that there was no direct link between glass transition and inactivation of microorganisms. It is often difficult to clearly correlate glass transition with microbial activity, enzymatic or non-enzymatic reactions, e.g. the oxidation of ascorbic acid (Lin et al. 2006). This weak point can be overcome by including molecular mobility in the stability concept (Champion et al. 2000, Lin et al. 2006).

2.2.2 Molecular mobility

The mobility of water and solids, called molecular mobility in the following, plays an important role concerning the chemical and biological stabilities of food, pharmaceutical and biological products (Acevedo et al. 2008, Biliaderis et al. 2002, Champion et al. 2000, Lin et al. 2006, Yoshioka and Aso 2007). Low-resolution proton nuclear-magnetic resonance (^1H NMR) allows determining the molecular mobility of heterogeneous systems, i.e., the dynamics of the systems, in a non-invasive way with short analysis times (Champion et al. 2000, Lin et al. 2006, Mariette 2009). Water protons have a spin value of $\frac{1}{2}$ and, consequently, possess a magnetic moment μ , i.e., they orientate parallel or antiparallel to an external homogenous

magnetic field B_0 (Fig. 2.4) (Hinrichs 2004, Schmidt 2004). The parallel orientation has a slightly lower energy level than the antiparallel orientation. Therefore, more nuclei arrange parallel to the external magnetic field B_0 , which results in a magnetization vector. If a second oscillating magnetic field B_1 is applied, which is usually generated by a radio frequency (rf) coil around the sample, the equilibrium is disturbed. The magnetic moments change their position relative to the z-axis to get in phase with one another and the magnetization vector precesses about B_1 . The duration and amplitude of B_1 is normally chosen in such a way that the sample magnetization is focused in the x-y-plane, i.e., a rotation angle of 90° . When the 90° -impulse, i.e., the magnetic field B_1 , is turned off, the nuclear spins return to their equilibrium position. This relaxation phenomenon creates a voltage which can be measured with the rf-coil. The relaxation phenomenon can be divided into the transversal or spin-spin relaxation component, called free induction decay (FID), and the longitudinal or spin-lattice relaxation component. The longitudinal relaxation time T_1 characterizes the temporal development of the magnetization in z-direction and describes how fast the spins transfer the absorbed energy as heat to their environment. Thus, it is a measure for the interactions between the spins and their environment. The transversal relaxation time T_2 characterizes the temporal development of the magnetization in the x-y-plane and describes the mobility of nuclear spins. Hence, it can be used to measure the molecular mobility in heterogeneous systems in a fast way without laborious sample preparation. To reduce the impact of field inhomogeneities, diffusion and chemical exchange processes on the transversal relaxation time T_2 , 180° -impulses are transmitted at certain time intervals after the 90° -impulse. This procedure is called Carr-Purcell-Meiboom-Gill (CPMG) sequence. Thus, fanning of the signal can be reduced and erroneous interpretation of the signal avoided. This technique is recognized as a powerful non-destructive analysis tool to study molecular mobility in biological systems (Mariette 2009, Mateus et al. 2007, Schmidt 2004).

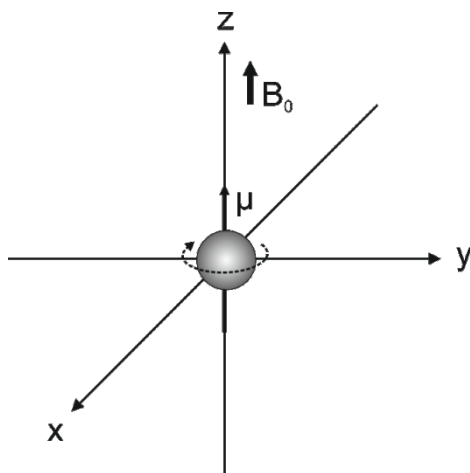


Fig. 2.4 Nucleus with the magnetic moment μ in a static external magnetic field B_0

Data available in the literature on chemical or microbiological stability as related to molecular mobility is rather scarce. Acevedo et al. (2008) related non-enzymatic browning kinetics in potato starch to glass transition and molecular mobility. They determined higher non-enzymatic browning rates in the rubbery state compared to the glassy state concomitant with an increasing molecular mobility. The decrease in the non-enzymatic browning rate at higher

water contents was attributed to the appearance of very mobile water. Foerst et al. (2010) demonstrated that the transition from liquid-like to solid-like behavior during drying as evaluated by means of molecular-mobility measurements coincided with the critical water content for a protective effect of sorbitol on the survival of lactic acid bacteria. Hinrichs et al. (2004) linked molecular mobility to the water-binding capacity of whey-protein concentrates. This knowledge can serve to minimize the extent of syneresis in dairy products. Yoshioka and Aso (2007) concluded that global mobility and/or local mobility can be decisive for the chemical stability of amorphous pharmaceuticals, depending on the degradation reaction. The global mobility can be measured by differential scanning calorimetry and the local mobility by nuclear magnetic resonance. To sum up, the use of molecular mobility measured by low-resolution nuclear magnetic resonance to describe the chemical or biological stability is not widespread but seems promising to fill the gap of the established stability concepts. Probably, combining the water-activity concept with the glass-transition concept and the molecular-mobility concept will lead to an improved understanding of chemical and biological stabilities.

2.3 Spray drying³

Spray drying was identified to be the critical production step concerning lysine loss in infant formula (Ferrer et al. 2000, Finot 1983). This can be explained by the fact that the rate of lysine loss is higher in the dry state than in the liquid state with a maximum at low or intermediate water activities depending on the experimental conditions (Malec et al. 2002, Morgan et al. 1999). Thus, the extent of lysine loss during spray drying is influenced by the drying kinetics and particle flow inside the spray dryer. These two factors determine the particle history and, consequently, the extent of lysine loss.

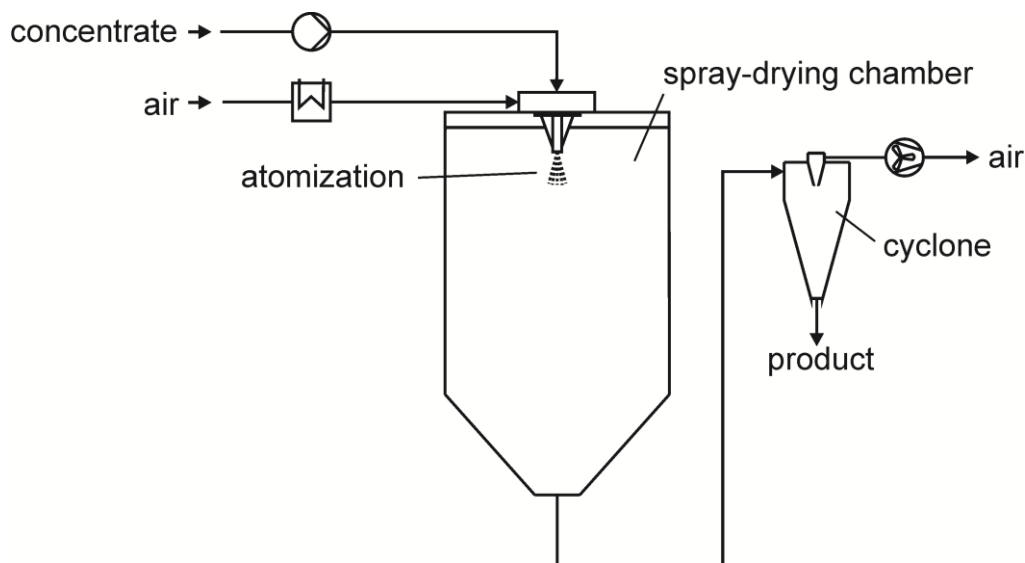


Fig. 2.5 Scheme of the spray-drying process

Spray drying is a rather gentle drying process, i.e., a liquid is transformed into a powder with little thermal alterations (Filková and Mujumdar 1995, Masters 1991, Písecký 1997). A concentrate is atomized into fine droplets in a hot air flow leading to the drying of the droplets and to the formation of powder particles (Fig. 2.5). Three different principle process stages can be distinguished: atomization of the concentrate, drying of the droplets in contact with the hot air and separation of the powder particles from the drying air. Powder particles are normally separated from the drying air with the aid of cyclones and filters. Special attention must be paid to the atomization of the concentrate because the droplet size is directly linked to the size of the powder particles as well as to the evaporation rate and, consequently, to the efficiency of the drying process. The droplet-size distribution, which depends on the characteristics of the concentrate, on the type of atomizer and on the energy input, is crucial for the drying rate, particle residence-time and thus, final product quality. Rotating wheels, pressure nozzles or two-fluid nozzles are types of atomizers typically used in spray-drying applications. The hot air flow furnishes on the one hand the energy that is necessary for evaporation and transports on the other hand the evaporated water. The drying air cools down and takes up

³ Partly published in: Schmitz-Schug I, Foerst P, Kulozik U (2013) Impact of the spray drying conditions and residence time distribution on lysine loss in spray dried infant formula. *Dairy Science & Technology* 93(4):443-462

the humidity while the product is being dried. The typical evolution of the water content and the temperature of the particles is illustrated in Fig. 2.6. The product temperature stays close to the wet bulb temperature as long as the product surface is humid and then rises reaching the air temperature if the residence time is sufficiently long (Fu and Chen 2011, Gianfrancesco 2009, Mezhericher et al. 2010b). The first part of the drying process, which is called first drying stage, ends when the critical water content is attained. It is characterized by a constant drying rate and a product temperature close to the wet bulb temperature. The critical water content specifies the moment when moisture cannot any longer be transported as fast from the droplet center to the surface as it evaporates at the droplet surface. From this moment on, the drying rate declines and the droplet temperature rises until it attains the air temperature. This period is called second drying stage and finishes when the equilibrium water content is reached.

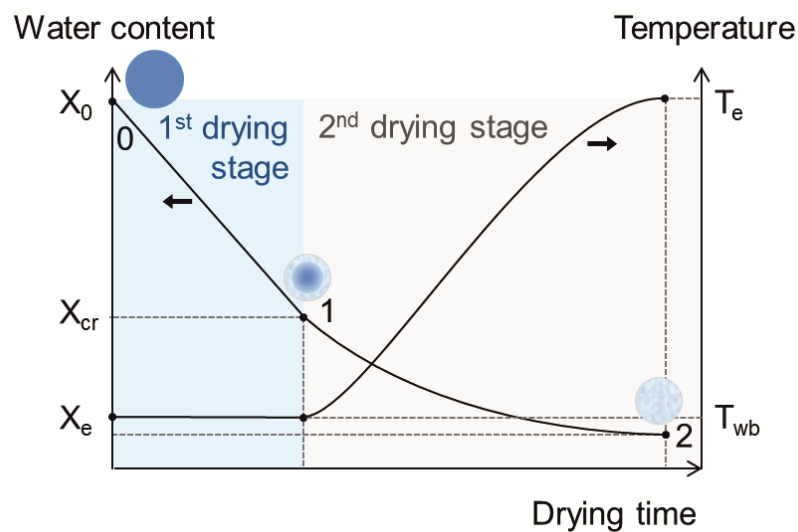


Fig. 2.6 Convective drying kinetics: typical evolution of the water content and the product temperature (X_0 : initial water content; X_{cr} : critical water content; X_e : equilibrium (final) water content; T_{wb} : wet bulb temperature; T_e : equilibrium (final) temperature)

Several authors have studied drying kinetics and how it can be applied to spray drying. Usually, drying-kinetics models are integrated in computational fluid dynamics (CFD) simulations in order to characterize the spray-drying behavior of various products (Woo et al. 2008b, Patel and Chen 2005). Accurate experimental data to fit the model parameters is necessary to predict the drying kinetics e.g. in a CFD simulation. Drying kinetics and computational fluid dynamics of spray drying will be discussed in detail in chapters 2.4 and 2.5, respectively.

Apart from the drying kinetics, the residence time is an important factor with regard to product quality. On the one hand, the particle residence-time has to be long enough to ensure dehydration to the desired residual water content. On the other hand, long residence times lead to longer exposure times to high temperatures when the particles are already in dry-state. This can result not only in the loss of lysine but also in the denaturation of proteins, for exam-

ple. Gianfrancesco (2009) measured median particle residence-times of 2-3 min in a pilot-scale spray dryer equipped with a rotary atomizer. Mazza et al. (2003) determined mean particle residence-times of 69-77 s for a co-current pilot-scale spray dryer with a rotary atomizer. Kieviet and Kerkhof (1995) obtained a median residence time $\tau_{50} = 58.5$ s for a co-current pilot-scale spray dryer with a pressure nozzle. Jeantet et al. (2008) determined mean particle residence-times of 9-12 min for a pilot-scale spray dryer with a pressure nozzle as atomization device, a fines-return system and an internal fluid bed. These studies have in common that the mean particle residence-time was always significantly longer than the mean residence time of the air. In contrast, Zbicinski et al. (2002) showed for a long-form co-current spray dryer that smaller particles had longer residence times than bigger particles. In this case, the residence time of the particles was shorter than the average residence time of the drying gas. This was explained by the high initial velocity of the particles which were atomized using a pneumatic nozzle. In summary, these results show on the one hand that there is a wide range of residence times according to the dryer configuration and on the other hand that particle residence-times can be quite long during spray drying.

Thus, important process parameters are the temperature and mass-flow rate of the drying air, the mass-flow rate and concentration of the product to be dried as well as the atomization parameters which are responsible for the droplet size distribution. These parameters determine the drying kinetics and particle residence-time which in turn are decisive for the final product quality. Despite spray drying being generally known as a rather gentle drying process, product deterioration can occur, especially if heat sensitive products are dried, as will be shown in the following.

Despite the principle awareness that sensitive compounds can be damaged during spray drying, there are only a few studies that investigate the spray-drying process with the aim of reducing the damage of sensitive food, pharmaceutical or biological products. For this class of products, the drying process has not only to fulfill the basic requirement to obtain a dry powder but also to preserve sensitive compounds. Menshutina et al. (2010) studied spray drying of probiotics and showed that the drying process can be optimized with regard to microorganism inactivation by taking into account the drying kinetics together with the inactivation kinetics. Similarly, Mestry et al. (2011) employed the response-surface method to improve the nutritional quality of fermented carrot and watermelon juice. In addition, a good knowledge and control of the spray-drying process makes it possible to combine two processing steps in one. Reinhold et al. (2001) showed that a targeted conversion of ingredients during spray drying is possible if the reaction is faster than drying. To sum up, spray drying can be employed to dry sensitive food, pharmaceutical or biological products given that the spray-drying conditions are carefully chosen. However, these have had to be found by trial and error so far and no published data is available on the impact of the thermal and dehydration stresses on lysine loss during spray drying (cf. chapter 2.1).

2.4 Drying kinetics

Detailed knowledge of the drying kinetics is essential for the design of drying processes with regard to dryer configuration, drying parameters and product quality (Chen and Patel 2008, Putranto et al. 2011). Drying-kinetics models can for example be used to describe the drying of particles in a computational fluid-dynamics simulation of spray drying. To adapt existing drying-kinetics models to specific products, the drying kinetics must be determined experimentally.

2.4.1 Experimental methods to determine the drying kinetics

Several methods exist to determine the drying kinetics experimentally which can be divided into three classes: single-droplet drying, multiple-droplets drying and thin-film drying. All these methods are based on convective drying conditions. Each method has its advantages and disadvantages. These have to be considered carefully because they can impair the transferability to the spray-drying process. Special attention has to be paid to variations in sample geometry, the characteristics of the flow field and crust formation at the sample surface. None of the methods described in the following reproduces exactly the drying conditions of the spray-drying process but they are able to approximate them sufficiently well. However, the drying-kinetics data obtained has to be analyzed carefully and the simplifications have to be taken into account when the results are transferred to the spray-drying process.

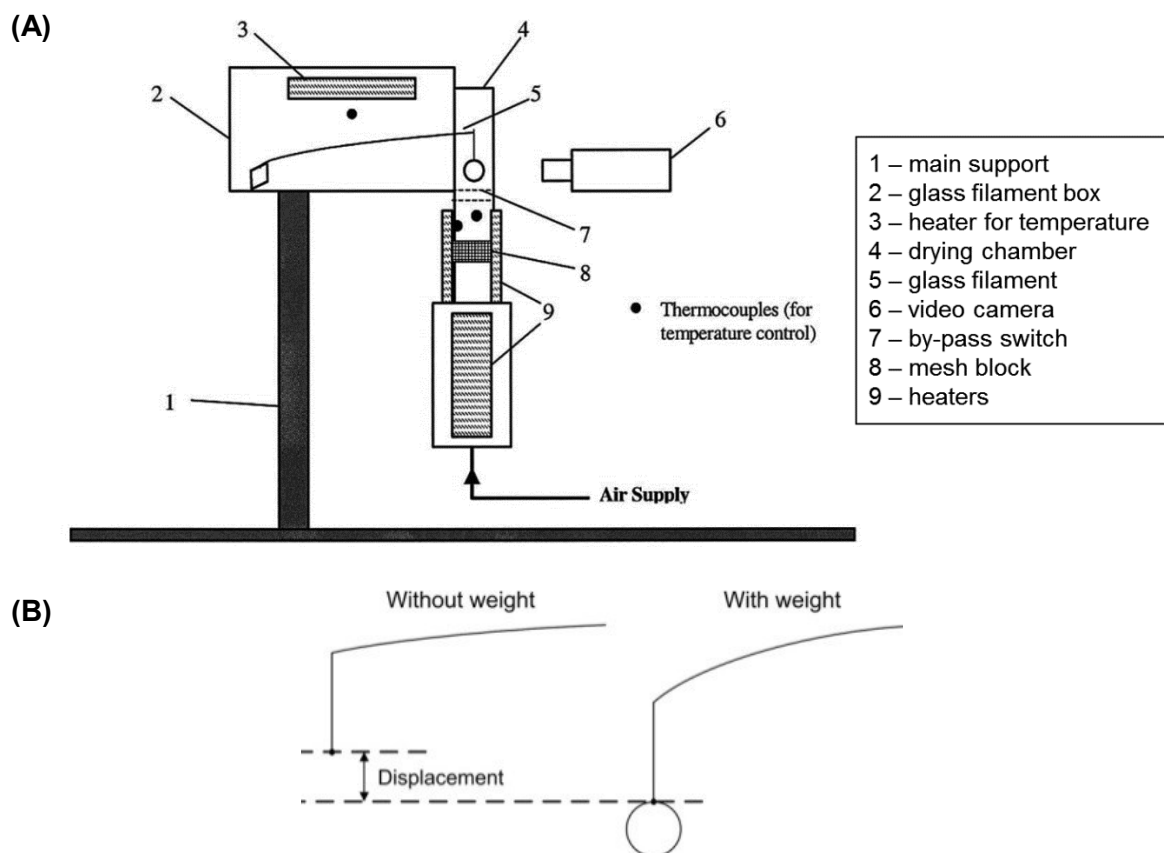


Fig. 2.7 (A) Experimental set-up of the glass filament method (Lin and Chen 2002), (B) detail of the glass filament (Fu et al. 2011)

Single-droplet drying

Single-droplet drying can be realized, e.g. by the glass-filament method or by acoustic levitation. In the glass-filament method (Fig. 2.7; Charlesworth and Marshall 1960, Cheong et al. 1986, Fu et al. 2011, Lin and Chen 2002, Yamamoto and Sano 1994), a droplet with a diameter of $\geq 400 \mu\text{m}$ is positioned at the end of a glass filament. The weight of the droplet is deduced from the displacement of the glass filament which is recorded using a camera. The contact area between the glass filament and the droplet is minimized by using thin glass filaments with a diameter of $< 100 \mu\text{m}$, which leads to a relatively spherical droplet. For the drying experiments, the glass filament with the droplet is positioned in an air flow with controlled temperature, humidity and flow rate. The air flow normally occurs vertically from the bottom to the top so that the glass filament does not influence the flow profile around the droplet. This configuration, which is characterized by convection flows to the top with the air flow, represents a good approximation of the free fall of droplets. The droplet is recorded by a video camera during the experiment to monitor continuously the diameter, morphology and position of the droplet. This allows determining the weight and, thus, the water content if the flow forces are considered. The glass filament can be equipped with a thermocouple to monitor the product temperature. However, the droplet size is above the order of magnitude typical of spray drying, the droplet cannot rotate and the glass filament can influence the drying progress.

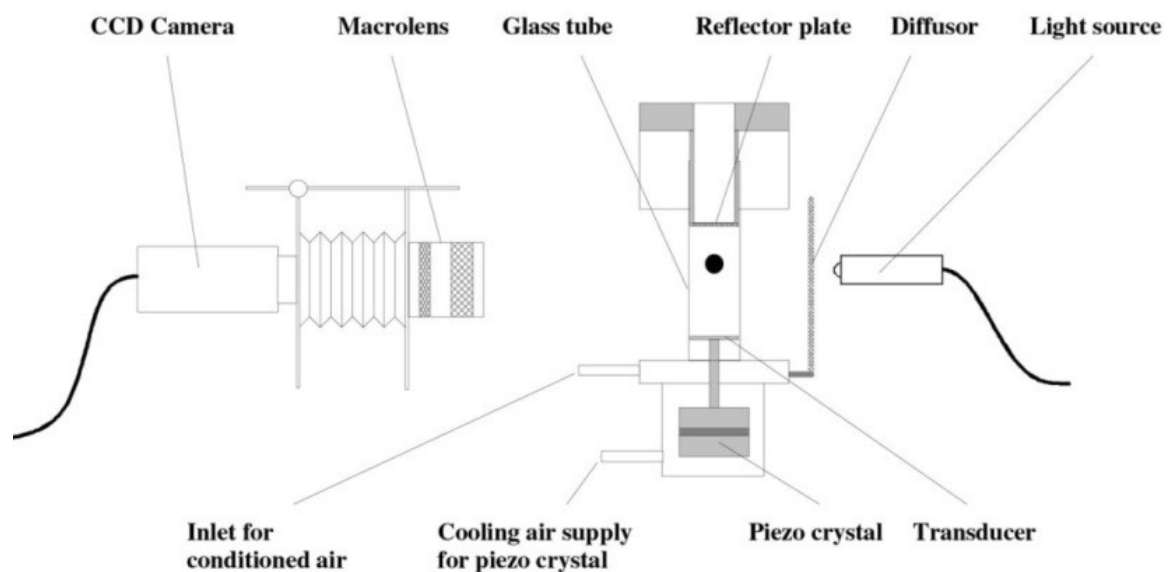


Fig. 2.8 *Experimental set-up of the acoustic levitation method (Yarin et al. 2002)*

The acoustic levitation method uses a standing ultrasonic wave to keep a droplet suspended (Fig. 2.8; Groenewold et al. 2002, Kastner et al. 2001, Räderer 2001, Sloth et al. 2006, Yarin et al. 1999, Yarin et al. 2002). The standing ultrasonic wave is produced between a piezoelectric exciter and a concave reflector which allows positioning contactlessly a droplet in the nodes of the wave. The droplet is continuously filmed with a camera to determine the drying kinetics. The weight and hence the drying kinetics can be derived from the position of the

droplet. Due to the weight of the droplet, the droplet is not positioned exactly in the node of the wave but below it. The displacement is directly linked to the weight of the droplet. Droplet sizes are normally <1.5 mm. A characteristic flow field forms around the droplet (Fig. 2.9). The inner acoustic streaming is responsible for the removal of humidity from the surroundings of the droplet and, thus, for the drying of the droplet. However, humidity is deposited in the outer acoustic streaming which forms circulating vortices. Consequently, drying is limited. As a countermeasure, an additional controlled air stream can be passed through the ultrasonic field in order to remove the humidity of the outer acoustic streaming. However, convective drying is not possible since the air velocity of the supplementary air stream is limited because otherwise it would entrain the droplet. Furthermore, the droplet is not spherical but deformed and resembles a donut.

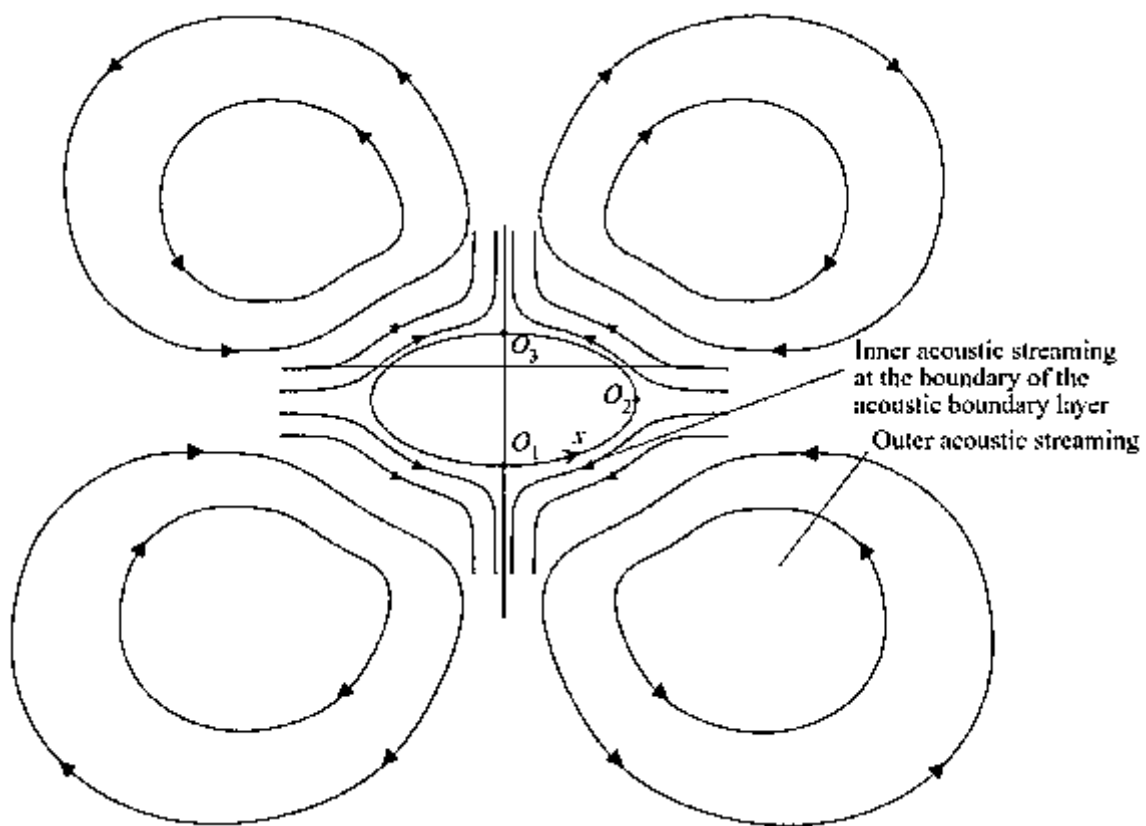


Fig. 2.9 Acoustic flow around a droplet (Yarin et al. 1999)

Multiple-droplets drying

Multiple-droplets drying has the advantage that sufficient material is available for subsequent analyses. Possible applications are the drying of sessile droplets and the drying of droplets in a falling-droplet dryer. The falling droplet comes relatively close to the conditions in a spray dryer (El-Sayed et al. 1990, Sloth et al. 2009, Wallack et al. 1990). Droplets are generated using a nozzle or specially designed devices that create a single stream of equally sized droplets. Typical droplet sizes are in the range of 200-1500 μm . The droplets are dried in the falling tower in a stream of air with controlled properties. At different positions of the tower

samples can be taken to measure the water content and, consequently, to determine the drying kinetics. Samples are collected in sampling devices filled e.g. with liquid nitrogen or paraffin oil to stop further evaporation. To ensure a uniform residence time of the droplets, plug flow must be guaranteed inside the falling tower. However, it is hardly possible to measure the droplet temperature.

Drying of sessile droplets is a method that can be implemented more easily than the methods described above. One or more droplets are deposited on a flat surface and dried in a drying channel (Perdana et al. 2011, Schutyser et al. 2012). An air stream with controlled temperature, humidity and flow characteristics is passed through the drying channel. The mass change can be recorded by linking a balance to the droplet holder. The sample temperature can be monitored using thermocouples. Special attention must be paid to the sample holder. On the one hand, it should be hydrophobic for hydrophilic samples to enable the formation of droplets which are as spherical as possible. On the other hand, it should avoid entrainment of the droplets by the air stream. Moreover, a possible heat transfer from the sample holder to the sample must be considered.

Thin-film drying

Thin-film drying is a method which is quite similar to the drying of sessile droplets. Instead of droplets, a thin film of the sample is put on a sample holder (Li et al. 2010a, Men-shutina et al. 2010, Räderer 2001, Zbiciński et al. 2005). The sample holder is usually equipped with a cavity for this purpose. The material of the sample holder must be chosen in such a manner that wide spreading of the film is ensured to minimize the thickness of the film. Recording of the sample weight for drying kinetics and of the sample temperature can be realized in the same way as it has been described for the drying of sessile droplets. Advantages are that the film keeps its geometry during drying and that, due to the higher sample volume, the temperature and weight of the sample can be measured more easily and probably more accurately than with other methods. However, data should be carefully transferred to spray drying due to the geometry which deviates from a sphere. This results in modified conditions for the heat transfer and flow field around the sample.

In conclusion, each method has advantages and disadvantages. Consequently, the choice of the method depends on the aim of a study and on the available technical equipment.

2.4.2 Modeling approaches to describe drying kinetics

In general, there are two approaches to modeling drying kinetics (Chen 2008, Wang and Langrish 2009, Woo et al. 2008a): the lumped-parameter approach and the distributed-parameter approach. The distributed-parameter approach resolves the temperature and concentration profiles inside the product to be dried, i.e., the mass and heat transfer. In contrast, the lumped-parameter approach neglects the temperature and the concentration profiles inside the product to be dried. This assumption is justified if the product to be dried is sufficiently small, i.e., if the Biot number is less than 0.1 (Incropera 2007). This usually applies to spray drying, droplet drying or thin-film drying (Adhikari et al. 2007, Chen and Lin 2005, Patel and Chen 2008a). Examples of lumped-parameter approaches are the characteristic drying-rate curve model (CDRC) and the reaction-engineering approach (REA). The energy balance (eq.

2.1), which assumes a uniform product temperature, forms the basis of the heat transfer in these models (Woo et al. 2008b).

$$m \cdot c_p \cdot \frac{dT_p}{dt} = h \cdot A_p \cdot (T_b - T_p) + r_v \cdot \frac{dm_w}{dt} \quad 2.1$$

The characteristic drying-rate curve model (CDRC) was extensively used in the past to predict the drying behavior of droplets during spray drying (Langrish and Kockel 2001, Woo et al. 2008b). This approach assumes that the drying curve dX/dt (eq. 2.2) is governed by a characteristic product-specific function ξ of the dimensionless water content φ (eq. 2.3). It relates the specific drying rate of the second drying stage to the unhindered drying rate of the first drying stage (Woo et al. 2008b). The characteristic drying rate ξ is product-specific but independent of the drying conditions.

$$\frac{dX}{dt} = -\xi \cdot \frac{A_p \cdot h}{m_s \cdot r_v} \cdot (T_b - T_{wb}) \quad 2.2$$

$$\xi = \frac{N}{N_{\max}} = \begin{cases} 1 & \text{for } X > X_{cr} \\ f(\varphi) = \left(\frac{X - X_e}{X_{cr} - X_e} \right)^a & \text{for } X \leq X_{cr} \end{cases} \quad 2.3$$

The advantages of the CDRC model are its simplicity, flexibility and little computational effort. Furthermore, you do not need the product and surface temperatures, which are often difficult to measure accurately. However, the assumption of wet-bulb temperature during the whole drying process might create errors because the product temperature rises during the second drying stage. This might influence the drying rate. Moreover, the critical water content, which often depends on the drying conditions, must be determined experimentally (Chen 2008). A lot of experimental data is necessary to determine the parameters of the CDRC model in a reliable manner.

The reaction-engineering approach (REA) model applies the chemical reactor-engineering principle to drying kinetics and was introduced by Chen and Xie (1997). It is assumed that evaporation is an activated process, i.e., an energy barrier has to be overcome, that can be described as zero-order kinetics other than condensation or adsorption, which is described as first-order kinetics without activation energy (Putranto et al. 2011). The drying rate is described as follows:

$$\frac{dm_p}{dt} = m_s \frac{dX}{dt} = -h_m \cdot A_p \cdot (\rho_{v,s}(T_s) - \rho_{v,b}) \quad 2.4$$

The vapor concentration on the sample surface $\rho_{v,s}$, i.e., at the interface between the sample and the drying gas, can hardly be obtained from experiments. This is due to the fast evolution of the water content at the sample surface. However, it is known that the vapor concentration at the surface is equal to the saturated vapor concentration as long as the surface is saturated with water, i.e., during the constant drying-rate period. The vapor concentration decreases

during the falling drying-rate period and can be linked to the saturated vapor concentration via the relative air humidity at the surface (Chen and Xie 1997):

$$\rho_{v,s} = RH_s \cdot \rho_{v,sat}(T) \quad 2.5$$

The relative air humidity on the surface is expressed as a function of the apparent activation energy ΔE_v and the product temperature T_p (Chen and Xie 1997):

$$RH_s = \exp\left(\frac{-\Delta E_v}{R_G \cdot T_p}\right) \quad 2.6$$

The apparent activation energy describes the increasing difficulty to remove water as the water content decreases. The apparent activation energy must be determined from experimental drying kinetics data for each product. Relating the apparent activation energy to the equilibrium apparent activation energy leads to a function that is product specific and independent of the drying conditions (Chen and Xie 1997, Woo et al. 2008b):

$$\frac{\Delta E_v}{\Delta E_{v,e}} = f(X - X_e) = a \cdot \exp(-b \cdot (X - X_e)^c) \quad 2.7$$

The equilibrium apparent activation energy can be calculated using the properties of the drying gas:

$$\Delta E_{v,e} = -R_G \cdot T_b \cdot \ln(RH_b) = -R_G \cdot T_b \cdot \ln\left(\frac{\rho_{v,b}}{\rho_{v,sat}}\right) \quad 2.8$$

The REA model is generally seen as an accurate and simple drying-kinetics model that could successfully be applied to various materials, e.g. cream and whey concentrates, skim milk, fruit tissue, silica-gel particles and grains (Chen and Xie 1997, Lin and Chen 2007, Putranto et al. 2011). It accurately predicts the water content and temperature evolution even at fluctuating drying-gas conditions (Chen and Lin 2005, Putranto et al. 2011). However, it often overestimates the drying rate at the start of the drying process. Moreover, the REA model requires the exact measurement of the product temperature as well as a good determination of the mass-transfer coefficient (Chen and Lin 2005, Chen 2008).

2.5 Computational fluid dynamics

Spray drying belongs to the rather complex multiphase convective-drying processes which involve the atomization of droplets, particle transport, the evaporation of droplets as well as the interaction between particles and/or droplets and/or dryer walls (Blei and Sommerfeld 2011). For this reason, designing, optimizing or scaling-up spray-drying processes are complicated tasks which are often accomplished by time-consuming trial-and-error experiments. Computational fluid dynamics (CFD) can be an effective way to facilitate this process. Therefore a lot of research is conducted on simulating spray-drying. Using CFD, Gianfrancesco et al. (2010) studied the stickiness of maltodextrin solutions during spray drying. They aimed at reducing wall deposition of particles and achieving a controlled agglomeration of particles. Rogers et al. (2012) investigated the formation of insoluble material during the spray drying of skim milk in a CFD-based study. In general, fields like a better understanding of the spray-drying process, particle history during spray drying and wall deposition have been widely studied using CFD. (Anandharamakrishnan et al. 2010, Birchal et al. 2006, Huang et al. 2003, Huang et al. 2005, Langrish and Zbicinski 1994, Mezhericher et al. 2009, 2010a, Ullum et al. 2010, Zbiciński and Li 2006). Although pilot-scale dryers were used in most studies, industrial-scale simulations were conducted, too (Huang and Mujumdar 2007, Jin and Chen 2009, Lo 2005, Straatsma et al. 1999). It is generally accepted that special attention has to be paid to droplet-drying kinetics (Mezhericher et al. 2010a, Patel and Chen 2008b). Woo et al. (2008b) used two drying-kinetics models, the characteristic drying-rate curve and the reaction-engineering approach, in combination with a CFD simulation of the spray drying of a sucrose-maltodextrin mixture. They found no significant differences in the particle trajectories and outlet conditions although the predicted drying curves were slightly different. However, validating the simulation results is still a challenging task because detailed measurements of the flow field inside a spray dryer are hardly possible (Huang and Mujumdar 2007). This, on the other hand, makes spray drying interesting for simulation studies.

Computational fluid dynamics (CFD) is the computer-based simulation of applications which include fluid flow, heat transfer and associated phenomena like chemical reactions. These need to be described using partial differential equations that cannot be solved analytically in most cases (Ferziger and Perić 2008, Versteeg and Malalasekera 2007). The principal components of a numerical solution procedure in CFD are shown in Fig. 2.10. In a first step, the problem has to be defined, a geometrical model of the fluid domain of interest has to be drawn and a mathematical model of the problem has to be set up. The mathematical model is based on physical and chemical models and leads to a system of differential equations. A discretization method has to be chosen to approximate the differential equations by a system of algebraic equations for discrete points in space and time. There are various discretization methods, for instance the finite difference, finite volume (used in most commercial CFD codes) or the finite element method. To solve algebraic equations in the computational domain, a coordinate system is defined, the geometry is divided into a numerical grid and the equations will be solved for nodes inside the grid cells. The solution will be more accurate the finer the grid is. However, fine grids lead to high computational efforts. Therefore, grid optimization is important because grid independence is one of the quality criteria of a CFD model. Next, a finite approximation method has to be chosen to interpolate between the nodes, for surface and volume integrals, gradients, etc. Then, the solution procedure has to be select-

ed and convergence criteria defined. Convergence, consistency, stability, conservativeness, boundedness and accuracy are among the most important properties of numerical solution procedures. As numerical solutions are approximate solutions, special attention must be paid to systematic errors, namely model errors, discretizing errors and iteration errors. Validation of a model, which is best done by experiments, have to take into account the quality criteria mentioned.

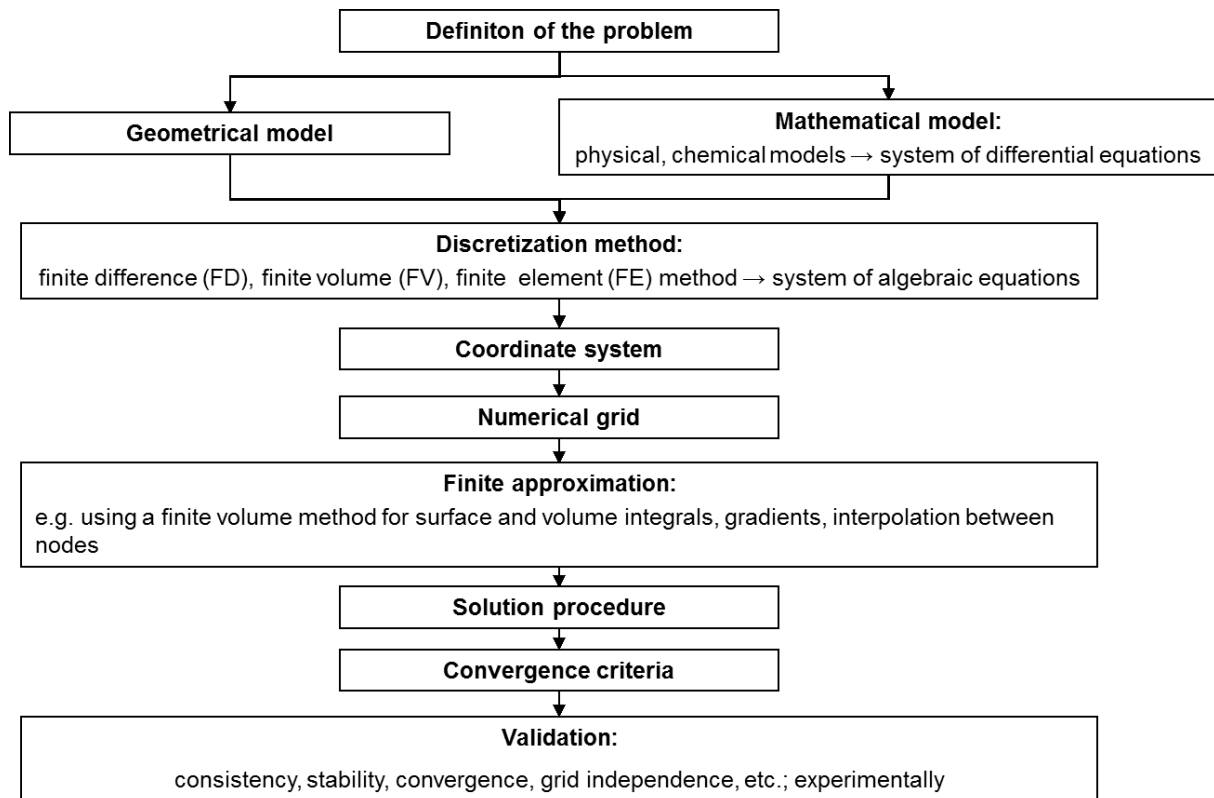


Fig. 2.10 Components of a numerical solution procedure in computational fluid dynamics

In the case of spray drying, 3D simulations, transient calculations, hindered drying-kinetics models and particle-wall interaction models are necessary to obtain good results with regard to flow stability and the wall deposition of particles because of the asymmetric flow field and significant flow instabilities inside spray dryers (Fletcher et al. 2006, Fletcher and Langrish 2009, Langrish 2009). The formation of flow instabilities, which can be considered as one of the key elements of a spray-dryer simulation, is especially pronounced in short-form spray dryers (Fletcher et al. 2006). Generally, the flow inside a spray dryer can be considered as incompressible and Newtonian and the Euler-Lagrange approach is applied (Anandharamakrishnan et al. 2010, Blei and Sommerfeld 2011, Fletcher and Langrish 2009, Gianfrancesco et al. 2010, Langrish 2009, Jin and Chen 2009, Mezhericher et al. 2009, 2010a). The Reynolds-averaged Navier-Stokes (RANS) equations are solved for the flow field, i.e., the flow field, which is the continuous phase, is treated by the Eulerian approach. The Lagrangian approach is applied to the discrete phases, i.e., to the droplets/particles (Birchal et al. 2006, Fletcher et al. 2006, Blei and Sommerfeld 2011, Langrish 2009). The product mass-flow rate is divided into a certain number of parcels (Birchal et al. 2006, Blei and Sommerfeld 2011, Langrish 2009). Each parcel comprises many particles with the same characteristics (diame-

ter, water content, temperature, etc.) so that the parcels sum up to the product flow-rate and particle-size distribution created by the atomizer. Due to the high interchange rate between the two phases, which occurs in both directions, the conservation equations of mass, momentum and energy are coupled iteratively using two-way coupling procedures (Anandharamakrishnan et al. 2010, Blei and Sommerfeld 2011, Fletcher et al. 2006, Huang et al. 2003, Huang et al. 2005, Langrish 2009). The initial droplet-size distribution is often defined by a Rosin-Rammler distribution (Huang et al. 2003, Huang et al. 2005, Jin and Chen 2009). For the correct tracking of the particles, the drag force, gravity and buoyancy forces have to be taken into account (Blei and Sommerfeld 2011). The flow field around the particles is usually not resolved because the particles are considered as point particles.

A common solution procedure for steady-state computation is to converge the flow field first and to start tracking the particles once the flow field has converged. These steps are coupled and repeated until a quasi-constant converged solution is obtained (Fletcher et al. 2006, Mezhericher et al. 2010a). The advantage of this approach is that only the droplet source-terms have to be stored, which reduces the memory requirements compared to unsteady calculations. In unsteady calculations, the position and state of the droplets have to be stored after each time step, new droplets have to be injected at each time step and the computational time has to be long enough to represent the particle residence-time leading to long simulation times. Moreover, the grid has to be sufficiently fine to reproduce the transient behavior of the flow field because otherwise a steady solution is obtained.

There are several models for the kinetics of hindered drying, which are described in detail in chapter 2.4 and can be integrated in the CFD simulation via user-defined functions (Mezhericher et al. 2010a). The particle-wall interactions can be defined in different ways (Fletcher et al. 2006, Mezhericher et al. 2010a). One possibility is to consider all particles that hit the wall as “escaped”, i.e., these particles are not tracked any longer. It is also possible to use reconstitution coefficients, which can either be constant or dependent on the local state. Jin and Chen (2009) obtained better results with the “reflecting wall” (reconstitution coefficient = 1) than with the “escaping” boundary condition when simulating the industrial-scale spray drying of milk. Likewise, Mezhericher et al. (2010a) pointed out the importance of the particle-wall boundary condition for the particle residence-time and, consequently, for the final product quality. They compared the “escape” with the “reflecting wall” (tangential reconstitution coefficient of 0.5 and perpendicular one of 0.9) boundary condition.

Turbulence modeling, i.e., the selection of a turbulence model, is still a difficult issue. Despite the drawbacks of the k - ϵ model, it is considered to give acceptable results with manageable computational effort, thus suitable for spray-drying modeling (Langrish 2009, Mezhericher et al. 2009, 2010a). In unsteady simulations, it is possible to represent the precession of a jet in an expansion flow using the k - ϵ model if the mesh is sufficiently fine and the time step short enough (Fletcher et al. 2006). As the instantaneous fluid velocity, which is averaged by solving the RANS equations, is decisive for the particle tracks, the calculation of the particle tracks is based on stochastic approaches (Anandharamakrishnan et al. 2010, Blei and Sommerfeld 2011, Birchal et al. 2006, Huang et al. 2005).

3 Objective

Although it is known that processing, especially spray drying, plays a major role regarding lysine loss in dairy powders, research has until now mainly been focused on lysine loss occurring during the storage of powdered dairy products. The importance of heating and drying rates is unknown at conditions relevant to spray drying. Moreover, there is a lack of knowledge about the importance of the physical state and of molecular mobility on lysine loss. Choosing the correct processing parameters is crucial for producing high-quality products. However, trial and error, a time-consuming procedure, and statistical methods are the only way to determine adequate drying conditions at the moment. The knowledge of the reaction kinetics in the relevant parameter range is a prerequisite for the correct choice of the processing parameters. Coupling the reaction kinetics with computational fluid dynamics will result in a powerful tool to optimize the nutritive quality of spray-dried dairy powders in a targeted and efficient way.

In this study, a model dairy-formulation will be used. On the one hand, this model system will be prone to the loss of available lysine due to its high content of lysine-rich proteins and lactose. On the other hand, it easily tends to phase transitions, i.e., glass transition and crystallization, which is accompanied by a change in molecular mobility. Thus, a wide range of factors affecting lysine loss are taken into account so that the results can be transferred to a variety of products.

As pointed out in chapter 2, it is not possible to directly determine the drying kinetics and reaction kinetics during spray drying. Therefore, this study will be based on three pillars, starting with more fundamental investigations besides spray drying. The results of these fundamental investigations will then be coupled with spray drying. This procedure represents an innovative way of combining different scientific disciplines in order to gain a deeper understanding of the spray-drying process.

The first part of the project focuses on the reaction kinetics of lysine loss. To start with, the reaction kinetics of lysine loss will be studied at conditions relevant to spray drying, i.e., in the dry-state at temperatures that the product might experience during spray drying. The impact of temperature and concentration will be assessed. Special attention will be paid to physical state and to molecular mobility. Molecular mobility as measured by low resolution $^1\text{H-NMR}$ will be related to water activity and physical state as well as chemical stability expressed by the loss of available lysine. In a second step, the impact of the dehydration conditions on the loss of available lysine will be elaborated. Vacuum dehydration at moderate temperatures will be used as a tool to work out the impact of dehydration on lysine loss and to largely exclude the impact of thermal treatment. The longer drying times during vacuum dehydration compared to spray drying will allow recording lysine losses as a function of the dehydration progress as well as of the dehydration rate. To evaluate the impact of the composition of the dairy formulation on lysine loss, the lactose-protein ratio as well as the whey protein-casein ratio will be varied and the resulting differences in thermally and dehydration-induced lysine losses will be analysed. The experimental data will be used to build a reaction-kinetics model that can be used to minimize lysine loss when processing milk powders. Thus, a deeper understanding of the mechanism of lysine loss in milk systems will be obtained and it will be possible to distinguish between thermally and dehydration-induced lysine losses.

Moreover, the importance of a combined stability concept based on water activity, physical state and molecular mobility will be demonstrated.

In the second part of the project, the spray-drying process of the model dairy-formulation will be studied and the process characteristics will be correlated with the extent of lysine loss. The residence-time distribution of the particles will be measured because of its relevance for the powder quality. Lysine loss during the storage of the spray-dried powders will be included in the investigations. Thus, a comprehensive and differentiated analysis of the spray-drying process will be obtained, which is necessary for a targeted improvement of the nutritive quality of spray-dried dairy powders.

In the third part of this study, the drying kinetics of the model dairy-formulation will be investigated and integrated into a computational fluid-dynamics simulation of the spray-drying process. The reaction-kinetics model will be linked to the simulation. The experimental data will be used to validate the resulting model of lysine loss during spray drying. This model will be capable of predicting lysine losses during spray drying and, consequently, will allow determining the appropriate spray-drying conditions in a targeted way to guarantee high-quality dairy powders.

To sum up, this study aims at gaining a deeper understanding of the mechanism of lysine loss during spray drying. A step-wise procedure is chosen to achieve this objective. The obtained knowledge will then be used to develop a tool for optimizing the spray-drying process with regard to product quality. This will allow producing higher-quality dairy powders. The approach of this study can be transferred easily to other applications in the future.

4 Material and methods⁴

4.1 Composition and preparation of the model dairy-formulation

The composition of the model dairy-formulation was derived from the typical composition of infant formulas based on cow's milk. The standard composition was characterized by a lactose-protein ratio of 5:1 and a whey protein-casein ratio of 60:40. Skim-milk powder (22.2%), whey-protein isolate (8.4%), lactose (68.3%), potassium citrate (1.0%) and monosodium phosphate dihydrate (0.1%) (all provided by Nestec Ltd.) were reconstituted in deionized water to 20% dry matter. Unless otherwise stated, the model dairy-formulation with this standard composition was used throughout this study.

To study the impact of the matrix composition on the loss of available lysine, the lactose-protein ratio and the whey protein-casein ratio was modified (Table 4.1). This was achieved by adjusting the amount of lactose and whey-protein isolate in the model dairy-formulation. Departing from the standard composition, the lactose-protein ratio (L:P) was set to 3:1 and to 7:1 keeping the whey protein-casein ratio (WP:C) constant at the standard ratio of 60:40. Additionally, the whey protein-casein ratio was adjusted to 40:60 and 20:80 keeping the lactose-protein ratio at 5:1. All the compositions were within the limits of European commission directive 2006/141/EC (European Commission 2008). Thus, it was possible to evaluate the sensitivity to lysine loss of the different proteins and the role of the lactose content, as well as the importance of physical state.

Table 4.1 Dry matter composition of the model dairy-formulations

Composition	Standard composition	High lactose content	Low lactose content	Medium casein content	High casein content
Lactose-protein ratio	5:1	7:1	3:1	5:1	5:1
Whey protein-casein ratio	60:40	60:40	60:40	40:60	20:80
Skim-milk powder [%]	22.2	16.8	32.8	32.9	43.4
Whey-protein isolate [%]	8.4	6.4	12.4	4.2	0
Lactose [%]	68.3	75.8	53.7	61.8	55.5
Potassium citrate [%]	1.0	1.0	1.0	1.0	1.0
Monosodium phosphate dihydrate [%]	0.1	0.1	0.1	0.1	0.1

⁴ Partly published in: Schmitz I, Gianfrancesco A, Kulozik U, Foerst P (2011) Kinetics of lysine loss in an infant formula model system at conditions applicable to spray drying. *Drying Technology* 29(16):1876-1883; Schmitz-Schug I, Gianfrancesco A, Foerst P, Kulozik U (2013) Impact of dehydration on lysine loss in a model dairy formulation. *Drying Technology* 31(13-14):1477-1484; Schmitz-Schug I, Foerst P, Kulozik U (2013) Impact of the spray drying conditions and residence time distribution on lysine loss in spray dried infant formula. *Dairy Science & Technology* 93(4):443-462; Schmitz-Schug I, Gianfrancesco A, Kulozik U, Foerst P (2013) Physical state, molecular mobility and chemical stability of powdered dairy formulations. *Food Research International* 53(1):268-277; Schmitz-Schug I, Kulozik U, Foerst P (2014) Reaction kinetics of lysine loss in a model dairy formulation as related to the physical state. *Food and Bioprocess Technology* 7:877-886

4.2 Freeze drying

For the characterization of the model system and the determination of the reaction kinetics of thermally and dehydration-induced lysine loss, the solution was frozen (-40°C) and freeze-dried (0.37 mbar, shelf temperature: 15°C , >48 h, freeze dryer Delta 1-24 LSC, Martin Christ, Osterode, Germany) in order to obtain a homogeneous amorphous powder without applying elevated temperatures. The freeze-dried materials were ground immediately after freeze drying. The freeze-dried powder had a water content of $4.5 \pm 0.6\%$ and a water activity (a_w) of 0.09 ± 0.03 . For the experiments of dehydration-induced lysine loss, the freeze-dried powder was reconstituted at 20% dry matter. For the experiments on thermally-induced lysine loss and for the characterization of the model system, the freeze-dried powder was stored over saturated salt solutions at 25°C (Table 4.2) until equilibrium was reached, i.e., for at least 7 days, in order to adjust the water activity and the water content, respectively.

Table 4.2 Water content of the model system after storage over saturated salt solutions and equilibrium water activities at 25°C

Salt	Relative humidity ^a /%	Water activity a_w /-	Water content X^{*b} /% wb
LiBr	6	0.06	4.07 ± 0.11
NaOH	8	0.08	4.01 ± 0.05
LiCl	11	0.11	4.68 ± 0.09
CaBr ₂	17	0.17	5.25 ± 0.08
CH ₃ COOK	23	0.23	5.66 ± 0.06
MgCl ₂	33	0.33	6.66 ± 0.05
K ₂ CO ₃	43	0.43	8.59 ± 0.07
MgNO ₃	53	0.53	6.95 ± 0.05
NaBr	58	0.58	7.40 ± 0.80
KJ	69	0.69	8.22 ± 1.86
NaCl	75	0.75	8.86 ± 0.07
KCl	84	0.84	9.87 ± 0.42
K ₂ SO ₄	97	0.97	19.55 ± 2.58

^a(Greenspan 1977), ^b $\pm 95\%$ confidence limit

4.3 Thermal treatment

After equilibrating the water activity and thus the water content at 25°C , the freeze-dried powders were transferred to specially designed cans (Fig. 4.1A, \varnothing 50 mm, height 8 mm) and heated in a water bath with optimized heating-up periods of about 30 s (Fig. 4.1B). The temperature was set to 60 - 90°C and the heating time was 30 s to 30 min. After heating, the samples were cooled down to room temperature in an ice bath to stop any ongoing reactions. For further analysis the samples were reconstituted in deionized water at 10% (w/w) dry matter. Samples that were not analyzed immediately were frozen and kept at -40°C until analysis.

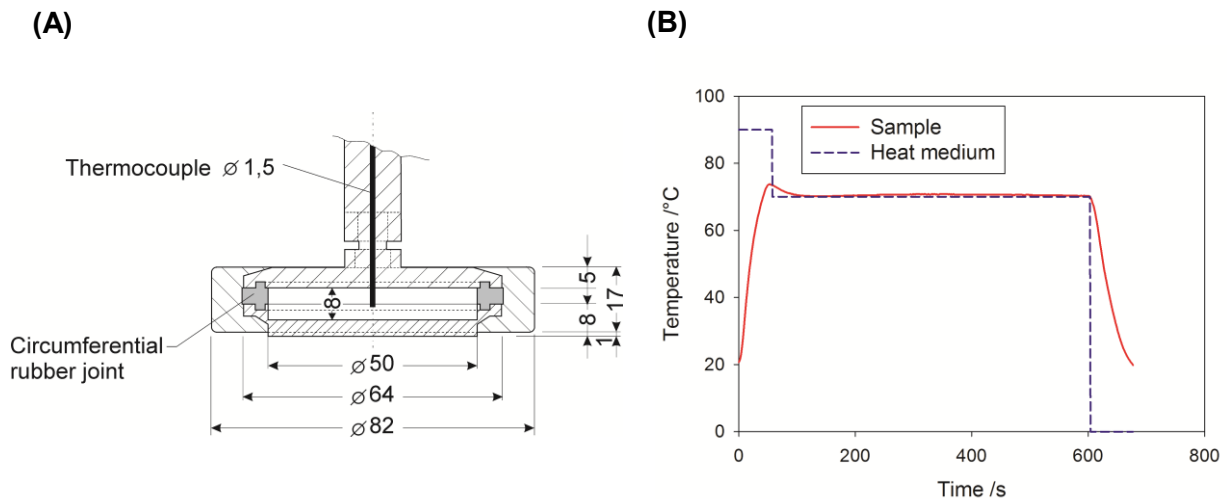


Fig. 4.1 Device used to heat the samples (A) and typical temperature profile of the water bath and the sample during the thermal treatment at 70°C (B)

4.4 Vacuum dehydration

Vacuum dehydration was done in a laboratory batch vacuum-drier (VO 400, Memmert, Schwabach, Germany). The freeze-dried powder was reconstituted in water at 20% dry matter. 8 ml of the concentrate were filled into a steel petri dish. The petri dishes had diameters of 6, 9 and 12 cm, i.e., surfaces of 28.3, 63.6 and 113.1 cm², respectively, leading to sample heights of 2.8, 1.3 and 0.71 mm, respectively. By increasing the sample surface and keeping the volume constant, the drying rate was increased due to the higher surface-volume ratio. Three different dehydration conditions were used that are listed in Table 4.3. At two dehydration conditions, zeolite was positioned around the sample in the drying chamber in order to accelerate the dehydration process. Zeolite works as a water absorbent, thus keeping the relative humidity low in the drying chamber. This procedure was chosen because the vacuum drier was neither equipped with a condenser nor with a humidity trap and the vacuum pump only removed the evaporated water after a certain pressure difference had been attained. The chamber pressure and shelf temperature of the dehydration conditions were chosen in such a manner that the difference between the shelf temperature and the evaporation temperature was equal for the three dehydration conditions. Consequently, the relative energy input was kept constant. The sample temperature was monitored in the middle and at the rim of the sample during vacuum dehydration. The dehydration was stopped after discrete drying times (1-85 min) to monitor the progress of lysine loss and residual water content. Weighing by difference was applied to determine the residual water content (wet basis) after vacuum dehydration. After vacuum dehydration, the samples were reconstituted to 20% (w/w) dry matter before measuring the content of available lysine. Samples that were not analyzed immediately after vacuum dehydration were kept frozen at -40°C until they were analyzed.

Table 4.3 Vacuum dehydration conditions

Nr.	Abbreviation	Shelf temperature /°C	Chamber pressure /mbar	Evaporation temperature /°C	Use of zeolite
1	45 mbar/60°C	60	45	≈ 32°C	No
2	45 mbar/60°C/zeolite	60	45	≈ 32°C	Yes
3	20 mbar/46°C/zeolite	46	20	≈ 18°C	Yes

4.5 Spray drying on a laboratory and pilot scale

4.5.1 Spray drying on a laboratory scale

Spray drying on a laboratory scale was performed using a laboratory-scale spray dryer (B-290, BÜCHI Labortechnik AG, Flawil, Switzerland). This spray dryer was a tall-form co-current spray dryer equipped with a two-fluid nozzle working with compressed air. The inlet temperature of the air (T_{in}) was set to 152-208°C and the product mass-flow rate to 0.22-1.3 kg.h⁻¹. The temperature of the concentrate before spray drying was kept constant at 30°C. The air volume-flow rate was 35 m³.h⁻¹. The dried powders were recuperated and analyzed as described in the following.

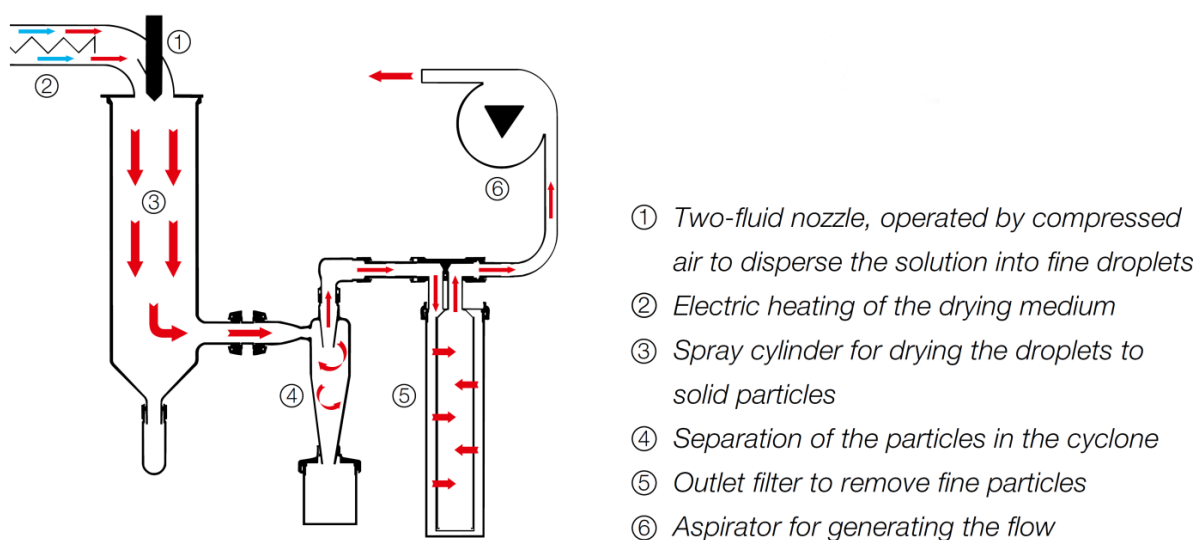


Fig. 4.2 Scheme of the laboratory-scale spray dryer (Büchi Labortechnik AG 2013)

For the experimental range of the spray-drying conditions, a 2² central composite factorial experimental design was drawn up with 8 center points in total so that a rotatable and orthogonal design was obtained. The experiments were run in six blocks, three blocks for the square which included five center points each and 3 blocks for the star which included three center points each. The order of the experiments was randomized. Three replicates of each factor combination were run. Response surfaces were built with the results.

4.5.2 Spray drying on a pilot scale

On a pilot scale, spray drying was carried out in a short-form co-current spray dryer (PRODUCTION MINOR™, GEA Niro, Søborg, Denmark) with a two-fluid nozzle that works with compressed air as atomizing device (Fig. 4.3). Air inlet temperatures were in the range of 160-200°C, the air volume-flow rate was 411 m³.h⁻¹ and product mass-flow rates were in the range of 11.0-18.7 kg.h⁻¹. The produced powders were analyzed in the same way as the samples of laboratory-scale spray drying.

Similarly to the laboratory-scale experiments, a 2² central factorial experimental design was chosen for pilot-scale drying. Three replicates of each parameter combination were run in three blocks with one center point each and response surfaces were established.

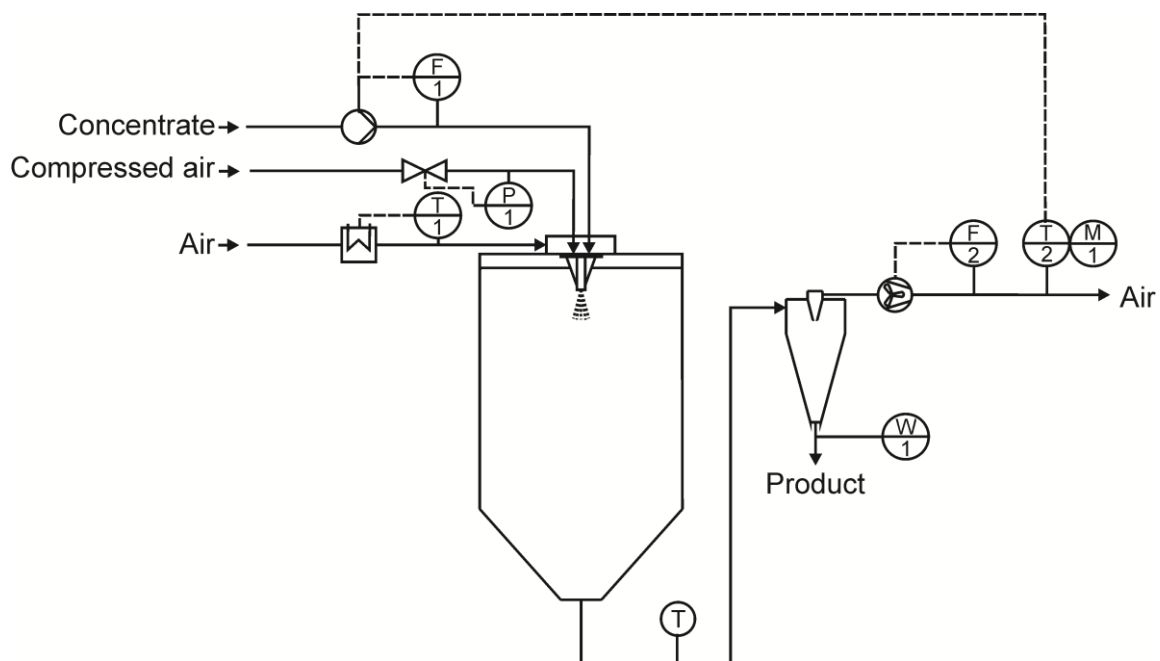


Fig. 4.3 Scheme of the pilot-scale spray dryer

4.5.3 Scale up of the spray-drying process

Scale-up from laboratory scale to pilot scale was done by maintaining the air-liquid ratio of the nozzle (ALR_{nozzle}). The air-liquid ratio of the nozzle was defined as the mass-flow rate of the compressed air $\dot{m}_{compressed\ air}$ in relation to the product mass-flow rate $\dot{m}_{product}$:

$$ALR_{nozzle} = \frac{\dot{m}_{compressed\ air}}{\dot{m}_{product}} \quad 4.1$$

The air inlet temperatures on a pilot scale were in the same range as on a laboratory scale. Additionally, the air-liquid ratio of both spray dryers (ALR_{dryer}) was calculated according to eq. 4.2 where \dot{m}_{air} is the air mass-flow rate and \dot{m}_{water} is the mass-flow rate of the water contained in the concentrate.

$$ALR_{dryer} = \frac{\dot{m}_{air}}{\dot{m}_{water}} \quad 4.2$$

By using the air-liquid ratio of the dryer (ALR_{dryer}), it became possible to compare the process characteristics of spray drying on a pilot scale and on a laboratory scale despite the differences in geometry and, consequently, in the air-flow pattern. On a laboratory scale, ALR_{dryer} of 36-118 were used whereas on a pilot scale ALR_{dryer} were in the range of 25-47. The different ALR_{dryer} ranges were due to the different geometries of the dryers and the different drying efficiencies.

4.5.4 Residence-time distribution of the particles

The particle residence-time distribution was determined for both spray dryers under the spray-drying conditions described above. Sodium chloride (NaCl, neoLab, Heidelberg, Germany) at a concentration of 0.1 mol.l^{-1} and Cochineal Red A (E124, Brauns-Heitmann, Warburg, Germany) at a concentration of 0.125 mg.g^{-1} were added as tracers to the model dairy-formulation. Step marking was realized by switching the product supply from the standard model dairy-formulation to the model dairy-formulation supplemented with the tracers. Samples were collected at the bottom of the cyclone in regular time steps. Time was set to zero when the product reached the atomizer. On a laboratory scale, sampling times were 5 s, 10 s, 20 s, 30 s, 40 s, 50 s, 60 s, 70 s, 80 s, 120 s, 160 s and 220 s. On a pilot scale, samples were taken after 20 s, 40 s, 60 s, 2 min, 4 min, 7 min, 15 min, 20 min, 30 min and 40 min. Samples were reconstituted in deionized water for further analyses. NaCl-concentration was determined with a flame photometer (ELEX 6361, Eppendorf, Hamburg, Germany). Conductivity was measured with a dual meter pH/conductivity (SevenMultiTM S47, Mettler-Toledo, Gießen, Germany) equipped with a conductivity probe (InLab®730, Mettler-Toledo, Gießen, Germany) that had a measuring range of $0\text{-}1000 \text{ mS.cm}^{-1}$ and an integrated temperature sensor. The color was measured with a spectrophotometer (SP68, X-Rite, Köln, Germany). The CIE $L^*a^*b^*$ color system with the coordinates lightness L^* , red/green value a^* and yellow/blue value b^* was used to express the color of the samples. The color saturation index C^* (chroma) was calculated according to eq. 4.3:

$$C^* = \sqrt{a^{*2} + b^{*2}} \quad 4.3$$

The NaCl-concentration, the conductivity and the color saturation index C^* at the different time steps were used to calculate the residence-time distribution of the particles. In order to obtain the non-dimensional cumulative residence-time distribution $F(t)$, the tracer concentration $C(t)$ at time t was normalized with the concentration C_0 of the model dairy-formulation without any tracers added and the concentration C_∞ of the model dairy-formulation supplemented with the tracer:

$$F(t) = \frac{C(t) - C_0}{C_\infty - C_0} \quad 4.4$$

Particle residence-time distributions were characterized by the median residence time τ_{50} , which is the 50% percentile, and the 10% and 90% percentiles τ_{10} and τ_{90} , respectively. To compare the particle residence-time with the air residence-time, the mean residence time of the particles \bar{t} was calculated according to eq. 4.5 where \bar{t}_i denotes the mean time of interval i and ΔC_i the concentration difference in interval i :

$$\bar{t} = \sum_{i=1}^n \bar{t}_i \cdot \Delta C_i \quad 4.5$$

Assuming plug flow inside the spray dryer, the mean residence time of the air \bar{t}_{air} was estimated based on the volume of the spray dryer V_{dryer} and the air volume-flow rate \dot{V}_{air} :

$$\bar{t}_{air} = \frac{V_{dryer}}{\dot{V}_{air}} \quad 4.6$$

4.6 Thin-film drying and droplet drying

The drying kinetics of the model dairy-formulation was determined by thin-film drying experiments and by drying sessile droplets in a drying channel. These methods were chosen because they can be realized in the drying channel available at the Chair for Food Process Engineering and Dairy Technology (TU München) and were successfully employed in the past (Perdana et al. 2011, Räderer 2001). The characteristic drying-rate curve (CDRC) and the reaction-engineering approach were used to model drying kinetics.

4.6.1 Experimental set up of the drying channel

The drying channel (Fig. 4.4 and Fig. 4.5) had a height of 20.3 mm and a width of 50 mm. Compressed air at 2 bar was used as drying-air supply. The drying air was heated to temperatures of 80-120°C (Table 4.4) and the relative humidity was adjusted to 0-20% by injecting and evaporating water in the dry air stream using a controlled evaporator mixer (W101A, Bronkhorst High-Tech B.V., Ruurlo, the Netherlands). Air velocity was set to 0.15-0.30 m.s⁻¹ with the aid of two dosing valves (EL Flow Select and Liqui Flow, Bronkhorst High-Tech B.V., Ruurlo, the Netherlands). The drying channel was surrounded by a second pipe with an insulating air flow that was heated using an electric pipe heater (type 5000, Herz GmbH, Neuwied, Germany). The temperature of the insulating air was adjusted depending on the experimental conditions in order to obtain a stable temperature in the drying channel. Before starting an experiment, the drying channel and the sample holder were equilibrated at the desired temperature for 30 min. All parameters were controlled and recorded using a Labview automatic control system. The relative humidity of the air was not measured continuously but before positioning the sample in the drying channel.

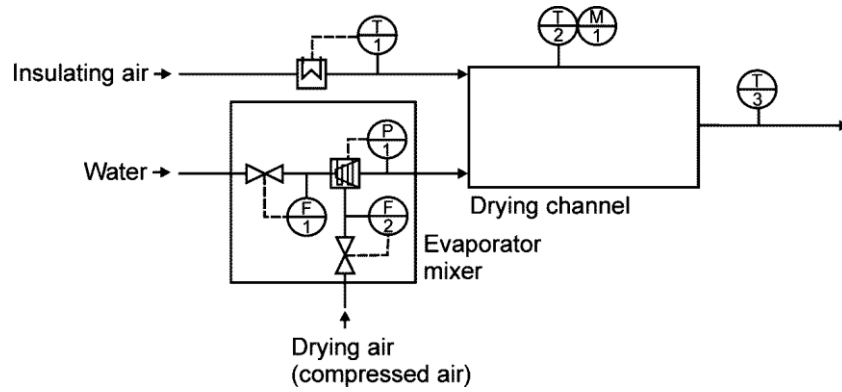


Fig. 4.4 Experimental set-up of the drying channel

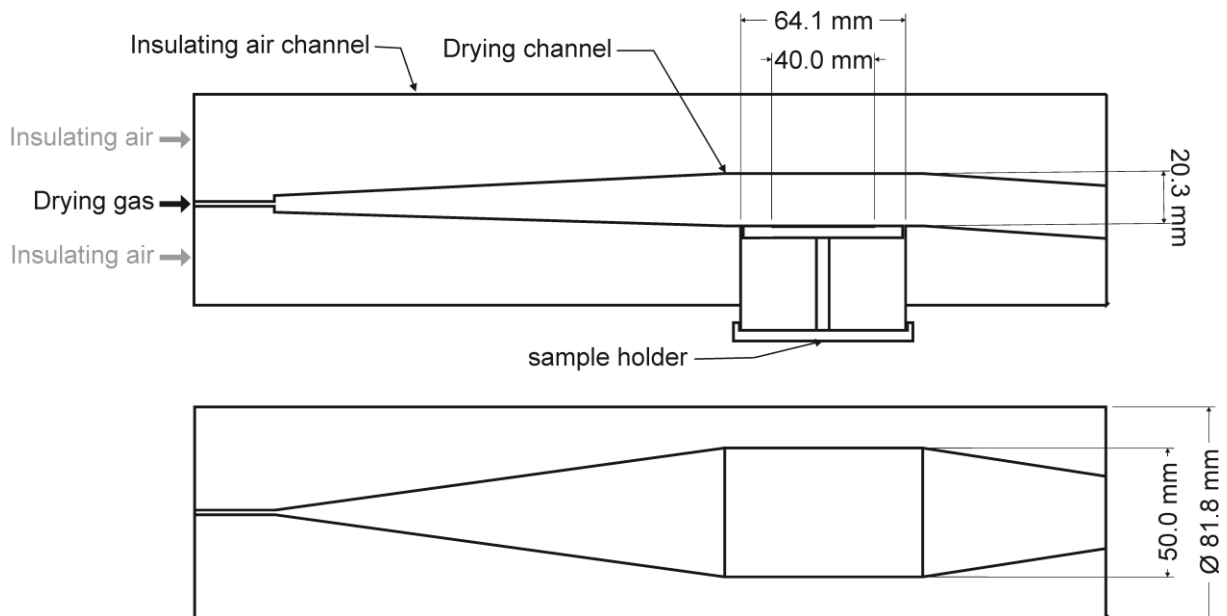


Fig. 4.5 Details of the drying channel

The freeze-dried model dairy-formulation was reconstituted to 20% dry matter and tempered at 25°C. Aliquots were positioned on a sample holder which formed the bottom of the drying channel. Two different sample holders were used, one for the drying of sessile droplets and one for the drying of thin films. The surface of the sample holder for droplet drying was made of a flat Teflon plate. As Teflon is a hydrophobic material, the spreading of droplets could be minimized and spherical sessile droplets were obtained. Either one droplet of 50 μl or 40 droplets of 2.5 μl were placed on the sample holder. When the droplet size was decreased the droplet number had to be increased due to the measuring range of the balance. The sample holder for film drying was made of aluminum, a hydrophilic material, in order to obtain thin films. A cavity with a diameter of 40 mm and a depth of 0.6 mm was milled into the aluminum plate and 1000 μl of the sample were filled in it. To determine the drying kinetics, i.e., the weight loss over time, the sample holder was taken out of the drying channel after

discrete time steps and put on a precision balance (WZ64S, Sartorius AG, Göttingen, Germany). To avoid experimental errors, samples were discarded after weighing and a new aliquot was taken for the next time step. A thermocouple was positioned in the middle of the sample to measure the product temperature which was continuously recorded. The experimental set up was validated by drying deionized water

Table 4.4 Experimental conditions for the drying kinetics experiments (T_{air} : drying air temperature; v_{air} : drying air velocity; RH: relative humidity; h_F : film thickness; V : sample volume)

	Film drying					Droplet drying				
	F1	F2	F3	F4	F5	T1	T2	T3	T4	T5
$T_{air} / ^\circ\text{C}$	80	120	80	120	80	80	120	80	120	80
$v_{air} / \text{m}\cdot\text{s}^{-1}$	0.15	0.15	0.3	0.3	0.3	0.15	0.15	0.3	0.3	0.3
RH /%	0	0	0	0	20	0	0	0	0	0
h_F / mm	0.6	0.6	0.6	0.6	0.6	-	-	-	-	-
$V / \mu\text{l}$	1000	1000	1000	1000	1000	1 x 50	1 x 50	1 x 50	1 x 50	40 x 2.5

4.6.2 Modeling drying kinetics

The experimental drying kinetics data was modeled using the characteristic drying-rate curve (CDRC) and the reaction-engineering approach (REA) (cf. chapter 2.4.2). In both modeling approaches, the mean temperature T_m (eq. 4.7) of the air temperature T_{air} and the product temperature T_p was used as bulk temperature T_b because this is a good approximation for the temperature of the boundary layer between the product and the surrounding air (Chen and Mujumdar 2008).

$$T_b = T_m = \frac{T_{air} + T_p}{2} \quad 4.7$$

The CDRC model compares the specific drying rate at each water content to the unhindered drying rate during the first drying stage (Chen 2008, Langrish and Kockel 2001, Woo et al. 2008b). The drying rate is represented by eq. 4.8 where X denotes the water content, t the time, ξ the relative drying rate, A_p the product surface area, h the heat transfer coefficient, m_s the mass of dry matter, r_v the latent heat of vaporization and T_{wb} the wet bulb temperature.

$$\frac{dX}{dt} = -\xi \cdot \frac{A_p \cdot h}{m_s \cdot r_v} \cdot (T_b - T_{wb}) \quad 4.8$$

The definition of the relative drying rate ξ depends on the water content X and on the critical water content X_{cr} :

$$\xi = \frac{N}{N_{max}} = \begin{cases} 1 & \text{for } X > X_{cr} \\ f(\varphi) = \left(\frac{X - X_e}{X_{cr} - X_e} \right)^a & \text{for } X \leq X_{cr} \end{cases} \quad 4.9$$

where N is the specific drying rate, N_{max} the maximum drying rate, X_e the equilibrium water-content and a a product-specific constant. The equilibrium water-content can be derived from the sorption isotherm (cf. chapter 4.7.12; Lin and Chen 2007). The critical water content, i.e., the water content at the transition from the constant drying rate period to the decreasing drying rate period, and the constant a have to be deduced from experimental data. To do this, the experimental relative drying rates were calculated according to eq. 4.8. Eq. 4.9 was then fitted to the experimental relative drying rates with the critical water content X_{cr} and the constant a as fitting parameters. Predicted water contents were computed by including eq. 4.9 in eq. 4.8 and subsequent integration.

The product surface equated the surface of the cavity in the sample holder in the case of thin-film drying. In the case of droplet drying, it was determined from the contact angle measurements. The heat transfer coefficient was obtained from the experimental data at the start of drying, i.e., when the drying rate was unhindered ($X > X_{cr}$). The existing Nusselt correlations, which are often used to determine heat transfer coefficients, did not give correct results because heat conduction from the sample holder to the sample occurs apart from heat convection from the air to the sample. The physical characteristics of water and air were taken from VDI-Wärmeatlas (Gesellschaft Verfahrenstechnik und Chemieingenieurwesen 2006).

The reaction-engineering approach (REA), which was introduced by Chen and Xie (1997), expresses the drying rate as:

$$\frac{dm_p}{dt} = m_s \frac{dX}{dt} = -h_m \cdot A_p \cdot (\rho_{v,s}(T_s) - \rho_{v,b}) \quad 4.10$$

where m_p denotes the product mass, m_s the mass of the dry matter, X the water content, h_m the mass-transfer coefficient, A_p the product surface, T_s the interface temperature, $\rho_{v,s}$ the vapor concentration at the sample-gas interface and $\rho_{v,b}$ the bulk vapor concentration. The vapor concentration at the solid-gas interface can be derived by the following equation (Chen & Xie, 1997):

$$\rho_{v,s} = \exp\left(\frac{-\Delta E_v}{R_G \cdot T_P}\right) \cdot \rho_{v,sat} \quad 4.11$$

where ΔE_v is the activation energy, which represents the difficulty of removing water, R_G the specific gas constant and $\rho_{v,sat}$ the saturated vapor concentration. The apparent activation energy ΔE_v was determined experimentally by inserting eq. 4.11 in eq. 4.10. The drying rate was derived from the experimental drying kinetics data. The product surface area A_p was calculated in the same way as for the CDRC-model, the bulk vapor concentration $\rho_{v,b}$ with eq. 4.12 and the saturated vapor concentration $\rho_{v,sat}$ using eq. 4.13 (Putranto et al. 2011).

$$\rho_{v,b} = \frac{m_w}{V_{air}} = \frac{x \cdot m_{air}}{\frac{m_{air} \cdot R_G \cdot T_{air}}{P_{air}}} \quad 4.12$$

$$\rho_{v,sat} = \left(\begin{array}{l} 4.844 \cdot 10^{-9} \text{ } ^\circ\text{C}^{-4} \cdot (T_{P,^\circ\text{C}})^4 - 1.4801 \cdot 10^{-7} \text{ } ^\circ\text{C}^{-3} \cdot (T_{P,^\circ\text{C}})^3 \\ + 2.6572 \cdot 10^{-5} \text{ } ^\circ\text{C}^{-2} \cdot (T_{P,^\circ\text{C}})^2 - 4.8613 \cdot 10^{-5} \text{ } ^\circ\text{C}^{-1} \cdot T_{P,^\circ\text{C}} \end{array} \right) \cdot 1 \text{ kg m}^{-3} \quad 4.13$$

In the case of droplet drying, the mass-transfer coefficient h_m was computed with the Ranz-Marshall correlation for spherical particles (eq. 4.14) where Sh denotes the Sherwood number, d_s the equal volume sphere diameter, D_v the vapor-air diffusivity (eq. 4.15; Patel et al. 2009), Re the Reynolds number (eq. 4.16) and Sc the Schmidt number (eq. 4.17). In the case of thin-film drying, satisfactory results were neither obtained by the Ranz-Marshall correlation nor by the correlation for flow over a flat surface. Therefore, the mass-transfer coefficient was calculated using the experimental results of the first data point at the beginning of drying with the hypothesis that the vapor concentration at the sample-gas interface $\rho_{v,s}$ equals the saturated vapor concentration $\rho_{v,sat}$ (eq. 4.18). This hypothesis is justified because the film surface was saturated with water at the beginning of drying and was checked for droplet drying by comparing the mass-transfer coefficients calculated using the Ranz-Marshall correlation and using the data at the start of drying.

$$Sh = \frac{h_m \cdot d_s}{D_v} = 2 + 0.6 \cdot Re^{1/2} \cdot Sc^{1/3} \quad 4.14$$

$$D_v = (1.963 \cdot 10^{-7} \text{ K}^{-1} \cdot T_m - 3.33307 \cdot 10^{-5}) \cdot 1 \text{ m}^2 \text{ s}^{-1} \quad 4.15$$

$$Re = \frac{v \cdot d_s}{\nu_G} \quad 4.16$$

$$Sc = \frac{\nu_G}{D_v} \quad 4.17$$

$$h_m = - \frac{m_s \cdot \frac{dX}{dt}}{A_P \cdot (\rho_{v,sat}(T_s) - \rho_{v,b})} \quad 4.18$$

Eq. 4.19 was then fitted to the experimental data in order to derive a relation for the apparent activation energy ΔE_v (Chen & Xie, 1997).

$$\frac{\Delta E_v}{\Delta E_{v,e}} = a \cdot \exp\left(-b \cdot (X - X_e)^c\right) \quad 4.19$$

where a , b and c are constants and X_e the equilibrium water content. According to eq. 4.19 the relative activation energy $\Delta E_v/\Delta E_{v,e}$ is only a function of the water content for a given product.

The maximum apparent activation energy $\Delta E_{v,e}$ can be calculated with the relative humidity (RH_b) and temperature of the surrounding drying gas (Chen, 2008):

$$\Delta E_{v,e} = -R_G \cdot T_b \cdot \ln(RH_b) \quad 4.20$$

4.7 Analytical methods

4.7.1 Available lysine

Fluorimetric method with o-phthaldialdehyde (OPA)

The fluorimetric method with *o*-phthaldialdehyde (Ferrer et al. 2000, 2003a, Goodno et al. 1981, Morales et al. 1995) was established and validated at the institute to determine the content of available lysine. At alkaline conditions and in the presence of β -mercaptoethanol *o*-phthaldialdehyde (OPA) reacts with free amino groups, e.g. the ϵ -amino group of lysine and a fluorescent isoindole is formed (Fig. 4.6). The detected fluorescence intensity is directly related to the amount of free amino groups. When the impact of the amino groups of free amino acids and small peptides is taken into account, the amount of free amino groups is equivalent to the amount of available lysine.

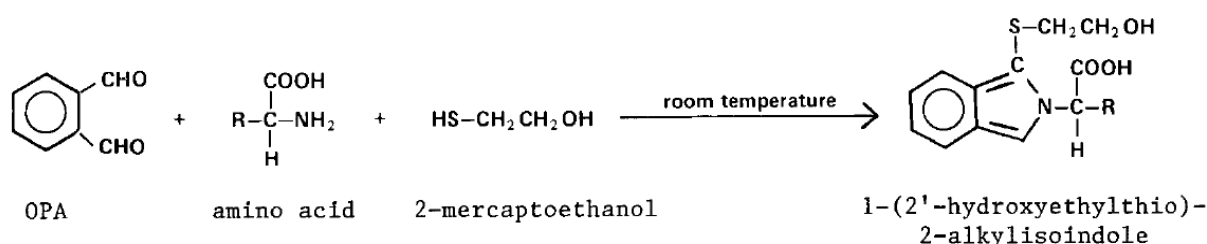


Fig. 4.6 Reaction of *o*-phthaldialdehyde with free amino groups (Dai et al., 1997)

50 μ l of the dissolved samples were mixed with 950 μ l water and 1 ml 12% SDS (Serva, Heidelberg, Germany) solution and the resulting mixtures were allowed to cool at 4°C overnight. After sonication in an ultrasonic bath (frequency: 35 kHz, HF power: 80 W_{eff}, ultrasonic peak output: 320 W; Sonorex Super RK 100 H, Bandelin, Berlin, Germany) at 25°C for 15 min, a 5 μ l aliquot was transferred to a black 96-well microtiter plate (Greiner Bio-One, Frickenhausen, Germany) and 150 μ l OPA reagent (80 mg OPA (Merck Darmstadt, Germany) dissolved in 2 ml ethanol (Merck Darmstadt, Germany), 0.2 ml β -mercaptoethanol (Merck Darmstadt, Germany), 5 ml 20% SDS solution, 50 ml 0.1 M sodium tetraborate (Sigma-Aldrich, Steinheim, Germany) buffer (pH 9.7-10) and diluted to 100 ml with water) were added. Fluorescence was measured with a microtiter-plate reader (Genios Plus, Tecan, Crailsheim, Germany) at $\lambda_{\text{excitation}} = 340$ nm and $\lambda_{\text{emission}} = 455$ nm. The OPA reagent was prepared daily.

Possible interferences from small peptides, free amino acids and amines were measured after precipitation with 10% TCA (2 ml 10% TCA (Scharlau, Barcelona, Spain) added to a dissolved sample of 2 ml, centrifuged at 3000 rpm for 15 min, then treated as described above). Blanks were prepared by adding 1 ml of water to 1 ml of 12% SDS solution. The fluorescence intensity of the blank and of the interferences was subtracted from the total fluorescence intensity. The resulting fluorescence intensity is proportional to the content of available lysine.

The calibration curve was obtained from a N_α-acetyl-L-lysine (Sigma-Aldrich, Steinheim, Germany) standard ranging from 0.9 to 19 mM (Fig. 4.7). The results were expressed as mol NH₂.(g dry matter)⁻¹. The method described above was validated for the model system. A linear relationship (Fig. 4.8) was obtained for the fluorescence intensity as a function of the concentration with an intraday precision of ±3.25% and an interday precision of ±5.78%. The recovery rate (Fig. 4.9) was determined by adding a β-lactoglobulin standard ranging from 0.9 to 1.9 mM to the model system (5% dry matter). A recovery rate of 100.6% was obtained. From these measurements it can be concluded that the chosen method is precise and suitable for this study.

Furosine method

The quantification of furosine represents another wide-spread method to determine the content of available lysine. The early Maillard reaction product ε-deoxylactulosyllysine is partly converted into furosine under defined hydrolysis conditions. According to Finot et al. (1983), 32% of protein-bound lactulose-lysine is converted to furosine upon acid hydrolysis and 40% to lysine. The furosine method of Fenaille et al. (2003) was used and the percentage of blocked lysine was calculated based on the conversion rate mentioned.

4.7.2 Contact angle

In order to determine the surface of sessile drops on the Teflon plates, which were used for the drying kinetics experiments, the contact angle between the drops and the Teflon plate was measured. Drops of deionized water and model dairy-formulation (20% dry matter) were placed on a Teflon plate. Three different volumes of 5, 50 and 100 μl were analyzed at 20°C with the contact angle measuring instrument DSA100 (Krüss, Hamburg, Germany). The drop was photographed 646 times in 6.25 s and the results were treated according to the Young-Laplace procedure with the software DSA1 (Krüss, Hamburg, Germany). In this way, the contact angle, the base diameter, the height and the surface of the drop were obtained.

4.7.3 Density

The density of the concentrates (10-30% dry matter) was measured with a digital density meter (Density Master DMA 4100M, Anton Paar, Ostfildern-Scharnhausen, Germany) based on the oscillating U-tube method. Measurements were done at 20-70°C.

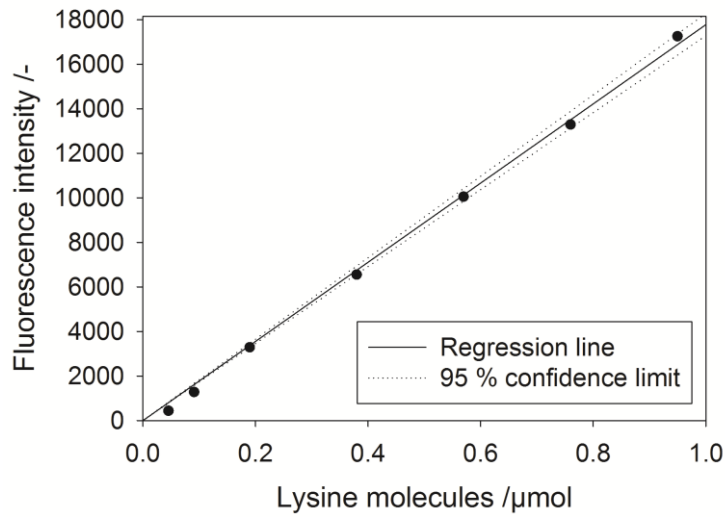


Fig. 4.7 Calibration curve obtained with the *N_α-acetyl-L-lysine* standard

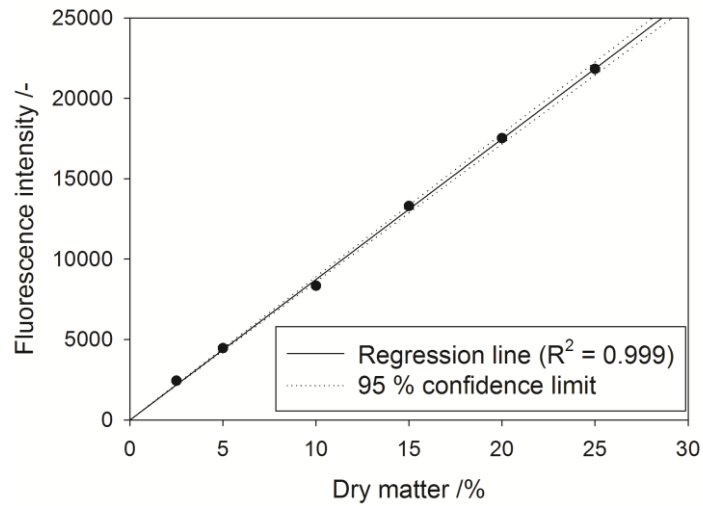


Fig. 4.8 Linearity determined with the model system

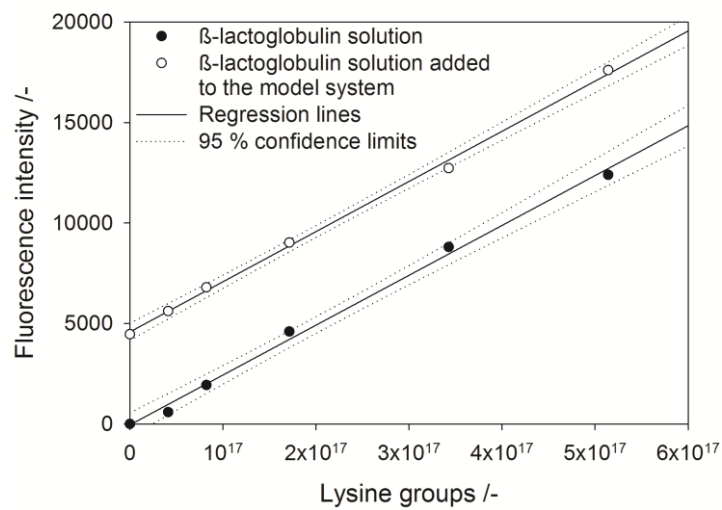


Fig. 4.9 Determination of the recovery rate

4.7.4 Glass-transition temperature and crystallization of lactose

Glass-transition temperature

The glass-transition temperature was measured after equilibrating the water activity of the freeze-dried samples (cf. chapter 4.2). Differential scanning calorimetry (DSC, Q1000, TA Instruments, Eschborn, Germany) in the modulated mode (modulated $\pm 0.50^\circ\text{C}$ every 60 seconds and a heating rate of $2.00^\circ\text{C}\cdot\text{min}^{-1}$ from 0 to 250°C) was used to measure the glass transition temperature. Hermetically sealed aluminum pans were used for the measurements with an empty aluminum pan as reference. Sample aliquots of about 20 mg were weighed in the aluminum pans. The glass-transition temperature was expressed as midpoint temperature.

To establish the glass-transition curve, aliquots of freeze-dried model dairy-formulation were equilibrated to water activities of 0-0.97 (Table 4.2). The Gordon & Taylor equation (Gordon and Taylor 1952) was fitted to the experimental data using least-square non-linear regression:

$$T_g = \frac{w_1 \cdot T_{g1} + K \cdot w_2 \cdot T_{g2}}{w_1 + K \cdot w_2} \quad 4.21$$

where T_g is the glass-transition temperature, T_{g1} is the glass-transition temperature of the dry matter, T_{g2} is the glass-transition temperature of water, w_1 and w_2 are the weight fractions of the dry matter and the water, respectively, and K is a constant. T_{g2} was set at -135°C (Vuataz 2002).

Crystallization kinetics

Lactose crystallization was determined by differential scanning calorimetry (DSC, Q1000, TA Instruments, Eschborn, Germany). An empty aluminum pan was used as reference. After equilibration of the water activity (Table 4.2), aliquots of about 20 mg of freeze-dried samples were transferred to aluminum pans which were subsequently hermetically sealed. The measurement was conducted in the isothermal mode. The samples were heated to the set temperature (60 - 90°C) and kept at this temperature until the crystallization peak was observed. The measurement was stopped if there had been no crystallization peak within 6 hours. The time at the peak maximum was taken as crystallization delay. Thus, the crystallization delay indicates after which time a sample crystallizes at a given temperature above the glass-transition temperature and it can be used to differentiate samples in the rubbery state from samples in the crystalline state, e.g. during isothermal heating experiments for the analysis of the kinetics of lysine loss

The delay of lactose crystallization as a function of $T - T_g$ was modeled using the Williams-Landel-Ferry equation (Williams et al. 1955):

$$\log \frac{\tau}{\tau_{T_g}} = \frac{-C_1 \cdot (T - T_g)}{C_2 + (T - T_g)} \quad 4.22$$

where τ denotes the crystallization delay at the temperature T and τ_{T_g} the crystallization delay

at the glass-transition temperature T_g . C_1 and C_2 are constants. As the crystallization time at the glass-transition temperature is difficult to obtain, it must be estimated. To avoid extensive extrapolation, the concept of reduced variables was applied where a reference temperature within the experimental range is chosen instead of the glass-transition temperature (Mazzobre et al. 2001, Peleg 1992):

$$\log \frac{\tau}{\tau_{T_r}} = \frac{-C_{1,r} \cdot (T - T_r)}{C_{2,r} + (T - T_r)} = \frac{-C_{1,r} \cdot (T - T_r)}{(T - T_\infty)} \quad 4.23$$

with τ_{T_r} being the crystallization delay at the reference temperature $T_r = T_g + 55.46$ K, $C_{1,r}$ and $C_{2,r}$ the corresponding relative constants. These constants were obtained with the aid of a temperature that is characterized by an infinite crystallization delay. According to Mazzobre et al. (2001) this is the case at $T_\infty = T_g - 50$ K and leads to the definition of $C_{2,r} = T_r - T_\infty$ (see eq. 4.23). Linear transformation was applied to evaluate $C_{1,r}$. The constants C_1 and C_2 were calculated using eq. 4.25 and eq. 4.26 and τ_{T_g} was then determined by non-linear regression.

$$\partial = T_r - T_g \quad 4.24$$

$$C_1 = \frac{C_{1,r} \cdot C_{2,r}}{C_{2,r} - \partial} \quad 4.25$$

$$C_2 = C_{2,r} - \partial \quad 4.26$$

The kinetics of lactose crystallization was analyzed by integrating the crystallization peak. Thus, the crystallinity α was obtained as a function of time. The induction time until the beginning of the peak was subtracted from the experimental time to obtain time t of the crystallization process. It was assumed that lactose was entirely amorphous ($\alpha = 0$) before the measurements and totally crystalline ($\alpha = 1$) after the measurements. This assumption is justified because of the proper choice of the freeze-drying conditions and the absence of glass transition after crystallization. The Avrami equation was used to analyze the degree of crystallinity (Avrami 1940):

$$1 - \alpha = \exp(-k_{Av} \cdot t^{n_{Av}}) \quad 4.27$$

where α denotes the crystallinity, k_{Av} the rate constant, t the crystallization time and n_{Av} the Avrami index.

4.7.5 Interfacial tension

The surface or interfacial tension of the concentrates (10-30% dry matter) was determined with the aid of a drop-volume tensiometer (TVT 2, Lauda, Königshofen, Germany) at 20-70°C. In the tensiometer, a drop was formed at the tip of a capillary surrounded by air. When

the weight of the drop exceeds the sum of the buoyancy and interfacial tension forces, the drop breaks of. The interfacial tension is then calculated with the critical volume V_{crit} that the drop has at the moment of disruption, the density difference $\Delta\rho$ between the droplet and the surrounding medium and the capillary radius r :

$$\sigma = \frac{V_{crit} \cdot \Delta\rho \cdot g}{2 \cdot \pi \cdot r_{capillary}} \quad 4.28$$

4.7.6 Molecular mobility

The molecular mobility was evaluated by measuring the transversal relaxation time T_2 with a low resolution $^1\text{H-NMR}$ spectrometer (MINISPEC mq20, Bruker Analytik GmbH, Rheinstetten, Germany). Longer transversal relaxation times correspond to higher molecular mobilities in the samples. After equilibrating the water activity (Table 4.2), 0.5 g of the sample to be analyzed was weighed in a glass tube and heated to the temperature of the analysis (20-70°C) in a bath thermostat (RL 6 CP, Lauda, Lauda-Königshofen, Germany). The same thermostat was used to temper the sample chamber of the NMR spectrometer. The resonance frequency was 20 MHz at a magnetic field strength B_0 of 0.47 T and a magnet temperature of 40°C. A combination of a free induction decay (FID) and a Carr-Purcell-Meiboom-Gill (CPMG) sequence was used. Each sample was analyzed at three different 90°-180° impulse spacing times τ_i of 0.05, 0.1 and 1 ms, respectively. No significant impact of the impulse spacing time on the results was observed. The envelope curve of the echoes was described by a gauss-exponential equation with a sinus term (Fig. 4.10):

$$U(t) = a_0 + f_S \cdot \exp\left(-\frac{t^2}{2 \cdot T_{2,1}^2}\right) \cdot \frac{\sin(b_1 \cdot t)}{b_1 \cdot t} + f_L \cdot \exp\left(-\frac{t}{T_{2,2}}\right) \quad 4.29$$

where $U(t)$ represents the intensity of the NMR signal, t the time, a_0 the offset value, b_1 a constant, f_S the proton fraction of the immobile, mostly solid component, f_L the proton fraction of the mobile component, mostly from water, and $T_{2,1}$ and $T_{2,2}$ the corresponding relaxation times. The sinus term is used for systems with a highly structured solid phase which shows a sinusoidal oscillation at the end of the Gaussian phase in the echoes (Mariette 2009). Eq. 4.29 was fitted to the experimental data using the software Table Curve™ 2D v4.07 (Systat Software Inc., San Jose, USA). An example is shown in Fig. 4.10. A mean relaxation time T_2 was calculated according to eq. 4.30 and the second moment M_2 according to eq. 4.31. The second moment expresses the strength of hydrogen dipolar interactions (Mateus et al. 2007).

$$T_2 = f_S \cdot T_{2,1} + f_L \cdot T_{2,2} \quad 4.30$$

$$M_2 = \frac{1}{T_{2,1}^2} + \frac{1}{3} b_1^2 \quad 4.31$$

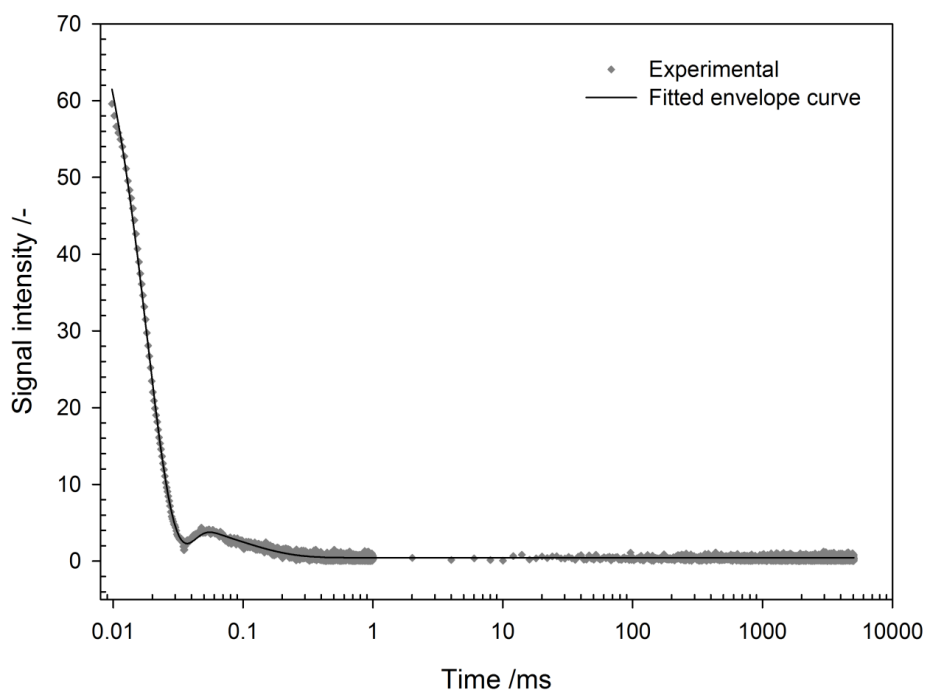


Fig. 4.10 T_2 relaxation curve of the standard composition with a water activity of 0.23 at 60°C

4.7.7 Particle size

The particle size distribution was analyzed by laser diffraction with the particle size measuring instrument Mastersizer 2000 in combination with the powder dispersion unit Scirocco 2000 (Malvern Instruments Ltd., Worcestershire, UK). The analyses were carried out with a particle refraction index of 1.41 and a particle absorption index of 0.001. The background measurement lasted 25 s and the duration of the particle size measurement 20 s. All samples were analyzed with dispersion pressures of 0.5 bar, 1.5 bar and 3 bar, respectively. At higher dispersion pressures, agglomerates of powder particles are destroyed. Consequently, it is possible to determine the degree of agglomeration and the strength of the formed agglomerates by comparing the particle size distributions obtained at the different dispersion pressures.

4.7.8 Solubility

The solubility of the model dairy-formulation was determined as a function of the temperature. Supersaturated solutions of the model dairy-formulation were prepared by reconstituting freeze-dried powders in deionized water. The samples were stored with stirring at 4°C overnight to ensure complete hydration. The supersaturated solutions were then maintained at 20–80°C in a first step with stirring for at least 30 min to ensure complete solution of the soluble dry matter. In a second step, they were maintained at the same temperature for at least 50 min without stirring to allow precipitation of the amount of dry matter above the solubility limit. The supernatant was analyzed for its dry matter content, protein content and lactose content. The dry matter content was determined by Karl-Fischer titration (see chapter 4.7.11). The protein content was measured according to the method of Dumas with the nitrogen/protein analyzer FP-528 (LECO Instrumente GmbH, Mönchengladbach, Germany). The lactose content was quantified by isocratic HPLC (Agilent 1100, Agilent Technologies, Santa Clara,

USA) using 0.005 M sulfuric acid as eluent with a flow rate of $0.6 \text{ ml}\cdot\text{min}^{-1}$ and a refraction index detector. Separations were performed on an Aminex® HPX-87H (300 x 7.8 mm) column with a precolumn (Bio-Rad Laboratories, Hercules, USA) at 50°C . For sample preparation, 50 μl of 60% perchloric acid was added to 1 ml of the sample to precipitate proteins and diluted with 9 ml of deionized water. The resulting solution was filtered through a RC-45/25 Chromafil® Xtra $\phi = 0.45 \mu\text{m}$ syringe filter (Macherey-Nagel, Düren, Germany) into a 1.5 ml HPLC vial (Macherey-Nagel, Düren, Germany). The standard injection volume was 20 μl . The obtained data was used to draw the solubility line of the model dairy-formulation.

4.7.9 Spray characteristics of the pneumatic nozzle

The spray characteristics of the pneumatic nozzle of the pilot-scale spray dryer (PRODUCTION MINOR™, GEA Niro, Søborg, Denmark) were analyzed visually. The nozzle was mounted in a specially designed test rig surrounded by a dark environment and the spray was photographed. The atomization conditions of the spray-drying experiments on a pilot scale were used (cf. chapter 4.5.2). The spray angle and droplet break-up characteristics were evaluated from the photographs.

4.7.10 Viscosity

The viscosity of concentrates was analyzed with a rotational viscometer (Advanced Rheometer AR1000, TA Instruments, Eschborn, Germany) using the rotor-stator principle. Samples were tempered in a water bath (30 min) before the analysis and then a 15 g aliquot of the concentrate was measured. Measurements were done at temperatures of $20\text{-}70^\circ\text{C}$ and at concentrations of 10-15% dry matter. A concentric aluminum cylinder with an outer radius of 14 mm was used. The inner radius of the stator was 15 mm, the immersed height of the cylinder was 42 mm and the gap between the cylinder bottom and the stator was 5.92 mm. Samples were equilibrated for 30 s and then a continuous shear ramp was applied from 0 to 200 s^{-1} in 120 s. The experimental data was analyzed with the software Rheology Advantage Data Analysis (TA Instruments, Eschborn, Germany). Viscosities at a shear rate of 200 s^{-1} will be reported in the following.

4.7.11 Water content and water activity

The water content X^* was determined using Karl-Fischer Titration (Karl-Fischer Titrator, Titro Line KF, Schott, Mainz, Germany). Analyses were carried out at 40°C in a 1.1:1 mixture of Hydranal®-Formamid dry and Hydranal®-Methanol Rapid (Sigma-Aldrich, Steinheim, Germany). Samples were stirred for 5 min to equilibrate the system and then titration was done with Hydranal®-Composite 5 (Sigma-Aldrich, Steinheim, Germany). The titrator was calibrated with Hydranal®-Water Standard (Sigma-Aldrich, Steinheim, Germany). Moisture contents were expressed as moisture contents on wet basis (wb).

The water activity a_w was measured using a Novasina Sprint (Novasina AG, Lachen, Switzerland). The measurements were carried out at 25°C .

4.7.12 Water sorption and desorption isotherm

To measure the water-sorption isotherm, aliquots of the freeze-dried powders were stored over saturated salt solutions at 25°C, 40°C and 60°C for at least 7 days (cf. Table 4.2) to adjust the water activity. The samples were weighed regularly until equilibrium was attained. The water content was deduced from the difference in weight. Samples with a water activity of 0.53 and above crystallized while equilibrating the water activity at 25°C. This was indicated by a weight loss, i.e., a decline of sorbed water after a certain time. The sorption isotherm was fitted with the Guggenheim-Anderson-de Boer (GAB) model, where X denotes the water content, X_m the monolayer water content, a_w the water activity, K' and C' constants (van den Berg and Bruin 1981):

$$\frac{X}{X_m} = \frac{K' \cdot C' \cdot a_w}{(1 - C' \cdot a_w) \cdot (1 + (K' - 1) \cdot C' \cdot a_w)} \quad 4.32$$

The water-desorption isotherm was measured for samples with amorphous and crystalline lactose. Aliquots of the freeze-dried model system were stored at a relative humidity of 43% for the amorphous case and of 75% for the crystalline case to humidify the powder. The humidified powders were then stored at relative humidities <43% and <75%, respectively, to equilibrate the water activity under desorption conditions. The desorption isotherm was established analog to the sorption isotherm at 25°C.

4.8 Statistical analysis

All experiments and analyses were carried out in triplicate. The Student t -test was applied to estimate differences between mean values at a confidence level of 95%. In the following, mean values $\pm 95\%$ confidence levels will be reported.

The analysis of the residuals and the F-test were used to judge the goodness-of-fit of the reaction-kinetics models (van Boekel 2009). The F-test compares the lack-of-fit mean squares SS_{lof} to the pure error mean squares SS_{pe} . If a model fits the experimental data well, this ratio is small.

Model discrimination tests, i.e., ratios of likelihood functions (odds ratios), the Akaike criterion and the Bayesian information criterion, were used to evaluate which model fits best the experimental data (van Boekel 2009). The likelihood function L was defined as

$$L = \exp\left(-\frac{SS_r}{2s^2}\right) \quad 4.33$$

where SS_r denotes the residual sum of squares and s^2 the experimental variance calculated from the replicate experiments. The Akaike criterion is a measure for the relative performance of a model. Given that the number of data points in relation to the model parameters is <40 in this study, the corrected Akaike criterion AIC_C was used:

$$AIC_C = n \cdot \ln\left(\frac{SS_r}{n}\right) + 2 \cdot (p+1) + 2 \cdot (p+1) \cdot \left(\frac{p+2}{n-p}\right) \quad 4.34$$

where n is the sample size and p the number of parameters in the model. A lower AIC_C means that a model is more likely. In order to compare two models, the AIC_C difference of two models 1 and 2 ΔAIC_C is calculated (eq. 4.35) and in a next step the probability P_{AIC} that one model is more likely than the other (eq. 4.36). Expressed in another way, the evidence ratio ER (eq. 4.37) tells how much more likely one model is compared to the other.

$$\Delta AIC_C = AIC_1 - AIC_2 \quad 4.35$$

$$P_{AIC} = \frac{\exp(-0.5 \cdot \Delta AIC)}{1 + \exp(-0.5 \cdot \Delta AIC)} \quad 4.36$$

$$ER = \frac{1}{\exp(-0.5 \cdot \Delta AIC)} \quad 4.37$$

The Bayesian information criterion BIC is defined by eq. 4.38. If a model has a lower BIC than another model, it is more likely.

$$BIC = n \cdot \ln\left(\frac{SS_r}{n}\right) + p \cdot \ln n \quad 4.38$$

5 Results and discussion

5.1 Characterization of the model dairy-formulation

A profound knowledge of the material and physical characteristics of the model dairy-formulation is essential to understand its behavior during processing and the kinetics of lysine loss. In the case of spray-drying model dairy-formulation, relevant material and physical characteristics are viscosity, interfacial tension, density, solubility, sorption behavior, glass transition, crystallization and molecular mobility. To implement these characteristics in a model for lysine loss, drying kinetics and computational fluid dynamics, they have to be expressed as a function of temperature and concentration.

5.1.1 Material characteristics of the model dairy-formulation concentrate

The model dairy-formulation concentrate was characterized by its viscosity, interfacial tension, density and solubility as a function of its concentration and temperature. The dynamic viscosity (apparent viscosity at 200 s^{-1}) increased with increasing dry-matter content and decreased with increasing temperature (Fig. 5.1). The values are in the typical range reported for dairy products (Kessler 1996). The interfacial tension (Fig. 5.2) was lower than the interfacial tension of pure water ($72\text{ mN}\cdot\text{m}^{-1}$ at 25°C ; Gesellschaft Verfahrenstechnik und Chemieingenieurwesen 2006) due to the surface coverage by the proteins and slightly lower than values reported for skim milk (Kessler 1996). The interfacial tension decreased with increasing temperature but the concentration had no impact on the interfacial tension. Consequently, the surface was already completely covered by proteins at the lowest concentration. The density increased with an increasing concentration and decreasing temperature. However, concentration had a bigger impact than temperature. The density of the dry matter was calculated to be $1.57\text{ g}\cdot\text{cm}^{-3}$, taking into account the density of water and the mixture properties. In the literature, values of $1.52\text{ g}\cdot\text{ml}^{-1}$ are reported for non-fat milk solids and $1.58\text{ g}\cdot\text{ml}^{-1}$ for whey solids (Písecký 1997). Thus, the density of the model dairy-formulation agrees well with known densities of milk products.

Fig. 5.4 shows the solubility line of the model dairy-formulation together with the solubility of the protein and lactose content. The solubility increased with increasing temperature. At 20°C the determined solubility limit was $21.5 \pm 1.6\%$ dry matter. As a consequence, a concentration of 20% dry matter was chosen for the drying experiments in order to ensure complete solubility of the ingredients. The lactose and protein solubility increased with increasing temperature. At temperatures $<50^\circ\text{C}$ disproportionately more lactose precipitated than protein, leading to a lower lactose-protein ratio in the supernatant than in the precipitate. The lactose-protein ratio increased from 3.0:1 at 20°C to 4.2:1 at 40°C . At temperatures $\geq 50^\circ\text{C}$, the lactose-protein ratio of the supernatant agreed well with the overall lactose-protein ratio of 5:1, i.e., lactose and protein precipitated to the same degree. At 80°C , browning of the sample was observed during the experimental time which means that the Maillard reaction took place. Thus, this data point has to be taken with caution.

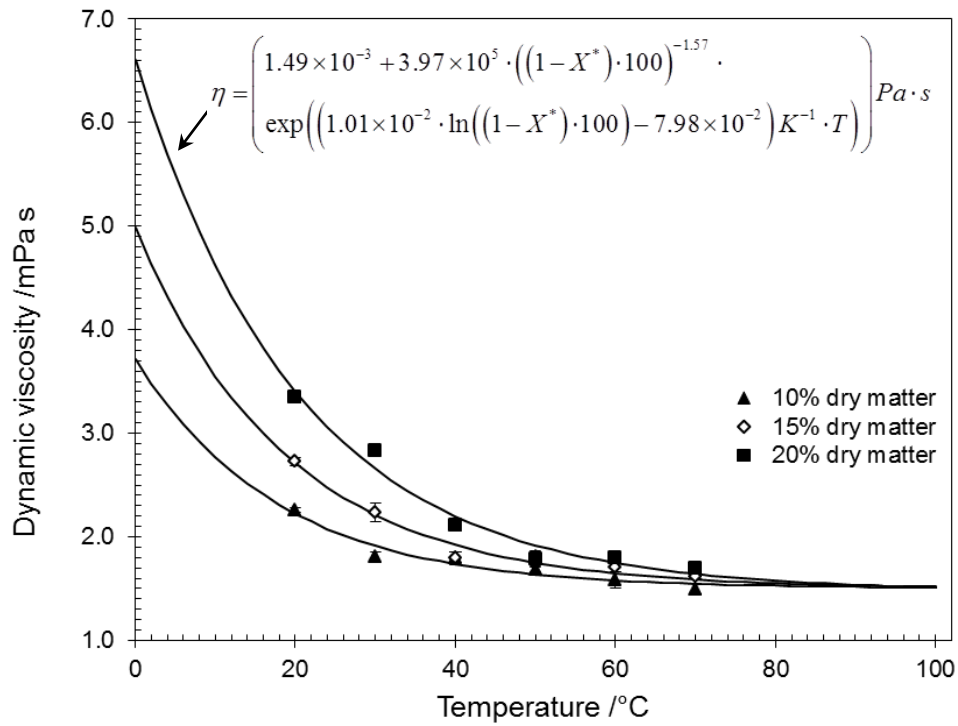


Fig. 5.1 Dynamic viscosity (apparent viscosity at 200 s^{-1}) as a function of the concentration and temperature

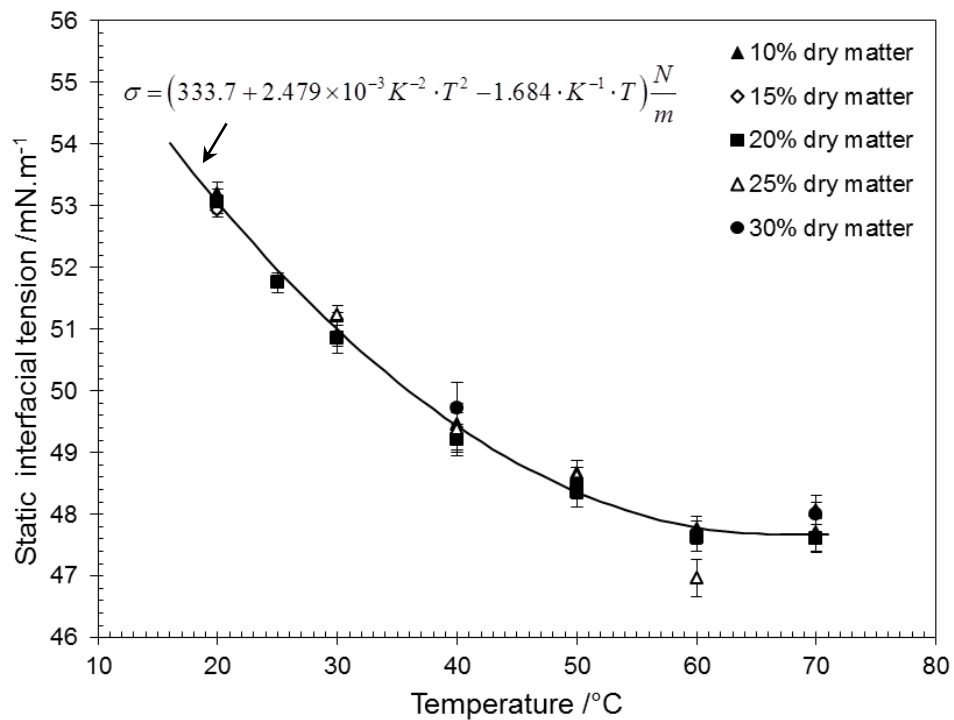


Fig. 5.2 Interfacial tension as a function of concentration and temperature

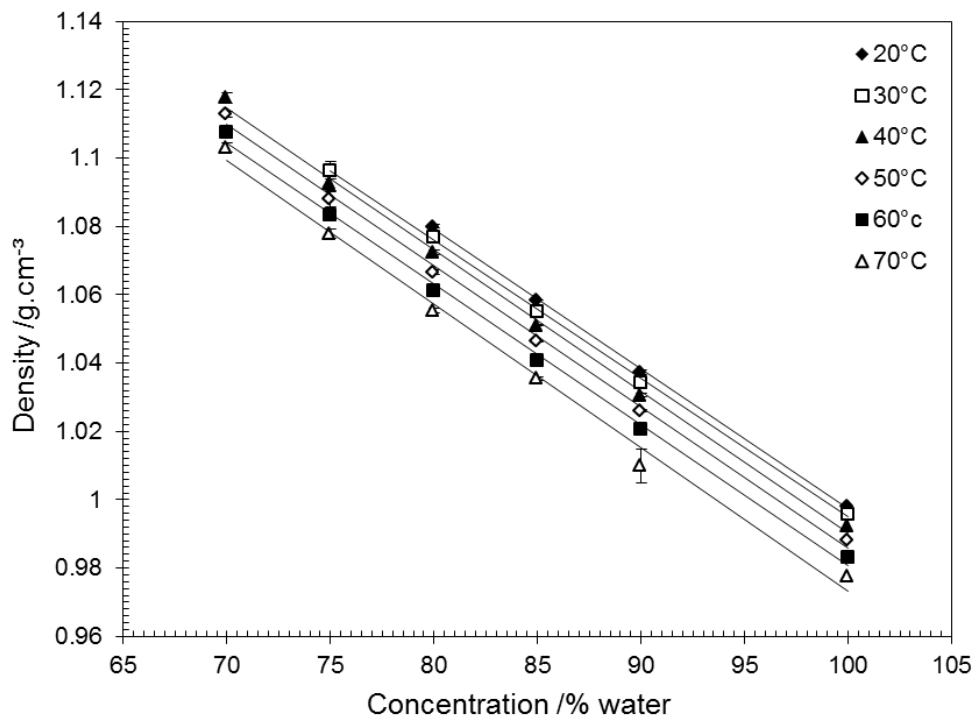


Fig. 5.3 Density as a function of concentration and temperature

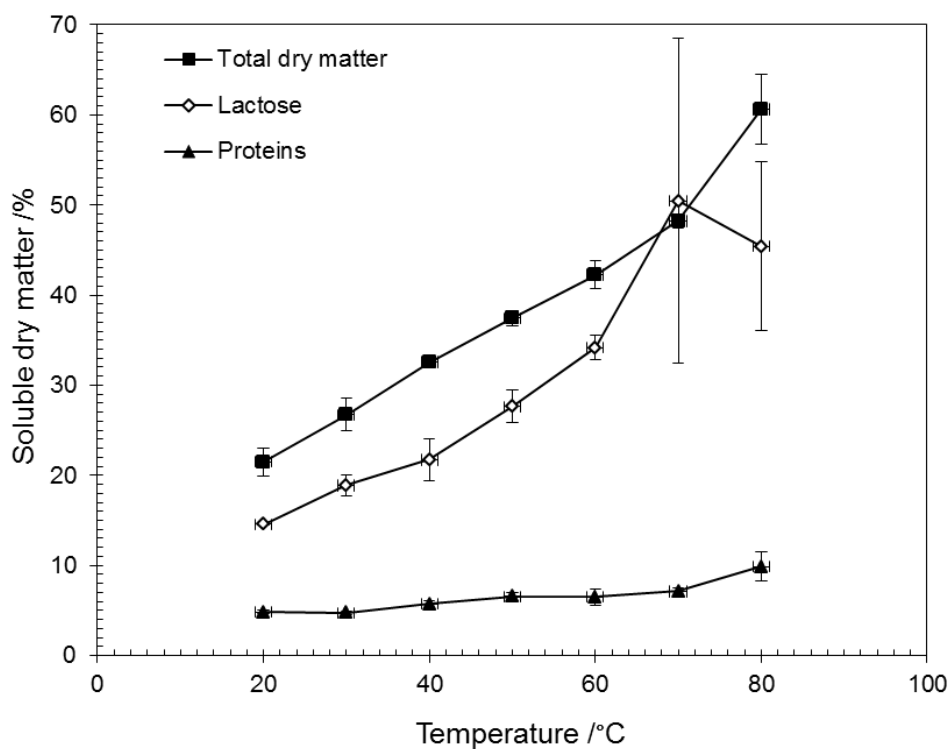


Fig. 5.4 Solubility of the model dairy-formulation concentrate as well as of the lactose and protein fractions

5.1.2 Sorption behavior and physical state⁵

When speaking of the physical state of powdered dairy products, usually the physical state of lactose is meant. Lactose contained in the model dairy-formulation might exist in the glassy, rubbery or crystalline states depending on temperature and water activity.

Fig. 5.5 and Fig. 5.6 show the experimental and calculated glass-transition curve and sorption isotherm of the model dairy-formulation with the standard composition. The Gordon & Taylor equation was fitted to the experimental data by non-linear regression (cf. eq. 4.21). The fitted parameters for the model system were $T_{gl} = 117.1 \pm 10.2^\circ\text{C}$ and $K = 5.6 \pm 1.0$ ($R^2 = 0.92$). The glass-transition temperature of the model dairy-formulation lies in the same range as the glass-transition temperature reported for pure lactose (Mazzobre et al. 2003, Roos 2010). This confirms the assumption that the physical state of the model dairy-formulation is governed by the physical state of lactose. At room temperature (25°C), the model dairy-formulation is in the glassy state for water activities of ≤ 0.43 . The experimental water sorption isotherm at 25°C displays a rupture between the water activities of 0.43 and 0.53 indicating the crystallization of lactose. During crystallization sorbed water is released, which leads to a decrease of the water content at constant water activity conditions. The Guggenheim-Anderson-de-Boer (GAB) equation (cf. chapter 4.7.12) was fitted to the experimental sorption isotherm for water activities ≤ 0.43 , i.e., for the amorphous range. The monolayer value X_m was 4.5% db, the constant K' was 71.8 and the constant C' was 1.2. In the literature, monolayer values X_m of 4.9% (Bronlund and Paterson 2004) and of 4.1% (Miao and Roos 2004) can be found for lactose powders and of 4.3% for skim milk powder (Timmermann et al. 2001). These values are in good accordance with this study as well as the values of the constant C' of 1.2 (Bronlund and Paterson 2004) and of 1.4 (Miao and Roos 2004) for lactose powders and of 0.9 for skim milk powder (Timmermann et al. 2001). In contrast, the constant K' differs between the mentioned studies with values of 3.23 (Bronlund and Paterson 2004) and 7.54 (Miao and Roos 2004) for lactose powders and of 38.0 for skim milk powder (Timmermann et al. 2001). Especially the data points at low water activities have an impact on the constant K' . Therefore, the observed differences can be attributed to the different experimental ranges and to uncertainties in the determination of the water contents at low water activities.

Increasing the temperature to 40 and 60°C does not lead to any significant changes in the sorption isotherm (Fig. 5.5). At 60°C , severe browning of the samples occurred while the sorption isotherm was established (Fig. 5.7). No hysteresis can be observed when the sorption isotherm at 25°C is compared with the desorption isotherms of amorphous powders at 25°C (Fig. 5.8). In the same way, the desorption isotherm of crystalline powder agrees well with the crystalline part of the sorption isotherm.

⁵ Partly published in: Schmitz I, Gianfrancesco A, Kulozik U, Foerst P (2011) Kinetics of lysine loss in an infant formula model system at conditions applicable to spray drying. *Drying Technology* 29(16):1876-1883; Schmitz-Schug I, Gianfrancesco A, Kulozik U, Foerst P (2013) Physical state, molecular mobility and chemical stability of powdered dairy formulations. *Food Research International* 53(1):268-277

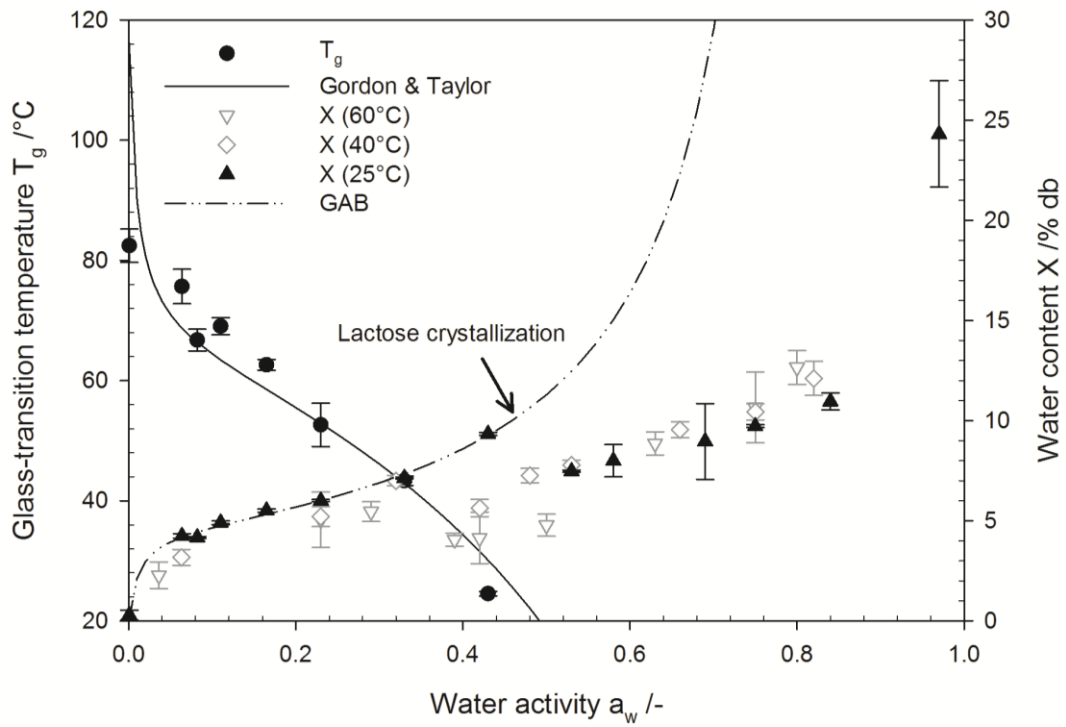


Fig. 5.5 Glass-transition curve and water-sorption isotherm at 25°C, 40°C and 60°C of the model dairy-formulation with the standard composition

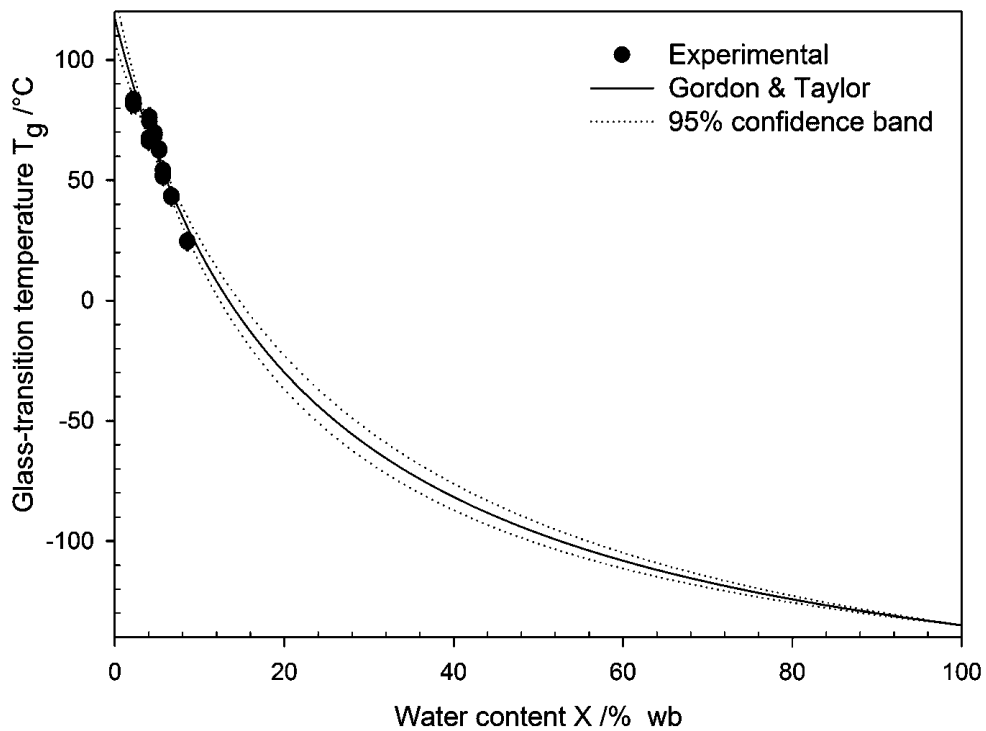


Fig. 5.6 Glass transition curve: experimental values and Gordon & Taylor equation



Fig. 5.7 Browning of the model dairy-formulation during equilibration of the sorption isotherm at 60°C (the values written on the vials indicate the water activity)

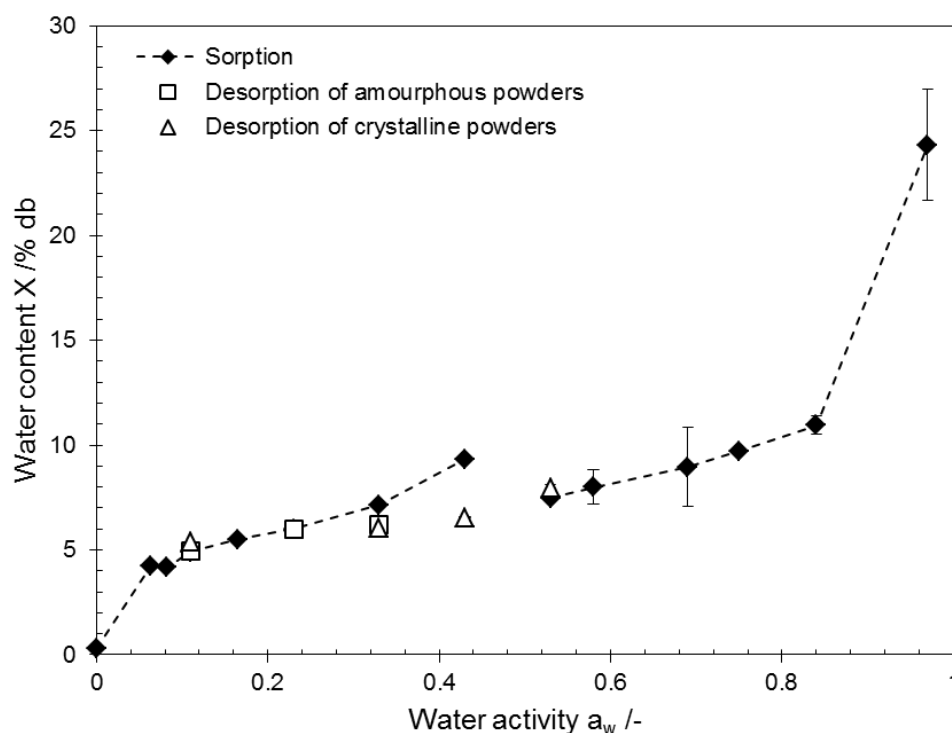


Fig. 5.8 Sorption and desorption isotherms of the model dairy-formulation at 25°C

Crystallization kinetics was determined by isothermal differential scanning calorimetry. The time at the peak maximum was taken as crystallization delay, i.e., after this timespan lactose crystallized at a given humidity and temperature in the model dairy-formulation. From Fig. 5.9 it becomes evident that the crystallization delay was a function of the temperature difference to the glass-transition temperature. While the measured crystallization delay was in the range of several minutes for $T - T_g > 30^\circ\text{C}$, a sharp rise of the crystallization delay was observed at $T - T_g$ of 20-30°C. Langrish (2008) observed a similar trend for pure lactose. The Williams-Landel-Ferry equation (WLF, Williams et al. 1955) has often been criticized because it does not account for the concentration, implicitly implies a zero-order reaction and disregards nucleation and crystal growth (Langrish and Wang 2009). Nevertheless, it was used in this study to model the crystallization delay because it is a rather simple approach that describes the experimental data reasonably well. The procedure of Mazzobre et al. (2001) was

used to fit the WLF equation to the experimental data. It avoids extrapolation to the crystallization delay at the glass-transition temperature T_g by using instead a reference temperature $T_r = T_g + 55.46$ K. Thus, C_{2r} was evaluated to be 105.46 K and C_{1r} to be 3.58 ± 1.68 by linear regression analysis. Converting these constants to the equivalent constants with the glass-transition temperature as reference temperature gave $C_1 = 7.55$ and $C_2 = 50$ K. Hence, the WLF constants are material-specific in the case of the model dairy-formulation because they differ from the “universal” WLF constants $C_2 = 51.6$ K and $C_1 = 17.44$ reported by Williams et al. (1955). The use of material-specific WLF constants is widely spread and the validity of the “universal” constants is challenged in the literature (Aschenbrenner et al. 2012, Langrish 2008, Langrish and Wang 2009, Mazzobre et al. 2001, Peleg 1992). The “universal constants” are queried because they were obtained by averaging data of a certain number of polymers. However, this does not inevitably mean that the “universal” constants are valid for any kind of product. Contrariwise, it seems quite logical that in complex systems additional factors are interacting. For example, Langrish and Wang (2009) found similar crystallization delays for lactose and sucrose while the glass-transition temperatures were different. Moreover, crystallization delays of this study are longer than the crystallization delays reported for pure lactose by Mazzobre et al (2003). As will be discussed later, this divergence can be attributed to the presence of proteins in the model dairy-formulation of this study.

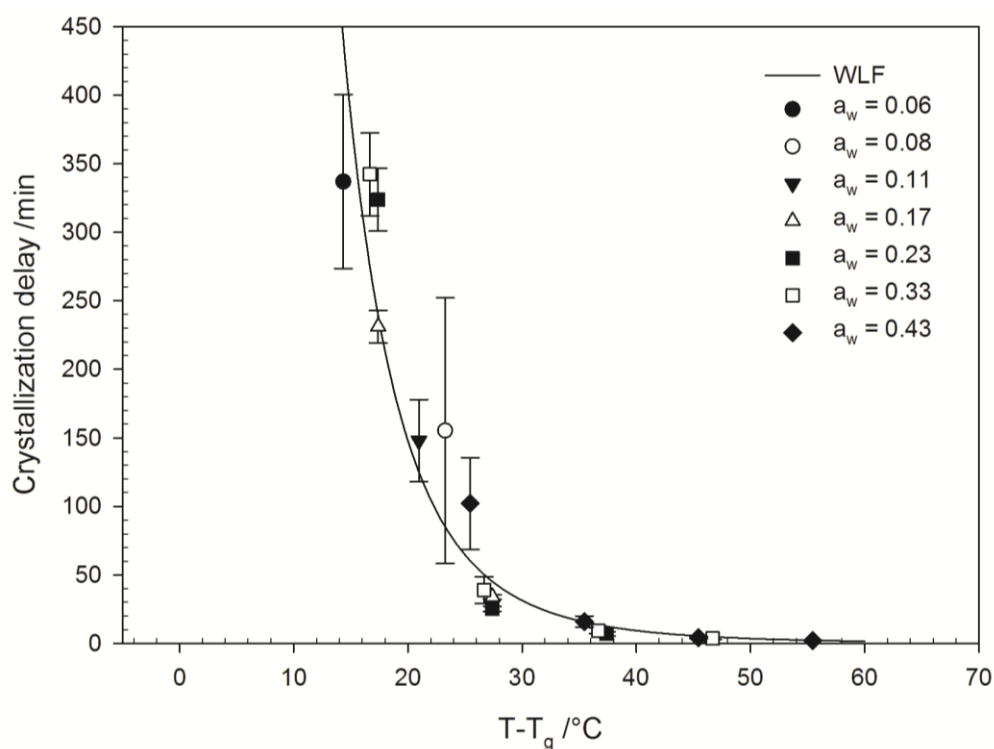


Fig. 5.9 Lactose-crystallization delay of the model dairy-formulation with the standard composition

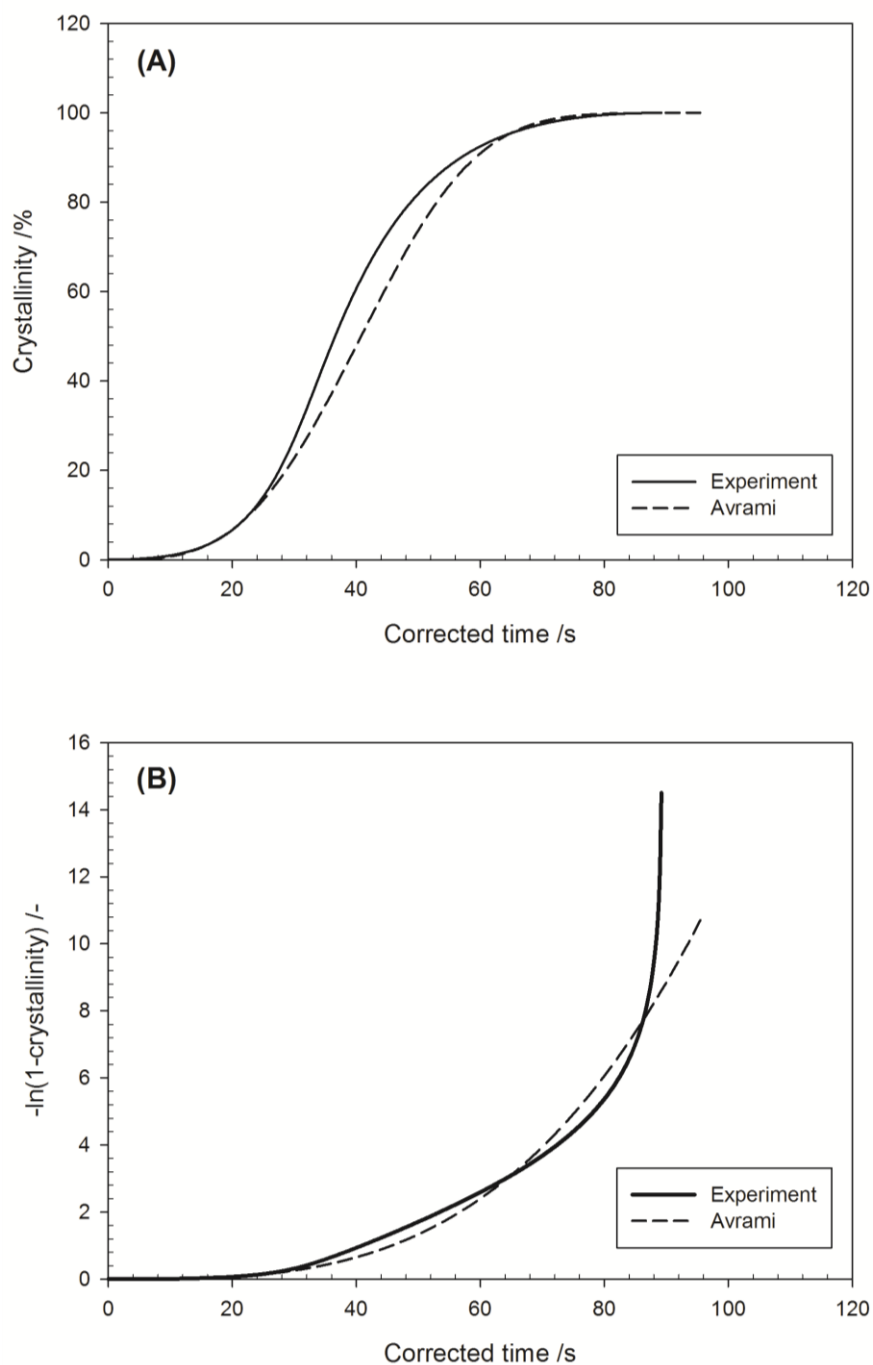


Fig. 5.10 Lactose crystallization kinetics at $a_w = 0.43$ and $T = 80^\circ\text{C}$ modeled with the Avrami-equation

The kinetics of lactose crystallization was analyzed by integrating the crystallization peaks of the isothermal differential scanning calorimetry measurements (Fig. 5.10A). The Avrami equation (Avrami 1940) is often used to model crystallization kinetics. However, it was not possible to fit the Avrami equation to the experimental data of this study. From the transformed crystallinity in Fig. 5.10B, which is often used to fit the Avrami equation to experimental data, it becomes obvious that the experimental data shows two shifts in the slope, the first at about 30 s and the second at about 85 s. In contrast, the Avrami equation predicts a smooth curve. This trend might be explained by the formation of different crystal forms

which can be α -lactose monohydrate, α -lactose anhydrate, β -lactose anhydrate or mixed crystals of α - and β -lactose. The formation of different crystal forms will be discussed more in detail below. Jouppila et al. (1997) observed similar crystallization characteristics for pure lactose powders and attributed the divergence from the Avrami equation to restricted water removal and structural changes. Difficulties with applying the Avrami equation have often been reported in the literature (Ibach and Kind 2007, Jouppila et al. 1997, Langrish 2008, Mazzobre et al. 2001). Ibach and Kind (2007) could only fit the Avrami equation to lactose crystallization in whey and whey-permeate powder at relative humidities $\leq 70\%$ and temperatures of 50-100°C. In contrast, Jouppila et al. (1997) only managed to model lactose crystallization in skim-milk powder with the Avrami equation at relative humidities $\geq 66.2\%$. Kedward et al. (2000) and Mazzobre et al. (2001) concluded that the different lactose crystal forms had a major impact on the crystallization characteristics and, consequently, the Avrami analysis could only be used as a rough approximation. In conclusion, lactose crystallization is a rather complex process that can apparently only be modeled with the Avrami equation under specific conditions.

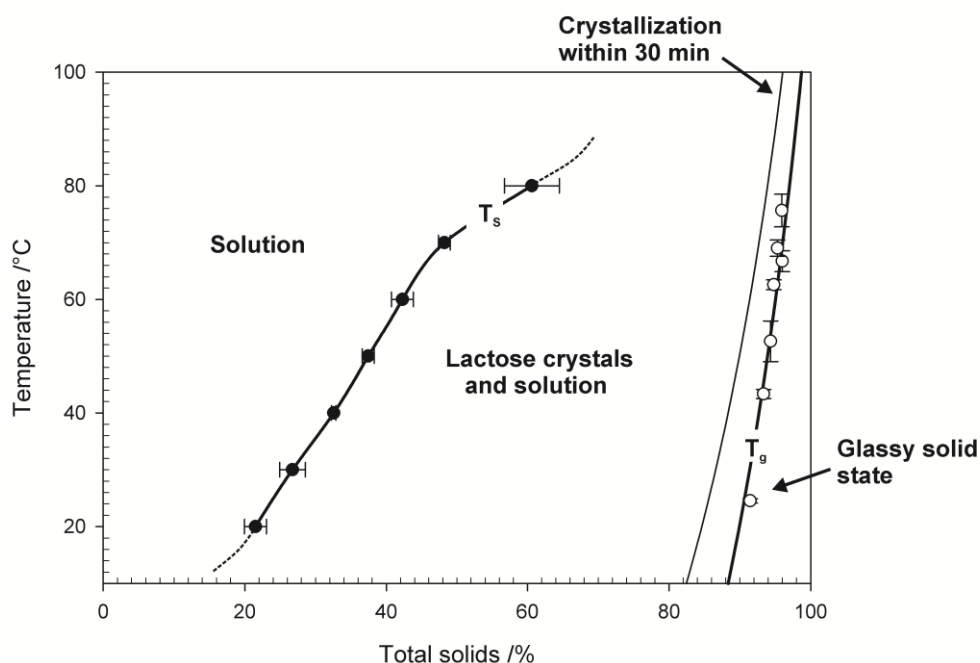


Fig. 5.11 The state diagram of the model system (the error bars indicate a confidence limit of 95%)

The information concerning the solubility, glass transition and crystallization of the model dairy-formulation is summarized in the state diagram (Fig. 5.11). Several regions can be distinguished in the state diagram. Left of the solubility line, the model system exists as a solution. Between the solubility line and the glass-transition curve, the model system contains crystalline structures. Below the glass-transition curve, the model system, i.e., lactose, can be in the glassy amorphous state. During drying, the glassy state is reached when the water is removed sufficiently fast. Otherwise lactose will be crystalline after drying. After conventional spray drying lactose is mainly in the glassy state (Písecký 1997). When the temperature is above the glass-transition temperature, lactose will crystallize within 30 min at the conditions indicated in Fig. 5.11.

5.1.3 Molecular mobility⁶

The transversal relaxation time T_2 determined by low resolution $^1\text{H-NMR}$ was taken as a measure for the molecular mobility or, more precisely, for the proton mobility in the model dairy-powder. Longer transversal relaxation times correspond to higher molecular mobilities. In Fig. 5.12 the transversal relaxation time T_2 of the model dairy-powder (standard composition) is depicted as a function of water activity and temperature. The samples were tempered for 30 min at the analysis temperature before the analysis. As could be expected, the transversal relaxation time T_2 and accordingly the molecular mobility increased significantly with increasing water activity at water activities ≥ 0.53 . Comparing this with Fig. 5.5 reveals that the samples in this water activity range had already been crystalline before heating. At water activities ≤ 0.43 , which corresponds to samples that were glassy before heating, the molecular mobility remains almost constant. In contrast, the impact of the temperature is much less pronounced for the whole water activity range.

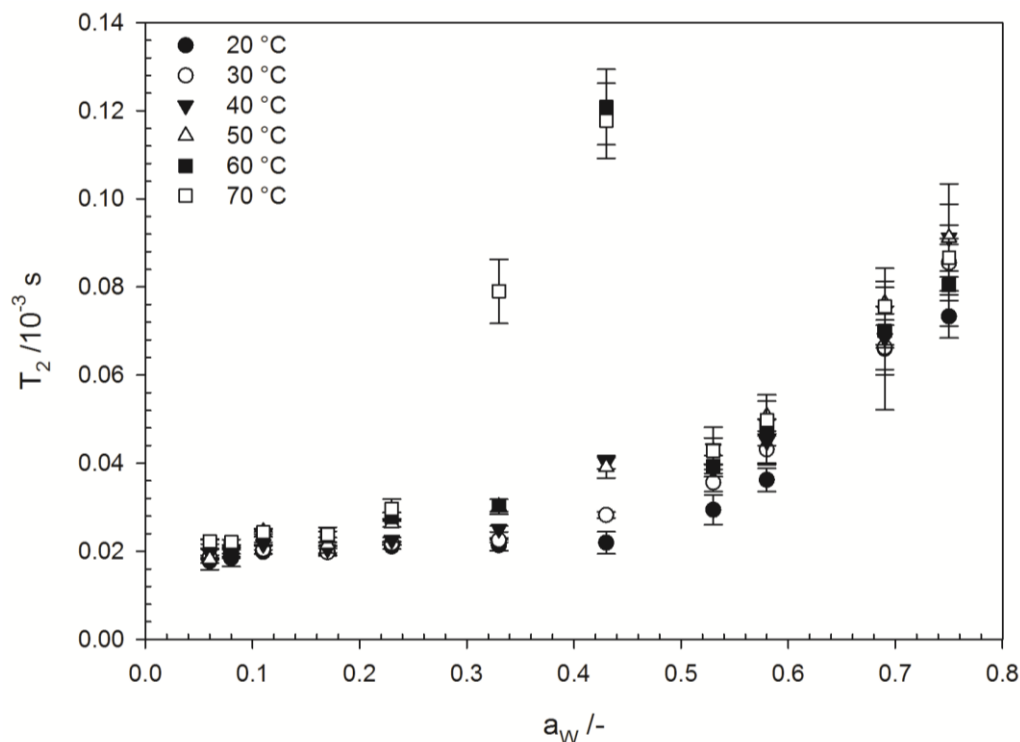


Fig. 5.12 Molecular mobility expressed as transversal relaxation time T_2 as a function of water activity and temperature after heating the model dairy-powder with the standard composition for 30 min

Of particular note are the molecular mobilities at $a_w = 0.33/T = 70^\circ\text{C}$, $a_w = 0.43/T = 60^\circ\text{C}$ and $a_w = 0.43/T = 70^\circ\text{C}$ which deviate significantly from the trend observed from the majority of the results. This can be explained by the physical state which becomes obvious from Fig. 5.13. For all water activities, mobility is low in the glassy state and rises after glass transition

⁶ Published in: Schmitz-Schug I, Gianfrancesco A, Kulozik U, Foerst P (2013) Physical state, molecular mobility and chemical stability of powdered dairy formulations. Food Research International 53(1):268–277

in the rubbery state. In general, crystalline samples are characterized by a higher molecular mobility than samples in the rubbery state. However, the crystalline region can be divided into two zones: samples that had already been crystalline before the heating period and samples that became crystalline during the heating period.

When the crystallization of lactose takes place during the heating time, a steep rise in the relaxation time is noticed in the transition zone from the rubbery to the crystalline state ($T - T_g \approx 26^\circ\text{C}$). During crystallization, bound water is liberated leading to the plasticization of the matrix, thus increasing the mobility. The NMR measurements were made in closed tubes so that the water content was fixed and water activity increased when sorbed water was released. The water content of amorphous samples with a water activity of 0.43 was between the water contents of crystalline samples of $a_w = 0.69$ and 0.75. The water content of amorphous samples with $a_w = 0.33$ was just below the water content of crystalline samples with $a_w = 0.53$. Consequently, the molecular mobility of samples that had crystallized during heating before the analysis was higher than the mobility of samples that had already crystallized while equilibrating the water activity at 25°C , i.e., that had already been crystalline before heating. These distinct mobility characteristics might be attributed to the formation of different lactose-crystal forms.

Lactose-crystallization forms have been studied by various research groups. It was found that α -lactose monohydrate, the most stable lactose crystal, is preferentially formed at lower crystallization temperatures, given a sufficient water content, as well as mixed anhydrous crystals of α - and β -lactose in a molar ratio of 5:3 (Ibach and Kind 2007, Jouppila et al. 1997, Jouppila et al. 1998, Nijdam et al. 2007). At lower humidities, β -lactose anhydrate was measured, too. At higher temperatures, β -lactose anhydrate and mixed crystal forms developed which were not stable under normal storage conditions. The amount of α -lactose monohydrate also depended on the rate of mutarotation in the amorphous state and on the rate of hydration of α -lactose during crystallization (Nijdam et al. 2007). When crystallizing skim-milk powder, Chiou and Langrish (2007) noted that other than β -lactose, α -lactose could only be detected after 118 h with a maximum at 168 h. After this time, α -lactose transformed to β -lactose. Moreover, Letho et al. (2006) found differences in the crystal forms of recrystallized amorphous and partially crystalline lactose. The latter also contained anhydrate crystals. To sum up, the development of the lactose-crystal composition depends on a complex set of factors. Coming back to this study, it seems probable that the lactose crystals formed during equilibration of the water activity at 25°C differ from the crystal forms that develop during heating at $60\text{--}70^\circ\text{C}$ in closed systems. As a consequence, this suggests that different crystal forms, or, more precisely, the amount of hydrate water bound to the crystals leads to the differences in molecular mobility of crystalline samples. So far no data has been available on the impact of the lactose crystal form on molecular mobility expressed as transversal relaxation time. Measurements of the spin-lattice relaxation time T_1 of crystalline lactose revealed that the spin-lattice relaxation time of α -lactose monohydrate is significantly longer than that of β -lactose anhydrate (Lubach et al. 2007). In general, the spin-lattice relaxation time T_1 correlates inversely with the transversal relaxation time T_2 in crystalline systems (Hinrichs 2004, Lubach et al. 2007). Thus, this supports the hypothesis that the differences in molecular mobility are due to the formation of different crystal forms. Further measurements are needed to evaluate the relation between specific lactose crystal forms and molecular mobility expressed as transversal relaxation time.

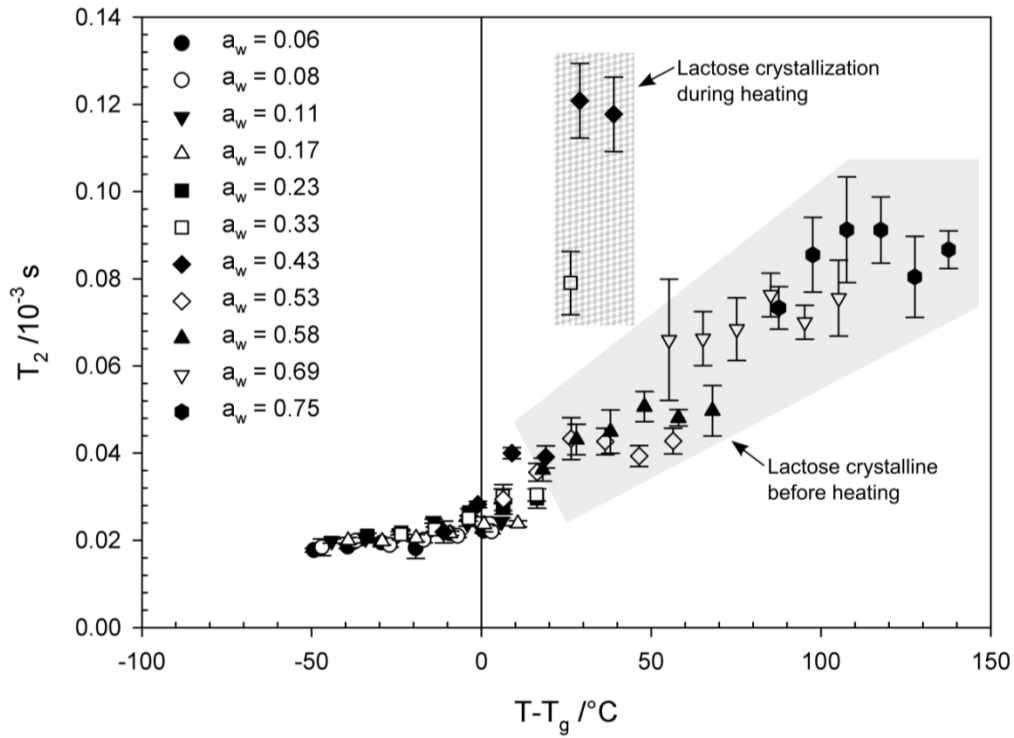


Fig. 5.13 *Molecular mobility expressed as transversal relaxation time T_2 as a function of the temperature difference from the glass-transition temperature after heating the model dairy-powder with the standard composition for 30 min*

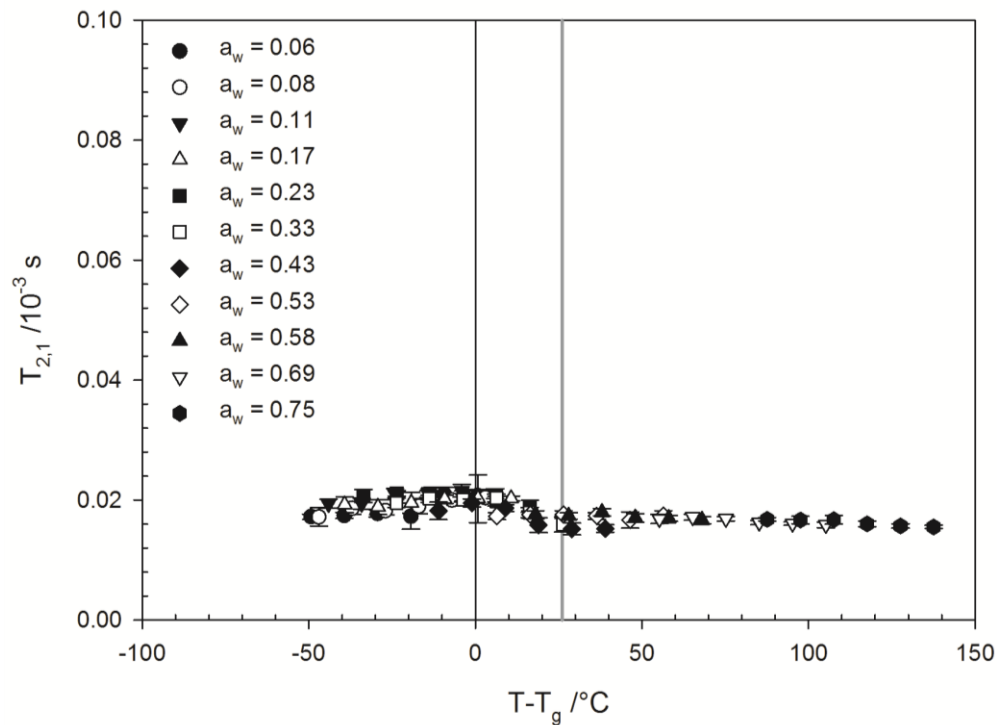


Fig. 5.14 *Transversal relaxation time $T_{2,1}$ of the immobile component as a function of the temperature difference from the glass-transition temperature after heating the model dairy-powder with the standard composition for 30 min ("applies only to water activities ≤ 0.43)*

Detailed analysis of the transversal relaxation times and fractions of the immobile and mobile component as well as of the second moment provides further insight into the mobility conditions of the model dairy-powder. Fig. 5.14 shows the transversal relaxation time $T_{2,1}$ of the immobile component of the model dairy-powder (standard composition) after heating for 30 min at the analysis temperature T as a function of the temperature difference from the glass-transition temperature T_g . The immobile component can be ascribed to non-exchangeable protons of proteins and polysaccharides (Mariette 2009). The transversal relaxation time $T_{2,1}$ of the immobile component remains relatively constant over the whole experimental range independently of the physical state. The fluctuations and uncertainties are slightly higher in the glassy state compared with the crystalline state, which is probably due to the shorter overall relaxation time and thus, due to the higher uncertainty in fitting the envelope curve to the experimental NMR signal. Hence, water activity, temperature and physical state do not have a significant impact on the molecular mobility of the immobile component.

Matters are quite different when the transversal relaxation time $T_{2,2}$ of the mobile part is considered (Fig. 5.15). The mobile part is usually ascribed to protons of water and to exchangeable protons of proteins, polysaccharides or carbohydrates (Mariette 2009). Here, a similar pattern to the mean transversal relaxation time T_2 is observed that is characterized by short relaxation times in the glassy state and increasing relaxation times above the glass-transition temperature. Thus, the physical state has a major impact on the transversal relaxation time $T_{2,2}$ of the mobile component. Again, the relaxation times of the conditions $a_w = 0.33/T = 70^\circ\text{C}$, $a_w = 0.43/T = 60^\circ\text{C}$ and $a_w = 0.43/T = 70^\circ\text{C}$ were longer than the relaxation times of the other crystalline conditions. This can be explained in the same way as for the mean relaxation time T_2 . Other than the transversal relaxation times, the proton fractions of the immobile component f_S and of the mobile component f_L remained relatively constant in the whole experimental range. The proton fraction of the immobile component f_S totaled about 90% and the proton fraction of the mobile component f_L about 10%, accordingly.

Crystalline model dairy-powders can clearly be distinguished from amorphous powders, i.e., glassy or rubbery ones, when the second moment M_2 is regarded (Fig. 5.16). The strength of hydrogen dipolar interactions is represented by the second moment M_2 (Mateus et al. 2007). The second moment decreased linearly with an increasing temperature difference from the glass-transition temperature $T-T_g$ when lactose was in the glassy or rubbery state. This means that the strength of hydrogen dipolar interactions decreased. These findings are in accordance with results reported by Roudaut et al. (2009) for gelatinized starch and starch-sucrose mixtures and by Aeberhardt et al. (2007) for oligosaccharide-water mixtures. Crystallization of lactose led to a step change in the second moment M_2 which rose to $7.6 \times 10^9 \text{ s}^{-2}$. This is probably due to dipole forces between the lactose molecules in the crystal lattice. The second moment remains constant when lactose is crystalline independently of water content and temperature. Consequently, low resolution $^1\text{H-NMR}$ represents a fast and easy-to-handle method to measure lactose crystallization in dairy powders.

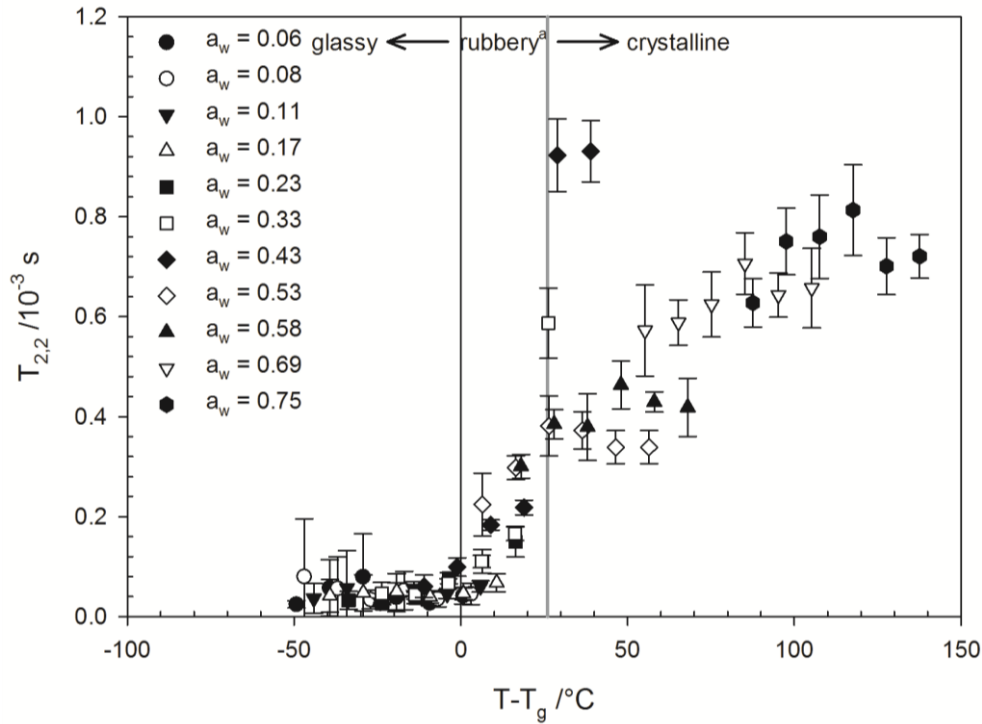


Fig. 5.15 Transversal relaxation time $T_{2,2}$ of the mobile component as a function of the temperature difference from the glass-transition temperature after heating the model dairy-powder with the standard composition for 30 min (^aapplies only to water activities ≤ 0.43)

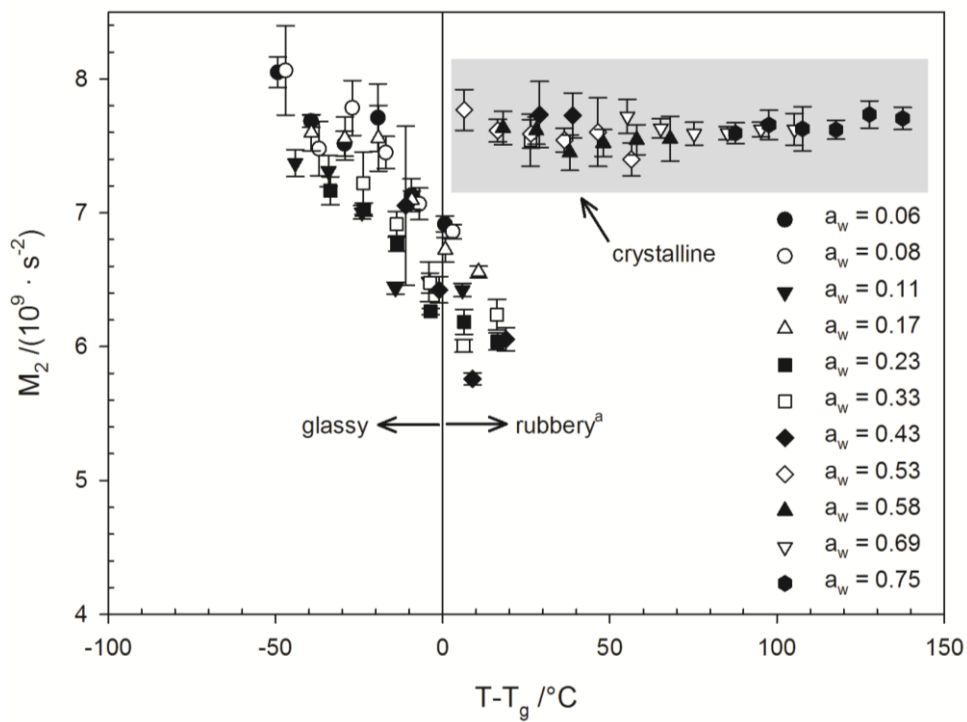


Fig. 5.16 Second moment M_2 as a function of the temperature difference from the glass-transition temperature $T - T_g$ after heating the model dairy-powder with the standard composition for 30 min

5.1.4 Impact of the protein and lactose content on the physical state of lactose⁷

The glass-transition temperature T_g decreased with increasing lactose content although the water content was not influenced at a water activity of 0.33 (at 25°C; Fig. 5.17). Consequently, the milk proteins retarded the glass transition. This led to higher glass-transition temperatures at higher protein contents. Similar observations were made for spray-dried mixtures of lactose and whey-protein isolate by Haque and Roos (2004). At the highest casein content (WP:C = 20:80), a lower glass-transition temperature was determined compared to the standard composition. This is probably due to the higher water content of this matrix composition at a water activity of 0.33 because water decreases the glass-transition temperature.

The delay of lactose crystallization for the different lactose-protein ratios as a function of the temperature is displayed in Fig. 5.18. No lactose crystallization was observed within 6 hours in this temperature range for a lactose-protein ratio of 3:1. Lactose crystallization was accelerated with increasing lactose content. Consequently, the proteins contained in the dairy formulation impede lactose crystallization which is in accordance with results of Ibach and Kind (2007) for whey-permeate and whey powders and of Haque and Roos (2004) for spray-dried mixtures of lactose and whey-protein isolate. Chiou and Langrish (2007) attributed the reduced crystallization rate in skim-milk powder to water being bound to proteins instead of interacting with sugars. At a whey protein-casein ratio of 40:60, the crystallization delay was shorter than at the standard ratio of 60:40. However, increasing the casein content further did not further decrease the crystallization delay.

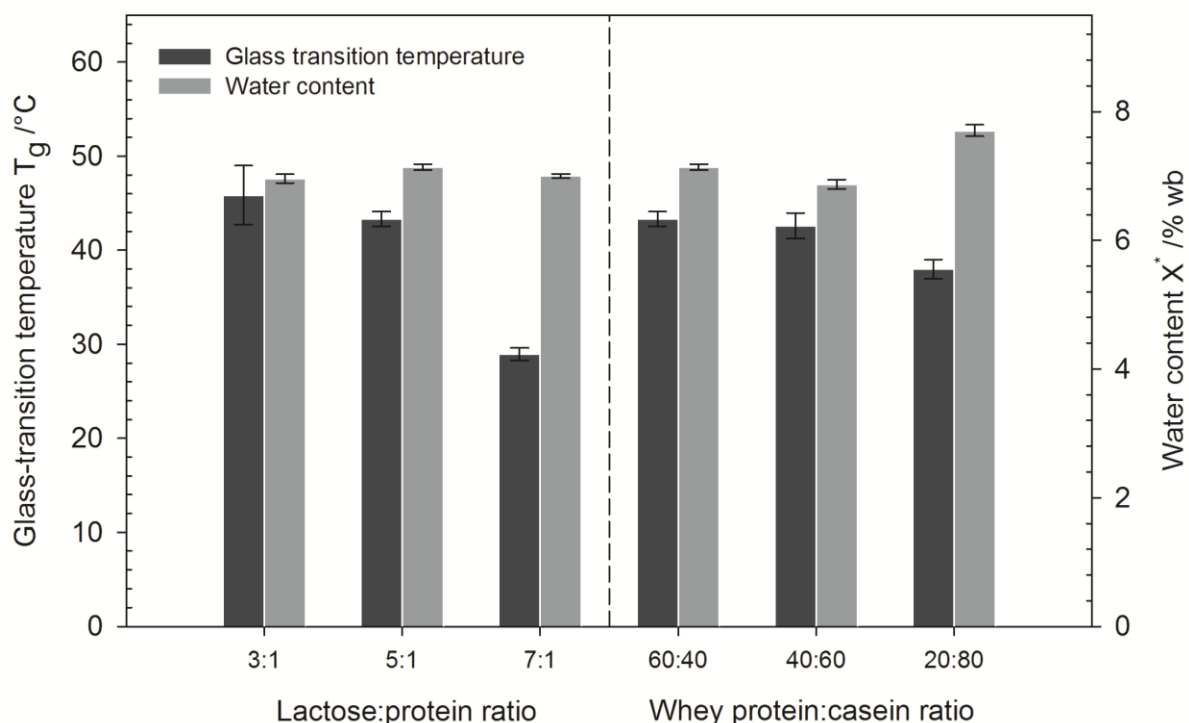


Fig. 5.17 Glass-transition temperature T_g and water content X at a water activity of 0.33 (at 25°C)

⁷ Partly published in: Schmitz-Schug I, Gianfrancesco A, Kulozik U, Foerst P (2013) Physical state, molecular mobility and chemical stability of powdered dairy formulations. Food Research International 53(1):268–277

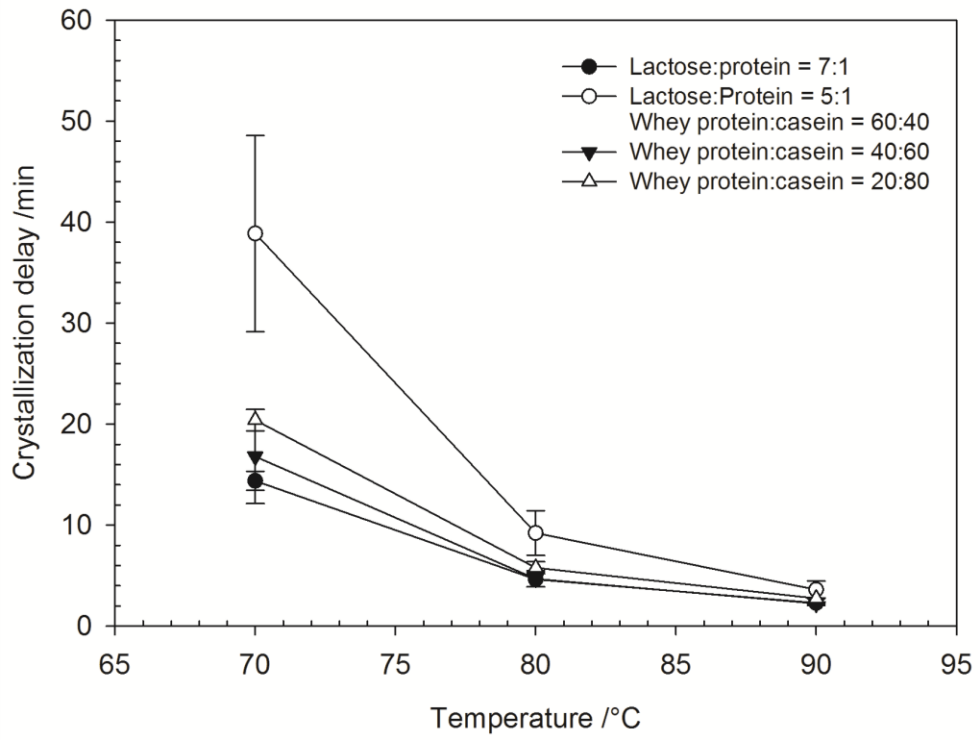


Fig. 5.18 Crystallization delay at a water activity of 0.33 (at 25°C)

5.2 Thermally-induced lysine loss

Thermal stress is one of the main reasons for degradation reactions during spray drying (Langrish 2007). So far, little is known about the loss of available lysine at conditions relevant to spray drying. This part will focus on thermally-induced lysine losses at constant concentrations. The impact of concentration, physical state, molecular mobility and composition will be elaborated.

5.2.1 Impact of the heating conditions⁸

Lysine loss was monitored during the heating of the model system at 60-90°C for 30 s to 30 min. During heating the water content of the model system was kept constant. This was ensured by using hermetically closed heating cans. However, in the event of lactose crystallization during heating, sorbed water was released and the water activity increased. When dealing with systems existing in the amorphous and crystalline states, the same water content can be associated with different physical states and water activities. For this reason, water activity will be used to describe the experimental results. As it is possible that water activity evolves along the experiments, water activities reported in the following correspond to the original water activities at 25°C before heating. Compared to the particle residence-time during spray drying, much longer heating times were chosen in order to obtain a higher extent of lysine loss. This allows a more detailed characterization of lysine loss, which can also be applied to further processing steps.

Lysine loss occurred in the model system for all conditions that had been applied. Lysine loss at a water activity of 0.43 (at 25°C), which corresponds to a water content of $8.54 \pm 0.07\%$ wb, is plotted in Fig. 5.19. Lysine loss increased with increasing heating temperature and heating time. A sharp increase in lysine loss was measured at the beginning of heating, corresponding to the time scale relevant for spray drying. After 2-3 min, lysine loss proceeded more slowly. After 30 min of heating, lysine loss reached $70.4 \pm 2.4\%$ at 90°C, $50.4 \pm 3.0\%$ at 80°C, $27.0 \pm 5.8\%$ at 70°C and $10.9 \pm 8.2\%$ at 60°C. Lysine losses followed a similar pattern at all other water activities studied (data not shown). However, the extent of lysine loss and the temperature dependence were a function of the water activity as will be shown in the following.

With the aim of assessing the impact of the concentration on lysine loss, Fig. 5.20 shows the extent of lysine loss after 30 min of heating. For all water activities, lysine losses increased with increasing temperature. Rather small lysine losses were measured at 60°C (max. $13.8 \pm 3.5\%$) and the impact of the water activity was not significant. At 70°C, lysine losses were significantly higher than at 60°C with a lysine loss of up to $29.2 \pm 5.7\%$. At 80°C lysine loss reached $53.8 \pm 6.1\%$ and at 90°C $81.1 \pm 1.1\%$. A maximum in lysine loss can be distinguished at each temperature, except at 60°C, where no significant impact of the water activity can be observed. The location of the maximum depends on the temperature. At 70°C the maximum is found at a water activity of about 0.43. At 80°C and 90°C, the maximum is shifted to

⁸ Partly published in: Schmitz I, Gianfrancesco A, Kulozik U, Foerst P (2011) Kinetics of lysine loss in an infant formula model system at conditions applicable to spray drying. *Drying Technology* 29(16):1876-1883; Schmitz-Schug I, Kulozik U, Foerst P (2014) Reaction kinetics of lysine loss in a model dairy formulation as related to the physical state. *Food and Bioprocess Technology* 7:877-886

lower water activities in the range of 0.2. As will be demonstrated in the next chapter, these differences are due to the physical state of the system.

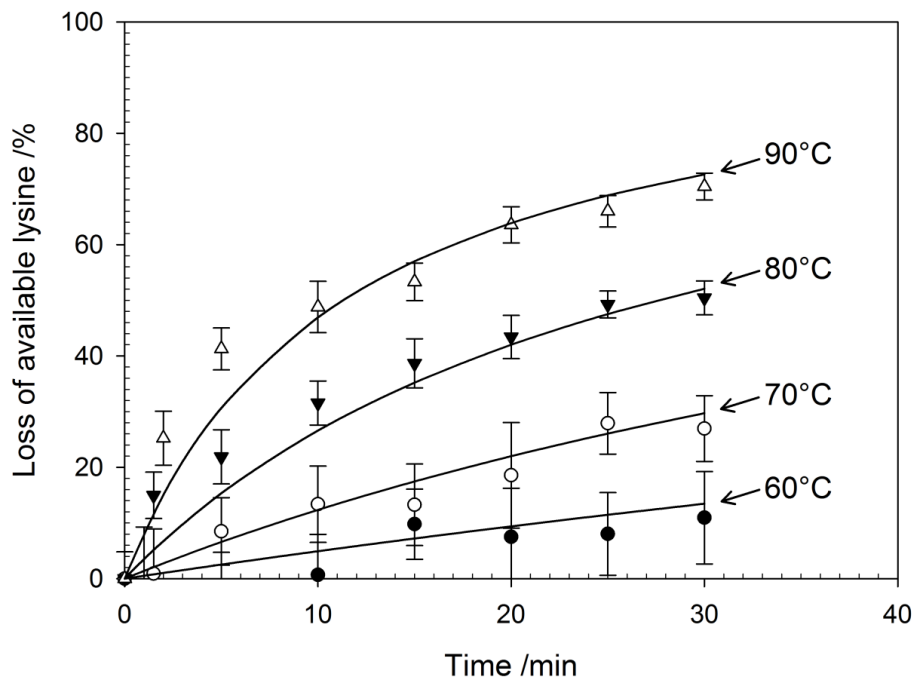


Fig. 5.19 Heat-induced lysine loss at a water activity of 0.43 at 25°C, i.e., a water content of $8.54 \pm 0.07\%$ wb

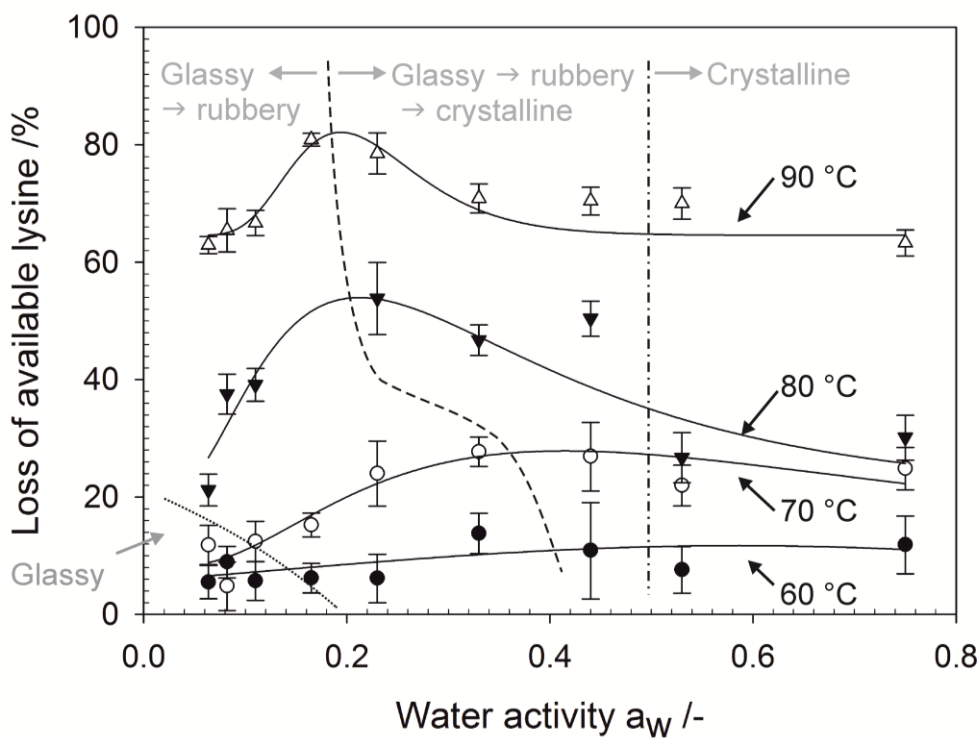


Fig. 5.20 Lysine loss after 30 min of heating as a function of the concentration and the physical state

The lysine-loss pattern obtained during this study is comparable to the results published in other studies that investigated the lysine loss in dairy products or simple model systems for various temperature-time combinations (Fenaille et al. 2003, Ge Pan and Melton 2007, Morgan et al. 2005, Vuataz 1988). However, the model system and the experimental conditions of this study differ from those of the cited studies. As this approach aims at developing a tool to optimize spray drying with regard to lysine loss, the parameter range was adapted to the needs for spray drying. Especially the time scale is much shorter and the temperatures are higher. The maximum in lysine loss is shifted to lower water activities in this study compared to the studies cited above. For example, Malec et al. (2002) found the highest reaction rates at a water activity of 0.52 in a milk-like system at 37 and 50°C at prolonged heating times (several days to some weeks). In agreement with this study, they could not determine significantly different reaction rates at 60°C for water activities between 0.33 and 0.98. To further analyze the obtained kinetics of lysine loss, it is necessary to consider the physical state of lactose.

5.2.2 Role of physical state⁹

The physical state of the system is mainly determined by the physical state of the lactose contained in the model dairy-formulation (cf. chapter 5.1.2). According to the experimental conditions, lactose can be in the glassy, rubbery or crystalline states. The physical state at the experimental conditions is shown in Fig. 5.21. Below the glass-transition curve (T_g), lactose is in the glassy state. Above the glass-transition curve, lactose can be in the rubbery or crystalline states. Before heating, i.e., at 25°C, the samples were in the glassy state for water activities of 0.06-0.43 and in the crystalline state for water activities of 0.53-0.75. At a water activity of 0.17 and below, no lactose crystallization was observed during heating for 30 min. In the water activity range of 0.23-0.43, lactose crystallized within 30 min of heating (points right of the grey line in Fig. 5.21).

Coming back to the loss of lysine as a function of the temperature and water activity after 30 min of heating (Fig. 5.20), lysine losses can now be linked with the physical state of the model system. The region of low lysine losses at 60 and 70°C at water activities of 0.06 to 0.11 (to the left of the dotted line) coincides with the fraction of the samples that remained in the glassy state throughout the experiments. The values between the dotted and the dashed lines belong to the samples that became rubbery during heating for 30 min. To the right of the dash-dotted line, the lactose had already been crystalline before heating. Between the dashed line and the dash-dotted line, the lactose contained in the model dairy-formulation crystallized during heating for 30 min. Comparing the regions of the glassy, rubbery and crystalline states with the lysine losses, it becomes obvious that the maximum of lysine loss coincides with the transition zone from the rubbery to the crystalline state. The rubbery state as well as the crystalline state is characterized by a high mobility in the system which might favor lysine loss to occur. However, as expected, the availability of lactose for the early Maillard reaction between lactose and the amino group of lysine is obviously higher in the rubbery state than in the crystalline state. This results in a maximum of lysine loss in the transition zone.

⁹ Partly published in: Schmitz I, Gianfrancesco A, Kulozik U, Foerst P (2011) Kinetics of lysine loss in an infant formula model system at conditions applicable to spray drying. *Drying Technology* 29(16):1876-1883; Schmitz-Schug I, Gianfrancesco A, Kulozik U, Foerst P (2013) Physical state, molecular mobility and chemical stability of powdered dairy formulations. *Food Research International* 53(1):268-277

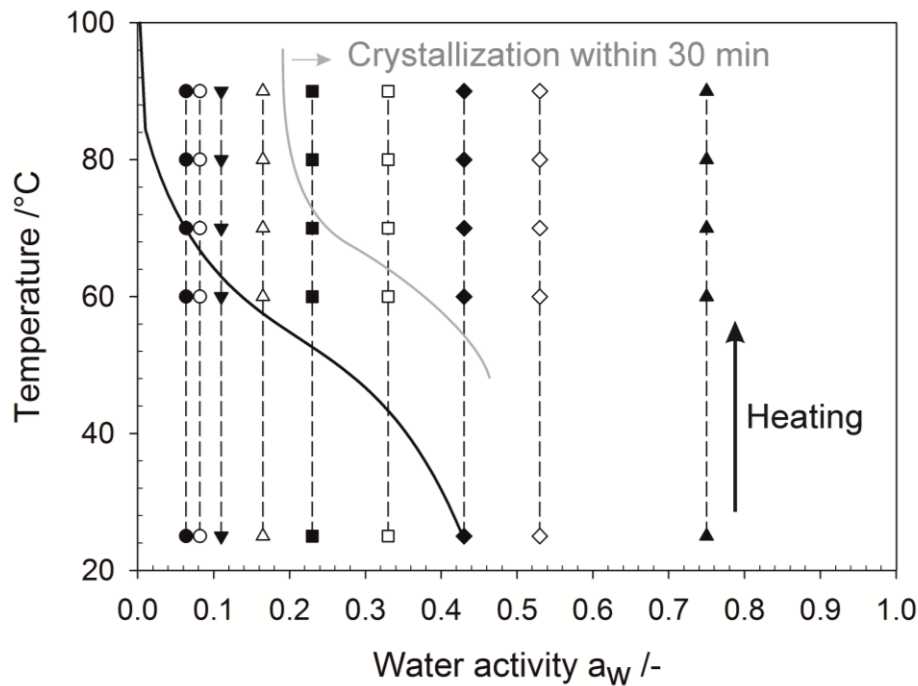


Fig. 5.21. Glass-transition curve of the model dairy-formulation. The points represent the experimental heating conditions.

In accordance with Pereyra-Gonzales et al. (2010) who studied lysine losses in skim-milk powder during the storage (several months) at water activities of 0.31-0.98 and at temperatures of 37-60°C, the reaction rate in this study is low near the glass-transition temperature. In contrast to the results found by other authors, the extent of lysine loss could be linked to lactose crystallization in this study. Thomsen et al. (2005a) noted that the formation of furosine, an indicator of the early Maillard reaction, was not affected by lactose crystallization. Likewise, Morgen et al. (2005) figured out that lactose crystallization had no apparent impact on the early Maillard reaction in skim-milk powder. This difference might be due to the different matrix composition, the higher temperatures and shorter heating times applied in this study. These results highlight the importance of monitoring the physical state of the model system to understand the kinetics of lysine loss. The relation between lysine loss and physical states gets even more important when applying the kinetics of lysine loss to spray drying. In this case the impact of the drying conditions both on lysine loss and on the physical state of the system has to be taken into consideration. Even though water is removed very quickly during spray drying and, consequently, most of the lactose is amorphous after spray drying, lactose can partly crystallize during spray drying (Langrish 2008, Langrish and Wang 2009). This might either happen when the solution passes the solubility limit or when particles are exposed to high temperatures due to recirculation inside the drying chamber.

5.2.3 Role of the molecular mobility

As the loss of available lysine is a bimolecular reaction, it should be influenced by the mobility in the system. In this study, the mobility was expressed as the proton or molecular mobility which was measured by low resolution $^1\text{H-NMR}$ relaxometry (compare chapter 5.1.3). To evaluate the impact of the molecular mobility on lysine loss, results of chapter 5.1.3 will be compared to results of chapter 5.2.1.

In chapter 5.2.1 it was concluded that lysine losses after 30 min of heating were low in the glassy state. According to chapter 5.1.3 the molecular mobility was low in the glassy state, which limits bimolecular reactions (van Boekel 2001). Above the glass-transition temperature, a sharp increase of the molecular mobility was observed which was accompanied by increasing lysine losses. However, once lactose crystallizes during the heating experiments, lower lysine losses were determined compared to completely rubbery conditions. This leads to the conclusion that the rubbery state was the most reactive with regard to lysine loss. In contrast, molecular mobility continued to increase after crystallization. Consequently, the lower reaction rates of lysine loss in the crystalline state cannot be attributed to a reduced molecular mobility. Hence, confirming the hypothesis of chapter 5.2.1, crystalline lactose must be less reactive than amorphous lactose. Other reaction pathways resulting in a loss of available lysine could become important, too. This will be discussed in more detail in chapter 5.2.6.

5.2.4 Reaction mechanism of lysine loss

Generally, the early stage of the Maillard reaction, i.e. the formation of the Amadori product lactuloselysine out of the ϵ -amino group of lysine and the reducing sugar lactose, is considered to be the main cause for lysine loss. However, there are several other pathways that can lead to lysine losses, e.g. the advanced Maillard reaction, the formation of lysinoalanine or the development of isopeptides (Meade et al. 2005, Moughan and Rutherfurd 2008). It is possible to differentiate between these pathways when available or blocked lysine is measured by different analytical methods that are based on different measurement principles.

Two measurement techniques were compared within this work. On the one hand, the fluorescence method with *o*-phthaldialdehyde (OPA) according to Ferrer et al. (2003a) was used. With this method free amino groups are detected. Thus, a value of blocked lysine is obtained independently of the reaction pathway. On the other hand, the furosine method of Fenaille et al. (2003) was used for selected experimental conditions. The early Maillard reaction product ϵ -deoxylactulosyllysine is partly converted into furosine under defined hydrolysis conditions. According to Finot et al. (1983), 32% of protein-bound lactulose-lysine is converted to furosine upon acid hydrolysis and 40% to lysine. Thus, only the early stage of the Maillard reaction can be detected by this method. Contreras-Calderón (2008) measured the available lysine contents of protein ingredients which contained whey protein, casein and soy protein, respectively, by the OPA and the furosine method. They found no correlation between the results of both methods because the furosine method only detected the lysine loss due the early Maillard reaction. Consequently, the comparison of both measurement techniques can give a hint to the extent of the Maillard reaction or possible other reactions occurring.

The lysine loss, measured with both methods, at a water activity of 0.33 (at 25°C) after heating at 70-90°C is shown in Fig. 5.22. At 70 and 80°C, both methods give the same lysine loss after 5 min of heating. At longer heating times (for all heating temperatures) the OPA method amounts to a higher lysine loss than the furosine method. Consequently, the early Maillard reaction is not the only cause for lysine loss at these conditions but the Maillard reaction probably proceeds to advanced stages. This is indicated by the fact that the samples slightly changed their color after heating. Other reactions leading to lysine loss (mentioned above) might also become important. In short, lysine loss seems to be caused by the early Maillard reaction at the beginning of heating but at more severe heating conditions other reaction pathways become important.

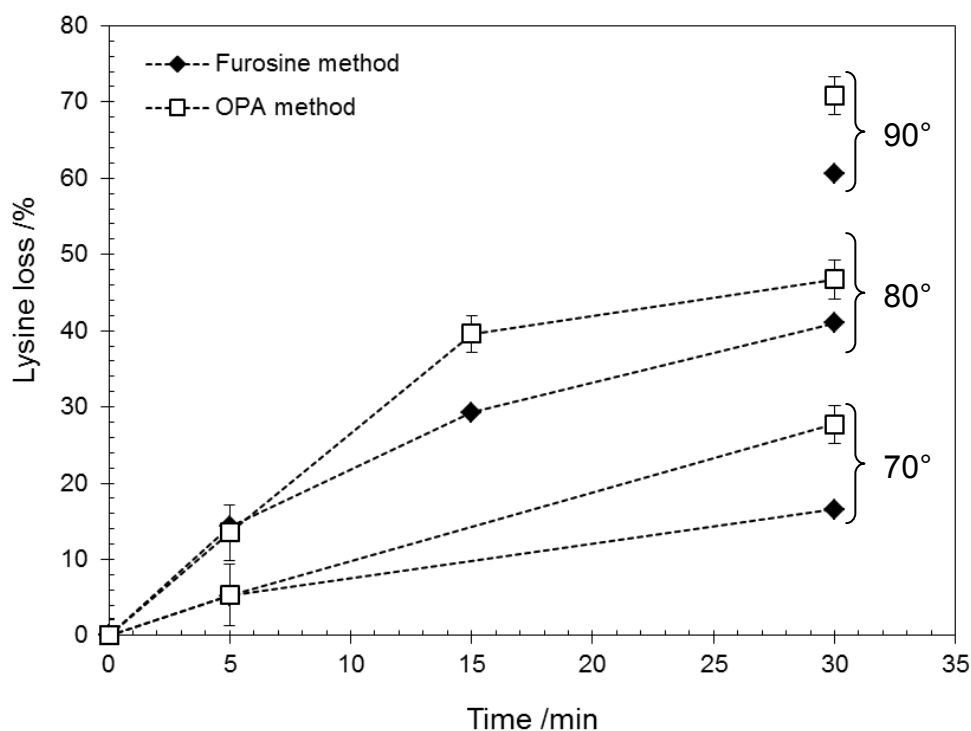


Fig. 5.22 Lysine losses at a water activity of 0.33 (at 25°C) determined by the OPA method and by the furosine method.

5.2.5 Modeling reaction kinetics of lysine loss¹⁰

In order to obtain a tool that describes lysine loss in powdered dairy formulations, thermally-induced lysine loss at different concentrations was modeled by reaction kinetics. Lysine loss during the storage of milk powder was reported to follow pseudo-first order kinetics (Pereyra Gonzales et al. 2010). For skim-milk powder and pasteurized whole milk, second-order reaction kinetics were applied to describe the loss of available lysine (Vuataz 1988, Fink and Kessler 1986a, Horak and Kessler 1981). Thomsen et al. (2012) did a more detailed analysis of the reaction scheme of the lactosylation of β -lactoglobulin leading to pseudo-first

¹⁰ Published in: Schmitz-Schug I, Kulozik U, Foerst P (2014) Reaction kinetics of lysine loss in a model dairy formulation as related to the physical state. Food and Bioprocess Technology 7:877-886

order reaction-rate constants for the formation of mono- and di-lactosylated β -lactoglobulin. To sum up, the reported reaction orders are contradictory which might be due to the fact that different products were studied or that the data range was too small to determine the reaction order in a reliable way. Consequently, the data of this study was fitted to a pseudo-first order (eq. 5.1) and to a pseudo-second order reaction-kinetics model (eq. 5.2) in order to find the reaction order that fits best the experimental data:

$$\frac{C_t}{C_0} = \exp(-k \cdot t) \quad 5.1$$

$$\frac{C_t}{C_0} = (1 + k \cdot t)^{-1} \quad 5.2$$

where C_t is the concentration of available lysine at time t , C_0 the initial concentration of available lysine, k the reaction rate constant and t the reaction time.

Non-linear regression was applied with a global fitting for all temperatures and water activities. The goodness-of-fit of the two models was evaluated by residual analysis and the F-test. The normal probability plot for a water activity a_w of 0.43 and a heating temperature of 60°C is exemplarily shown in Fig. 5.23. The fact that the data points follow a straight line indicates that the residuals are distributed normally, i.e., the model predicts the data well. The results of the F-test are given in Table 5.1. The smaller the F-value, the better is the goodness-of-fit of the corresponding model. Accordingly, the higher the probability P that the model fits well, the better the goodness-of-fit of the corresponding model. Consequently, the analysis of Table 5.1 leads to the conclusion that the pseudo-second order reaction-kinetics model predicts the experimental data more adequately than the pseudo-first order reaction-kinetics model. However, the differences between the two models are small. To confirm the hypothesis that the loss of available lysine follows a pseudo-second order reaction, further statistical tests for model discrimination (ratios of likelihood functions (odds ratios), Akaike criterion, Bayesian information criterion) were performed (Table 5.2). An odds ratio of more than 1 indicates that the pseudo-second order reaction-kinetics model supports the experimental data better than the pseudo-first order reaction-kinetics model. For two water activities, namely 0.17 and 0.33, the odds ratio is bigger than 10 which is usually taken as strong evidence that one model is superior to another (van Boekel 2009). The bigger the values of ΔAIC_C the better the pseudo-second order reaction-kinetics model performs compared to the pseudo-first order reaction-kinetics model. This indicates that, except at a water activity of 0.06 and 0.75, the pseudo-second order reaction-kinetics model gives better results. Analysis of the associated probability P_{AIC} for the pseudo-first order reaction-kinetics model leads to the same conclusion as well as the evidence ratio ER which expresses how many times more likely the pseudo-second order reaction-kinetics model is than the pseudo-first order reaction-kinetics model. The same is confirmed by the Bayesian information criterion BIC where the model that yields the lower BIC is the more probable one. Although the two models sometimes come quite close in the statistical tests, it can be concluded that the loss of available lysine follows pseudo-second order reaction kinetics because this model predicts the experimental values more accurately for all tested conditions than the pseudo first-order reaction-kinetics model.

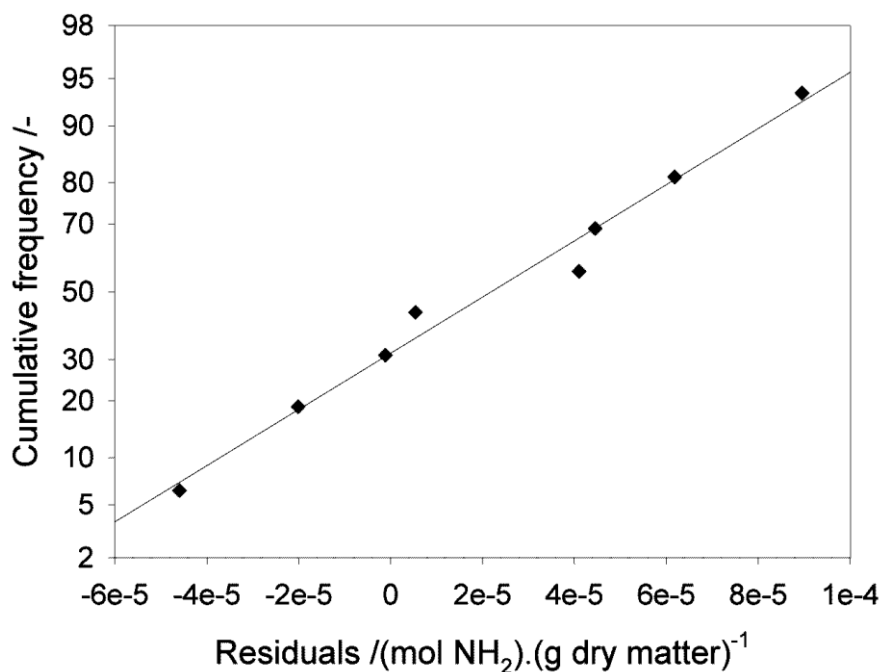


Fig. 5.23 Normal probability for lysine loss at $a_w = 0.43$ and $T = 60^\circ\text{C}$

Table 5.1 Goodness-of-fit for the pseudo-first and pseudo-second order reaction-kinetics model

Water activity a_w /-	F-value		Probability P	
	n = 1	n = 2	n = 1	n = 2
0.06	3.11×10^{-1}	3.12×10^{-1}	0.959	0.959
0.08	7.86×10^{-2}	5.98×10^{-3}	1.000	1.000
0.17	6.73×10^{-1}	3.50×10^{-1}	0.756	0.942
0.33	5.99×10^{-1}	2.19×10^{-1}	0.780	0.989
0.53	3.40×10^{-1}	1.89×10^{-1}	0.947	0.994
0.75	1.86×10^{-2}	1.21×10^{-1}	1.000	0.999

Table 5.2 Model discrimination between the pseudo-first and pseudo-second order reaction-kinetics model

Water activity a_w / -	Odds ratio $L(n=2)/L(n=1)$	AIC_C		ΔAIC_C	P_{AIC}	ER	BIC		ΔBIC
		n = 1	n = 2				n = 1	n = 2	
0.06	1.0	-633.7	-633.6	-0.1	5.13×10^{-1}	9.48×10^{-1}	-631.5	-631.4	-0.1
0.08	2.4	-637.6	-651.7	14.1	8.57×10^{-4}	1.17×10^3	-635.4	-649.5	14.1
0.11	1.2	-678.9	-681.7	2.8	2.00×10^{-1}	4.01×10^0	-676.2	-678.9	2.8
0.17	48.2	-616.0	-632.6	16.6	2.50×10^{-4}	4.01×10^3	-613.8	-630.3	16.6
0.23	2.4	-603.5	-625.7	22.2	1.51×10^{-5}	6.63×10^4	-601.2	-623.5	22.2
0.33	96.2	-593.0	-616.9	23.9	6.62×10^{-6}	1.51×10^5	-590.8	-614.7	23.9
0.43	3.0	-594.2	-615.1	20.8	3.00×10^{-5}	3.33×10^4	-592.0	-612.9	20.8
0.53	6.1	-611.4	-624.0	12.5	1.88×10^{-3}	5.30×10^2	-609.2	-621.8	12.5
0.75	0.3	-645.0	-627.8	-17.2	1.00×10^0	1.83×10^{-4}	-642.8	-625.6	-17.2

Fig. 5.19 shows the experimental values for the loss of available lysine (points) and the losses that were calculated with the pseudo-second order reaction-kinetics models (lines) for a water activity of 0.43 (at 25°C). The coefficient of determination R^2 was 0.97. The values of the reaction rate constant k at the different temperatures are given in Table 5.3. In Fig. 5.24 the linearized plot for the second-order reaction-kinetics model is depicted. It can be seen that the loss of available lysine can be described well by pseudo-second order reaction kinetics.

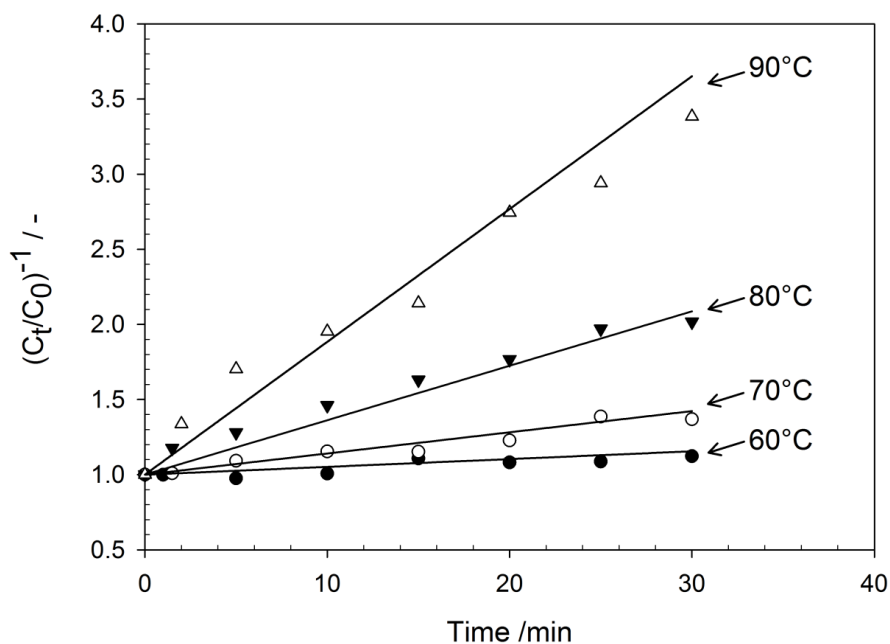


Fig. 5.24 Linearized second-order reaction kinetics of lysine loss at a water activity of 0.43 (C_t = concentration of available lysine at time t , C_0 = initial concentration of available lysine)

Table 5.3 Second-order reaction-rate constants for thermally-induced lysine loss at a water activity of 0.43 (at 25°C, $X^* = 8.54 \pm 0.07\%$ wb)

Temperature /°C	$k / 10^{-2} \text{ min}^{-1}$
60	0.29 ± 0.30
70	1.16 ± 0.40
80	3.86 ± 0.77
90	9.03 ± 1.53

The reaction rate-constant k increases with increasing temperature. The temperature dependence of the reaction-rate constant at a water activity of 0.43 (at 25°C) can be described by the reparametrized Arrhenius equation (Fig. 5.25):

$$k = k_0^* \cdot \exp\left(-\frac{E_A}{R} \cdot \left(\frac{1}{T} - \frac{1}{T^*}\right)\right) \quad 5.3$$

where k denotes the reaction-rate constant at temperature T , k_0^* is the preexponential factor, E_A is the activation energy and T^* a reference temperature. The advantage of the reparametrized form of the Arrhenius equation lies in statistics, i.e., the confidence limits obtained by the reparametrized form are narrower than by the standard Arrhenius equation (van Boekel 2009). At a water activity of 0.43, an activation energy E_A of $95 \pm 11 \text{ kJ}\cdot\text{mol}^{-1}$ was determined which is in the typical range of chemical reactions. However, it has to be noted that this is an activation energy that was determined from observed pseudo-second order reaction-rate constants of lysine loss. This means that it is composed of the activation energies of the individual reactions that lead to the loss of available lysine, e.g. the formation of the Schiff's base and the Amadori rearrangement. Thomsen et al. (2012) reported an activation energy of about $100 \text{ kJ}\cdot\text{mol}^{-1}$ for the lactosylation of β -lactoglobulin. Malec et al. (2002) determined activation energies in the range from 117 to $156 \text{ kJ}\cdot\text{mol}^{-1}$ in a lactose-casein model system. The preexponential factor k_0^* , determined by non-linear fitting, was $2.28 \pm 0.28 \times 10^{-2} \text{ min}^{-1}$ and the reference temperature T^* was set at 348.15 K which was the mean temperature of the experimental range.

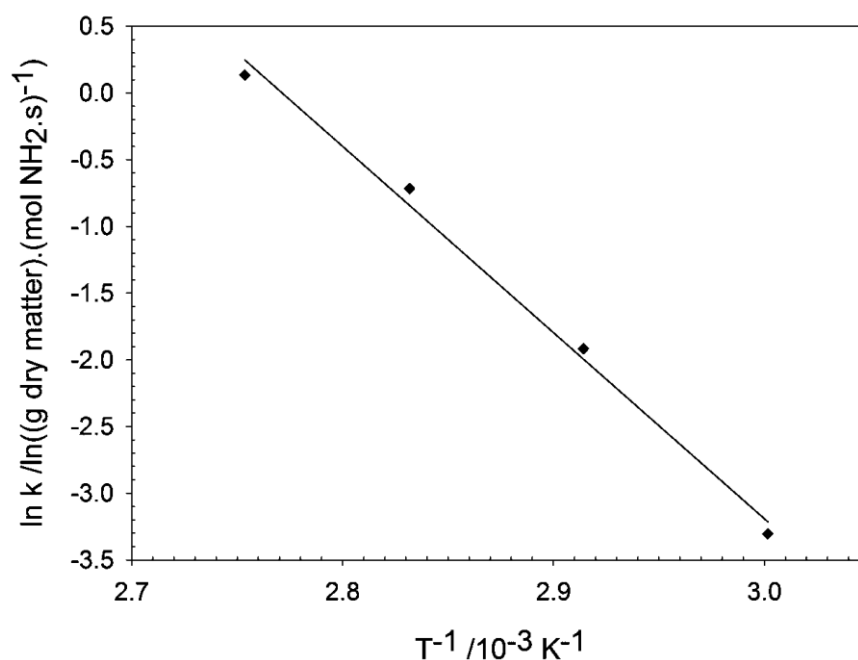


Fig. 5.25 Arrhenius plot of lysine loss at a water activity of 0.43 (at 25°C , $X^* = 8.54 \pm 0.07\% \text{ wb}$)

Reaction rates were calculated using the pseudo-second order reaction-kinetics model for all water activities and heating temperatures (Fig. 5.26). For all water activities, reaction rate constants increased with increasing temperature with a maximum reaction rate in the region of low to intermediate water activities. At 90°C the highest reaction rate constant is found at a water activity a_w of 0.23. At 80°C , there is a maximum at $a_w = 0.23\text{--}0.43$. At 60 and 70°C , reaction rates are rather low and no clear maximum can be distinguished. In contrast to this study, Pereyra Gonzales et al. (2010) concluded that the water activity did only affect the reaction rate constants in milk powder at high water activities ≥ 0.85 . However, they used temperatures in the range of $37\text{--}60^\circ\text{C}$, i.e., below the temperature range of this study, and water

activities higher than 0.3. Depending on the matrix composition, reported maximum rates for the Maillard reaction and lysine loss in powders are found at intermediate water activities of 0.3-0.8 (Labuza and Saltmarch 1981, Vuataz 1988, Malec et al. 2002, Ge Pan and Melton 2007). At high water activities the reactants are too diluted. At low water activities the concentration of reactants is so high that diffusion becomes limiting (van Boekel 2001).

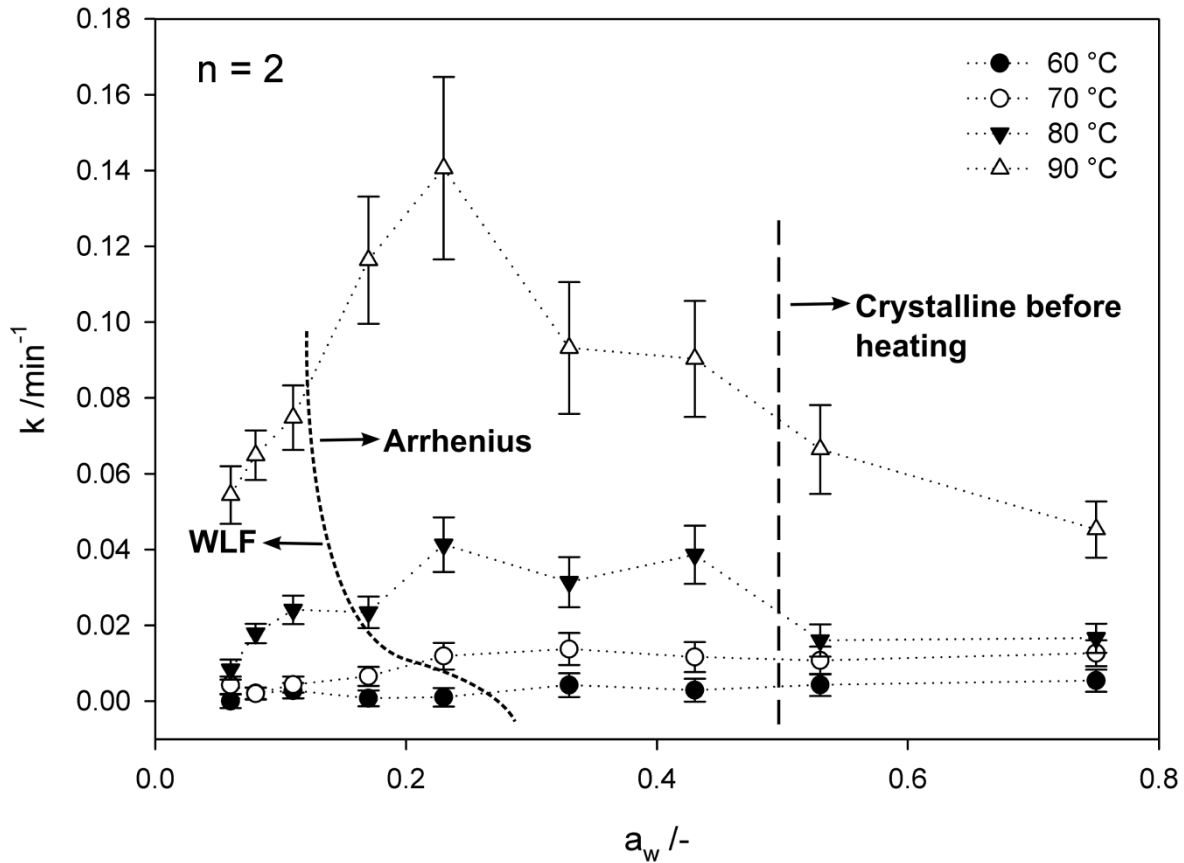


Fig. 5.26 Second-order reaction-rate constants of lysine loss.

Fig. 5.26 shows that a reaction-kinetics model describing the loss of available lysine in dairy formulation must take into account the impact of temperature, physical state and water activity. This was also concluded by Karmas et al. (1992), who evaluated non-enzymatic browning rates in various food systems. According to Fig. 5.9 (chapter 5.1.2), the data points to the right of the long-dashed line in Fig. 5.26 correspond to conditions where lactose is crystalline before thermal treatment whereas lactose is in the glassy state before heating at all conditions to the left of the long-dashed line. At 60°C and $a_w < 0.17$ as well as at 70°C and $a_w \leq 0.08$, lactose stays glassy during the thermal treatment. At the remaining conditions, lactose becomes rubbery at the heating temperature and might crystallize depending on the water activity and heating time. In order to analyze the temperature dependence and the impact of the physical state, the reaction rate constants were plotted as a function of the temperature difference to the glass-transition temperature $T - T_g$ (Fig. 5.27). Here, two regions can be defined.

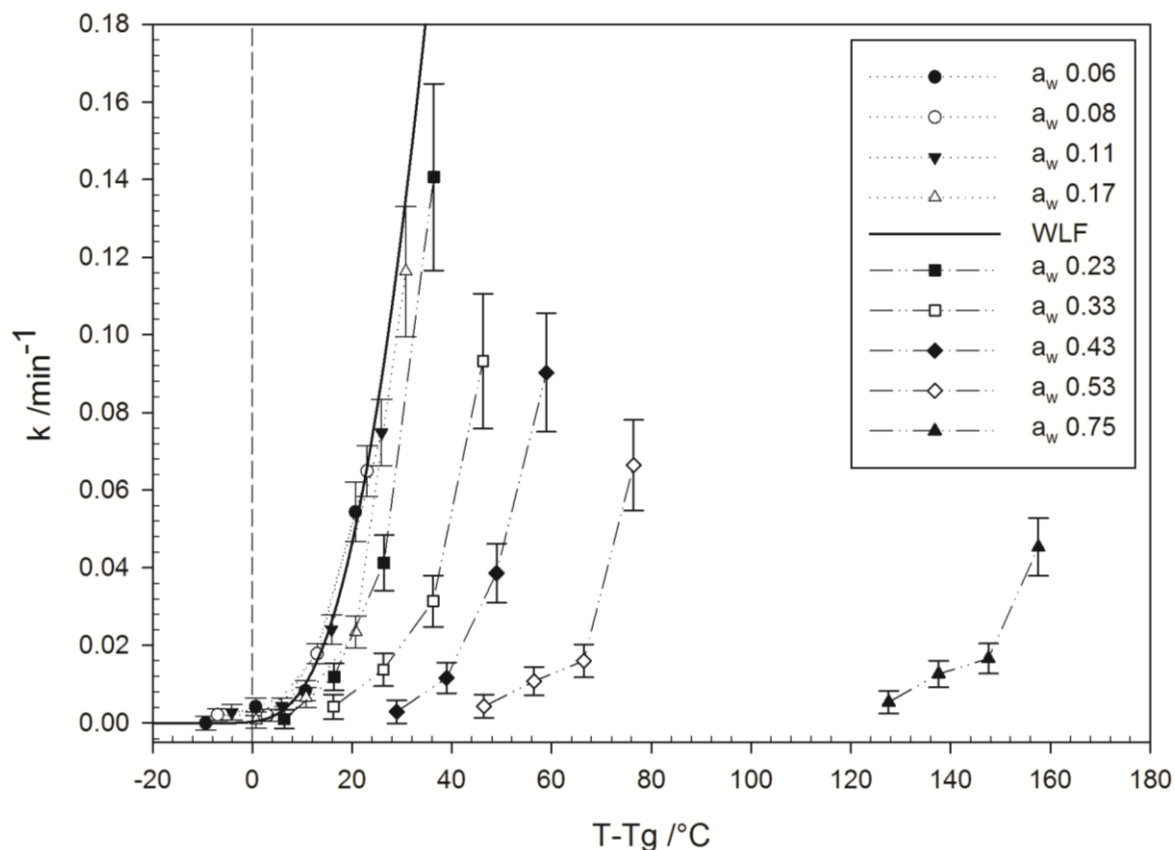


Fig. 5.27 Temperature dependence of the reaction rate constants and impact of the physical state

On the one hand, at $T-T_g < 16-30^\circ\text{C}$ (corresponding to the experimental conditions to the left of the short-dashed line in Fig. 5.26) the reaction rate constants are governed by $T-T_g$ because the experimental values of the different water activities lie on the same curve which indicates that the reaction rate constants might be related to viscosity (Roos and Himberg 1994). Such a behavior can be modeled with the Williams-Landel-Ferry (WLF) equation:

$$\log \frac{k_{T_g}}{k} = \frac{-C_1 \cdot (T - T_g)}{C_2 + (T - T_g)} \quad 5.4$$

with $C_1 = 4.4 \pm 0.4$, $C_2 = 20.7 \pm 13.8$ K and $k_{T_g} = 3.3 \times 10^{-4} \pm 4.4 \times 10^{-4} \text{ min}^{-1}$. An advantage of the WLF equation is that the impact of the concentration is directly included in the equation by the glass-transition temperature. The glass-transition temperature is a function of the concentration that can be described by the Gordon & Taylor equation (cf. chapter 5.1.2). Thus, the reaction rates can be calculated as a function of water content and temperature. Comparing the crystallization data of chapter 5.1.2 and Fig. 5.21 reveals that the experimental range where the WLF equation can be applied coincides with samples that are in the glassy or rubbery state during thermal treatment.

On the other hand, at $T-T_g > 16-30^\circ\text{C}$ (corresponding to the conditions to the right of the short-dashed line in Fig. 5.26) the reaction rate constants are no longer determined by the

temperature difference from the glass-transition temperature $T-T_g$ but by the actual heating temperature and the water content. This can be deduced from the fact that there is a separate curve for each concentration in Fig. 5.27. In this case, the Arrhenius equation can be used to describe the temperature dependence of the reaction rate constants as it was exemplarily shown above for a water activity of 0.43. For the non-linear regression, the reparametrized Arrhenius equation (eq. 5.3) was integrated in eq. 5.2 in order to enhance the statistical quality of the fitted constants.

The temperature dependence of lysine loss and the Maillard reaction has been studied by several authors. Roos and Himberg (1994) reported that non-enzymatic browning in a model food did not show WLF-like behavior but Arrhenius-type temperature dependence. Similarly, Miao and Roos (2004) modeled non-enzymatic browning kinetics in a carbohydrate-based model food using the WLF equation as well as the Arrhenius equation. However, they adapted the WLF constants to each experimental condition, which is not in accordance with the WLF concept. In contrast, Karmas et al. (1992) revealed for various food systems that the temperature dependence of the rate of non-enzymatic browning is different for different $T-T_g$ ranges. They found Arrhenius-type behavior below the glass-transition temperature T_g and above $T_g + 15^\circ\text{C}$. Between these limits they observed a transition zone where they hypothesized that WLF kinetics might apply. However, they lacked in experimental data to confirm this hypothesis. This gap can be filled with the results of this study. The discrepancies found in the literature can be attributed to the different food systems and experimental conditions. As shown in this study, lysine loss is characterized by WLF-like behavior as well as by Arrhenius-type behavior depending on temperature, concentration and physical state. This complex nature of the reaction kinetics of lysine loss can only be recognized when a broad range of experimental conditions is studied as was done in this study.

The samples at a_w 0.53 and 0.75 had already been crystalline before heating and therefore it is difficult to compare them with the other samples which had been glassy before heating. Despite the difference in the water activity, the water content might be the same as for glassy samples at lower water activities. Moreover, glassy samples crystallize under certain heating conditions. For this reason, these two conditions were excluded in the following analyses.

Other than for the WLF equation (eq. 5.4), the concentration is not directly taken into account in the Arrhenius equation (eq. 5.3). Several authors derived Arrhenius-type equations that take into account the water content (Li et al. 2006, Lievens et al. 1992, Luyben et al. 1982, Sloth et al. 2008). However, these equations did not support well the data of this study. For this reason, the impact of the concentration, i.e., the water content, on the activation energy E_A and the preexponential factor k_0^* were evaluated for the Arrhenius-type range of the experimental conditions (Fig. 5.28 and Fig. 5.29). The activation energy E_A reached a maximum at a water content of 5.09% ($a_w = 0.17$) and then decreases to a plateau value of 95 $\text{kJ}\cdot\text{mol}^{-1}$. The data points were interpolated with the following equation:

$$E_A = E_{A0} + \frac{C_{E1} \cdot \exp\left(-\frac{X - X_0}{C_{E2}}\right)}{\left(1 + \exp\left(-\frac{X - X_0}{C_{E2}}\right)\right)^2} \quad 5.5$$

where E_{A0} denotes the plateau value, X_0 the water content of the peak maximum, $C_{E1} = 2.78 \times 10^3$ and $C_{E2} = 0.37\% \text{db}$ are constants.

The experimentally determined preexponential factors k_0^* were around 0.012 min^{-1} for low water contents and around 0.023 min^{-1} for higher water contents. The experimental values were approximated by eq. 5.6, in which $C_k = 0.19\% \text{ db}$ is a constant in order to estimate the transition between these two levels (k_1^* and k_2^*):

$$k_0^* = k_1^* + (k_2^* - k_1^*) \cdot \exp\left(-\exp\left(-\frac{X - X_0 - C_k}{C_k}\right)\right) \quad 5.6$$

In Fig. 5.30 the reaction rate constants obtained from the experiments (compare Fig. 5.26) are plotted with the reaction rate constants that were calculated with the model described above. The calculated reaction rate constants agree well with the experimental reaction rate constants. More data points, which are difficult to obtain due to the transitions in physical state, would be needed to improve the model with regard to the impact of the temperature and concentration on lysine loss, especially in the Arrhenius range.

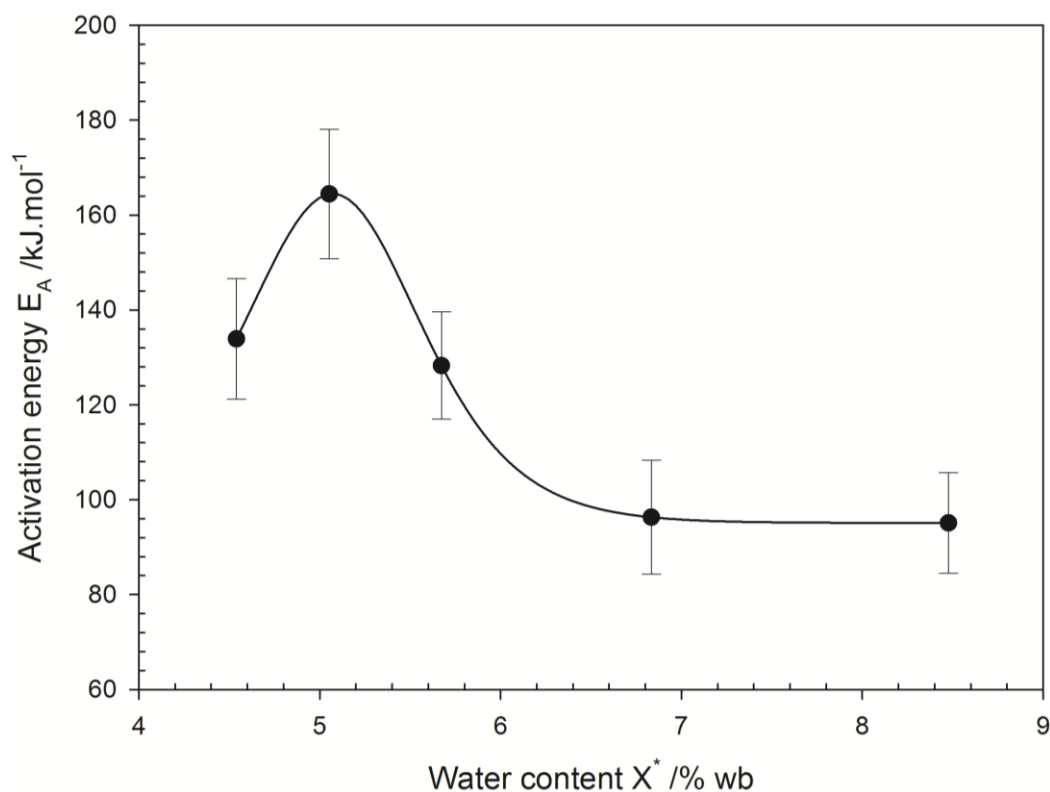


Fig. 5.28 Activation energy E_A as a function of water content (●) and regression curve (—)

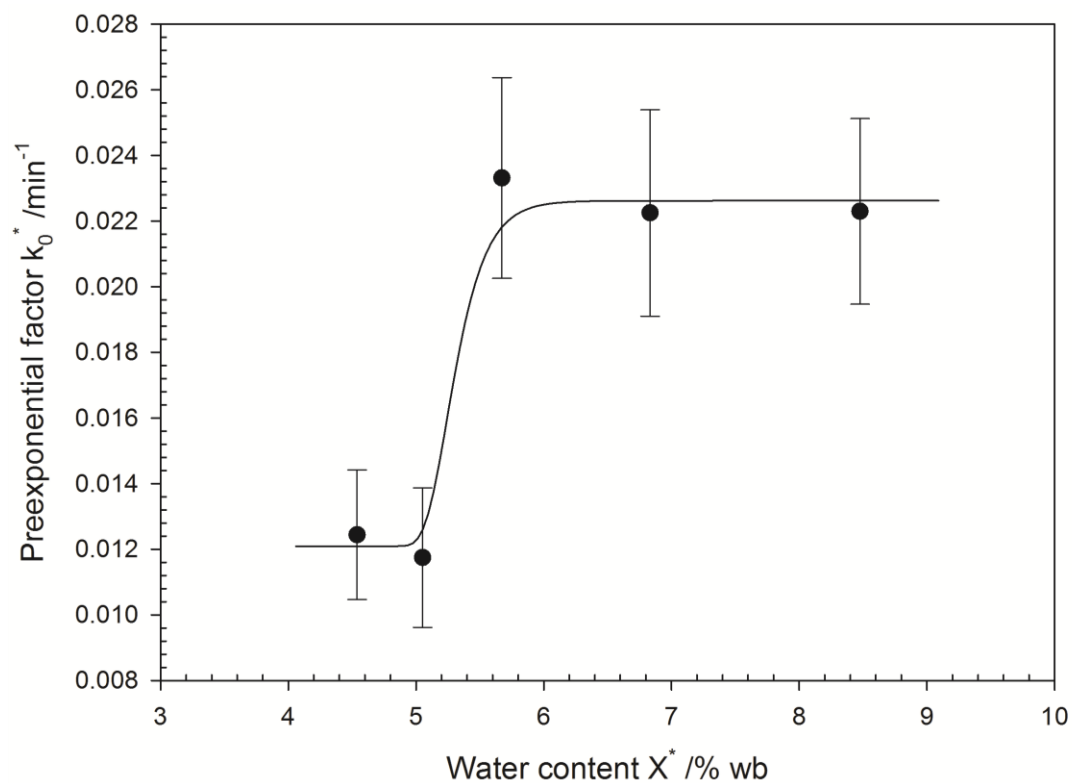


Fig. 5.29 Preexponential factor k_0^* as a function of water content (\bullet) and regression curve (—)

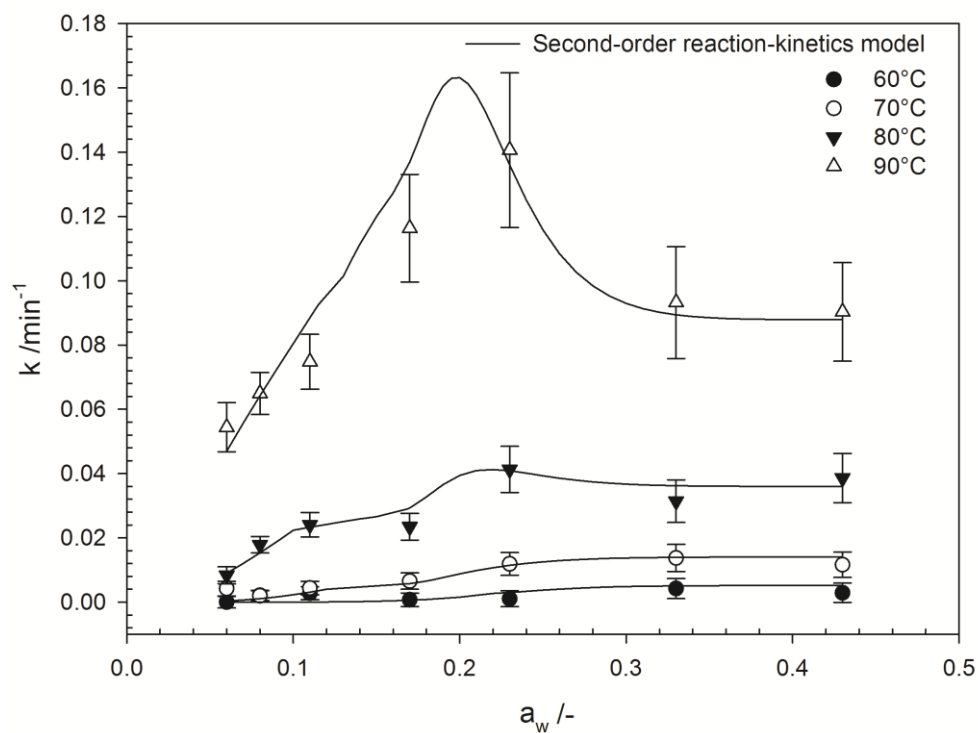


Fig. 5.30 Experimental second-order reaction-rate constants with the derived second-order reaction-kinetics model

5.2.6 Influence of the matrix composition¹¹

To study the impact of the matrix composition on the loss of available lysine, different lactose-protein ratios and whey protein-casein ratios were investigated. The results were analysed with regard to molecular mobility and physical state. The standard composition was characterized by a lactose-protein ratio of 5:1 and a whey protein-casein ratio of 60:40 (compare previous chapters). During this part of the project, the lactose-protein ratio (L:P) was set to 3:1 and to 7:1 keeping the whey protein-casein ratio (WP:C) constant at the standard ratio of 60:40. Additionally, the whey protein-casein ratio was adjusted to 40:60 and 20:80 keeping the lactose-protein ratio at 5:1. All the compositions were within the limits of commission directive 2006/141/EC (European Commission 2008). The prepared powders were equilibrated to a water activity of 0.33 at 25°C and then transferred to hermetically closed heating cans for isothermal heat treatment. After the equilibration of the water activity all samples were in the glassy state. Thus, it was possible to evaluate the sensitivity to lysine loss of the different proteins and the role of the lactose content, as well as the importance of the physical state.

The impact of the whey protein-casein ratio at heating temperatures of 70, 80 and 90°C and a heating time of 30 min is shown in Fig. 5.31. At 70°C and 80°C, lower lysine losses were detected at higher casein contents. This leads to the assumption that casein is less reactive with regard to lysine loss than whey protein. At 90°C, lysine losses were highest for the standard composition, i.e., the lowest casein contents. However, no significantly different lysine losses could be observed at 90°C between a whey protein-casein ratio of 40:60 and 20:80. The increase in the loss of available lysine in the course of heating at 90°C is depicted in Fig. 5.32 for the different compositions ($a_w = 0.33$ at 25°C). For all compositions, the loss of available lysine increased with increasing heating time. During the whole heating time, lysine losses were higher at higher whey protein-casein ratios. Similar lysine losses were measured for a whey protein-casein ratio of 40:60 and 20:80.

Concerning the lactose-protein ratio, lysine losses did not increase as a consequence of higher lactose contents at a heating temperature of 70, 80 and 90°C and a heating time of 30 min (Fig. 5.31). At 90°C and after five minutes of heating, no significant difference between the three formulations was determined (Fig. 5.32). However, at longer heating times, lysine loss depended on the lactose-protein ratio and more lysine was blocked at lower lactose-protein ratios. Thus, the lactose-protein ratio had an impact on the loss of available lysine but, inversely to what could have been suspected, lysine losses did not increase as a consequence of higher lactose contents. One reason for this might be that there was an excess of lactose compared to lysine in all three compositions. In this case, the question arises why lysine loss was not independent of the lactose-protein ratio then. To answer this question, the physical state of the different dairy powders as well as their molecular mobility has to be taken into consideration.

¹¹ Partly published in: Schmitz-Schug I, Gianfrancesco A, Kulozik U, Foerst P (2013) Physical state, molecular mobility and chemical stability of powdered dairy formulations. Food Research International 53(1):268–277

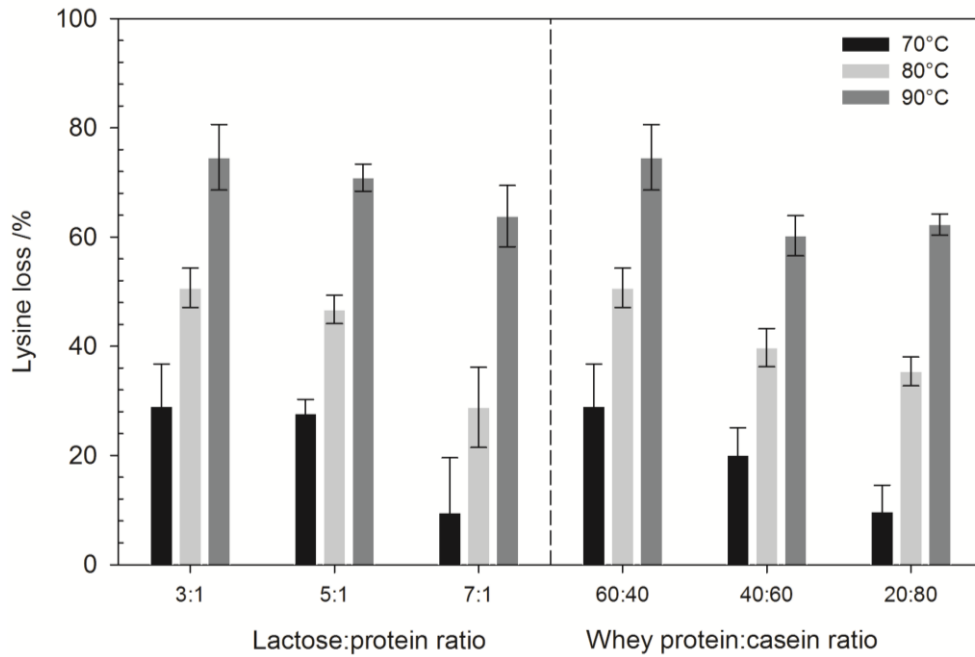


Fig. 5.31 Lysine loss due to a thermal treatment of 30 min at 70, 80 and 90°C in model dairy-powders that were equilibrated at a water activity of 0.33 at 25°C

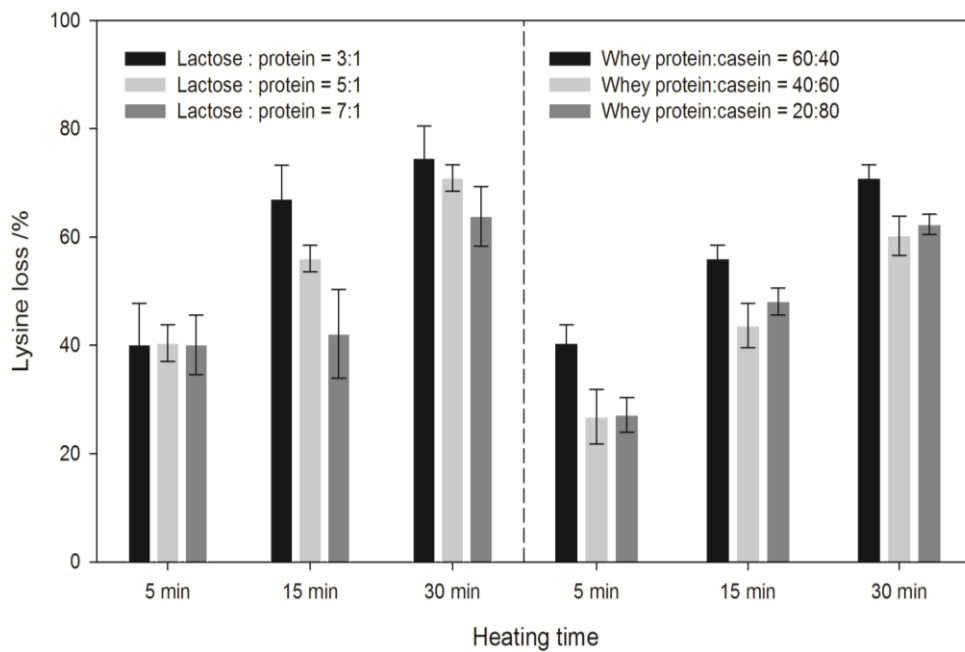


Fig. 5.32 Lysine loss caused by an isothermal heat treatment at 90°C in model dairy-powders that were equilibrated at a water activity of 0.33 (at 25°C)

Bearing the results on glass transition and crystallization in mind (chapter 5.1.4), lysine losses can be analyzed with regard to the physical state of the system. All matrix compositions were above the glass-transition temperature in the experimental range and, consequently, in the rubbery or crystalline state during thermal treatment. At all whey protein-casein ratios, lactose was crystalline after 2-3 min at 90°C (Fig. 5.18) and similar crystallization times

were determined for a whey protein-casein ratio of 40:60 and 20:80 at 70°C and 80°C. Consequently, the different lysine losses can be attributed to the whey protein-casein ratio because the physical state did not differ. Lactose contained in the powders with a lactose-protein ratio of 5:1 and 7:1 crystallized entirely within 2-3 min at 90°C (Fig. 5.18) whereas the powder with a lactose-protein ratio of 3:1 did not crystallize in the experimental range, i.e., remained in the rubbery state. After a heating time of 5 min, lysine loss ranged around 40% for all lactose-protein ratios and lactose was mostly rubbery during this heating period. At longer heating times, higher lysine losses were detected at the composition with a lactose-protein ratio of 3:1, which remained rubbery, than at higher lactose contents where lactose crystallized after 2-3 min. Therefore it can be concluded that crystalline lactose is less reactive with regard to lysine loss than rubbery lactose. However, the differences in lysine loss between the formulations with a lactose-protein ratio of 5:1 and with a lactose-protein ratio of 7:1 cannot be explained by the physical state. Thus, the stability concept based on the physical state is only capable to explain parts of the observed lysine losses. This gap might be filled by amending the stability concept based on the physical state with the stability concept based on the molecular mobility.

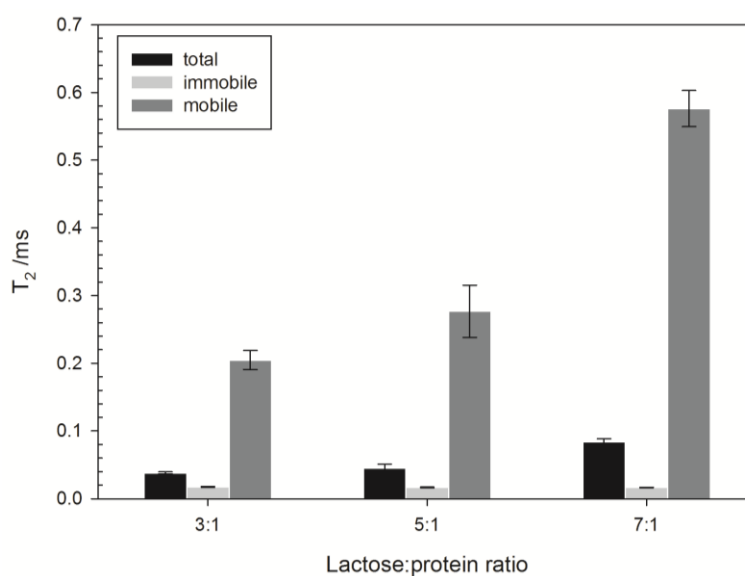


Fig. 5.33 Molecular mobility measured at 25°C after an isothermal treatment at 90°C for 30 min in model dairy-powders that were equilibrated at a water activity of 0.33 (at 25°C) which led to water contents of $6.96 \pm 0.07\%$ (3:1), $7.14 \pm 0.05\%$ (5:1) and $7.00 \pm 0.03\%$ (7:1)

The molecular mobility was measured at 25°C after heating the samples at 90°C for 30 min and cooling them down to room temperature in ice water. This procedure was necessary to quantify the impact of the lactose-protein ratio on the molecular mobility because a temperature of 90°C lies above the operating range of the ¹H-NMR instrument. Fig. 5.33 shows the obtained relaxation times for the mobile and the immobile fraction as well as the mean (total) relaxation time. The relaxation times of the immobile fraction hardly changed for the three compositions whereas the total relaxation times as well as the relaxation time of the mobile fraction increased significantly with increasing lactose content. Consequently, the loss of available lysine was lower at higher molecular mobilities under these conditions. This might

be explained by the system being too “diluted” at a lactose-protein ratio of 7:1 so that the reaction partners “meet” less frequently (van Boekel 2001). However, given the water content of about 7% wb of the three compositions, this seems to be unlikely. Another explanation for the lower lysine loss in the composition with a lactose-protein ratio of 7:1 than in the composition with a lactose-protein ratio of 5:1 despite the higher mobility could be that a more homogenous lactose crystal lattice might be formed at higher lactose concentrations. This would imply that at lower lactose concentrations the crystal structure was disturbed by proteins and salts so that more lactose molecules were exposed to lysine groups. This would lead to the conclusion that lactose molecules in a structured crystal lattice are less available for the Maillard reaction. Nijdam et al. (2007) reported that proteins and salts hinder the crystallization process. This could lead to a disrupted crystal lattice and support the hypothesis stated above. From Fig. 5.34 it becomes obvious that the fraction f_S of the immobile component as well as the fraction f_L of the mobile component did not change with an increasing lactose-protein ratio. This is in accordance with the findings of chapter 5.1.3 concerning the impact of temperature and water activity. The situation is different for the second moment (Fig. 5.34) which is a measure for the strength of hydrogen dipolar interactions (Mateus et al. 2007). The second moment increased with increasing lactose content. This shows that lactose contributed significantly to the dipolar interactions. The importance of the physical state of lactose for the second moment was already highlighted in Fig. 5.16, which demonstrated an increase of the second moment after crystallization. This might at least partly explain the increase of the second moment when the lactose-protein ratio is raised from 3:1 to 5:1. However, the second moment increased further when the lactose-protein ratio was raised to 7:1. Consequently, the composition with a lactose-protein ratio of 7:1 is characterized by the strongest dipolar interactions and at the same time by the highest molecular mobility of the mobile component. At the same time, the extent of lysine loss is smaller. This supports the hypothesis stated above that crystalline lactose is less reactive than amorphous lactose and apparently the reactivity of crystalline lactose is further reduced when stronger crystalline structures are formed.

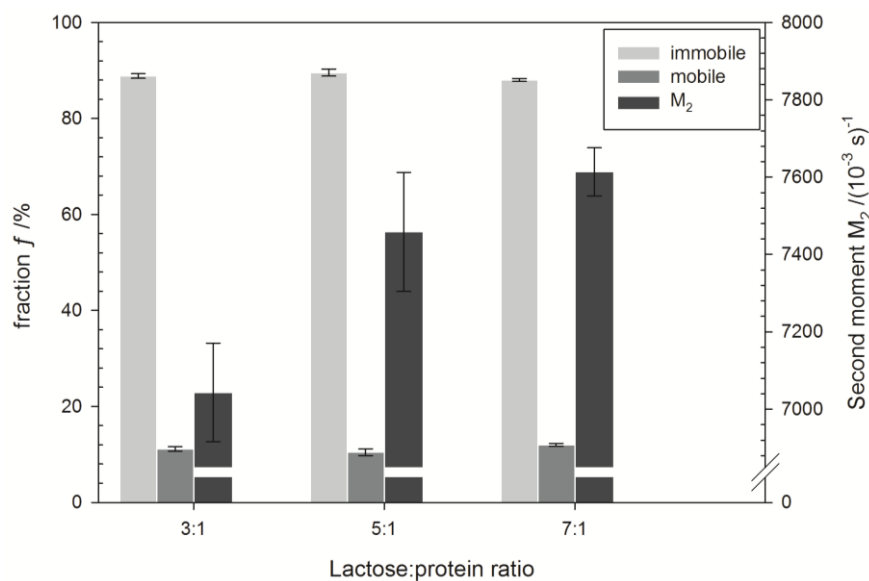


Fig. 5.34 Fractions of mobile and immobile components as well as the second moment measured at 25°C after an isothermal heat treatment at 90°C for 30 min in model dairy-powders that were equilibrated at a water activity of 0.33 (at 25°C)

5.3 Dehydration-induced lysine loss¹²

In order to evaluate the impact of the dehydration kinetics and temperature on lysine loss, the model dairy-formulation with the standard composition (lactose-protein ratio of 5:1 and whey protein-casein ratio of 60:40) was vacuum dried at three different dehydration conditions (45 mbar/60°C, 45 mbar/60°C/zeolite, 20 mbar/46°C/zeolite) and dehydration rates (high, medium and low). In the following, the dehydration kinetics will be characterized first and the impact of the dehydration kinetics on the loss of available lysine will be assessed afterwards. To gain a deeper insight into the factors affecting the loss of available lysine, the impact of the lactose-protein ratio and of the whey protein-casein ratio was studied in the second part.

5.3.1 Characterization of the dehydration kinetics

For all drying conditions, water evaporated fast after a short induction period until a water content of about 10% wb was reached. Then water evaporation slowed down until an equilibrium water content of about 5% wb was attained. At 45 mbar/60°C this water content was reached after 15 min for the high drying rate (Fig. 5.35), after 25 min for the medium drying rate and after 75 min for the low drying rate. Zeolite in the drying chamber decreased this time to 10 min for the high drying rate (Fig. 5.36), to 15 min for the medium drying rate and to 45 min for the low drying rate. Thus, the dehydration time was decreased by 40% when zeolite was positioned around the sample in the drying chamber. This shows that zeolites maintained a dry atmosphere in the drying chamber and, as a consequence, accelerated the dehydration process. However, at 20 mbar/46°C/zeolite the dehydration time was longer, namely 20 min for the high drying rate (Fig. 5.37), 45 min for the medium drying rate and 75 min for the low drying rate despite the same mean relative energy input. The higher uncertainties of the experimental results under this dehydration condition are due to the fact that this condition is at the extreme boundary of the operating range of the vacuum drier, which leads to a more unstable process control. Nevertheless, it seems that not only the relative energy input had an impact on the drying rate but also the actual temperature. A higher temperature leads to a higher mobility, thus perhaps facilitating evaporation.

¹² Published in: Schmitz-Schug I, Gianfrancesco A, Foerst P, Kulozik U (2013) Impact of dehydration on lysine loss in a model dairy formulation. *Drying Technology* 31(13-14):1477-1484

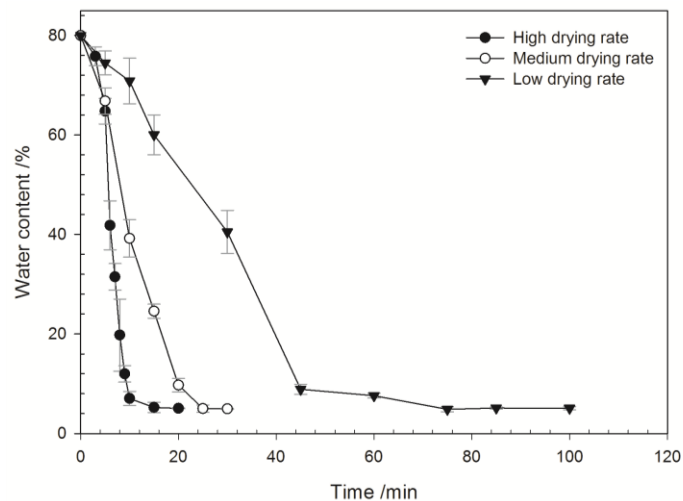


Fig. 5.35 Dehydration of the model system with the standard composition at 45 mbar/60°C

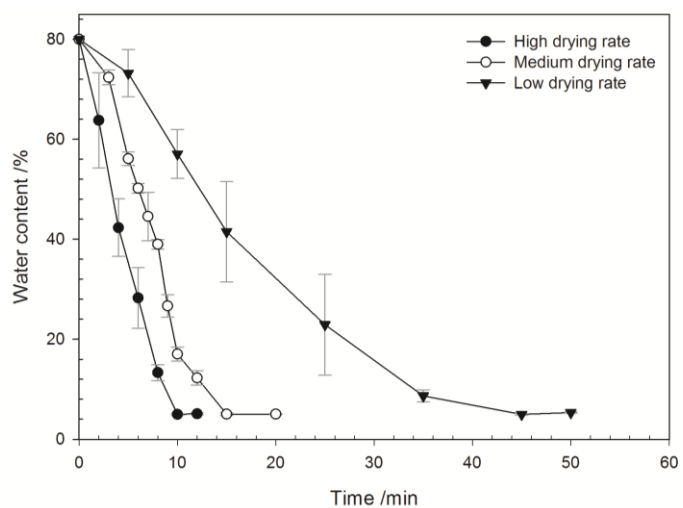


Fig. 5.36 Dehydration of the model system with the standard composition at 45 mbar/60°C/zeolite

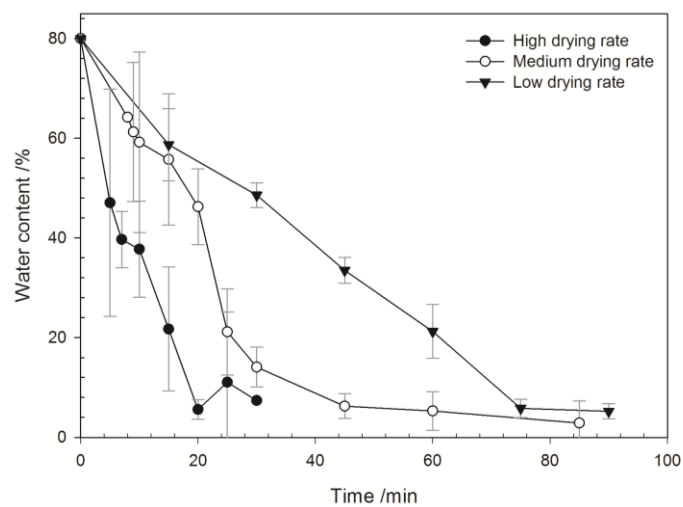


Fig. 5.37 Dehydration of the model system with the standard composition at 20 mbar/46°C/zeolite

In the first part of the drying process, the sample temperatures stayed close to the evaporation temperatures of about 32°C and 18°C, respectively (Fig. 5.38, Fig. 5.39, Fig. 5.40). As the dehydration proceeded, the samples got drier and the sample temperatures approached the shelf temperature of 60°C and 46°C, respectively. The temperatures increased with decreasing water content independently of the drying rate for all three dehydration conditions. Thus, the samples remained for a longer or a shorter time at a certain combination of water content and temperature, which might limit or favor degradation reactions. In general, the condition 20 mbar/46°C/zeolite was characterized by lower temperatures than the conditions 45 mbar/60°C and 45 mbar/60°C/zeolite. This suggests a lower extent of lysine loss because lysine loss increases with increasing temperature (cf. chapter 5.2.1). This will be discussed below in more detail.

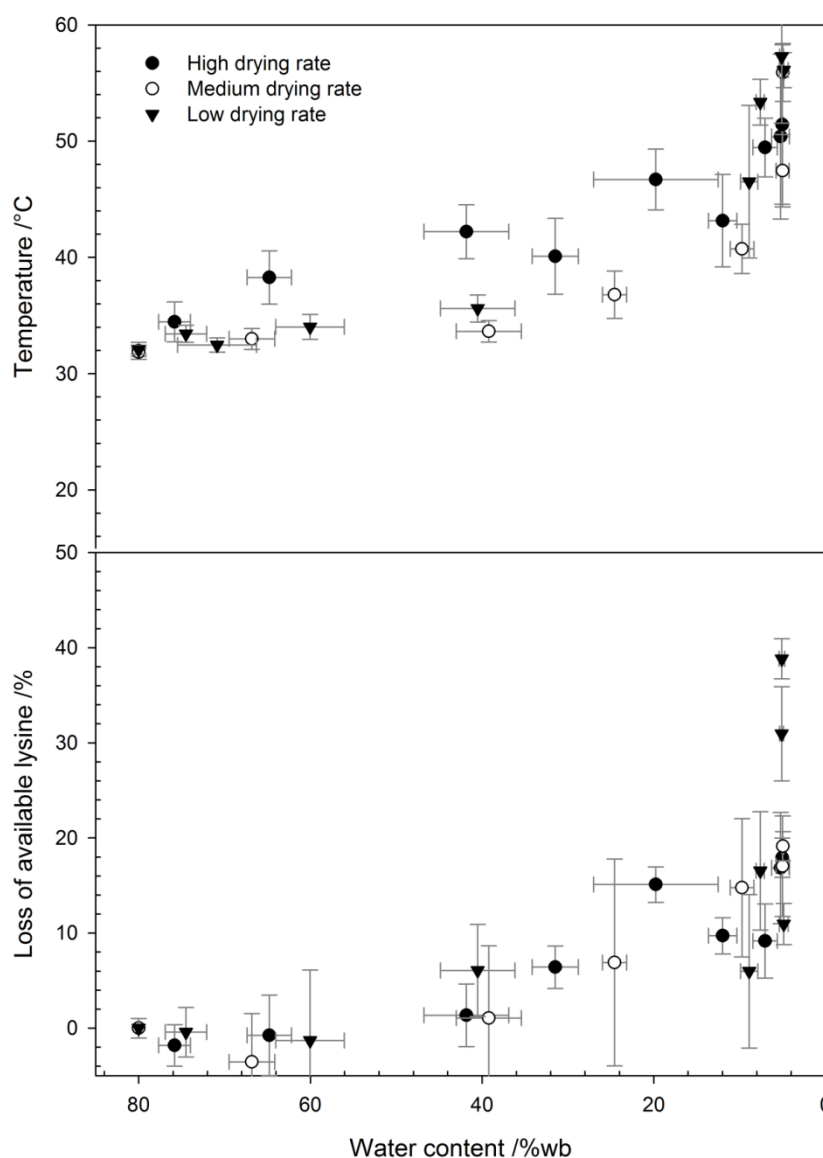


Fig. 5.38 Dehydration of the model system with the standard composition at 45 mbar/60°C: Product temperature and loss of available lysine as a function of the water content and of the drying rate

Fig. 5.39 Dehydration of the model system with the standard composition at 45 mbar/60°C/zeolite: Product temperature and loss of available lysine as a function of the water content and of the drying rate

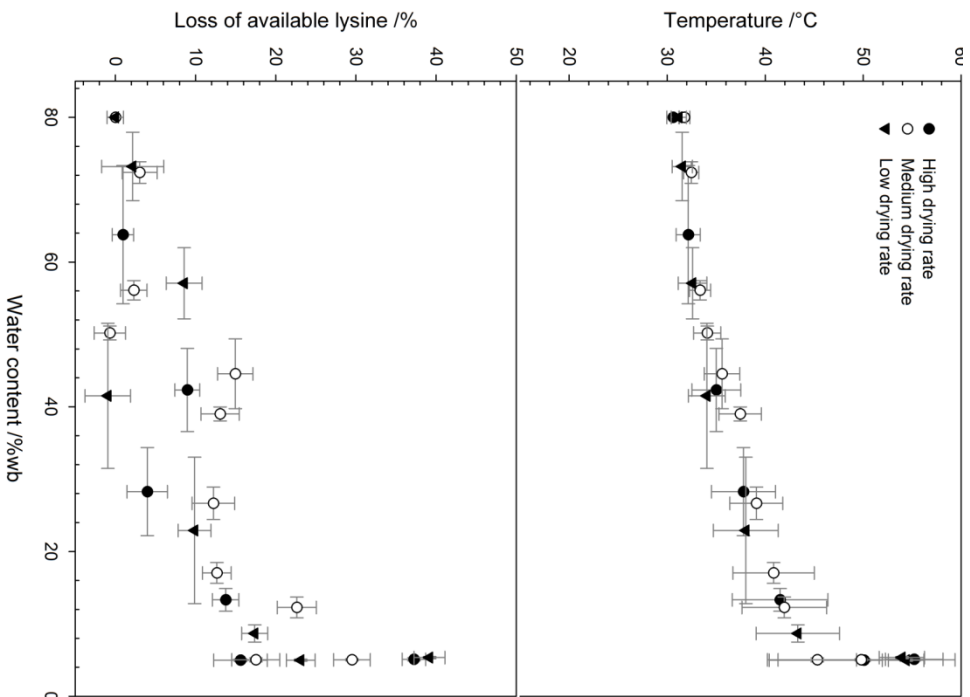
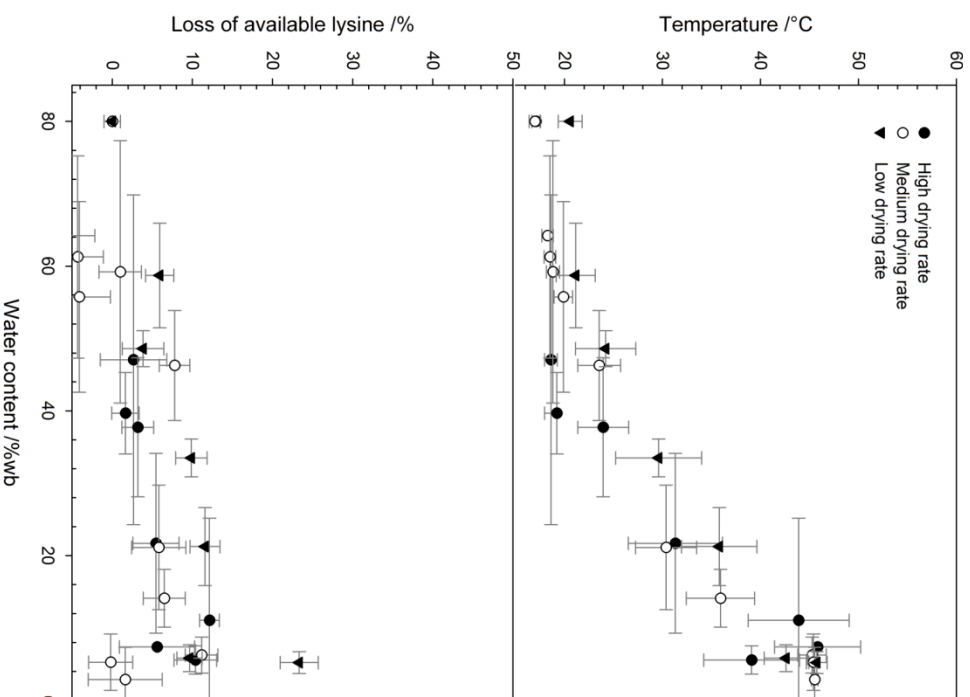


Fig. 5.40 Dehydration of the model system with the standard composition at 20 mbar/46°C/zeolite: Product temperature and loss of available lysine as a function of water content and drying rate



5.3.2 Impact of the dehydration conditions on lysine loss

The loss of available lysine was measured as a function of the dehydration degree for all dehydration conditions and drying rates (Fig. 5.38, Fig. 5.39, Fig. 5.40). At all experimental conditions, the loss of available lysine increased with dehydration time, i.e., with decreasing water content. During the first part of the dehydration process at water contents above 60%, no significant lysine loss was determined but below water contents of 60% lysine losses started to occur. A sharp increase in lysine loss was detected at water contents of less than 10%. This means that most of the lysine was blocked during the removal of the last remaining water when the sample temperature approached the shelf temperature. Interestingly, no significant impact of the drying rate can be derived from Fig. 5.38, Fig. 5.39 and Fig. 5.40. Hence, neither the rate of water removal nor the time at a certain temperature would influence the extent of lysine loss at a given dehydration condition. This indicates on the one hand that lysine loss was induced by water removal rather than by the heating effect above water contents of 10%. On the other hand, it can be assumed for water contents below 10% that the loss of available lysine was mainly caused by the elevated temperature towards the end of drying. Comparing the results obtained at 45 mbar/60°C and 45 mbar/60°C/zeolite with the results obtained at 20 mbar/46°C/zeolite supports this hypothesis because lower lysine losses were measured at the end of drying at 20 mbar/46°C/zeolite.

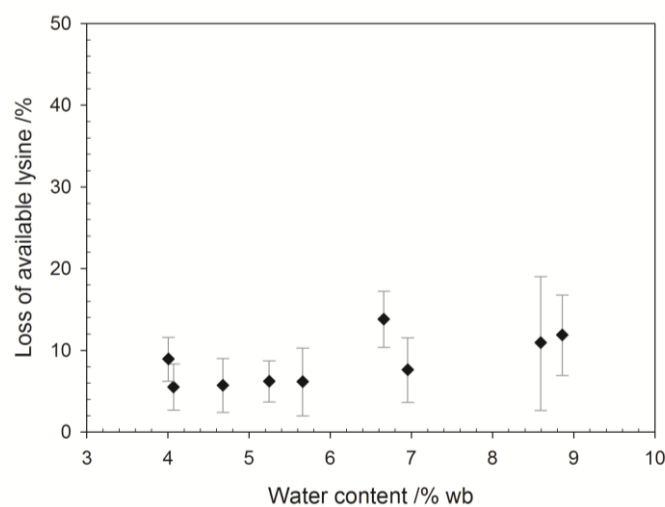


Fig. 5.41 Loss of available lysine after heating at 60°C for 30 min at constant water contents

In order to determine if these losses were caused by dehydration or if the moderate shelf temperature of 60°C and 46°C, respectively, was the reason for lysine loss, the impact of the shelf temperature was evaluated. To do this, samples were adjusted to water activities of 0.06-0.75, i.e., water contents of 4.1-8.9% wb, and heated at 60°C for 30 min (Fig. 5.41). These high concentrations were chosen because thermally-induced lysine losses were higher in concentrated systems than in low concentration systems (cf. chapter 5.2.1; Fenaille et al. 2003; Fink and Kessler 1986c; Horak and Kessler 1981). Lysine losses reached up to $13.8 \pm 3.4\%$ as a consequence of this thermal treatment whereas almost 40% was reached during dehydration at 45 mbar/60°C for the low drying rate as well as at 45 mbar/60°C/zeolite for the high and low drying rate. However, the product temperature was always below 60°C during dehydra-

tion. Moreover, the dehydration time did not exceed 12 min at 45 mbar/60°C/zeolite for the high drying rate compared to a heating time of 30 min for the thermally-induced lysine losses. Consequently, the loss of available lysine cannot only be caused by the shelf temperature of 60°C inside the drier but also has to be generated by the dehydration. Whether or not the extent of lysine loss can be controlled by the dehydration conditions will be discussed in the following.

In Fig. 5.42, the loss of available lysine is depicted as a function of the water content for the three dehydration conditions and drying rates. Despite the high scattering of the experimental results, it becomes evident that the loss of available lysine at the different dehydration conditions and drying rates was similar despite the different drying times and temperatures. A higher temperature means a higher mobility and a higher mobility usually favors chemical reactions like the loss of available lysine. However, no significant impact of the dehydration temperature was observed except at low water contents at the end of drying. Here, the lysine loss increased sharply for the dehydration conditions with a shelf temperature of 60°C whereas this sharp increase was not observed at a shelf temperature of 46°C. In this region, the water content was almost stable. Consequently, the extent of lysine loss was probably due to the residence time at the elevated temperature. In general, lysine losses due to vacuum dehydration were higher than due to a pure thermal treatment, which means that the dynamic change in the concentration seems to induce the loss of available lysine. In other words, a thermal treatment combined with a change in concentration appears to promote the loss of available lysine.

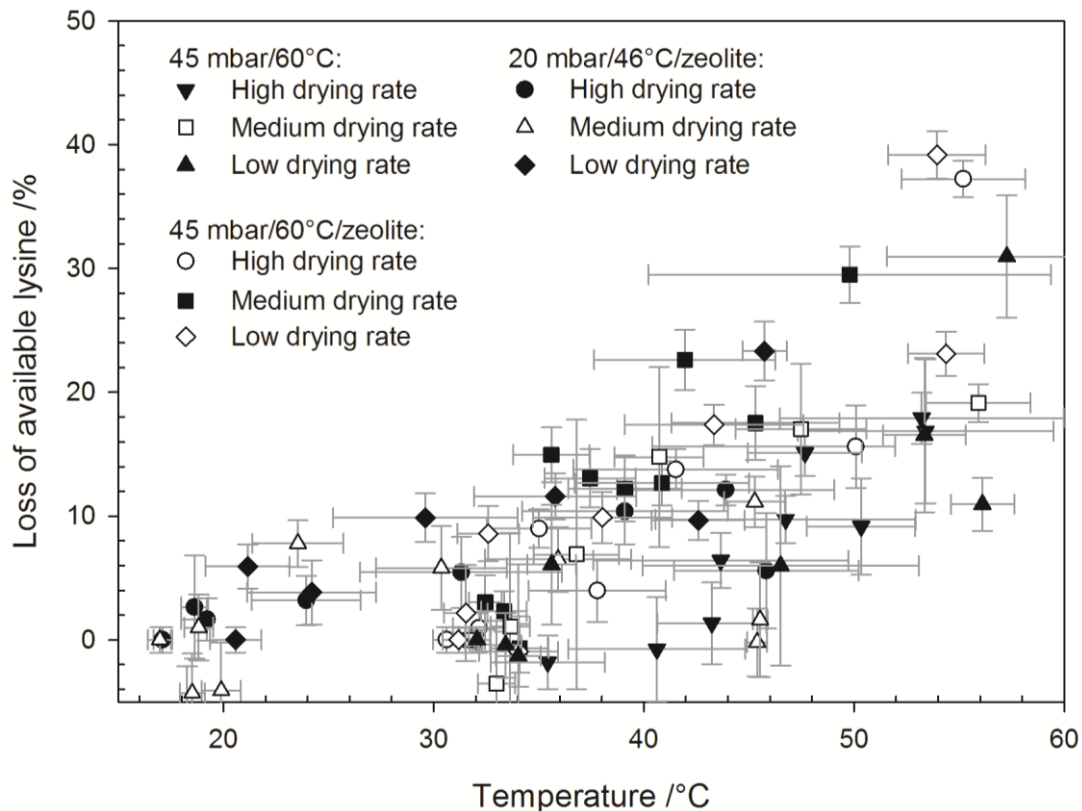


Fig. 5.42 Loss of available lysine as a function of the water content during dehydration of the model system with the standard composition

5.3.3 Impact of the lactose and protein content

The impact of the matrix composition on dehydration-induced lysine loss was studied during vacuum dehydration at 60°C shelf temperature, 45 mbar chamber pressure (evaporation at about 32°C) with zeolite in the drying chamber. To study the impact of the matrix composition, the lactose-protein ratio and the whey protein-casein ratio were varied. The lactose-protein ratio (L:P) was set to 3:1 and to 7:1 while keeping the whey protein-casein ratio (WP:C) constant at the standard ratio of 60:40. Additionally, the whey protein-casein ratio was adjusted to 40:60 and 20:80 keeping the lactose-protein ratio at 5:1.

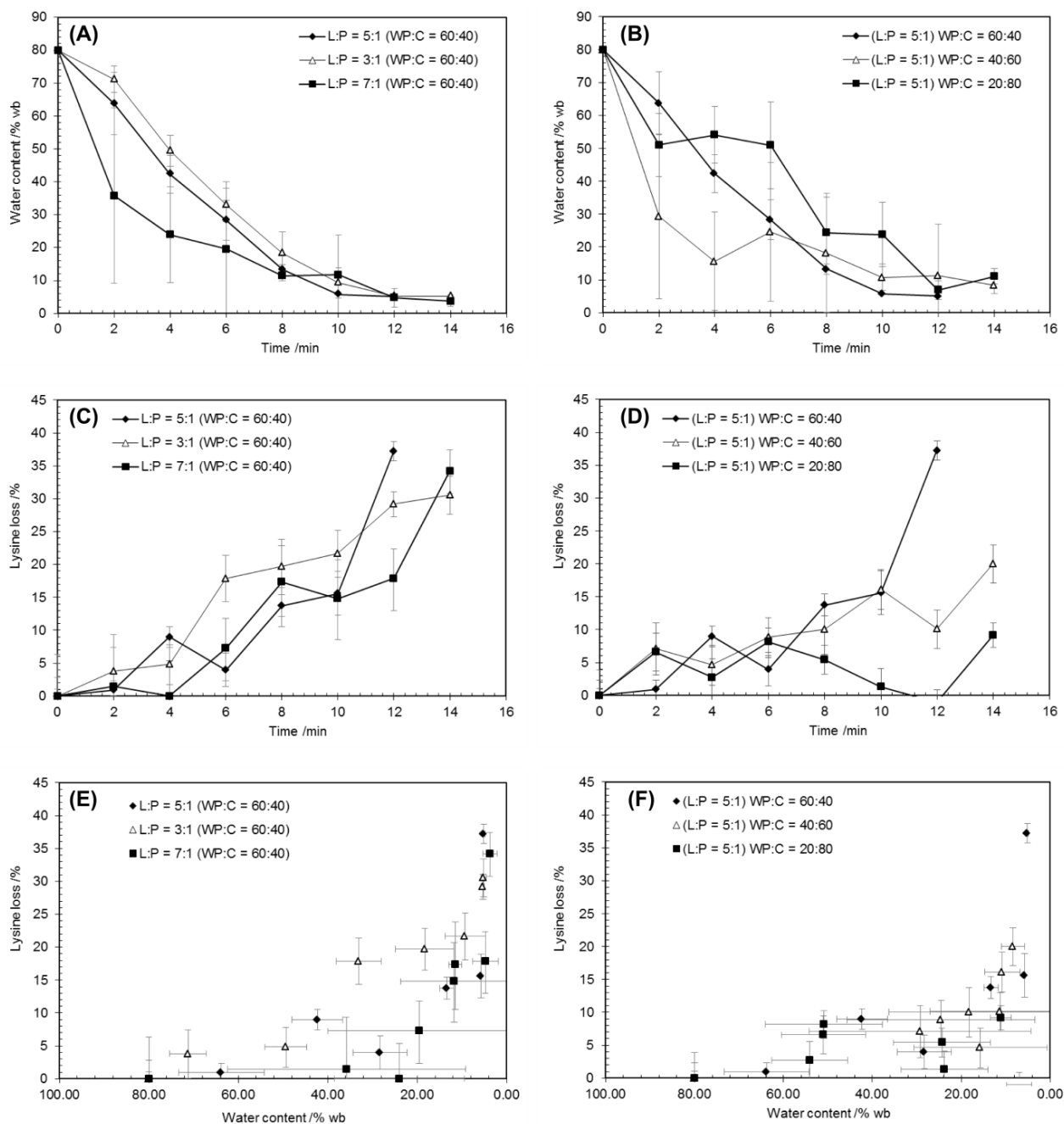


Fig. 5.43 Dehydration of the different model systems at 60°C/45 mbar with zeolite in the drying chamber: evolution of the water content with dehydration time (A, B); lysine loss as a function of the dehydration time (C, D) and as a function of the water content (E, F)

A higher lactose-protein ratio led to a faster dehydration at the beginning of drying (Fig. 5.43A) but the final water content and the time necessary to reach it seemed to be independent of the lactose-protein ratio. Lysine losses rose for all three compositions with dehydration time (Fig. 5.43C). To evaluate the impact of the lactose-protein ratio, lysine losses as a function of the water content have to be considered (Fig. 5.43E). For the three compositions, lysine losses increased with decreasing water content. In the region of high water contents, lysine losses in the system with a lactose-protein ratio of 7:1 were negligible whereas high lysine losses were measured at a lactose-protein ratio of 3:1. Below a water content of 20% a steep rise in lysine loss could be observed which was more pronounced in systems with a higher lactose-protein ratio. At the end of drying, no significant difference in lysine loss between the three lactose-protein ratios could be detected.

Variation of the whey protein-casein ratio led to a different drying behavior (Fig. 5.43B). At a whey protein-casein ratio of 40:60 dehydration was faster in the first half of drying than for the standard composition (whey protein-casein ratio of 60:40). In contrast, increasing the casein content further slowed down the dehydration rate. The higher the casein content, the higher was the residual moisture content at the end of drying. Lysine loss decreased with increasing casein content (Fig. 5.43D and F) and reached $37.2 \pm 1.5\%$ for the standard composition (whey protein-casein ratio of 60:40), $20.0 \pm 2.9\%$ at a whey protein-casein ratio of 40:60 and $9.2 \pm 2.8\%$ at a whey protein-casein ratio of 20:80. Consequently, casein seems to be less susceptible to lysine loss than whey protein.

5.4 Spray drying¹³

5.4.1 Process performance, powder characteristics and scale up

The model dairy-formulation was spray dried on a laboratory scale as well as on a pilot scale. On a laboratory scale, air inlet temperatures of 152-208°C led to air outlet temperatures of $49.5 \pm 8.1^\circ\text{C}$ to $106.7 \pm 12.7^\circ\text{C}$ (Fig. 5.44). Air-outlet temperatures increased with increasing air-inlet temperatures and decreasing product mass-flow rates. The temperature profile inside the spray dryer is an important factor regarding the quality of thermally sensitive products. The air temperature determines together with drying kinetics the temperature of the product to be dried (Gianfrancesco 2009, Mezhericher et al. 2010b). At the beginning of the drying process, as long as the water activity at the droplet surface stays close to $a_w = 1$, the product temperature equals the wet-bulb temperature. This corresponds to the first drying stage or constant-rate drying. Once the critical moisture content is attained, humidity cannot anymore be transported as fast from the droplet center to the surface as evaporation takes place on the droplet surface. During this second drying stage the drying rate is not constant but falling, the water activity decreases and the product temperature starts to rise. The product temperature is limited by the air temperature, i.e., the droplet or particle temperature cannot rise above the air temperature. Thus, the product temperature is determined by the drying kinetics, the air temperature profile inside the dryer and the particle residence-time.

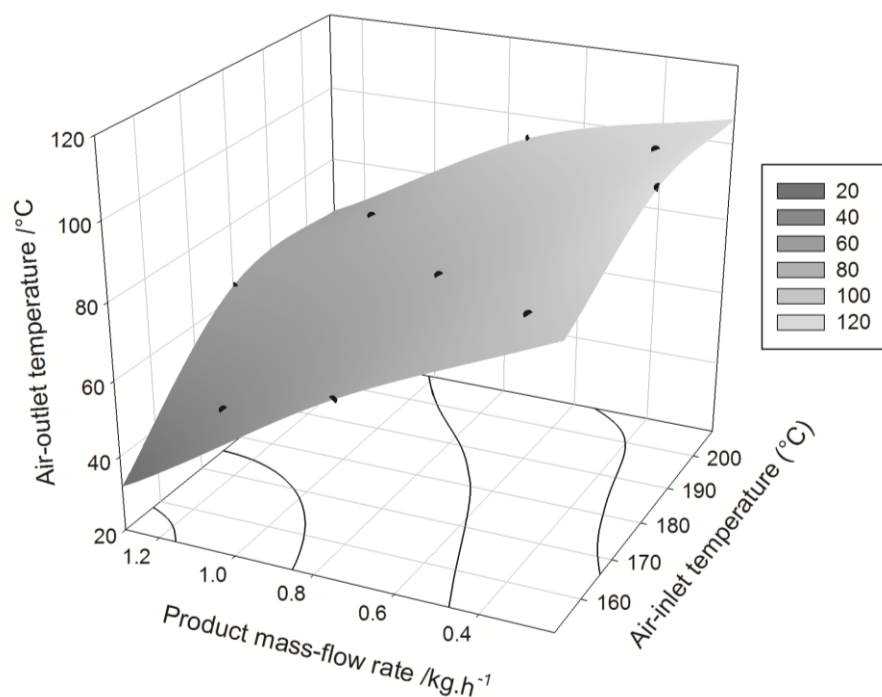


Fig. 5.44 Air-outlet temperatures depending on the drying conditions on a laboratory scale

¹³ Partly published in: Schmitz-Schug I, Foerst P, Kulozik U (2013) Impact of the spray drying conditions and residence time distribution on lysine loss in spray dried infant formula. Dairy Science & Technology 93(4):443-462

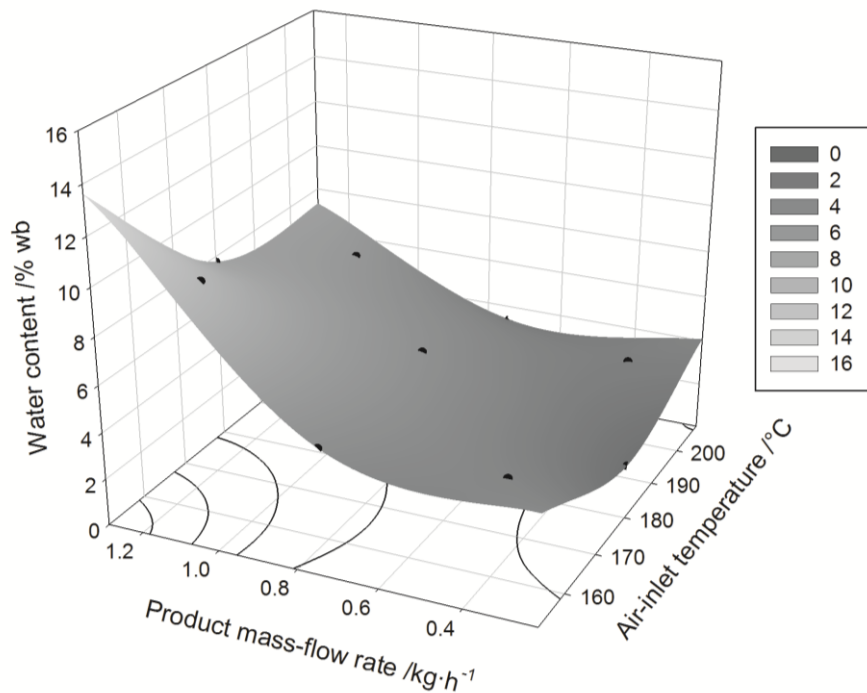


Fig. 5.45 Water content of the spray-dried powders produced on a laboratory scale

The water content of the powders, which were produced on a laboratory scale, was between $9.9 \pm 1.1\%$ wb and $3.7 \pm 0.6\%$ wb (Fig. 5.45), corresponding to water activities of 0.85 ± 0.04 to 0.10 ± 0.01 . Water content increased with an increasing product mass-flow rate and decreasing air-inlet temperature. Spray-drying conditions that led to high residual water contents in the powder were also characterized by low air-outlet temperatures. These findings are in accordance with results for whole-milk powder reported by Birchall et al. (2005). At a water content of $9.9 \pm 1.1\%$ wb ($a_w = 0.85 \pm 0.04$) drying was not completed and the powder was still humid. Moreover, in this case lactose was in the crystalline state contrary to the other spray-drying conditions that led to amorphous powders as shown in Fig. 5.46 and explained below. In Fig. 5.46 the sorption isotherm of the model dairy-formulation at 25°C is plotted with the experimental values of chapter 5.1.2. The values of the spray-dried powders agreed well with the values of the freeze-dried powders that were used to establish the sorption isotherm. Two different parts of the sorption isotherm can be distinguished. At a water activity of 0.43 and below, the lactose of the model dairy-formulation was in the amorphous state. Between a water activity of 0.43 and 0.53, a rupture in the sorption isotherm was observed that corresponded to the crystallization of lactose. At a water activity of 0.53 and above, lactose was in the crystalline state at 25°C. Consequently, the spray-dried powders were in the amorphous state except the powder with a moisture content of $9.9 \pm 1.1\%$ wb ($a_w = 0.85 \pm 0.04$). This was confirmed by DSC measurements. The glass-transition temperatures of the spray-dried powders were in accordance with the glass-transition temperatures of the freeze-dried powders that were used to determine the glass-transition curve (cf. chapter 5.1.2). The same was true for the molecular mobility expressed as transversal relaxation time T_2 . Consequently, the type of drying process did not influence the powder characteristics with regard to their sorption behavior, glass transition and molecular mobility. These powder properties were only dependent on the residual water content and physical state of the samples

after drying. Thus, the fundamental results of the previous chapters obtained with freeze-dried powders can be transferred to spray drying.

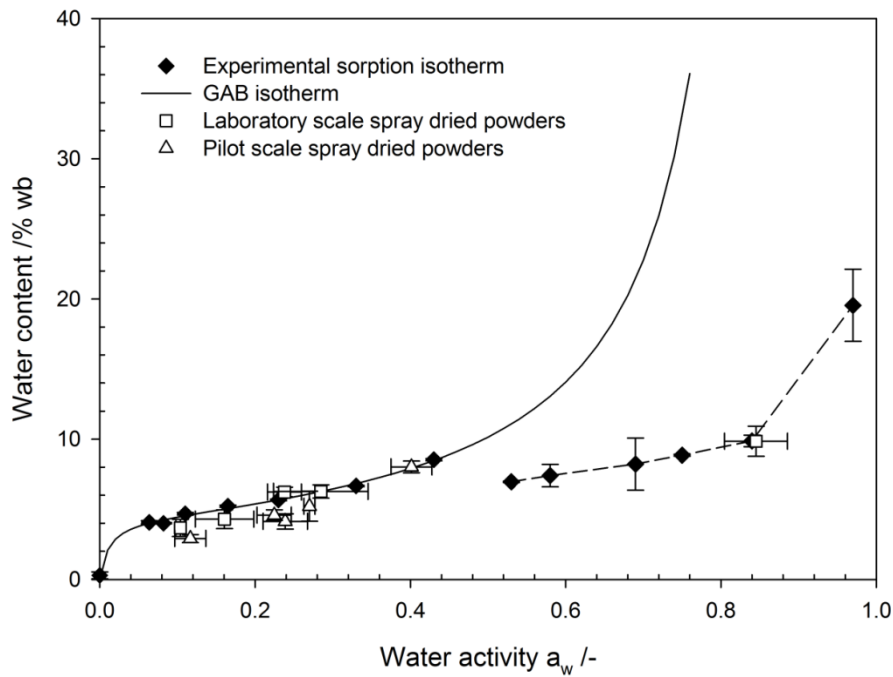


Fig. 5.46 Sorption isotherm of the model dairy-formulation in comparison with the spray-dried powders

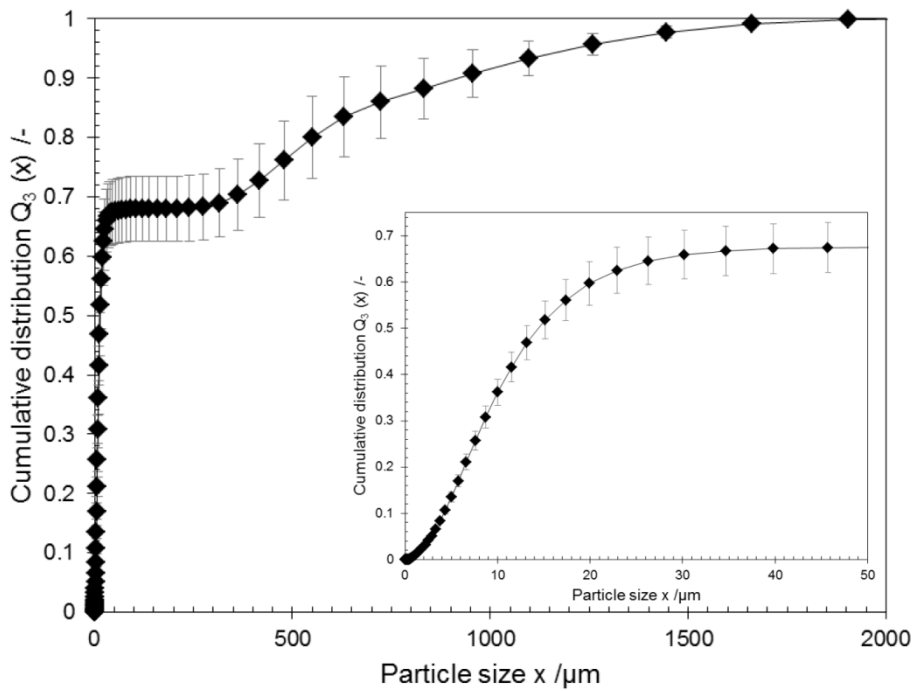


Fig. 5.47 Cumulative particle-size distribution $Q_3(x)$ of the powder produced by laboratory-scale spray drying at $T_{in} = 180^\circ\text{C}$ and $\dot{m}_{product} = 0.74 \text{ kg}\cdot\text{h}^{-1}$ (analysis pressure: 0.5 bar)

The cumulative particle-size distribution $Q_3(x)$ (analysis pressure of 0.5 bar) of the powder obtained by spray drying on a laboratory scale at $T_{in} = 180^\circ\text{C}$ and $\dot{m}_{product} = 0.74 \text{ kg}\cdot\text{h}^{-1}$ is depicted in Fig. 5.47. Two particle fractions can be distinguished: one fraction with particle sizes $<50 \mu\text{m}$ and one fraction with particles sizes $>200 \mu\text{m}$. The coarser fraction can be attributed to agglomerates which stayed intact at an analysis pressure of 0.5 bar and the finer fraction to non-agglomerated particles. The degree of agglomeration can be assessed further by increasing the analysis pressure. The median diameter d_{50} for laboratory scale powders together with the 10% and 90% percentiles (d_{10} and d_{90}) as a function of the analysis pressure are displayed in Fig. 5.48. With increasing analysis pressure agglomerates were destroyed to a higher degree, i.e., differences between the particle sizes at the different analysis pressures were a measure for the agglomeration degree. There was no significant difference between the d_{90} -values of the different spray-drying conditions but the d_{90} values decreased with an increasing analysis pressure. This shows the presence of agglomerates. The median diameter d_{50} was significantly higher at $T_{in} = 180^\circ\text{C}/\dot{m}_{product} = 0.74 \text{ kg}\cdot\text{h}^{-1}$ than under the other drying conditions, which indicates a higher portion of agglomerates. The same trend, however not significant, was observed for $T_{in} = 200^\circ\text{C}/\dot{m}_{product} = 1.10 \text{ kg}\cdot\text{h}^{-1}$. Both conditions were characterized by higher particle water contents (Fig. 5.45) and lower air outlet temperatures (Fig. 5.44) than the other spray-drying conditions. This might favor agglomeration during spray drying (Gianfrancesco et al. 2009). The d_{10} -values did not differ significantly in the experimental range. The particle sizes measured at an analysis pressure of 3 bar are a good indicator for the droplet size created by atomization. The atomization can be characterized by the air-liquid ratio of the nozzle (ALR_{nozzle}). A higher $ALR_{nozzles}$ means a higher relative energy input, which should lead to smaller droplet sizes (Masters 1991). However, no significant impact of the ALR_{nozzle} on the particle sizes measured at an analysis pressure of 3 bar was observed in the experimental range, which is probably due to the fact that the difference between the ALR_{nozzle} is rather small. The Sauter mean diameter is generally considered to be the most appropriate mean particle size for the characterization of the droplets created by atomization (Filková and Mujumdar 1995):

$$d_{3,2} = \frac{\sum_1^i D_i^3 \cdot f_i}{\sum_1^i D_i^2 \cdot f_i} \quad 5.7$$

where D_i is the particle diameter with the frequency f_i . Fig. 5.49 shows the Sauter mean diameter of the powders that were spray dried on a laboratory scale. Differences between the experimental conditions were small.

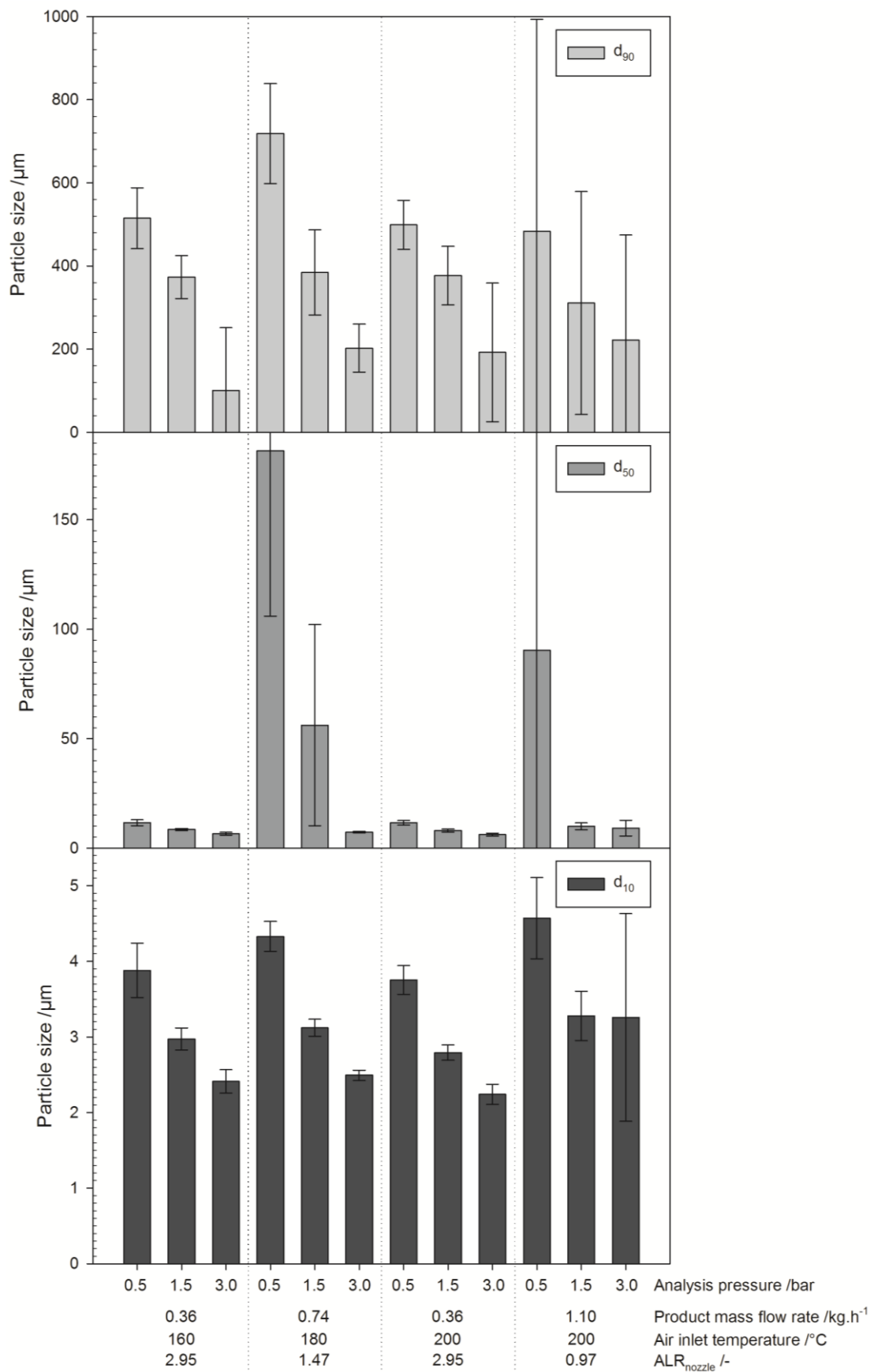


Fig. 5.48 Particle sizes and agglomeration degree of powders produced on a laboratory scale

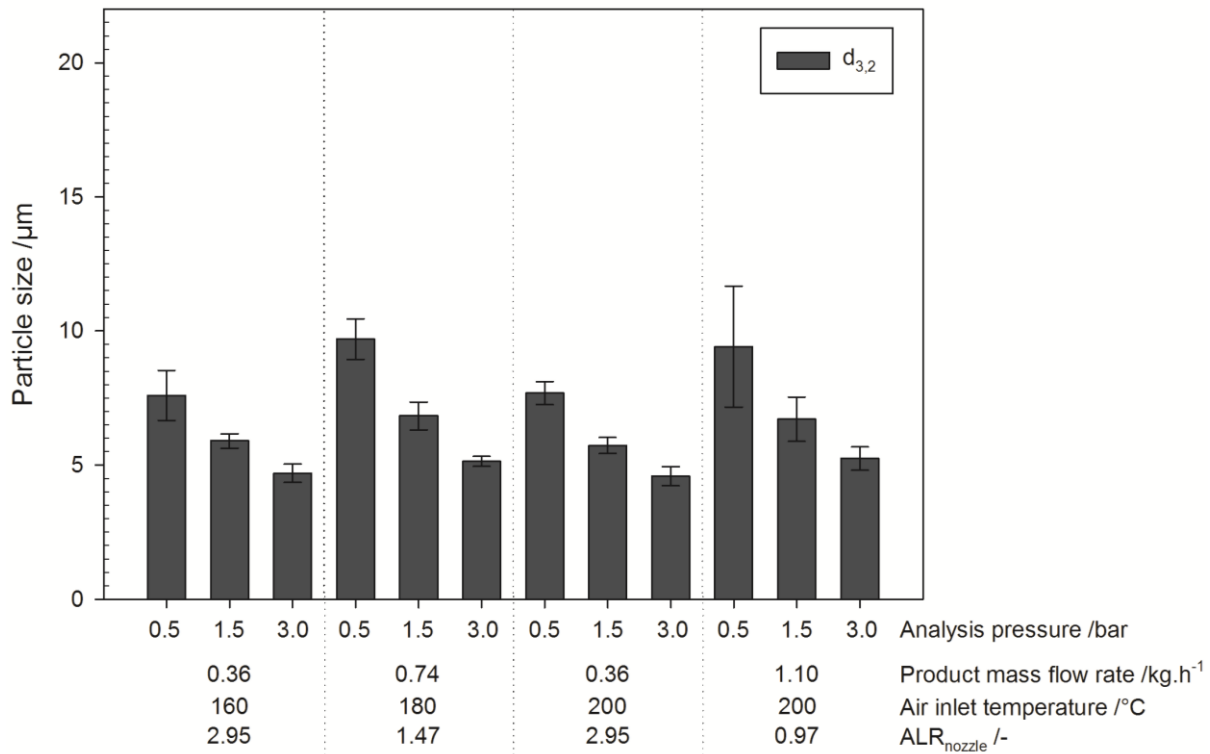


Fig. 5.49 Sauter mean diameter $d_{3,2}$ of powders produced on a laboratory scale

Spray drying on a pilot scale gave similar results. For air-inlet temperatures of 160-200°C, the air-outlet temperature was between $60.1 \pm 4.1^\circ\text{C}$ and $105.7 \pm 4.0^\circ\text{C}$ (Fig. 5.50). The measured water contents of the produced powders were between $8.0 \pm 0.4\%$ wb and $2.9 \pm 0.3\%$ wb and the corresponding water activities between 0.40 ± 0.03 and 0.12 ± 0.02 (Fig. 5.51). Comparing the powder characteristics with the sorption isotherm shows a good analogy (Fig. 5.46). On a pilot scale, no humid samples were obtained and all samples were in the amorphous state after spray drying. However, the drying condition that led to a powder with a water content of $8.0 \pm 0.4\%$ wb represented the upper limit of drying capacity and the process was unstable. In accordance with the observations of laboratory-scale spray drying, the glass-transition temperatures and the molecular mobility of the spray-dried powders agreed well with the results obtained for the freeze-dried powders. In the pilot-scale spray dryer it was possible to measure the humidity of the outlet air. In Fig. 5.52 the relative humidity of the outlet air is correlated with the water activity of the spray-dried powders. At all conditions, the water activity of the powder was only slightly higher than the relative humidity of the outlet air. Consequently, the particles were almost in equilibrium with the drying air at the spray-dryer outlet. The importance of the relative humidity of the outlet air was elaborated by Schuck et al. (2008). They demonstrated that it was necessary to control the relative humidity of the outlet air to regulate the water activity and moisture content of dairy powders. Similarly, Ozmen and Langrish (2003) concluded that dried powder particles were almost in equilibrium with the drying gas during the spray drying of skim milk on a pilot scale.

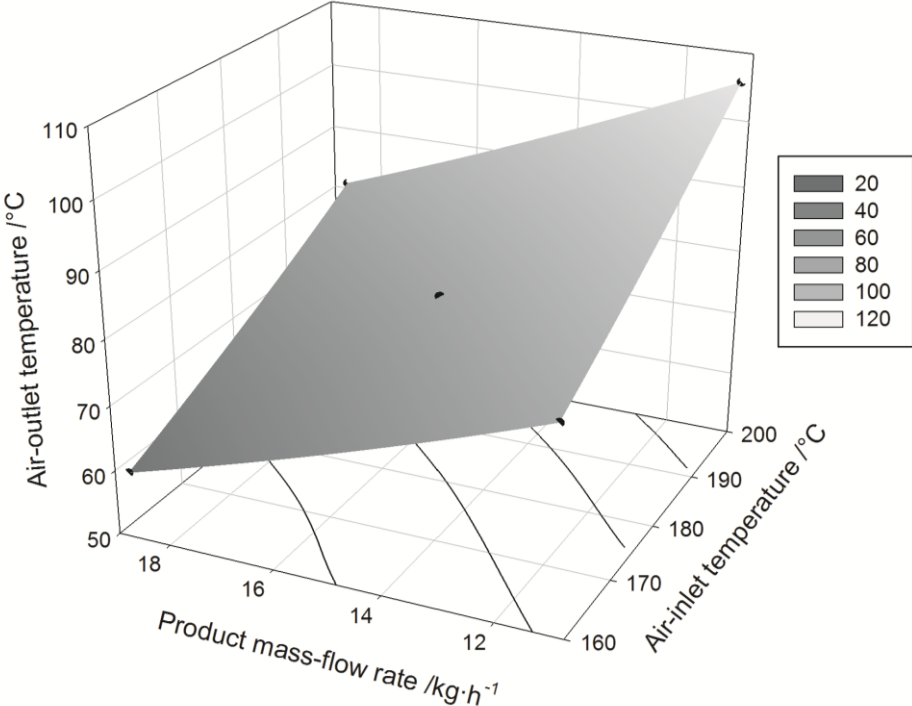


Fig. 5.50 Air-outlet temperature as a function of the spray-drying conditions on a pilot scale

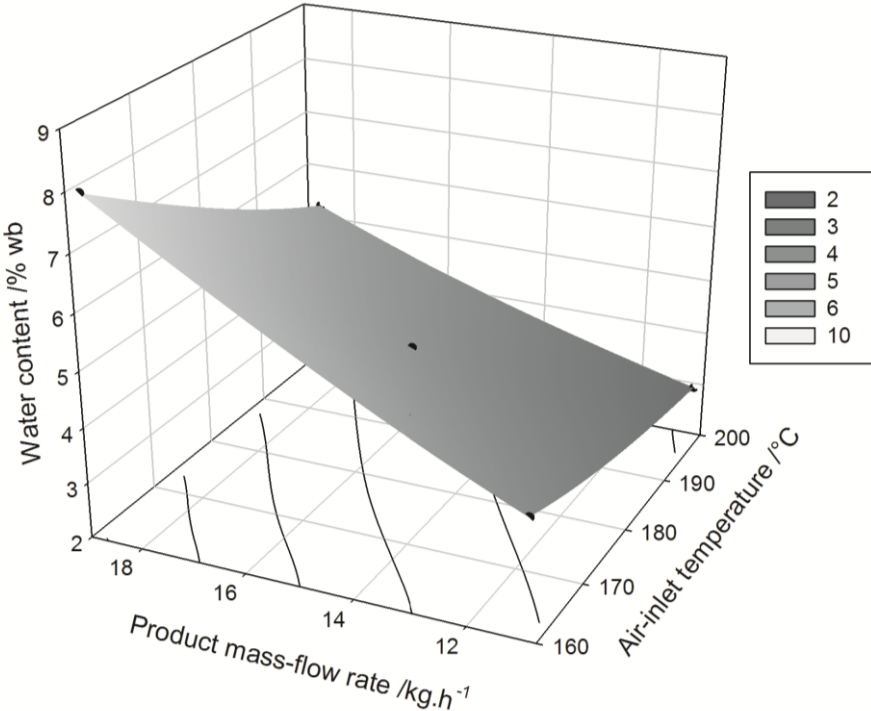


Fig. 5.51 Water content of the powders that were spray dried on a pilot scale

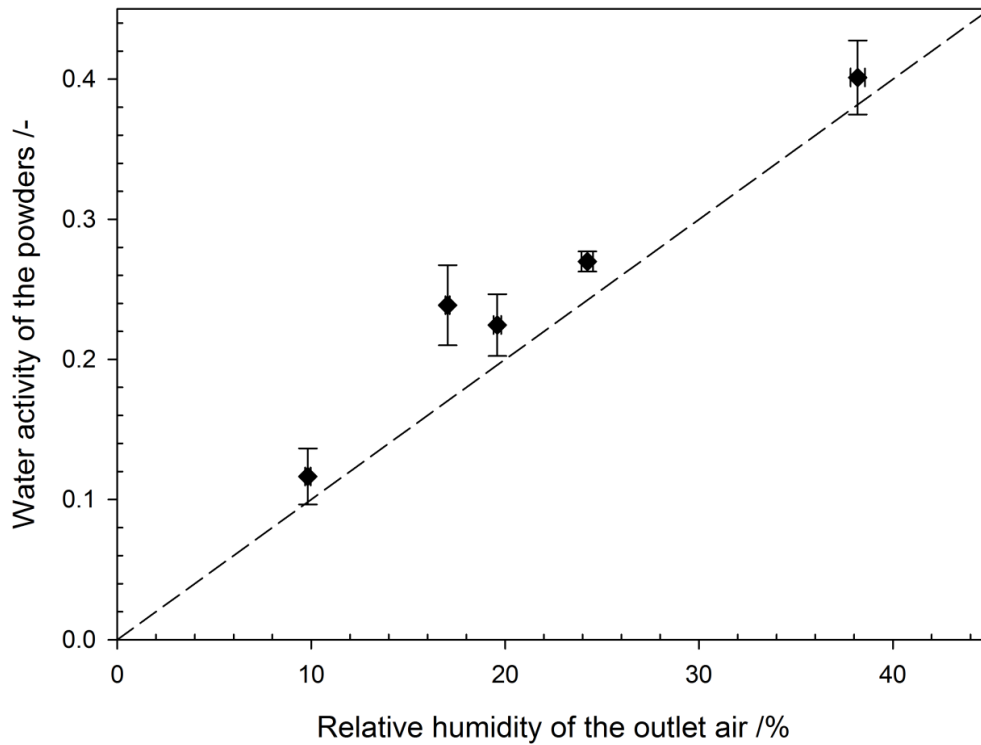


Fig. 5.52 Relation between the water activity of the spray-dried powders and the relative humidity of the outlet air for pilot-scale spray drying

As in laboratory-scale spray drying, powders were obtained with particle-size distributions that were composed of two different particle size fractions (Fig. 5.53). The coarser fraction was characterized by particle sizes $>250\ \mu\text{m}$ and the finer fraction by particle sizes $<60\ \mu\text{m}$ at an inlet air temperature $T_{in} = 180^\circ\text{C}$ and a product mass-flow rate $\dot{m}_{Product} = 14.9\ \text{kg}\cdot\text{h}^{-1}$. Thus, the particles-size distribution is in the same range as after laboratory-scale spray drying (cf. Fig. 5.47), which shows that the scale-up of the nozzle parameters was successful. However, the percentage of the coarser fraction is bigger than in the case of laboratory-scale spray drying, which means that more agglomeration occurs during pilot-scale spray drying. This is probably due to the different geometries of the two spray dryers which lead to different flow patterns and particle residence-time distributions. This observation is confirmed when the d_{10} , d_{50} and d_{90} -values are analyzed (Fig. 5.55). At first glance, a similar pattern is shown as for the laboratory scale powders. However, the d_{90} , d_{50} and d_{10} -values are shifted to bigger particle sizes which is due to the higher percentage of the coarser fraction. These results are supported by the Sauter mean diameters of spray drying on a pilot (Fig. 5.54) and laboratory scale (Fig. 5.49). At an analysis pressure of 0.5 bar, the Sauter mean diameter of the pilot-scale powders was significantly bigger than of the laboratory scale powders but when the analysis pressure was increased, the divergence decreased. At an analysis pressure of 3 bar, i.e., when the agglomerates were destroyed, the Sauter mean diameters were in the same range. This proves that the scale-up of the nozzle parameters was successful.

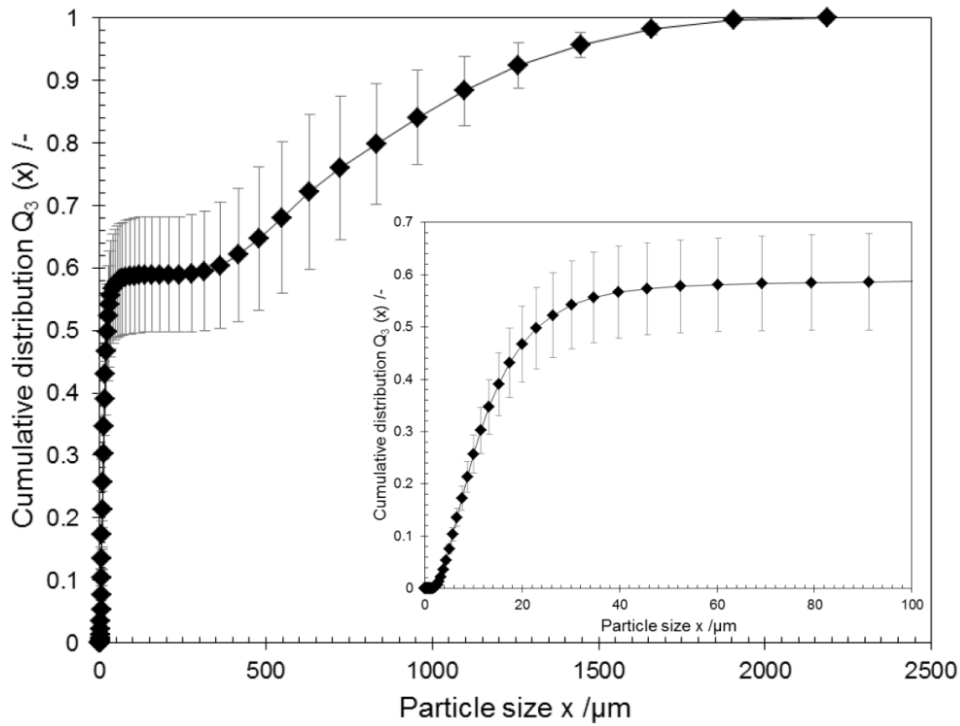


Fig. 5.53 Cumulative particle size distribution $Q_3(x)$ of the powder that was spray dried on a pilot scale at $T_{in} = 180^\circ\text{C}$ and $\dot{m}_{product} = 14.9 \text{ kg}\cdot\text{h}^{-1}$ (analysis pressure: 0.5 bar)

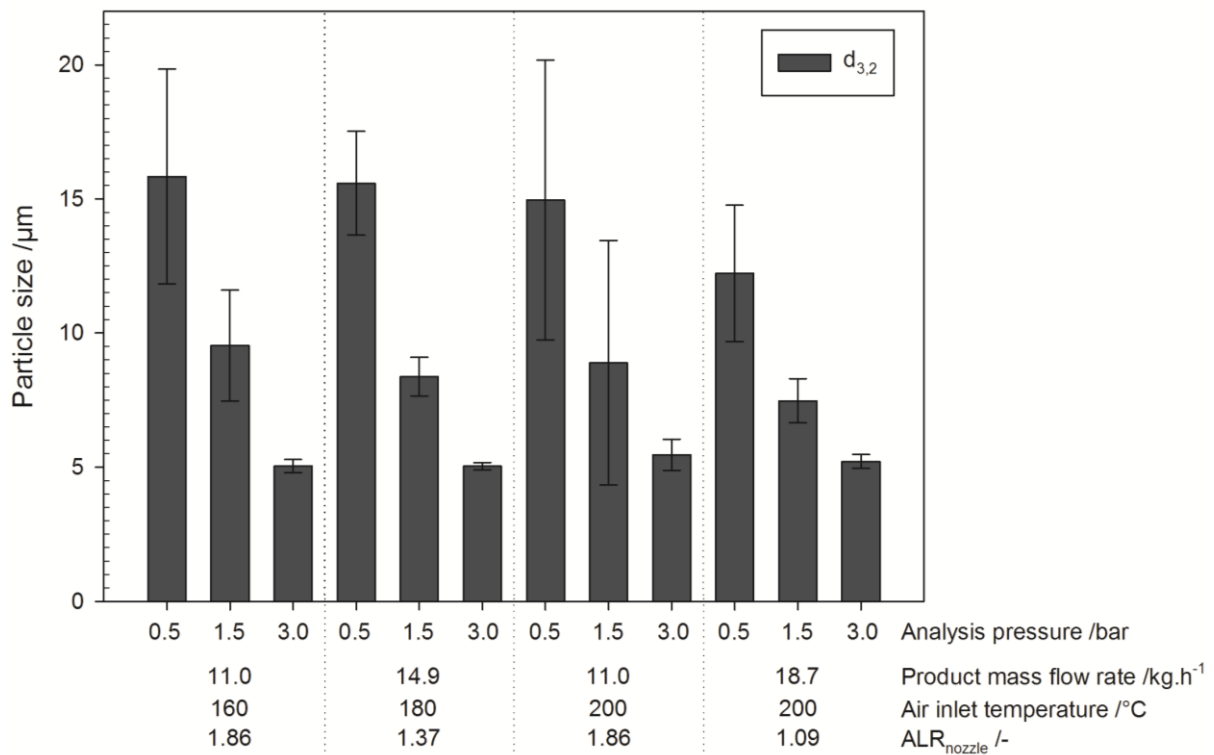


Fig. 5.54 Sauter mean diameter $d_{3,2}$ of the powders that were spray dried on a pilot scale

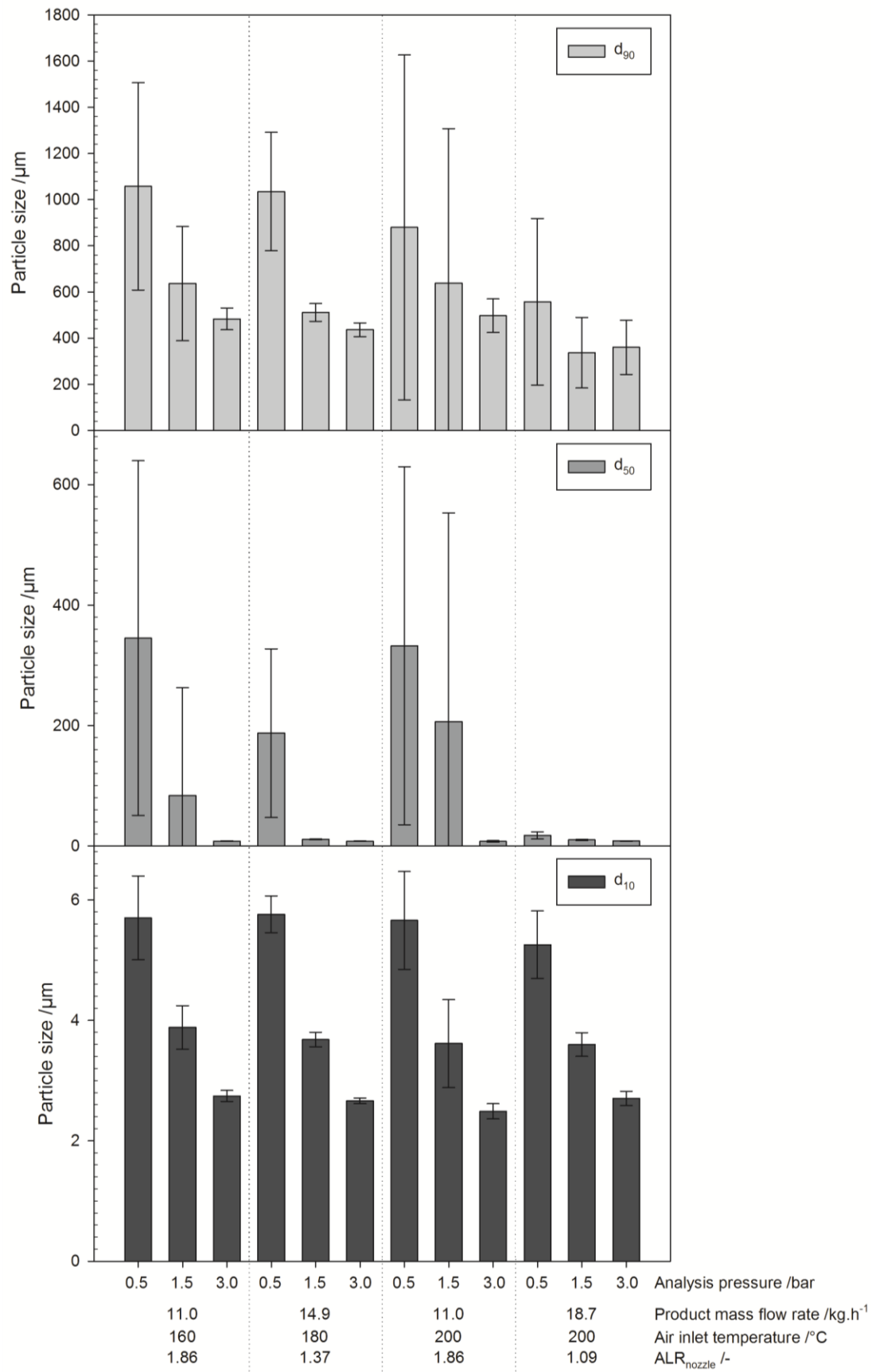


Fig. 5.55 Particle sizes and agglomeration degree of the powders that were spray dried on a pilot scale

To sum up, in pilot-scale spray drying, the powder characteristics and air outlet temperatures were similar to the laboratory scale experiments. However, higher air-liquid ratios (ALR_{dryer}) were needed on a laboratory scale ($ALR_{dryer} = 36-180$) than on a pilot scale ($ALR_{dryer} = 30-49$) to obtain the same drying result. This was probably due to the different form of the two dryers. The laboratory scale dryer resembled a tall-form dryer (height:diameter $\approx 3.2:1$). It was characterized by relatively short residence times in the spray dryer as will be shown below. As a consequence, a high energy input, i.e., a high air mass-flow rate, is needed to obtain the same drying result as in pilot scale drying. The pilot scale dryer was a short-form dryer (height:diameter $\approx 1.6:1$), in which recirculation and backflow of air and, consequently, powder particles might occur (Fletcher et al. 2006) and it was larger than the laboratory scale dryer. As will be shown in the following, this led to longer residence times and the energy of the air mass-flow could be used in a more efficient way.

5.4.2 Residence-time distribution of the particles

Particle residence-time distribution is an important parameter of the spray-drying process. On the one hand, particle residence-time has to be long enough to ensure the drying of the particles. On the other hand, long residence times can lead to the deterioration of sensitive products. As explained in chapter 5.4.1, the particle temperature rises when the particle concentration increases. Consequently, longer residence times result in longer times at high concentration and high temperature which is harmful to thermally sensitive ingredients, for example lysine. In order to assess the differences between laboratory-scale spray drying and pilot-scale spray drying, the particle residence-time distribution was measured in the range of the experimental conditions.

The particle residence-time distribution of the laboratory-scale spray dryer (Fig. 4.1) was characterized by a median residence time τ_{50} of 6 s as well as by τ_{10} and τ_{90} values of 0.2 s and 55 s, respectively. In contrast, longer particle residence-times were measured in the pilot-scale dryer (Fig. 5.57). Here, a median particle residence-time τ_{50} of 17 s was obtained, the τ_{10} and τ_{90} values being 4 s and 1 min 22 s, respectively. The last particles left the dryer after about 6 min. Particle residence-times measured in this study were in the same range as residence times reported in the literature (Gianfrancesco 2009, Jeantet et al. 2008, Kieviet and Kerkhof 1995, Mazza et al. 2003). These long particle residence-times indicate recirculation flows inside the drying chamber and possible wall deposition of particles. This hypothesis is confirmed by the comparison of the mean residence time of air with the mean residence time of particles. Assuming plug flow inside the spray dryer, the mean residence time of the air can be estimated by dividing the volume of the spray dryer by the air volume-flow. Using this approach, the calculated mean residence time of air is 1.1 s for the laboratory-scale spray dryer and 12 s for the pilot-scale dryer. In contrast to that, the mean particle residence-times, which were calculated from the experimental particle residence-time distributions, were 24.8 s for the laboratory-scale dryer and 90.2 s for the pilot-scale spray dryer. Consequently, the particle mean residence time is longer than the mean residence time of air. This is in accordance with the observations of other authors (Gianfrancesco 2009, Jeantet et al. 2008, Kieviet and Kerkhof 1995, Mazza et al. 2003). This divergence can be explained by the presence of recirculation zones and powder backflow inside the drying chamber as well as by temporary particle deposition on the dryer walls (Gianfrancesco 2009).

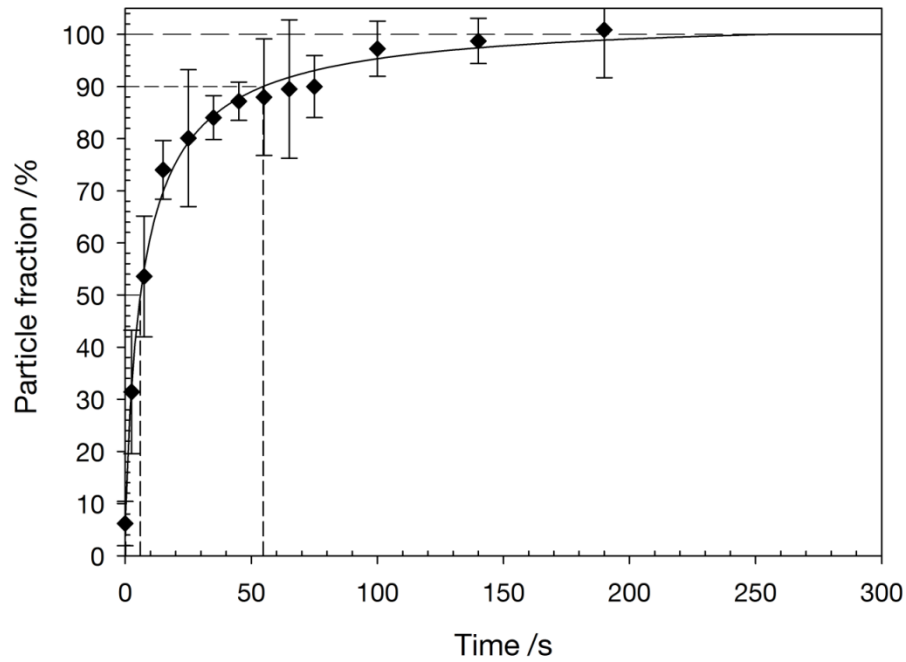


Fig. 5.56 Particle residence-time distribution of the laboratory-scale spray dryer

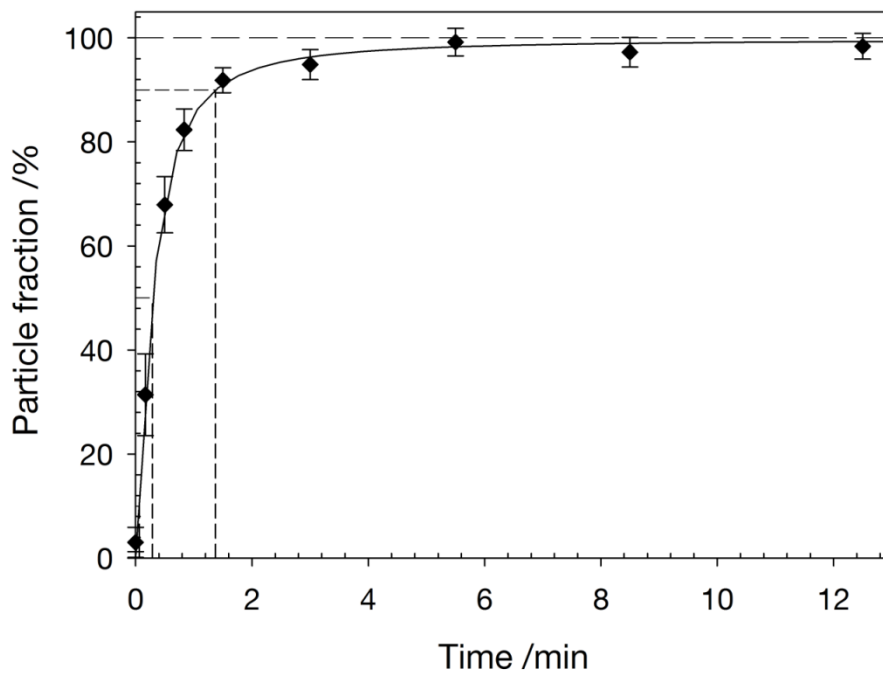


Fig. 5.57 Particle residence-time distribution of the pilot-scale spray dryer

In conclusion, the particle residence-time distribution in the laboratory-scale dryer differs significantly from the particle residence-time distribution in the pilot-scale spray dryer. As a consequence, the particle history is not equal in both dryers, which has an impact on the thermal stress and on lysine loss as will be shown in chapter 5.4.3. It was confirmed that particle residence-time distributions can assume considerable values. Thus, they cannot be neglected in attempts to minimize product damage of thermally sensitive components.

5.4.3 Lysine loss

Lysine loss caused by spray drying

The model dairy-formulation was spray dried on a laboratory scale as well as on a pilot scale and available lysine was measured as a function of the spray-drying conditions (Fig. 5.58 and Fig. 5.59). Lysine loss is reported as a function of the air-liquid ratio (ALR_{dryer}) of the respective spray dryer and not as a function of the product mass-flow rate so that laboratory scale conditions can be compared with pilot scale conditions. Despite partially high air outlet temperatures and low particle water contents reported for laboratory-scale spray drying in chapter 5.4.1, insignificant lysine losses were detected in the model dairy-formulation after spray drying on a laboratory scale (Fig. 5.58). The lysine loss did not exceed $\leq 3\%$.

Regarding lysine loss due to spray drying on a pilot scale, quite a different pattern than on a laboratory scale was determined (Fig. 5.59). Here, lysine loss of up to $10.4 \pm 2.9\%$ was measured after spray drying. Lysine loss increased with increasing air-inlet temperatures and increasing air-liquid ratio (ALR_{dryer}). This means that more severe drying conditions, i.e., conditions that lead to higher air outlet temperatures and, consequently, also to higher product temperatures and to lower residual water contents of the powders, cause higher lysine losses.

In order to highlight the importance of the particle history during spray drying, the impact of temperature, concentration and time on lysine loss has to be considered. The kinetics of lysine loss under conditions relevant to spray drying as a function of concentration, temperature and physical state were presented in chapter 5.1.4. It was shown that lysine loss increased with increasing temperatures and time following second-order reaction kinetics but most of all the role of the physical state was highlighted. The physical state of the system, glassy, rubbery or crystalline, is determined by the physical state of the lactose contained in the model dairy-formulation. From the results it became obvious that the maximum of lysine loss coincided with the transition zone from the rubbery to the crystalline state. The rubbery state as well as the crystalline state is characterized by a high mobility in the system (see chapter 5.1) which might favor lysine loss. However, the availability of lactose for the early Maillard reaction between lactose and the amino group of lysine is, as expected, obviously higher in the rubbery state than in the crystalline state. This results in a maximum of lysine loss in the transition zone. In summary, the lysine loss due to spray drying can only be understood and controlled by taking the physical state as well as the temperature of the particles and concentration into account. Moreover, the particle residence-time plays a major role as it determines the possible reaction time. As dehydration of small droplets is fast, particles will have high concentrations and temperatures in the case of long residence times. These are critical conditions regarding lysine loss and, consequently, high lysine losses will arise. The residence time on a laboratory scale was probably not long enough for the particles to reach air temperature whereas on a pilot scale the longer residence times would also lead to higher particle temperatures. This explains why no or little lysine loss was detected in powders that were spray dried on a laboratory scale but lysine losses of up to $10.4 \pm 2.9\%$ were measured in powders that were spray dried on a pilot scale. These results are consistent with values that can be found in the literature (Ferrer et al. 2000, Finot 1983).

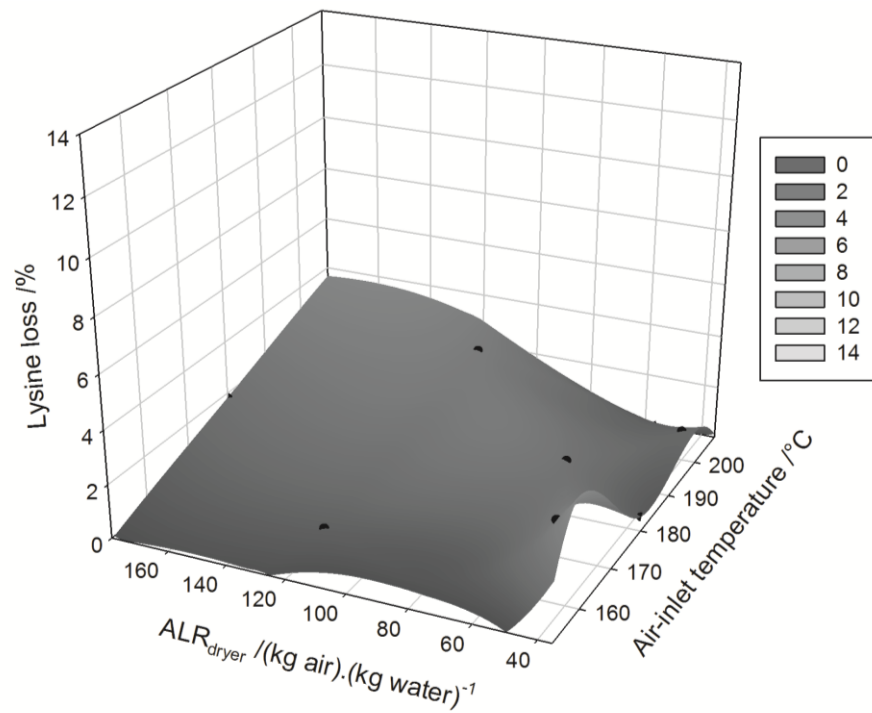


Fig. 5.58 Lysine loss due to spray drying on a laboratory scale

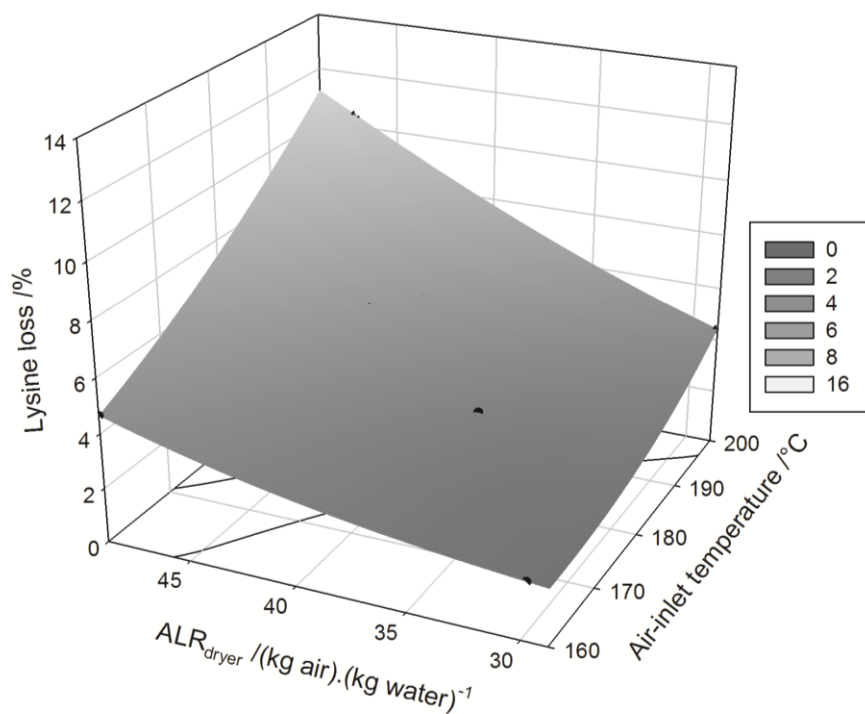


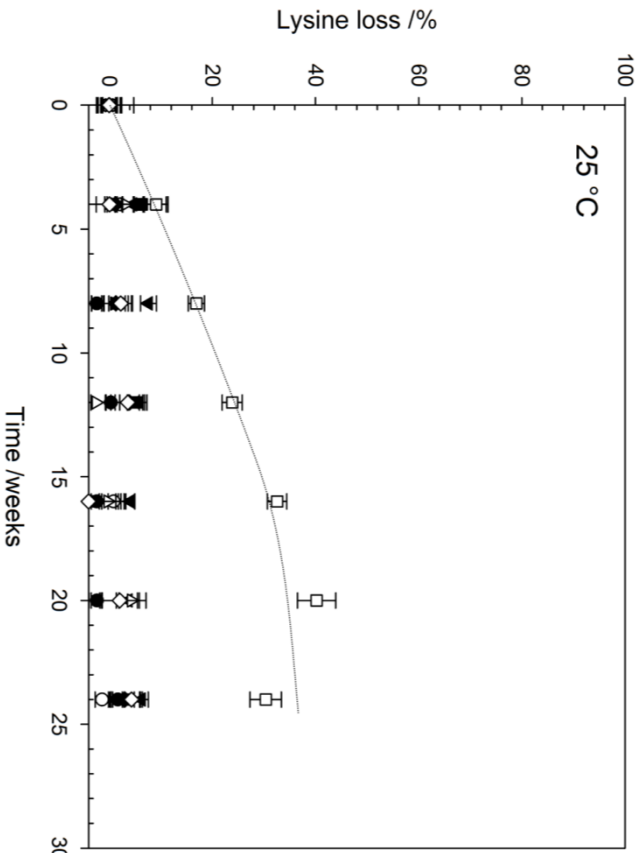
Fig. 5.59 Lysine loss due to spray drying on a pilot scale

Lysine loss during storage

The spray-dried powders were stored at 25°C and 37°C for 6 months and lysine loss was monitored throughout the storage period in order to assess the relative impact of storage vs. the drying stage. Lysine loss was expressed in percentage points of the initially available lysine (before spray drying) but only the fraction of lysine loss occurring during the storage is considered in Fig. 5.60 to Fig. 5.63. During the storage at 25°C of powders produced by laboratory-scale spray drying no significant lysine loss occurred with the exception of the following drying condition (Fig. 5.60). Lysine loss in samples that were spray dried on a laboratory scale at $T_{in} = 180^\circ\text{C}$ and $\dot{m}_{product} = 1.3 \text{ kg}\cdot\text{h}^{-1}$ ($X^* = 7.8 \pm 0.5\%$ wb) increased during the storage at 25°C and reached about 35% after 24 weeks. At 37°C higher losses were found than at 25°C (Fig. 5.61). Again, the highest losses ($88.9 \pm 2.2\%$ after 24 weeks) were measured in the powders that were spray dried at $T_{in} = 160^\circ\text{C}$ and $\dot{m}_{product} = 1.1 \text{ kg}\cdot\text{h}^{-1}$ ($X^* = 7.8 \pm 0.5\%$ b).

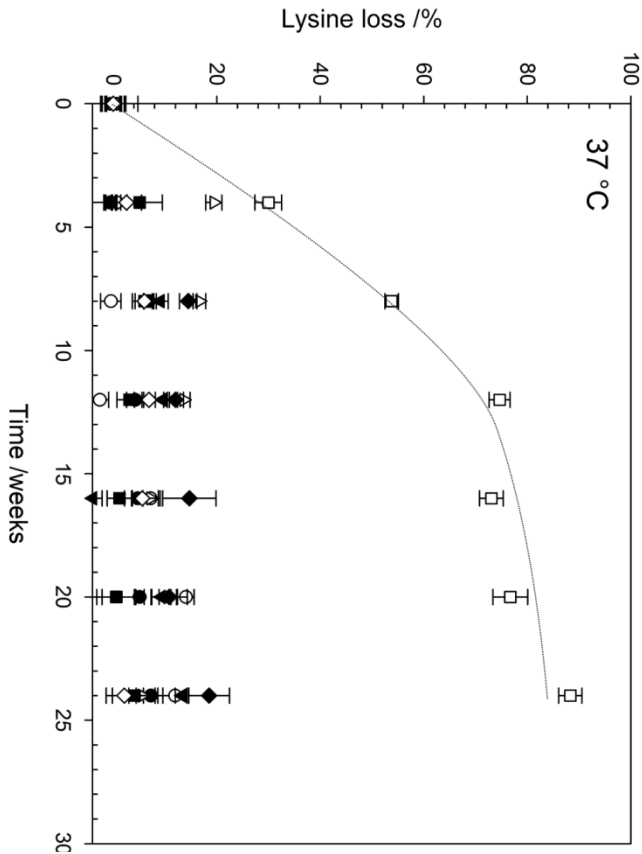
A similar trend was observed in the powders produced by pilot-scale spray drying. Here, at a storage temperature of 25°C, no significant lysine loss was measured during the first 20 weeks of the storage period except in the powders which were spray dried at $T_{in} = 160^\circ\text{C}$ and $\dot{m}_{product} = 18.7 \text{ kg}\cdot\text{h}^{-1}$ ($X^* = 8.0 \pm 0.4\%$ wb) where lysine loss of about 30% occurred within 24 weeks (Fig. 5.62). This will be discussed further below. The water content of this powder was in the same range as the water content of the laboratory scale powder with the highest lysine loss during storage ($T_{in} = 180^\circ\text{C}$ and $\dot{m}_{product} = 1.3 \text{ kg}\cdot\text{h}^{-1}$, $X^* = 7.8 \pm 0.5\%$ wb). After 24 weeks lysine loss reached about 35% in the laboratory-scale powder and about 30% in the pilot-scale powder. After spray drying, no significant lysine loss was measured in both powders and the air-outlet temperatures were in the same range with $63.3 \pm 7.4^\circ\text{C}$ on a laboratory scale and $60.1 \pm 4.1^\circ\text{C}$ on a pilot scale. In conclusion, lysine loss during the storage at a given temperature seems to be governed by the water content of the powder independently of the spray-dryer scale, particle residence-time and air-inlet temperature.

During the storage of the pilot scale powders at 37°C (Fig. 5.63), the highest losses of $89.0 \pm 1.8\%$ were observed in the samples of the same drying condition as at 25°C ($T_{in} = 180^\circ\text{C}$ and $\dot{m}_{product} = 1.3 \text{ kg}\cdot\text{h}^{-1}$, $X^* = 7.8 \pm 0.5\%$ wb). Comparing the corresponding laboratory-scale powder ($T_{in} = 180^\circ\text{C}$ and $\dot{m}_{product} = 1.3 \text{ kg}\cdot\text{h}^{-1}$, $X^* = 7.8 \pm 0.5\%$ wb) shows that the extent of lysine loss was similar. In the storage period the extent of lysine loss was less pronounced with decreasing water content of the pilot-scale powders. During pilot-scale spray drying (Fig. 5.59), the maximum of lysine loss ($10.4 \pm 2.4\%$) occurred at $T_{in} = 200^\circ\text{C}$ and $\dot{m}_{product} = 11.0 \text{ kg}\cdot\text{h}^{-1}$ with a water content of $2.9 \pm 0.3\%$ wb in the produced powder and $T_{out} = 105.7 \pm 4.0^\circ\text{C}$. During the storage of this powder at 25°C and 37°C no significant lysine loss took place (Fig. 5.62 and Fig. 5.63). The same is true for a powder with a similar water content $X^* = 2.3 \pm 0.3\%$ (Fig. 5.60 and Fig. 5.61) which was spray dried on a laboratory scale ($T_{in} = 180^\circ\text{C}$, $T_{out} = 106.7 \pm 12.7^\circ\text{C}$, $\dot{m}_{product} = 0.2 \text{ kg}\cdot\text{h}^{-1}$) without any significant lysine loss due to spray drying (Fig. 5.58). These observations support the assumption that the water content during the storage at a given temperature is the decisive factor concerning lysine loss during the storage. Furthermore, it is important to control the storage temperature because a temperature increase from 25°C to 37°C more than doubled the lysine loss. To optimize spray drying with regard to the overall lysine loss in the final product it is consequently necessary to



- $T_{in} = 180^{\circ}\text{C}, m_{product} = 0.7 \text{ kg}\cdot\text{h}^{-1}, X_i = 5.5\% \text{ wb}$
- $T_{in} = 160^{\circ}\text{C}, m_{product} = 0.4 \text{ kg}\cdot\text{h}^{-1}, X_i = 4.3\% \text{ wb}$
- ◊ $T_{in} = 200^{\circ}\text{C}, m_{product} = 0.4 \text{ kg}\cdot\text{h}^{-1}, X_i = 3.7\% \text{ wb}$
- ◻ $T_{in} = 200^{\circ}\text{C}, m_{product} = 1.1 \text{ kg}\cdot\text{h}^{-1}, X_i = 6.3\% \text{ wb}$
- ◼ $T_{in} = 180^{\circ}\text{C}, m_{product} = 0.2 \text{ kg}\cdot\text{h}^{-1}, X_i = 2.3\% \text{ wb}$
- ◼ $T_{in} = 180^{\circ}\text{C}, m_{product} = 1.3 \text{ kg}\cdot\text{h}^{-1}, X_i = 7.8\% \text{ wb}$
- ◆ $T_{in} = 152^{\circ}\text{C}, m_{product} = 0.7 \text{ kg}\cdot\text{h}^{-1}, X_i = 5.3\% \text{ wb}$
- ◇ $T_{in} = 208^{\circ}\text{C}, m_{product} = 0.7 \text{ kg}\cdot\text{h}^{-1}, X_i = 3.4\% \text{ wb}$

Fig. 5.60 Progress of lysine loss in the powder samples of laboratory-scale spray drying during storage at 25°C



- $T_{in} = 180^{\circ}\text{C}, m_{product} = 0.7 \text{ kg}\cdot\text{h}^{-1}, X_i = 5.5\% \text{ wb}$
- $T_{in} = 160^{\circ}\text{C}, m_{product} = 0.4 \text{ kg}\cdot\text{h}^{-1}, X_i = 4.3\% \text{ wb}$
- ◊ $T_{in} = 200^{\circ}\text{C}, m_{product} = 0.4 \text{ kg}\cdot\text{h}^{-1}, X_i = 3.7\% \text{ wb}$
- ◻ $T_{in} = 200^{\circ}\text{C}, m_{product} = 1.1 \text{ kg}\cdot\text{h}^{-1}, X_i = 6.3\% \text{ wb}$
- ◼ $T_{in} = 180^{\circ}\text{C}, m_{product} = 0.2 \text{ kg}\cdot\text{h}^{-1}, X_i = 2.3\% \text{ wb}$
- ◼ $T_{in} = 180^{\circ}\text{C}, m_{product} = 1.3 \text{ kg}\cdot\text{h}^{-1}, X_i = 7.8\% \text{ wb}$
- ◆ $T_{in} = 152^{\circ}\text{C}, m_{product} = 0.7 \text{ kg}\cdot\text{h}^{-1}, X_i = 5.3\% \text{ wb}$
- ◇ $T_{in} = 208^{\circ}\text{C}, m_{product} = 0.7 \text{ kg}\cdot\text{h}^{-1}, X_i = 3.4\% \text{ wb}$

Fig. 5.61 Increase of lysine loss in the powder samples of laboratory-scale spray drying during storage at 37°C

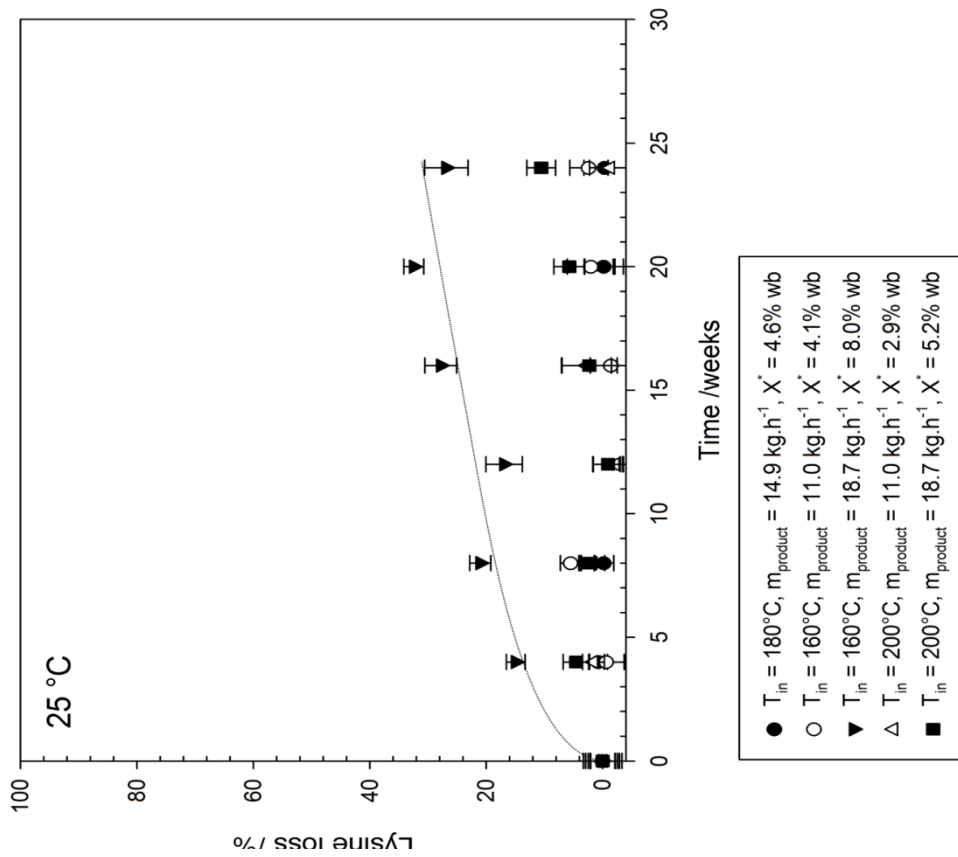


Fig. 5.62 Lysine loss occurring in the powders of pilot-scale spray drying during storage at 25°C.

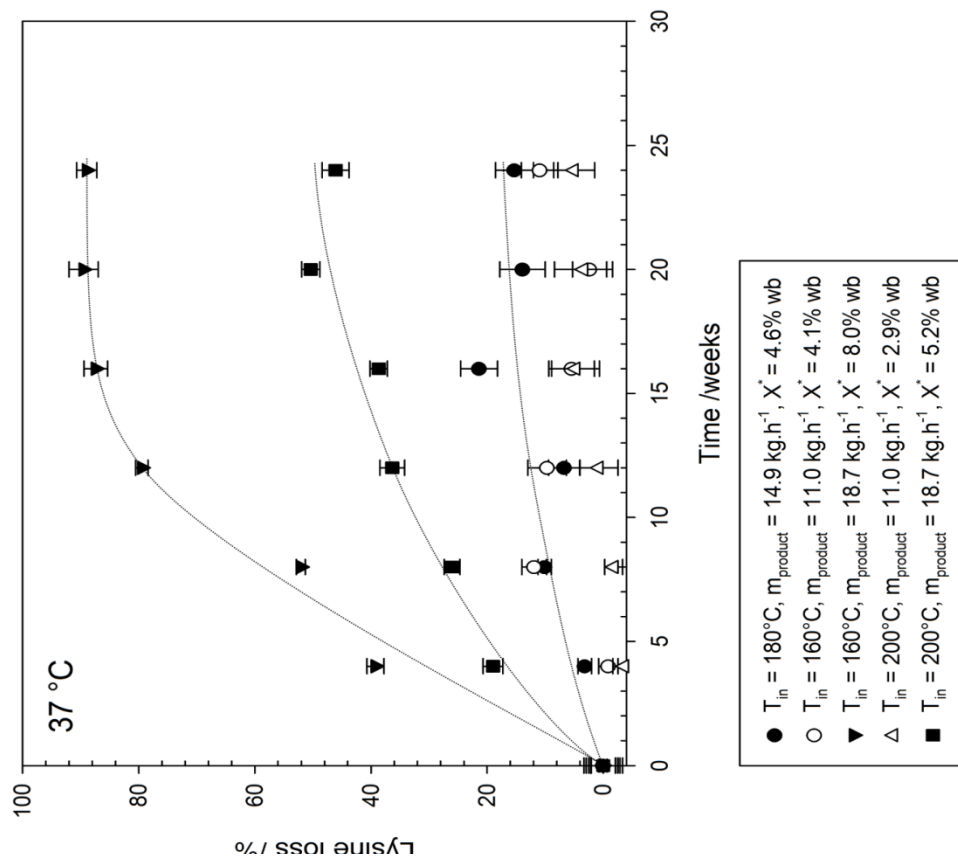


Fig. 5.63 Lysine loss in the powders of pilot-scale spray drying during storage at 37°C.

minimize lysine loss during spray drying and to ensure low residual water contents in the powder at the same time in order to minimize lysine loss during storage.

The results concerning the lysine loss during storage showed that in this study the extent of lysine loss is controlled by the storage temperature and the water content of the powders independently of the type of spray dryer used. Literature values for lysine loss during storage are quite scattered. Malec et al. (2002) found higher lysine losses than in this study. They observed a lysine loss of about 65% after the storage of a lactose-casein model system with a water activity of 0.52 at 37°C for 16 days and after 50 days for a water activity of 0.33. Chavez-Servin et al. (2008) measured a lysine loss of 7.98% in infant formula stored at 25°C for 6 months. These results are in good accordance with this study in contrast to the results published by Ferrer et al. (2000) who did not determine any significant lysine loss in adapted infant formula stored at 20 and 37°C for 6 months. These differences can probably be explained by the variations in composition, water content and physical state of the powders studied.

5.5 Drying kinetics

The knowledge of the product-specific drying kinetics is a prerequisite for simulating the spray-drying process. During this project, the applicability of drying sessile droplets and thin films in a drying channel for measuring the drying kinetics was assessed and the characteristic drying-rate curve model was compared to the reaction-engineering approach. The sample surface-size, which is needed for the drying-kinetics models, corresponded to the surface of the cavity in the sample holder in the case of thin-film drying. In the case of droplet drying, contact angle measurements were conducted to determine the surface size of the droplets (Fig. 5.64 and Table 5.4). The contact angle decreased with a decreasing droplet volume. Higher contact angles correspond to more spherical sessile droplets, which were desired for the drying kinetics study.

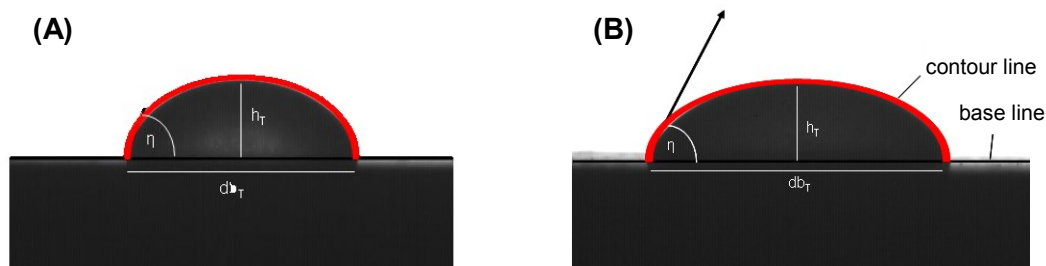


Fig. 5.64 Contact angle measurements of the model dairy-formulation (20% dry matter) at 20°C: droplet with a volume of 50 μl (A) and a volume of 100 μl (B)

Table 5.4 Contact angle and characteristic sizes of model dairy-formulation droplets on the Teflon plate of the sample holder

Droplet volume / μl	Contact angle η / $^\circ$	Bottom diameter db_T /mm	Height h_T /mm	Surface S / mm^2
5	104.52	2.09	0.99	9.92
50	95.36	3.29	1.17	13.12

5.5.1 Thin film and droplet drying

The model dairy-formulation was dried as sessile droplets and thin films at air temperatures of 80°C and 120°C, a relative air humidity of $\approx 0\%$ and air velocities of 0.15 $\text{m}\cdot\text{s}^{-1}$ and 0.30 $\text{m}\cdot\text{s}^{-1}$. In the case of sessile droplets, one droplet with a volume of 50 μl was dried during the standard experiments. To study the impact of the droplet size, an additional experiment with 40 droplets with a volume of 2.5 μl was conducted, i.e., the total volume was kept constant. In the case of thin-film drying, the impact of the relative humidity of air was evaluated using a relative humidity of 20%. The experimental drying curves, i.e., the water content as a function of time, are illustrated in Fig. 5.65 and Fig. 5.66.

In both cases, two drying stages could be distinguished. The first drying stage, until the critical water content was reached, was characterized by a constant drying rate, i.e., a linear decrease of the water content. The critical water content was 1.0 $\text{kg}\cdot\text{kg}^{-1}$ for droplet drying and 0.5 $\text{kg}\cdot\text{kg}^{-1}$ for thin-film drying. This difference can be attributed to the formation of a

crust at the product surface, which occurred for the droplets at a higher water content than for the thin films. The droplet size had no impact on the critical water content. The critical water content was attained faster when the droplet size was decreased from 50 μl to 2.5 μl and was then attained in the same time range as for the thin films. These observations are in accordance with results for lactose solutions found in the literature (Fu et al. 2011). The first drying stage was accelerated in all cases when the air temperature was increased from 80°C to 120°C. In contrast, the air velocity had no significant impact on the drying rate in the experimental range. This shows that the amount of air was no limiting factor for the drying rate. This would probably be the case if the air velocity was further decreased.

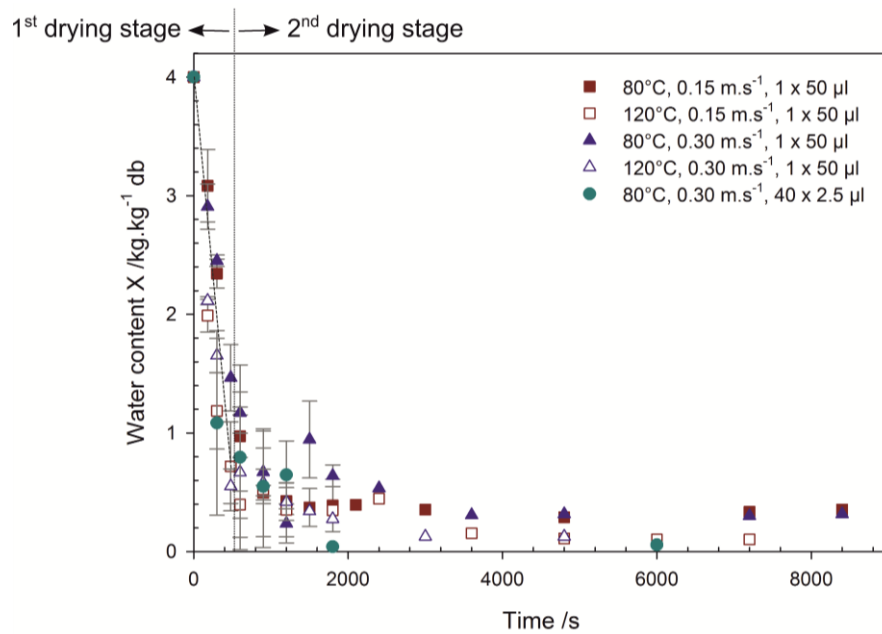


Fig. 5.65 Droplet drying: Impact of the drying conditions on the drying kinetics

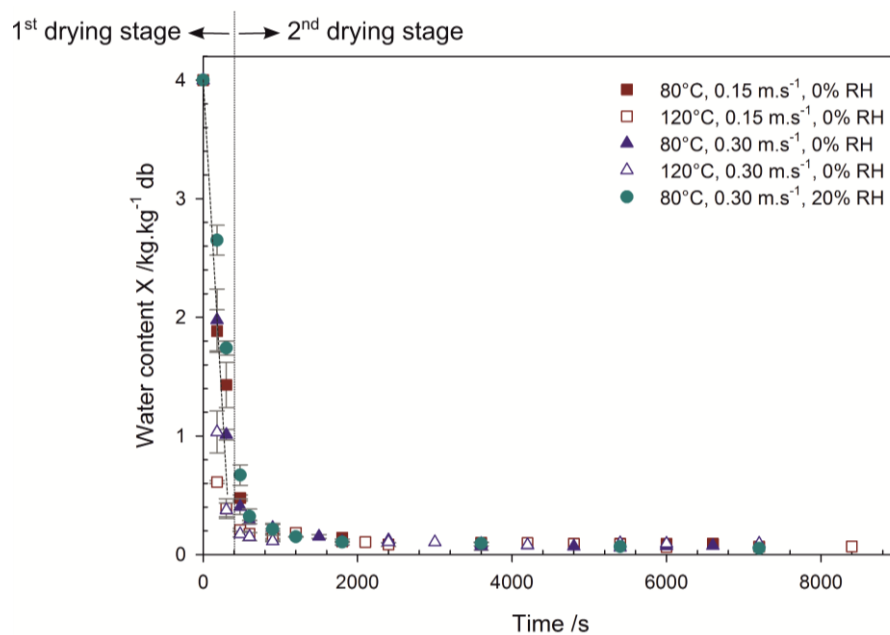


Fig. 5.66 Thin-film drying: impact of the drying conditions on the drying kinetics

During the second drying stage, the drying rate is limited by heat conduction through the dry outer parts of the sample to the core of the sample and diffusion of evaporated water in the opposite direction. As expected, higher drying rates and lower final water contents were determined during the second drying stage for an air temperature of 120°C compared to an air temperature of 80°C. However, drying droplets with a volume of 50 μl led to rather high final water contents at 80°C. This was probably due to a lower surface-volume ratio than in the case of droplets with a volume of 2.5 μl or thin films. Consequently, these results are hardly comparable to spray drying. Temperature influences the saturation pressure of air at the product surface as well as the diffusion coefficient. Higher air temperatures lead to higher saturation pressures at the product surface, which accelerates the evaporation rate during the first drying stage before a crust forms. Moreover, diffusivity increases with increasing temperature (Adhikari et al. 2003, Chen and Mujumdar 2008) which ameliorates the mass transfer during the second drying stage when on the other hand the diffusivity is reduced due to the low water contents.

The product temperature stayed close to the wet bulb temperature during the first drying stage and increased during the second drying stage approaching the air temperature (data not shown). At a relative humidity of air of 20% the evaporation rate during the first drying stage was decelerated. The relative humidity of air is linked to the partial water vapor pressure. Consequently, an increase of the relative humidity entails a decrease of the driving force for evaporation, namely the vapor concentration difference between the product surface and the surrounding air. The relative humidity had no significant impact on the critical water content or the final water content in the experimental range. In general, the results of droplet drying showed higher experimental uncertainties than the results of thin-film drying. High experimental uncertainties of drying kinetics data can also be found in the literature (Woo et al. 2008a). In conclusion, thin-film drying should be preferred to sessile droplet drying or the droplet size should be decreased in order to obtain reliable and reproducible drying kinetics data.

5.5.2 Characteristic drying-rate curve

The characteristic drying-rate curve (CDRC) model as described in chapter 4.6.2 was fitted to the experimental data of chapter 5.5.1. Due to the different drying behavior of the droplets and thin films used in this study, the characteristic drying-rate curve model was fitted separately to both geometries. The relative drying rate N/N_{max} as a function of the dimensionless water content $\varphi = (X - X_e)/(X_{cr} - X_e)$ is depicted in Fig. 5.67 and Fig. 5.68. In both cases, a good accordance between the calculated (CDRC-model) and the experimental values (symbols) was achieved. Above the critical water content, i.e., above a dimensionless water content of 1, the drying rate is equal to the maximum drying rate ($N/N_{max} = 1$) which corresponds to the first drying stage. Below the critical water content, i.e., during the second drying stage, the drying rate decreases with decreasing water content. The following functions were fitted to the experimental values by non-linear regression:

$$\frac{N}{N_{max}} = \left(\frac{X - X_e}{X_{cr} - X_e} \right)^{2.050} \quad \text{for droplet drying (R}^2 = 0.98, a = 2.050 \pm 0.197) \quad 5.8$$

$$\frac{N}{N_{max}} = \left(\frac{X - X_e}{X_{cr} - X_e} \right)^{1.483} \quad \text{for thin-film drying (R}^2 = 0.97, a = 1.4830 \pm 0.140) \quad 5.9$$

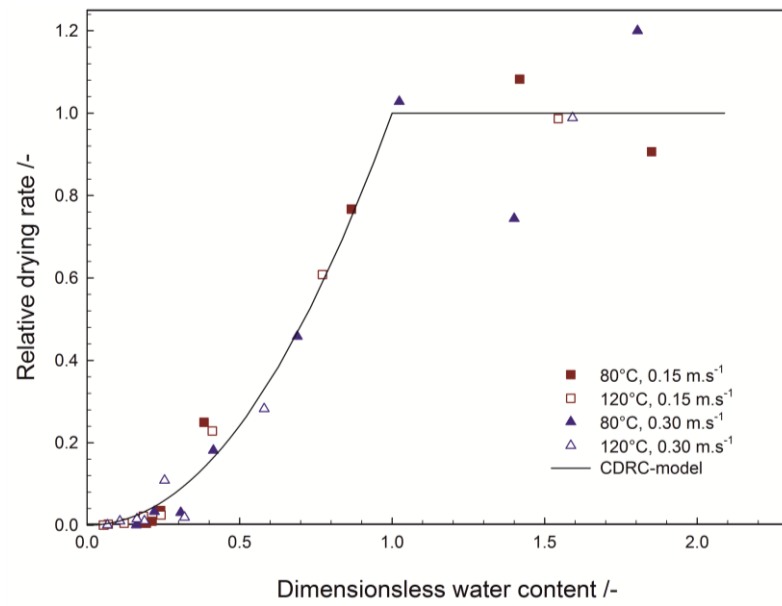


Fig. 5.67 Characteristic drying-rate curve fitted to the experimental droplet-drying data

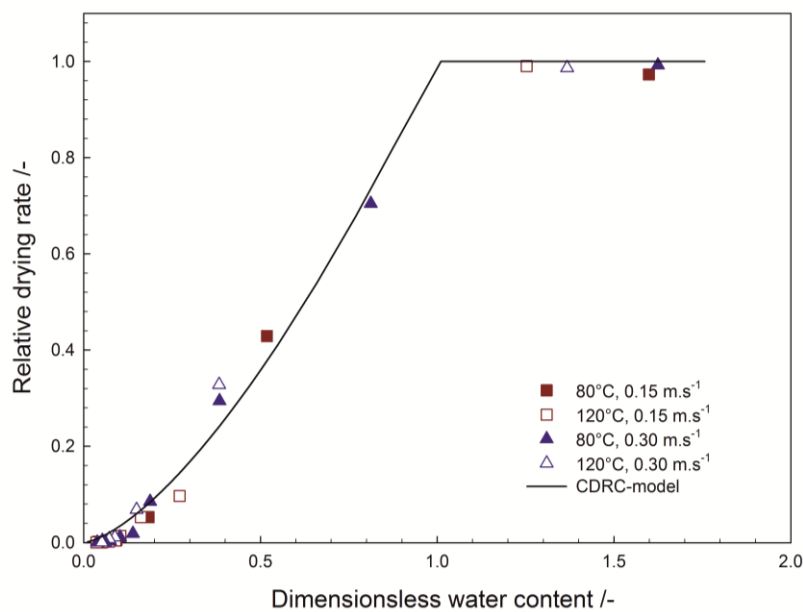


Fig. 5.68 Characteristic drying-rate curve fitted to the experimental thin-film drying data

The equilibrium water content X_e was derived from the sorption isotherm (cf. Fig. 5.6). The exponent a (droplet drying: 2.050 ± 0.197 , thin-film drying: 1.4830 ± 0.140) and the critical water content X_{cr} (droplet drying: 1.914 ± 0.056 , thin-film drying: 1.821 ± 0.110) were defined as fitting parameters. The fitted critical water contents differ significantly from the critical water contents that were estimated from the experimental drying curves. There was no significant difference between droplet and thin-film drying. Probably more data points of the drying curves are needed to avoid this divergence. Comparing the characteristic drying-rate curves of this study with correlations reported in the literature on dairy products and sugar solutions (Table 5.5), reveals that the obtained correlations are reasonable. In contrast to this

study, Chen and Lin (2005) neglected the constant drying rate period, i.e., they assumed that the initial water content was the critical water content. However, the experimental results of this study for the model dairy-formulation clearly show the existence of a constant drying-rate period. This divergence can probably be attributed to the differences in product composition and experimental conditions.

Table 5.5 Characteristic drying-rate curves of food products from the literature

Product	Correlation	Source
Maltodextrin	$\frac{N}{N_{\max}} = \left(\frac{X - X_e}{X_{cr} - X_e} \right)^{3.22}$	Woo et al. 2008a
Skim milk	$\frac{N}{N_{\max}} = \frac{X - X_e}{X_0 - X_e}$	Chen and Lin 2005
Sucrose-maltodextrin	$\frac{N}{N_{\max}} = \left(\frac{X - X_e}{X_{cr} - X_e} \right)^{1.98}$	Woo et al. 2008a
Sucrose	$\frac{N}{N_{\max}} = \left(\frac{X - X_e}{X_{cr} - X_e} \right)^{2.58}$	Woo et al. 2008a
Whole milk	$\frac{N}{N_{\max}} = \frac{X - X_e}{X_0 - X_e}$	Chen and Lin 2005

5.5.3 Reaction-engineering approach

In contrast to the characteristic drying-rate curve, the product temperature must be known for the reaction-engineering approach (REA) but the determination of the critical water content is not necessary. It was only possible to measure the product temperature during thin-film drying. Therefore, the temperatures measured during thin-film drying were transferred to droplet drying. This is possible because at the same drying conditions a characteristic relation between the water content and the product temperature exists (data not shown, cf. chapter 5.3.1). In the same manner as for the characteristic drying-rate curve model, the reaction-engineering approach was fitted separately to the experimental data of droplet drying and thin-film drying. Relative activation energies $\Delta E_v/\Delta E_{v,e}$ were plotted as a function of the water content difference to the equilibrium water content $X-X_e$ in Fig. 5.69 for droplet drying and in Fig. 5.70 for thin-film drying. In agreement with the principles of the reaction-engineering approach, a master curve was obtained with the experimental results (symbols) of all drying conditions for each geometry. Non-linear regression was applied to fit the reaction-engineering approach model to the experimental values. This resulted in the following equations for the relative activation energy:

$$\frac{\Delta E_v}{\Delta E_{v,e}} = 1.048 \cdot \exp\left(-3.189 \cdot (X - X_e)^{0.850}\right) \quad \text{for droplet drying (R}^2 = 0.82, a = 1.048 \pm 0.230, \\ b = 3.189 \pm 0.549, c = 0.850 \pm 0.340) \quad 5.10$$

$$\frac{\Delta E_v}{\Delta E_{v,e}} = 0.985 \cdot \exp\left(-2.798 \cdot (X - X_e)^{0.485}\right) \quad \text{for thin-film drying (R}^2 = 0.97, a = 0.985 \pm 0.054, \\ b = 2.798 \pm 0.367, c = 0.485 \pm 0.069) \quad 5.11$$

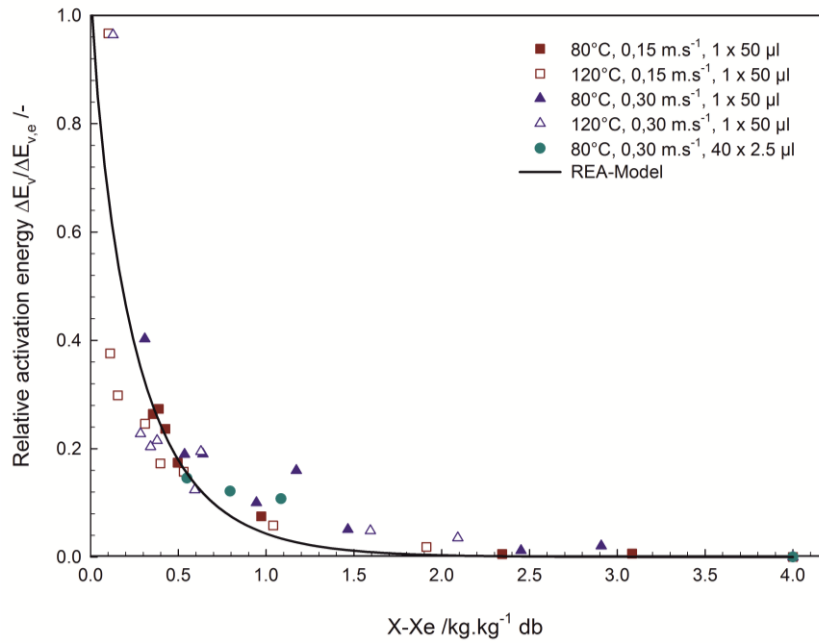


Fig. 5.69 Reaction-engineering approach fitted to the experimental droplet-drying data

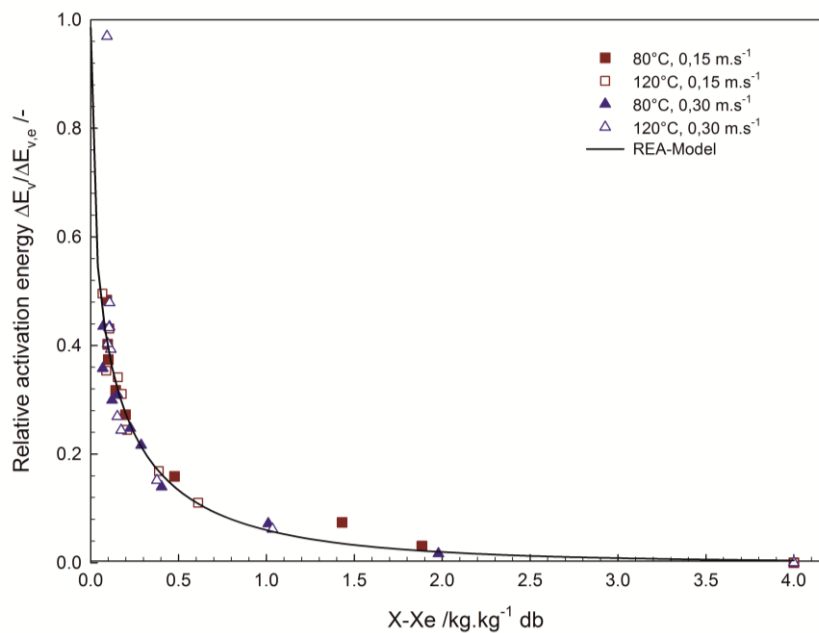


Fig. 5.70 Reaction-engineering approach fitted to the experimental thin-film drying data

Thin-film drying gave better results than droplet drying. This is probably due to the better quality of the experimental data of thin-film drying. In both cases, the relative activation energy rises only slightly at the beginning of drying which indicates that the energy barrier for evaporation is low, i.e., the surface is saturated with water. Below the critical water content, i.e., once a crust is formed, the relative activation energy rises sharply with decreasing water content, i.e., the activation energy that must be provided for evaporation increases. Reviewing data found in the literature (Table 5.6) reveals quite scattering correlations for the relative

activation energy even for the same product, for instance skim milk. Against this background, the correlations determined in this study agree well with these correlations when the differences in product composition are taken into account, which have an impact on the drying characteristics.

Table 5.6 Relative activation-energy correlations of food products from the literature

Product	Correlation	Source
Cream	$\frac{\Delta E_v}{\Delta E_{v,e}} = 1 - 0.6282 \cdot (X - X_e)^{0.5561}$	Lin and Chen 2007
Lactose	$\frac{\Delta E_v}{\Delta E_{v,e}} = 1.017 \cdot \exp(-1.678 \cdot (X - X_e)^{1.018})$	Lin and Chen 2006
Maltodextrin	$\frac{\Delta E_v}{\Delta E_{v,e}} = \exp(-1.793 \cdot (X - X_e)^{4.656})$	Woo et al. 2008a
Skim milk	$\frac{\Delta E_v}{\Delta E_{v,e}} = \exp(-0.408 \cdot (X - X_e)^{1.72})$	Chen and Xie 1997
Skim milk	$\frac{\Delta E_v}{\Delta E_{v,e}} = 0.998 \cdot \exp(-1.405 \cdot (X - X_e)^{0.930})$	Chen and Lin 2005
Sucrose-maltodextrin	$\frac{\Delta E_v}{\Delta E_{v,e}} = \exp(-0.892 \cdot (X - X_e)^{2.022})$	Woo et al. 2008a
Sucrose	$\frac{\Delta E_v}{\Delta E_{v,e}} = \exp(-1.688 \cdot (X - X_e)^{2.816})$	Woo et al. 2008a
Whey-protein concentrate	$\frac{\Delta E_v}{\Delta E_{v,e}} = 1.335 - 0.3669 \cdot (X - X_e)^{0.3011}$	Lin and Chen 2007
Whole milk	$\frac{\Delta E_v}{\Delta E_{v,e}} = 0.957 \cdot \exp(-1.291 \cdot (X - X_e)^{0.934})$	Chen and Lin 2005

5.5.4 Evaluation of the drying-kinetics models

To evaluate the prediction capabilities of the models, the derived model equations were used to predict the experimental drying curves. This way, a decision can be made which of the two drying-kinetics models should be used for the CFD simulation of spray drying. As thin-film drying proved to give more reliable results that seemed to be more adequate for a transfer to spray drying, the following explanations will be limited to thin-film drying. The predicted and experimental water contents as a function of the drying time are plotted in Fig. 5.71 for an air velocity of $0.15 \text{ m}\cdot\text{s}^{-1}$ and in Fig. 5.72 for an air velocity of $0.30 \text{ m}\cdot\text{s}^{-1}$. At first glance, it becomes obvious that the CDRC model does not predict realistic drying curves at drying times $>400 \text{ s}$ despite the good correlation coefficients of the characteristic drying-rate curve (cf. chapter 5.5.2). A closer look at the characteristic drying-rate curves of Fig. 5.67 and Fig. 5.68 reveals that the predicted relative drying rates are higher than the experimental relative

drying rates at non-dimensional water contents <0.2 . This leads to an overestimation of the drying rate and, consequently, to unrealistic predicted water contents. This behavior is more pronounced at 80°C than at 120°C . An equation that accounts for the reduced relative drying rates below non-dimensional water contents of 0.2 could reduce these discrepancies. In contrast, the predictions of the reaction-engineering approach (REA) follow the experimental values very well during both drying stages including the final water contents. Similarly, Woo et al. (2008a) concluded that the REA model predicted the drying rate better than the CDRC model for sucrose-maltodextrin solutions. Chen and Lin (2005) as well as Patel and Chen (2005) concluded the same for skim milk and whole milk. In conclusion, the reaction-engineering approach appears to be more suitable to predict the drying kinetics and will be used for the computational fluid-dynamics simulation of spray drying.

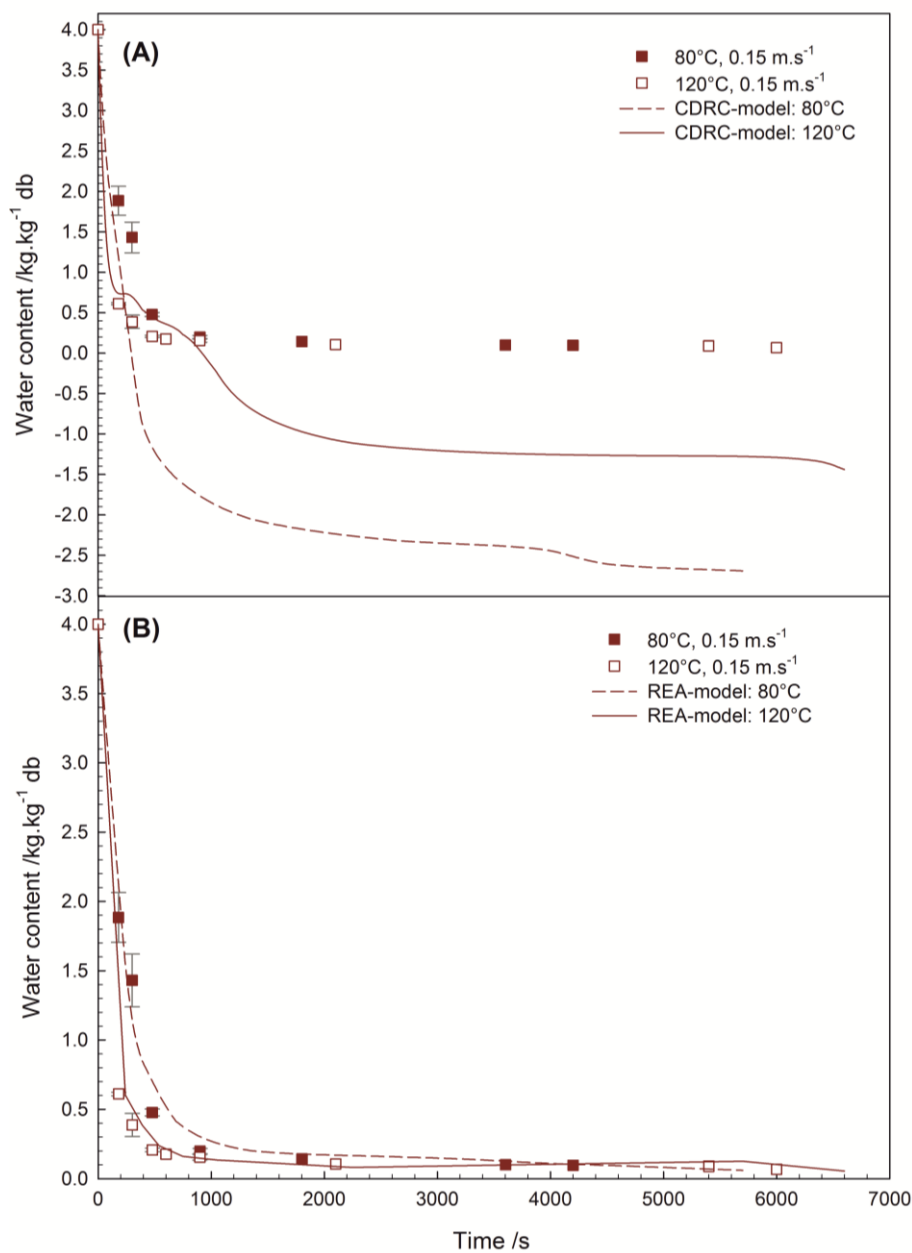


Fig. 5.71 Water contents predicted by the drying-kinetics models in comparison with the experimental water contents for thin-film drying at an air velocity of 0.15 m.s^{-1}

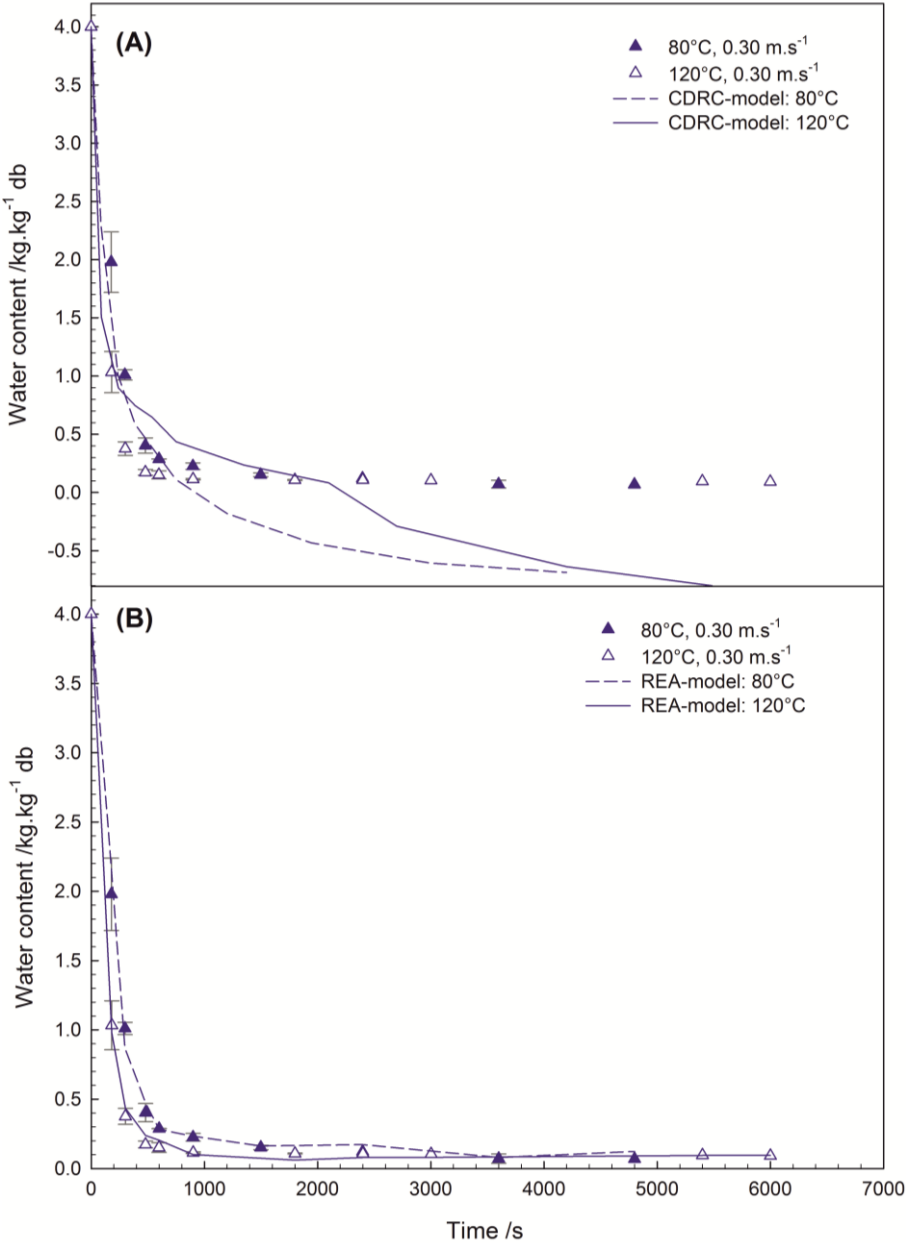


Fig. 5.72 Water contents predicted by the drying-kinetics models in comparison with the experimental water contents for thin-film drying at an air velocity of 0.30 m.s⁻¹

6 Modeling lysine loss during spray drying

6.1 Description of the computational fluid-dynamics model

The software STAR-CCM+ 7.04.011 (CD-adapco, USA) was used for the computational fluid-dynamics simulation of the spray-drying process. Details of the governing equations, turbulence model and solution procedures can be found in the STAR-CCM+ 7.04.011 user guide (CD-adapco 2012). A 3D model with a computational grid of 2 008 227 polyhedral cells was built using the meshing tool which is included in the STAR-CCM+ software (Fig. 6.1). The volume mesh at the pressure outlet was extended using the extruder mesher. Thus, the backflow of air and particles at the outlet can be avoided and the solution is stabilized. To improve the accuracy of the flow solution near the walls, the prism-layer mesh model was used. The mesh was refined at the air inlet, around the nozzle, in the atomization zone, at the outlet pipe and in the core flow region to adapt it to the flow characteristics. Generally, finer grid cells are needed in regions of higher particle concentrations (Mezhericher et al. 2009, 2010a). To verify the grid independency, four different base sizes were chosen (0.1 m, 0.0725 m, 0.045 m and 0.03 m) for meshing and the air-flow field was computed. When the base size was reduced from 0.1 m to 0.0725 m and further to 0.045 m, the air-flow field was resolved more accurately. However, the resolution was not further improved when the base size was decreased to 0.03 m. Consequently, the mesh created with a base size of 0.045 m was sufficiently fine to obtain a good resolution of the air-flow field with less computational effort than for the smaller base size of 0.03 m. However, a finer mesh was necessary for the accurate computation of the drying kinetics of the particles due to the fast evaporation of water. While the water is evaporating, the particle properties change a lot over short distances. To capture these changes, a fine mesh is necessary. Therefore, the final base size for the mesh generation was set to 0.025 m.

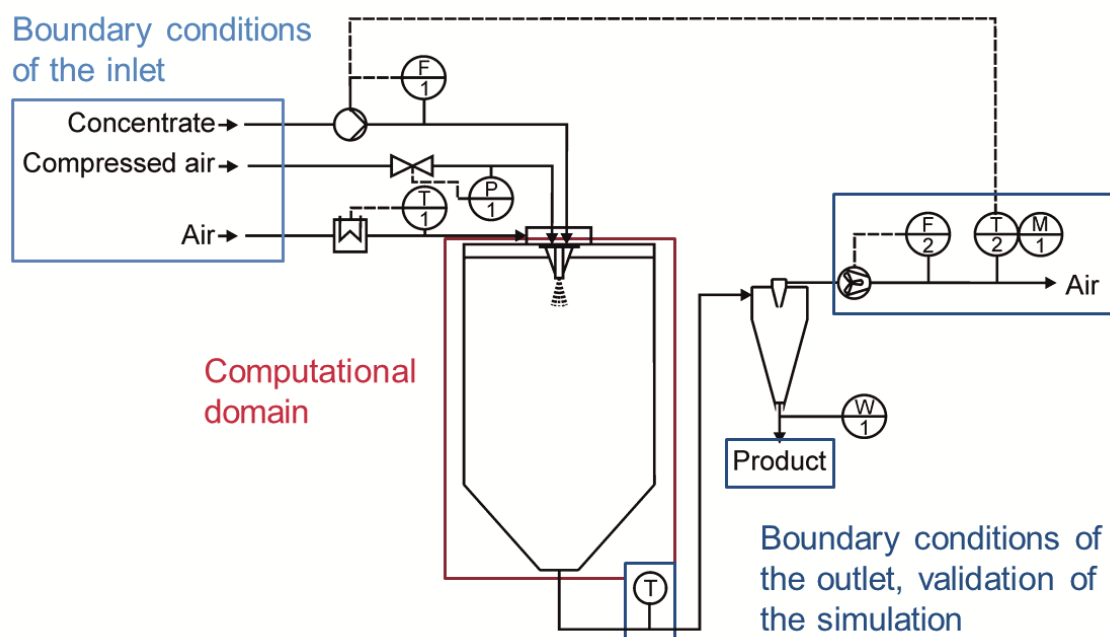


Fig. 6.1 Modeling approach for the computational fluid-dynamics simulation of spray drying

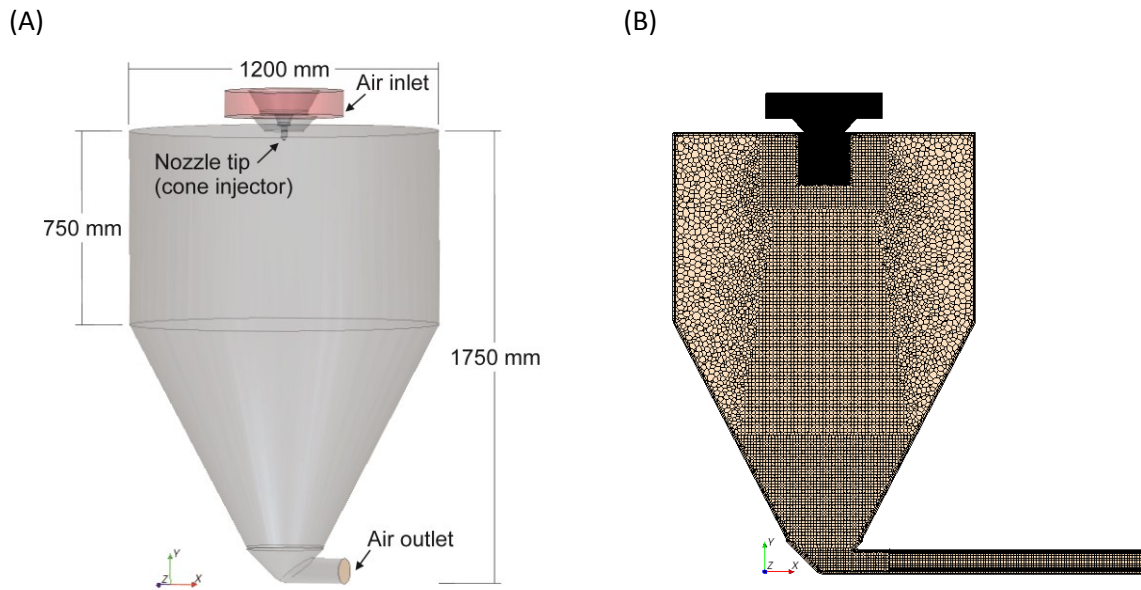


Fig. 6.2 Sketch of the geometry of the pilot-scale spray dryer (A) and computational grid at the center plane (B)

The Euler-Lagrange approach was chosen together with steady state calculations. Steady state calculations were chosen because in this way the computational time was considerably reduced. Due to the fast evaporation, very short time-steps, which are several orders of magnitude smaller than the particle residence-time, are needed to resolve the drying kinetics. This results in very long computational times. To justify this simplification, an unsteady simulation was compared to a steady simulation. No significant differences were determined, i.e., steady simulations are sufficiently accurate for the purpose of this study. The continuous phase (drying gas) was treated by the Eulerian approach using the Reynolds-averaged Navier-Stokes (RANS) equations (CD-adapco 2012). The realizable k - ϵ two-layer turbulence model with the standard coefficients together with the two-layer all y^+ wall treatment was employed for the Eulerian phase. According to the literature, the realizable k - ϵ turbulence model predicts flows which involve rotation, separation and recirculation better than the standard k - ϵ turbulence model (Kuriakose and Anandharamakrishnan 2010). The Eulerian phase consisted of a multi-component gas containing air and water vapor. The material properties of water and air (Table 6.1) were taken from VDI-Wärmeatlas (Gesellschaft Verfahrenstechnik und Chemieingenieurwesen 2006). The gas phase was considered an ideal incompressible gas. This assumption is justified because the Mach numbers were <0.3 . The gravity model was activated to account for the gravitational acceleration ($9.81 \text{ m}\cdot\text{s}^{-2}$ in $-y$ direction) which is important for the tracking of the Lagrangian particles (Blei and Sommerfeld 2011).

The spray-drying conditions of the experiments on a pilot scale were chosen as inlet, outlet and boundary conditions. The inlet of the drying gas was defined as velocity inlet with a velocity of $1.0 \text{ m}\cdot\text{s}^{-1}$ and a flow direction normal to the boundary. The turbulence conditions were specified by the turbulence intensity and length scale. The turbulence parameters for the inlet had to be estimated due to the lack of experimental values. This is a known difficulty (Ferziger and Perić 2008, Langrish 2009). The air-flow field was computed for three different turbulent intensities (0.01, 0.05 and 0.1) at the air inlet. Other than reported by Langrish (2009) and in accordance with Gianfrancesco (2009), the turbulent intensity had no signifi-

cant impact on the air-flow field in the tested range and was set to 0.01 in the final model. The turbulent length scale was 0.01 m. These values are in the same range as turbulent parameters reported in the literature (Birchal et al. 2006, Huang et al. 2005).

Table 6.1 *Material properties of water vapor and dry air (Gesellschaft Verfahrenstechnik und Chemieingenieurwesen 2006)*

Water vapor	
Dynamic viscosity	$\eta_w = (-0.10718 \cdot 10^{-5} + 0.35248 \cdot 10^{-7} K^{-1} \cdot T - 0.03575 \cdot 10^{-10} K^{-2} \cdot T^2) Pa \cdot s$
Specific heat:	$c_{p,w} = \left(\begin{array}{l} 1833.10 - 0.035 K^{-1} \cdot T + 6.96 \cdot 10^{-4} K^{-2} \cdot T^2 - 2.15 \cdot 10^{-7} K^{-3} \cdot T^3 \\ -2.6 \cdot 10^{-8} K^2 \cdot T^{-2} \end{array} \right) \frac{J}{kg \cdot K}$
Thermal conductivity	$\lambda_w = (0.46 \cdot 10^{-3} + 0.046 \cdot 10^{-3} K^{-1} \cdot T + 0.051150 \cdot 10^{-6} K^{-2} \cdot T^2) \frac{W}{m \cdot K}$
Dry air	
Dynamic viscosity	$\eta_{air} = (-0.03287 \cdot 10^{-5} + 0.77996 \cdot 10^{-7} K^{-1} \cdot T - 0.48801 \cdot 10^{-10} K^{-2} \cdot T^2) Pa \cdot s$
Specific heat	$c_{p,air} = \left(\begin{array}{l} 1070.30 - 0.564 K^{-1} \cdot T + 1.507 \cdot 10^{-3} K^{-2} \cdot T^2 - 1.102 \cdot 10^{-6} K^{-3} \cdot T^3 \\ -1.4 \cdot 10^{-8} K^2 \cdot T^{-2} \end{array} \right) \frac{J}{kg \cdot K}$
Thermal conductivity	$\lambda_{air} = (-0.37 \cdot 10^{-3} + 0.103 \cdot 10^{-3} K^{-1} \cdot T - 0.046570 \cdot 10^{-6} K^{-2} \cdot T^2) \frac{W}{m \cdot K}$

The outlet was defined as pressure outlet. In the pilot plant, the air is sucked through the spray dryer by a fan which is located behind the cyclone. This fan creates a depression of 100 Pa which is used as the outlet boundary condition.

To estimate the heat loss through the dryer walls, hot air was directed through the pilot plant without drying any product and the inlet, outlet and ambient temperatures were recorded. As no data of the actual wall temperature was available, the available data was used to calculate an approximate heat transfer coefficient. During the simulations, the heat transfer coefficient was adapted and verified by comparing the experimental air-outlet temperature to the computed air-outlet temperature. This resulted in a heat-transfer coefficient of $11 W \cdot (m^2 \cdot K)^{-1}$.

The dispersed droplets of the model dairy-formulation were treated by the Lagrangian approach. The material properties of the droplets, i.e., of the model dairy-concentrate with 20% dry matter, were defined based on the results of chapter 5.1 and Table 6.2. The density of the Lagrangian phase could not be entered as a function of the water content in STAR-CCM+. Therefore, a mean constant density of $1300 kg \cdot m^{-3}$ was used for the Lagrangian phase.

Table 6.2 Material properties of the model dairy-formulation (in addition to the results of chapter 5.1)

Material property	Constant value
Density of the dry matter ρ_s	1571 kg.m ⁻³
Density of the concentrate with 20% dry matter ρ_c	1076 kg.m ⁻³
Latent heat of vaporization r_v	2438 kJ.kg ⁻¹
Specific heat c_p	2580 J.(kg.K) ⁻¹

At present, it is not possible to incorporate satisfactorily the atomization of the concentrate into fine droplets in the Euler-Lagrange approach (Blei and Sommerfeld 2011, Hede et al. 2008). For that reason, simplified atomization models (Anandharamakrishnan et al. 2010, Duangkhamchan et al. 2012) or droplet injectors (Fries et al. 2011a, Fries et al. 2011b, Langrish and Zbicinski 1994) are usually used to model two-fluid nozzles. The atomization air is often supplied by a separate inlet and the inlet conditions can be obtained by a separate simulation of the nozzle (Anandharamakrishnan et al. 2010, Fries et al. 2011a, Fries et al. 2011b, Langrish and Zbicinski 1994, Li et al. 2010b). 150 parcels of spherical droplets with a temperature of 300 K and a diameter of 15 μm , which corresponds to the median droplet diameter of the spray-drying experiments on a pilot scale (cf. chapter 5.4.1), were injected using a cone injector. The whole product volume-flow was split into particles which were then grouped to 150 parcels. The particles of one parcel were considered to have the same properties. This is a common procedure because the computational effort to track each individual particle would be enormous. The injection conditions were obtained from experiments and a separate simulation of the two-fluid nozzle. A cone angle of 36° was derived for the cone injector from the visualization of the spray that is created by the two-fluid nozzle (Fig. 6.3). The droplet diameter d_d was estimated from the particle diameter d_p of the spray-dried powders assuming ideal shrinkage without taking into account particle porosity:

**Fig. 6.3 Spray created by the two-fluid nozzle ($\dot{m}_{\text{product}} = 14.9 \text{ kg}\cdot\text{h}^{-1}$)**

$$d_d = \sqrt[3]{\frac{d_p^3 \cdot \left(1 - \frac{X^*}{100}\right)}{c_s \cdot \rho_d \cdot \left(\frac{X^*}{100 \cdot \rho_w} + \frac{1 - X^*}{100 \cdot \rho_s}\right)}} \quad 6.1$$

where d_d is the droplet diameter, d_p the particle diameter, X^* the particle water content on a wet basis, c_s the solid concentration of the concentrate, ρ_d the density of the concentrate, ρ_w the density of water and ρ_s the density of the dry matter. This procedure ensures consistency with the calculation method of the particle diameter which is incorporated in STAR-CCM+.

However, it was not possible in STAR-CCM+ to define the particle size by a particle-size distribution and to use the user-defined evaporation model of this study at the same time. For this reason, the simulations were carried out with the median droplet diameter $d_{50,d}$ which was estimated from the median particle diameter d_{50} of the spray-dried powders. A sensitivity study on the impact of the droplet size is provided in chapter 6.2.

During atomization, the droplets are accelerated to the mixing-rate velocity v_{mr} by the atomization air (Walzel 1993):

$$v_{mr} = \frac{v_{air}}{1 + \frac{\dot{m}_{liquid}}{\dot{m}_{air}}} \quad 6.2$$

where v_{air} denotes the velocity of the compressed air at the nozzle exit, \dot{m}_{air} the mass-flow rate of the atomization air and \dot{m}_{liquid} the mass-flow rate of the concentrate. The mass-flow rates of the concentrate and of the atomization air were known from the experiments. The velocity of the compressed air at the nozzle tip was calculated in a separate computational fluid-dynamics simulation of the air flow in the nozzle (Fig. 6.4). Thus, the velocity of the droplets at the injection point was specified by their velocity magnitude and swirl. The atomization air was not included as a separate inlet stream but the inlet conditions of the drying gas were corrected for the atomization air.

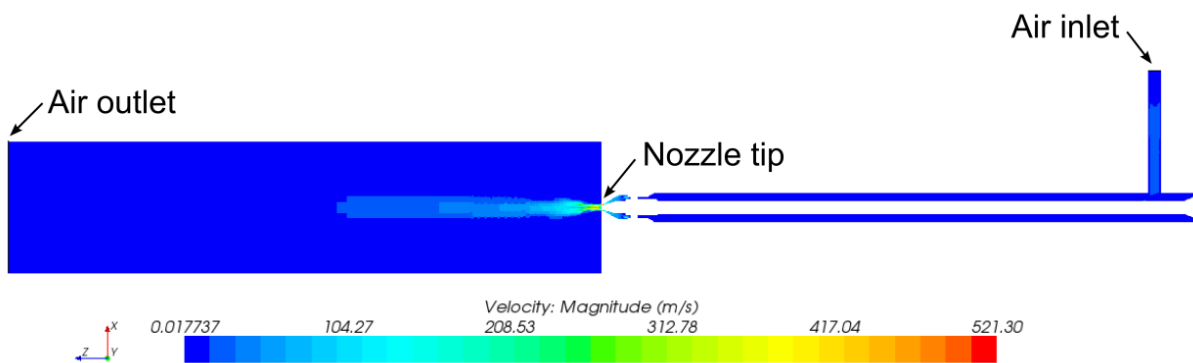


Fig. 6.4 Velocity profile of the compressed air at the center plane of the two-fluid nozzle

Two-way coupling was applied to take into account the impact of the discrete phase on the continuous phase. The built-in Bai-Gosman wall-impingement model of STAR-CCM+ was used as boundary condition for particles hitting the wall (CD-adapco 2012). In absence of experimental data for the model coefficients, the default values for water were applied. Parcels which would adhere to the dryer walls were considered as “escaped”. The drag force acting on the particles was modeled with the built-in Schiller-Naumann method of STAR-CCM+ for the drag coefficient of spherical particles (CD-adapco 2012). The heat transfer coefficient of the particles was defined by the Ranz-Marshall correlation for spherical particles (CD-adapco 2012). The particles were defined as material particles, i.e., they have a mass and volume, are internally homogenous and their behavior is governed by the physical conservation laws (CD-adapco 2012). As the turbulent eddies of the continuous phase, i.e., the Eulerian

drying gas, are not resolved when the RANS equations are used, the turbulent-dispersion model of STAR-CCM+ was selected to synthesize the impact of the fluctuating turbulent velocity field on the particle tracks (CD-adapco 2012). This stochastic approach is commonly used for particle tracking when the turbulent eddies of the flow pattern are not resolved (Anandharamakrishnan et al. 2010, Birchal et al. 2006, Huang et al. 2005). The drying kinetics was modeled with the reaction-engineering approach as described in chapter 5.5.3 and the lysine loss with the reaction kinetics model described in chapter 5.2.5.

To achieve convergence of the solution, first the flow field of the Eulerian phase was solved and after convergence of the flow field the Lagrangian solver was started. The segregated solver according to the SIMPLE algorithm was used with the Gauss-Seidel relaxation scheme and the second-order upwind convection scheme. The convergence of the solution was assessed by the residuals as well as by monitoring the outlet temperature, velocity and water content of the drying gas. The number of iterations depended on the convergence rate. The simulations were stopped once the monitored parameters leveled off at a constant value.

6.2 Analysis of the simulation results and validation of the model

The spray-drying simulations were run using the spray-drying conditions (air-inlet temperatures, air mass-flow rate, atomization conditions, product properties, etc.) of the spray-drying experiments on a pilot scale. The simulations were stopped when the solution converged. The drying-air properties inside the spray-drying chamber for an inlet-air temperature of 200°C and a product mass-flow rate of 11.0 kg.h⁻¹ are depicted in Fig. 6.5A-C. The air velocity is high in the center of the spray dryer where it is oriented downwards. It is lower in the peripheral zones where large vortex structures of recirculating air can be identified from the streamlines. Such vortex structures were also reported in the literature (Fletcher et al. 2006). The drying air is accelerated by the atomized droplets in the atomization zone. This air flow pattern is in good accordance with results found in the literature (Fletcher and Langrish 2009, Gianfrancesco 2009, Langrish and Zbicinski 1994, Mezhericher et al. 2010a) when it is taken into account that different atomization systems were used and the spray-dryer geometries were not identical. The temperature profile reflects the known principles of thermal process engineering. The temperature decreases near the dryer walls due to heat losses to the environment. Water of the atomized droplets evaporates which further cools down the drying-air temperature. This results in lower temperatures near the atomization zone and along the droplet spray. Further away from the atomization zone and the droplet spray, the drying air mixes due to the turbulent vortex flow. This balances the air temperature. These effects finally result in a mean outlet-air temperature which can be compared to experimental results. The relative humidity is high near the atomization zone where the air absorbs a lot of evaporated water and near the dryer walls. The heat loss through the dryer walls decreases the air temperature near the walls, which leads to higher relative humidities. Between these two zones, the relative humidity fluctuates according to the evolution of the air temperature and the evaporation of water from the droplets/particles.

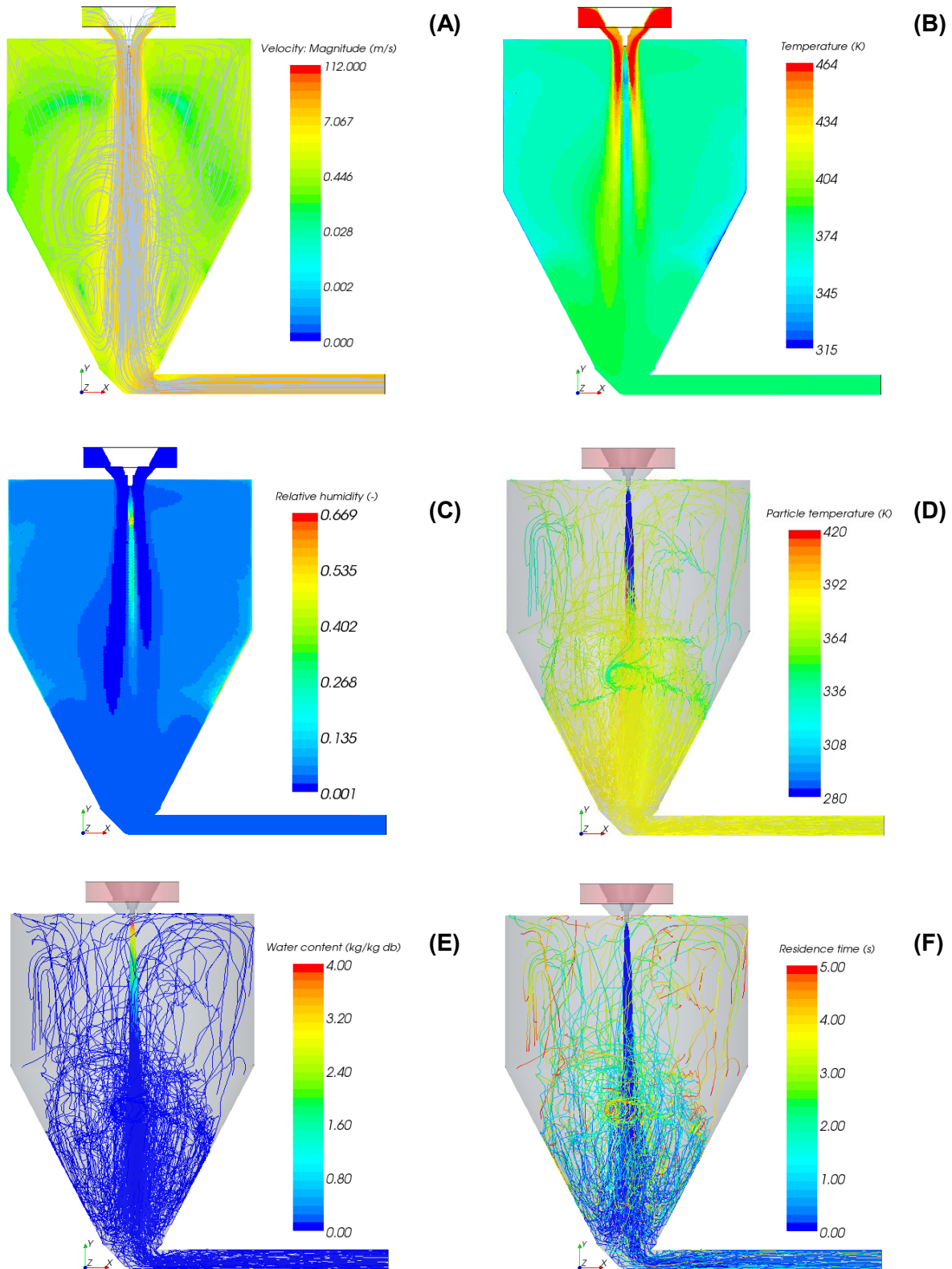


Fig. 6.5 Simulation results for an air-inlet temperature $T_{in} = 200^{\circ}\text{C}$ and a product mass-flow rate $\dot{m}_{product} = 11.0 \text{ kg}\cdot\text{h}^{-1}$ (particles were tracked for up to 5 s): air velocity profile and streamlines (A), temperature profile (B), relative humidity profile (C), particle tracks and particle temperature (D), particle tracks and water content of the particles (E), particle tracks and particle residence-time (F)

The whole product volume-flow was split into 150 parcels. The particle properties of the 150 parcels were tracked for up to 5 s during the CFD simulation. The tracking time was restricted to limit the computing time. The particle tracks are depicted in Fig. 6.5D-F together with the particle temperature, water content and residence time. At first glance, particle recirculation is apparent which causes the rather long residence times of the particles measured in the experiments (cf. chapter 5.4.2). The water content of the particles decreases quickly at the beginning of the particle tracks. This shows that water starts immediately to evaporate when the droplets get in contact with the hot drying air. The typical behavior of hindered drying kinetics can be noticed, which is expected from the drying-kinetics model that was used (cf. chapters 2.3, 2.4, 5.4 and 0). The drying rate falls when the critical water content is passed and approaches the equilibrium water content. The temperature of the particles stays close to the wet bulb temperature during the first drying stage, rises during the second one and approximates the air temperature at longer residence times. This reflects the characteristic temperature evolution during convective drying. Recirculating particles are in equilibrium with the drying air. Their water content and temperature fluctuates according to the properties of the drying air at their respective positions. These results are in accordance with results found for other spray-dryer configurations in the literature (Birchal et al. 2006, Gianfrancesco 2009, Jin and Chen 2009, Mezhericher et al. 2009, Woo et al. 2008b).

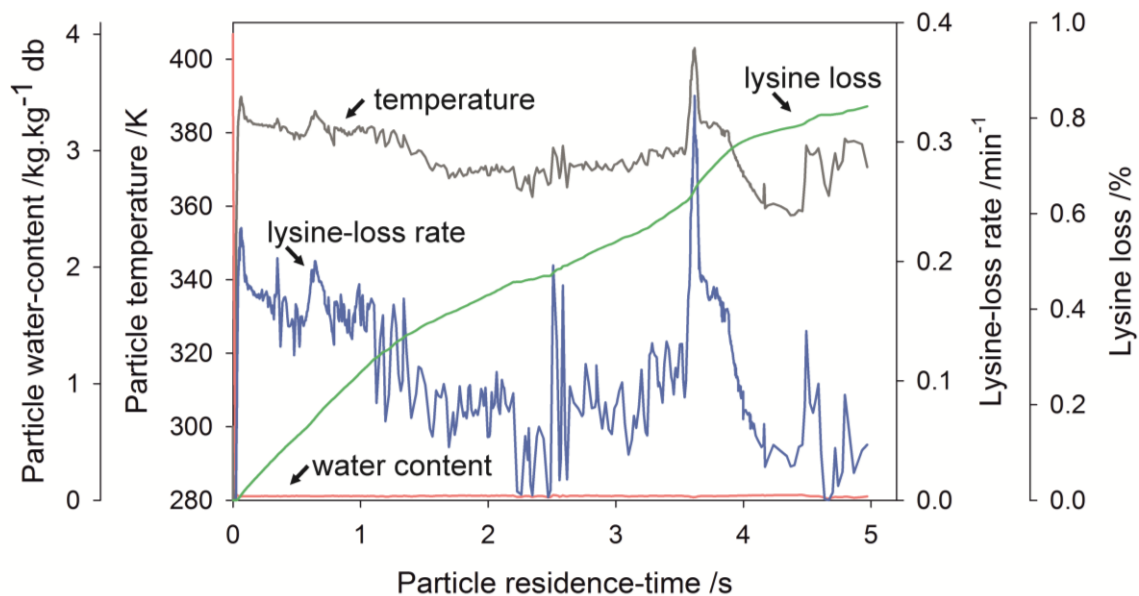


Fig. 6.6 Particle history of parcel 32 at an air-inlet temperature $T_{in} = 200^{\circ}\text{C}$ and a product mass-flow rate $\dot{m}_{product} = 11.0 \text{ kg}\cdot\text{h}^{-1}$ (particles were tracked for up to 5 s)

The temperature and water content evolution of one parcel is shown together with the rate of lysine loss and the accumulated lysine loss as a function of the particle residence-time in Fig. 6.6. The water content and the particle temperature follow the behavior which is specific to convective drying and was explained in the preceding paragraph. Lysine loss rates were calculated for each combination of particle temperature and water content. The loss of available lysine was determined by integrating the lysine-loss rates over the particle residence-time. According to the simulation results, no lysine loss occurs as long as the particle water-content is elevated and the particle temperature is moderate. When the particle temperature rises and

the water content reaches low values, the rate of lysine loss increases. This is the expected behavior in accordance with the kinetics of lysine loss that was presented in chapter 0. The lysine loss of parcel 32 amounts to 0.83% during the tracked residence time of the particles. Averaging the particle states and the resulting lysine-loss rates of all parcels and extrapolating to a residence time of 90 s leads to a lysine loss of 6.5% compared to $10.4 \pm 2.9\%$ in the experiments (cf. chapter 5.4.3). The residence time was extrapolated to 90 s because this is the average residence time of the particles according to the experimental results of chapter 5.4.2. Despite the simplifications made in the model of lysine loss during spray drying, the computed lysine loss is in the same order of magnitude as the experimental one. The divergence can probably be attributed to particle agglomeration and wall deposition inside the spray dryer, both of which are not considered in the model. The impact of these effects is particularly pronounced at adverse drying conditions with regard to lysine loss. This will be discussed in detail in the following section.

Table 6.3 Experimental and simulation results of pilot-scale spray drying (T_{in} : air inlet temperature; $\dot{m}_{product}$: product mass-flow rate; RH_{out} : relative humidity of the outlet air; X : water content; Exp.: experiment; Sim.: simulation)

Process conditions		Process characteristics				Powder characteristics			
T_{in} /°C	$\dot{m}_{product}$ /kg.h ⁻¹	T_{out} /°C		RH_{out} /%		X /% db		Lysine loss /%	
		Exp.	Sim.	Exp.	Sim.	Exp.	Sim.	Exp.	Sim.
160	11.0	81 ±11	91	8.2 ±4.2	6.6	4.31 ±0.55	4.24	4.7 ±2.1	2.0
180	14.9	80 ±6	83	9.7 ±1.7	11	4.58 ±0.38	4.60	3.4 ±2.2	2.9
200	11.0	106 ±4	107	3.3 ±1.3	3.9	3.00 ±0.29	3.73	10.4 ±2.9	6.5
200	18.7	81 ±12	81	11.0 ±5.5	15.3	5.22 ±1.07	4.99	4.4 ±2.5	4.2

To validate the simulations, the air-outlet temperature, the relative humidity of the outlet air, the water content of the powder and the lysine loss are compared with the experimental results (Table 6.3). The computed outlet temperatures and relative humidities of the air as well as the water content of the powders agree well with the experimental results. The simulation results always coincide with the confidence regions of the experimental results. Consequently, the simulation furnishes reliable and realistic results of the spray-drying process despite the assumptions and simplifications that were necessary. Concerning lysine loss, the simulations follow the trend observed from the experiments. Lysine loss increases with an increasing inlet temperature of the air and with a decreasing mass-flow rate of the product. At higher outlet temperatures and relative humidities of the air as well as at lower final water contents of the powders, bigger lysine losses were computed. At spray-drying conditions of $160^{\circ}\text{C}/11.0 \text{ kg.h}^{-1}$, $180^{\circ}\text{C}/14.9 \text{ kg.h}^{-1}$ and $200^{\circ}\text{C}/18.7 \text{ kg.h}^{-1}$, the calculated lysine loss is within the confidence region of the experimental result. However, at $200^{\circ}\text{C}/11.0 \text{ kg.h}^{-1}$, the simulation yields a lower lysine loss than the experiment. This spray-drying condition was identified as the most adverse one with regard to lysine loss in chapter 5.4.3. It is characterized by a high temperature level inside the spray dryer and low water content of the particles. According to the reaction kinetics established in chapter 5.2.5, this corresponds to conditions with

maximum lysine-loss rates. Small variations in the temperature or water content entrain significant changes of the lysine-loss rates in this region. Therefore, exact particle tracks are important to reproduce correctly this drying condition. Consequently, extrapolation of the status after a residence time of the particles of 5 s to 90 s might lead to erroneous results. For this reason, this simulation was repeated and the particles were tracked for their entire residence time (Fig. 6.7). Contrasting the simulated residence time of the particles with the experimental one reveals that the simulation predicts shorter residence times than were measured in the experiments. This divergence probably arises because the droplet size distribution, agglomeration and wall deposition were neglected in the model.

Models for agglomeration and wall deposition can be found in the literature (Blei and Sommerfeld 2011, Ullum et al. 2010). However, modeling wall deposition and agglomeration is still a difficult task. Such models might be included in the model set-up given that future versions of the software will allow integrating these models and high-performance cluster computers will be used.

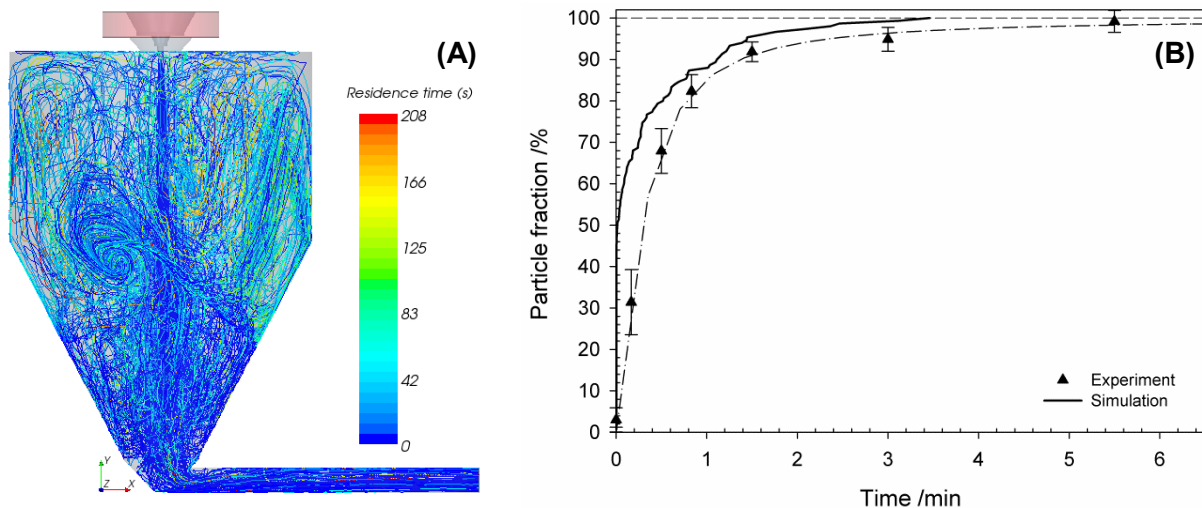
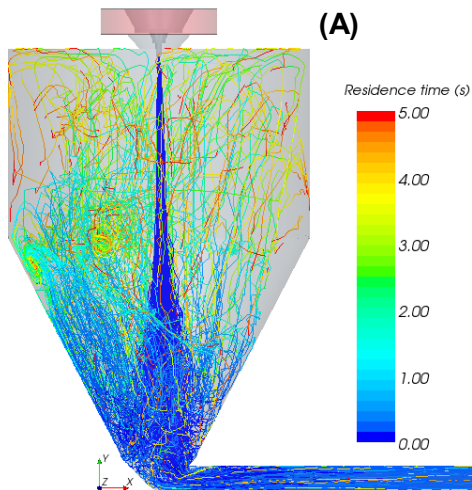


Fig. 6.7 Simulation results for an inlet temperature of the air $T_{in} = 200^{\circ}\text{C}$ and a mass-flow rate of the product $\dot{m}_{product} = 11.0 \text{ kg}\cdot\text{h}^{-1}$ (particles were tracked for their entire residence time): particle tracks colored according to their residence time (A); experimental and simulated residence time of the particles (B)

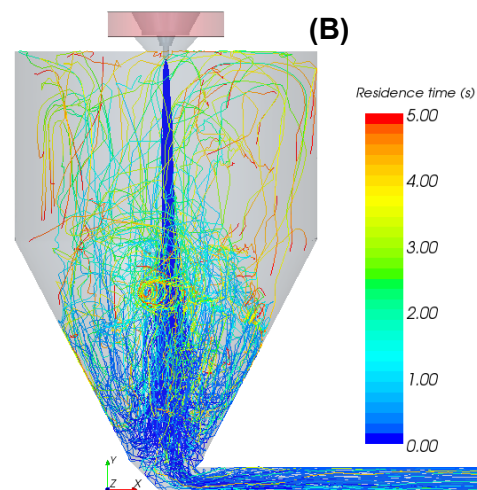
To evaluate the impact of particle size on residence-time distribution and particle properties, the simulation of the spray-drying condition $200^{\circ}\text{C}/11.0 \text{ kg}\cdot\text{h}^{-1}$ was additionally carried out for droplet sizes of $10 \mu\text{m}$ and $50 \mu\text{m}$, which corresponds to the largest diameter of the finer fraction of the experimental powder (cf. chapter 5.4.1). The particle tracks, which are colored according to the residence time, and the computed residence-time distributions are illustrated in Fig. 6.8. It is obvious that the particle size has an impact on the particle tracks. As expected, smaller particles are more influenced by the air flow pattern than bigger particles. Small particles have shorter residence times than bigger particles during the tracking time of 5 s. After 5 s, 49% of the particles with an initial diameter of $10 \mu\text{m}$ are still recirculating inside the spray dryer, 55% of the particles with an initial diameter of $15 \mu\text{m}$ and 61% of the particles with an initial diameter of $50 \mu\text{m}$. Moreover, smaller particles reach faster low water contents and their temperature and water content adapts faster to the surrounding air

conditions than is the case for bigger particles. This leads to bigger mean lysine losses after spray drying, with 9.1% for an initial droplet size of 10 μm , 6.5% for an initial droplet size of 15 μm and 5.8% for an initial droplet size of 50 μm .

10 μm :



15 μm :



50 μm :

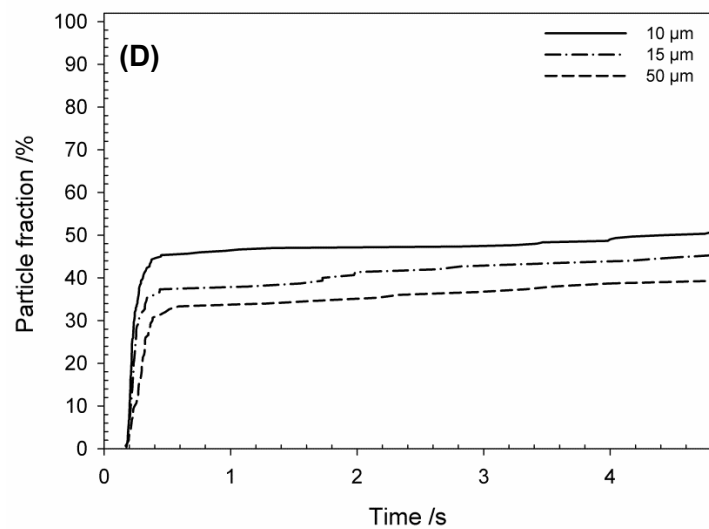
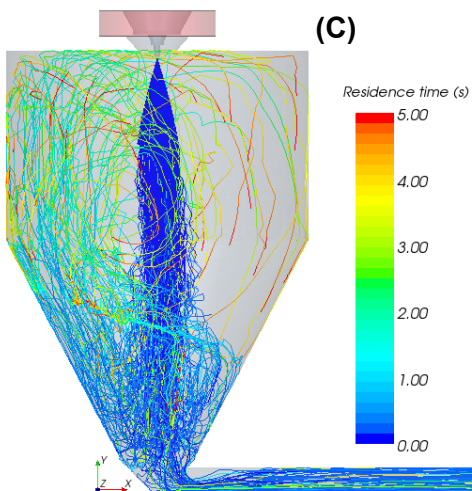


Fig. 6.8 Simulation results for an inlet temperature of the air $T_{in} = 200^\circ\text{C}$ and a mass-flow rate of the product $\dot{m}_{product} = 11.0 \text{ kg}\cdot\text{h}^{-1}$ (particles were tracked for up to 5 s): residence time of droplets with an initial size of 10 μm (A), 15 μm (B), 50 μm (C), particle residence-time distribution (D)

To sum up, the model of lysine loss during spray drying, which was developed in this study, is well capable of predicting the degree of lysine loss. However, to enhance its predictive power at adverse conditions with regard to lysine loss, it must be expanded to particle-size distributions, agglomeration of particles and wall deposition. Nevertheless, the model in its actual form is capable of distinguishing adverse conditions from gentle conditions and it can be used to optimize the spray-drying process as well as the spray-dryer geometry. Thus, a tool was successfully developed that renders superfluous work-intensive trial-and-error ex-

periments to find suitable spray-drying conditions. It is now possible to use the model to select potential spray-drying conditions and to restrict the experiments to a limited number which is necessary to validate the selected spray-drying conditions.

6.3 Optimization of the spray-drying process with regard to lysine loss

In order to ameliorate the nutritional product quality of spray-dried dairy powders, the particle residence-time inside the spray-drying chamber has to be reduced, i.e., the recirculation of powder particles inside the drying chamber has to be minimized. This implies that the flow profile of the drying gas is optimized from large vortex structures towards plug flow conditions. In this study, two approaches were chosen to achieve this goal. On the one hand, a secondary air inlet was defined in the roof of the spray-drying chamber to create a directed air flow from the top to the bottom. This should impede the formation of large vortices. On the other hand, a design study was conducted. The diameter of the spray-drying chamber was reduced step by step to eliminate recirculation zones.

6.3.1 Modification of the air profile by a secondary air inlet

To minimize recirculation of the drying air and thus of the particles, a secondary air inlet was defined at the roof of the spray-drying chamber. The entire roof of the spray-drying chamber was assigned to the secondary air inlet. The direction of flow was set perpendicular to the secondary inlet, i.e., the flow was directed from the top to the bottom. The inlet-air mass flow was split into one part which enters the spray-drying chamber through the primary inlet and one part which passes through the new secondary inlet. The expression “primary inlet” refers to the air inlet of the standard configuration (cf. chapter 6.1). The boundary conditions of the primary inlet remained unchanged except for the mass-flow rate. The mass-flow split ratios between the primary and the secondary air inlet were 75:25, 50:50 and 25:75. The simulation was run with the settings that are detailed in chapter 6.1. The air velocity profiles and the particle tracks, which are colored according to the particle residence-time, are shown in Fig. 6.9. The air-flow field is significantly altered by the air flow through the secondary inlet. The recirculation zones are reduced when mass flow through the secondary inlet is increased. Consequently, the residence time of the air is shorter. This results in higher outlet-air temperatures (Table 6.4) because less heat is lost through the dryer walls due to the shortened residence time. The vortex structures of the particle tracks become smaller with an increasing air mass flow through the secondary inlet (Fig. 6.9). Thus, the particle residence-time distribution is narrowed and the particle residence-times are shorter. Shorter particle residence-times mean less lysine loss. However, the vortex structures are not eliminated entirely and particles still recirculate, which leads to longer residence times. The mean final water content of the particles slightly decreases when the air flow through the secondary inlet is increased (Table 6.4). This can be attributed to the decreasing relative humidities of the air because the water content of the particles is in equilibrium with the air at this drying stage (cf. chapter 6.2). The lower relative humidities of the air result from the higher temperature level of the air. Low water contents in combination with high temperatures were shown to generate high lysine losses (cf. chapters 0 and 5.3). Hence, to which extent lysine loss can be diminished depends on the combined effect of the reduced residence-time, the reduced water content and the increased temperature. In conclusion, the desired amelioration degree can be achieved

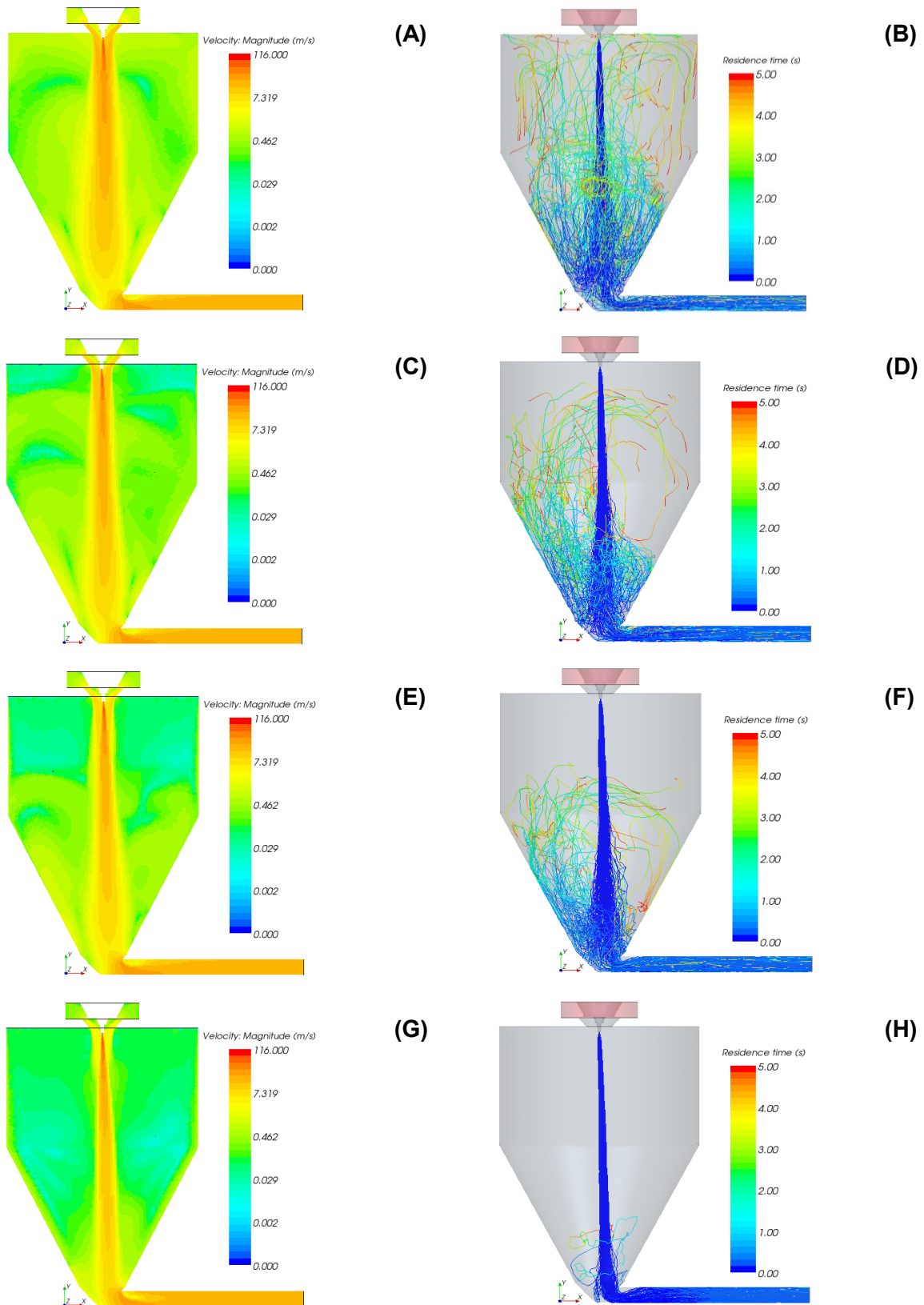


Fig. 6.9 Air-velocity profiles on the center plane with streamlines (left) and particle tracks with residence times (right) for different air inlet conditions ($T_{in} = 200^{\circ}\text{C}$; $\dot{m}_{product} = 11.0 \text{ kg}\cdot\text{h}^{-1}$): (A), (B) no secondary inlet (standard configuration); (C), (D) 25% of the inlet-air mass flow through the secondary inlet; (E), (F) 50% of the inlet-air mass flow through the secondary inlet; (G), (H) 75% of the inlet-air mass flow through the secondary inlet

with this approach. However, based on these results, the flow field should be optimized further taking into account process efficiency. The positioning and flow conditions of air inlets and outlets, e.g., should be carefully reconsidered to achieve a directed and controlled air-flow field. This would allow optimizing the spray-drying process.

Table 6.4 Simulation results of pilot-scale spray drying ($T_{in} = 200^{\circ}\text{C}$; $\dot{m}_{product} = 11.0 \text{ kg}\cdot\text{h}^{-1}$): Impact of the secondary air inlet

Mass-flow split ratio primary : secondary inlet /%	Process characteristics		Powder characteristics
	$T_{out} / ^{\circ}\text{C}$	$\text{RH}_{out} / \%$	X /% db
100 : 0	107	3.9	3.73
75 : 25	110	3.5	3.61
50 : 50	114	2.8	3.32
25 : 75	114	2.8	3.33

6.3.2 Variation of the spray-dryer geometry

A design study was conducted on the impact of the spray-dryer geometry on the air-flow field and particle tracks. The diameter of the spray-drying chamber was gradually reduced to avoid recirculation zones. Three different diameters (600 mm, 300 mm, 160 mm) were studied. The solver settings and boundary conditions were adopted as specified in chapter 6.1 and the simulations were run until the solutions converged. Fig. 6.10 displays the air flow fields and particle tracks as a function of the drying-chamber diameter. At smaller diameters, the recirculation zones diminish and the flow field approximates plug-flow conditions. This effect is accompanied by shortened particle residence-times, i.e., less lysine loss. The air outlet temperature increases with decreasing chamber diameter until a diameter of 300 mm. At the same time, the relative humidity of the outlet air and the average water content of the powder particles decrease. Consequently, the process efficiency is slightly improved. The increased temperature and reduced water content will only trigger lysine loss at long residence times. When the chamber diameter is further reduced to 160 mm, the air outlet temperature decreases again and the relative humidity of the outlet air and average water content of the powder particles increases. Recirculation of particles is avoided. This leads to very short residence times, which is desired to minimize lysine loss. However, many particles hit the dryer walls. This might lead to particle deposition depending on particle water content and temperature. The resulting long residence times combined with low water contents and high temperatures were shown to generate high lysine loss. To conclude with, optimizing the spray-dryer geometry makes it possible to ameliorate the flow field and particle tracks inside the spray dryer. Consequently, lysine loss can be minimized. This design study was based on simple geometry modifications and can be the basis for more sophisticated design optimizations. These could include the amount and position of air inlets and outlets as well as of atomizing devices. The geometry of the spray-drying chamber can then be adapted to the flow characteristics. In this way, the contact and mixing of the drying air with the droplets can be optimized. If controlled

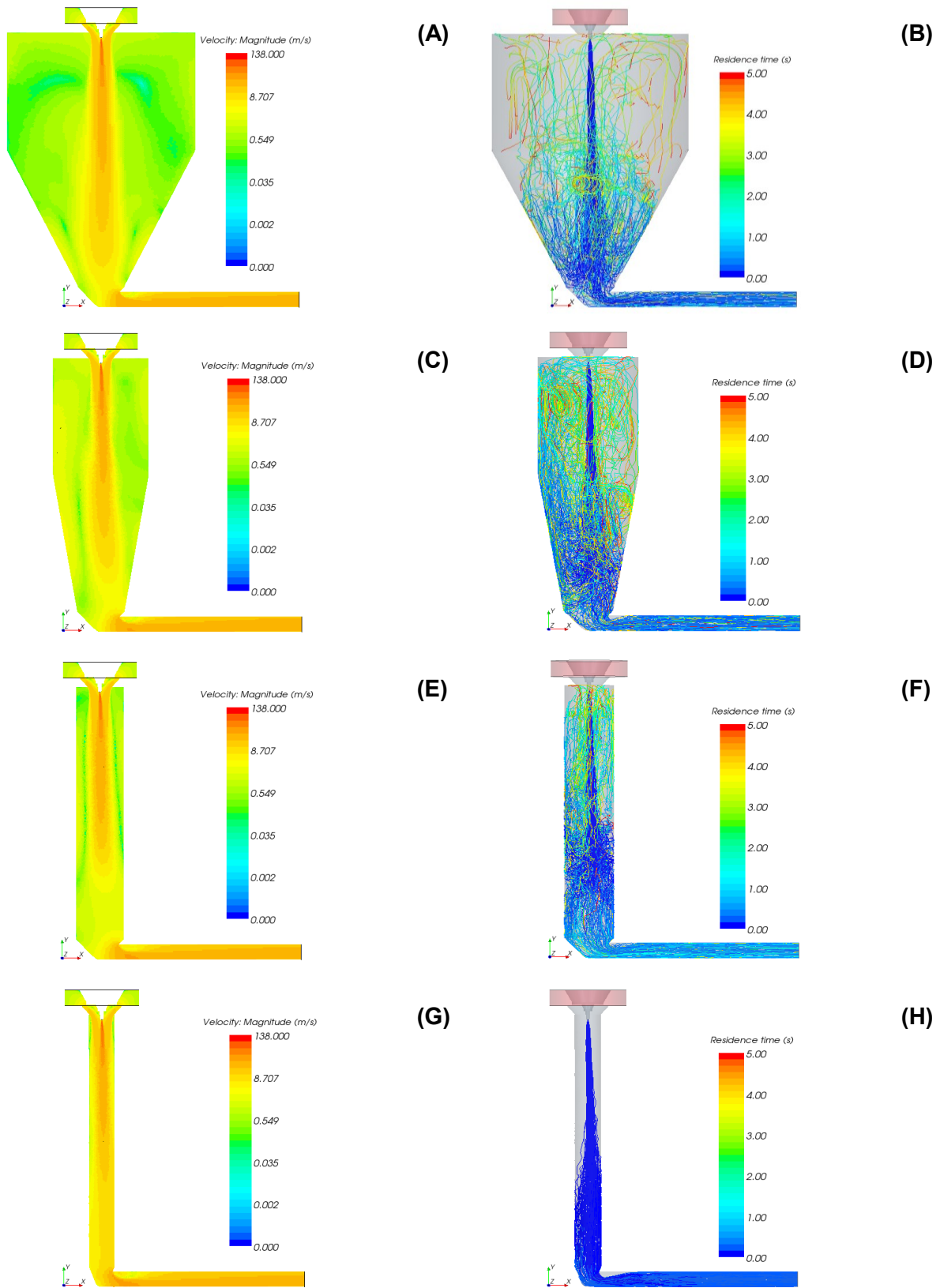


Fig. 6.10 Air velocity profiles on the center plane with streamlines (left) and particle tracks with residence times (right) for different spray-dryer geometries ($T_{in} = 200^{\circ}\text{C}$; $\dot{m}_{product} = 11.0 \text{ kg}\cdot\text{h}^{-1}$): (A), (B) spray-dryer diameter of 1200 mm (standard design); (C), (D) spray-dryer diameter of 600 mm; (E), (F) spray-dryer diameter of 300 mm; (G), (H) spray-dryer diameter of 160 mm

recirculation of the drying air and particles is achieved, the efficiency of the spray-drying process can be enhanced and at the same time the nutritional product quality ameliorated. Additionally, this will open a broad range of new applications. Thus, amongst others, novel engineered particles can be produced and controlled chemical modifications performed.

Table 6.5 Simulation results of pilot-scale spray drying ($T_{in} = 200^{\circ}\text{C}$; $\dot{m}_{product} = 11.0 \text{ kg}\cdot\text{h}^{-1}$): Impact of the diameters of the spray-drying chamber

Spray-drying chamber Diameter /mm	Process characteristics		Powder characteristics
	$T_{out} /^{\circ}\text{C}$	$\text{RH}_{out} /\%$	X /% db
1200	107	3.9	3.73
600	113	3.2	3.48
300	120	2.3	3.14
160	115	3.1	3.52

7 Conclusion

This study presents a new way of interpreting lysine losses in order to assess and understand lysine losses that occur during spray drying. The impact of heating on lysine loss has been separated from the impact of dehydration to establish the kinetics of lysine loss. It has been shown that the lysine loss in spray-dried dairy formulations can be controlled by the correct choice of the spray-drying conditions. Combining the kinetics of lysine loss with the drying kinetics of the model dairy-formulation and the particle tracks inside the spray dryer has allowed drawing conclusions on possible process optimizations.

Concerning dehydration-induced lysine losses, significant lysine losses could be observed for all vacuum dehydration conditions. Lysine losses increased with decreasing water content and the rate of lysine loss depended on the water content. Most of the lysine loss occurred towards the end of dehydration when the water content was below 10%. At the end of drying when the water content remained almost constant, thermal effects became more important, which resulted in a sharp increase in lysine loss at the higher shelf temperature. This increase was not comparably pronounced at the lower shelf temperature. Although dehydration induced considerable lysine losses, the drying rate did not significantly affect the extent of lysine loss. Further measurements are needed to elaborate the mechanism of lysine loss due to dehydration in more detail.

The loss of available lysine during heating in concentrated systems was influenced by various factors. Lysine loss increased significantly with increasing temperature and at prolonged heating times. The rate of lysine loss due to heating was fast during the first few minutes, which is the most relevant time scale for the spray-drying process. Then the rate of lysine loss slowed down for all water activities and temperatures. The water activity had a significant impact on lysine loss, as well. The water activity range of maximum lysine loss was shifted to lower water activities for higher temperatures applied. However, the mechanism of lysine loss is not that easy to determine. A complex system of competing reactions has to be taken into consideration to understand and describe the loss of available lysine in high concentration milk-systems. The importance of the physical state of lactose, of the transition phases and of molecular mobility arises and demonstrates the need to take these factors into account. The range of maximal lysine losses coincides with the transition zone from the rubbery to the crystalline states. This highlights the importance of monitoring the physical state and molecular mobility of the system.

It has been shown that the molecular mobility measured by low resolution ^1H NMR is a valuable tool to characterize the chemical stability of dairy powders and to complement the stability concept based on physical state. The loss of available lysine increased with increasing molecular mobility in the glassy and rubbery states and was decelerated by crystallization. This deceleration was in-line with an increase in the second moment, i.e., with an increase in the strength of the dipolar interactions. Consequently, a detailed analysis of the molecular mobility gave a deeper insight in the factors affecting chemical stability.

Differential scanning calorimetry and low resolution ^1H NMR both indicated that lactose crystallizes into different crystal forms depending on the crystallization conditions. Further

measurements are needed to determine which crystal forms develop. Then it might be possible to use low resolution ^1H NMR to analyze the crystalline structure of dairy powders.

Analyzing the molecular mobility together with the physical state can now be used to optimize dairy formulations with regard to their chemical stability. To enhance the chemical stability, the composition as well as the processing and storage conditions should be adapted with regard to the molecular mobility and physical state.

The reaction kinetics presented in this paper emphasizes the impact of the concentration, of the temperature and, linked to these two factors, of the physical state on the loss of available lysine in dairy formulations in the dry-state. It has been demonstrated that the loss of available lysine is a complex mechanism that can be modeled by pseudo-second order reaction kinetics when the physical state is included. The reaction-rate constants increased with increasing temperature showing a maximum at 90°C and $a_w = 0.23$. At lower temperatures this maximum was shifted to higher water activities. The temperature dependence of the reaction rate constants was modeled by the WLF equation in the vicinity of the glass transition temperature and in the rubbery state. Arrhenius-type behavior was determined for higher water contents and temperatures. Empirical relations were derived for water content dependence of the activation energy E_A and of the pre-exponential factor k_0^* .

To reduce the loss of available lysine while processing dairy products, high temperatures should be avoided especially at processing stages where the product is in the rubbery state. The reaction rate constants of lysine loss in the glassy state were rather small but increased fast above the glass transition temperature. In the glassy state, the system is characterized by a high viscosity and, consequently, lysine loss might be diffusion-limited. In the crystalline state, the reaction rate constants were lower than in the rubbery state. This can be explained by a lower reactivity of lactose in the crystalline state than in the rubbery state and/or by dilution of the reactants due to the higher water content.

During spray drying, the temperature profile inside the spray dryer and the particle residence time are important factors concerning lysine loss. Higher particle temperatures caused by higher air-outlet temperatures or by recirculation to zones with higher air temperatures will entrain higher lysine loss because lysine loss depends strongly on the temperature. This is especially true for conditions under which the particles are in the rubbery state.

Combining the kinetics of lysine loss with the drying kinetics of the model dairy-formulation and the particle tracks obtained from a CFD simulation gave a deeper insight into the evolution of lysine loss during spray drying. The reaction-engineering approach for the drying kinetics was successfully integrated into the CFD simulation. Thus, the dehydration time was shown to be much shorter than the particle residence time. However, special attention should be paid to the particle residence time. The longer a particle remains in the spray dryer, due to recirculation or because it sticks to a wall, the longer it is at elevated temperature and thus, at a critical concentration and physical state with regard to lysine loss. These relations were highlighted by coupling the reaction kinetics of lysine loss with the CFD simulation. Here, the need arose of further optimization regarding the air flow and particle deposition on the dryer walls. First promising optimization concepts were presented within the framework of this study. Atomization nozzles that create a controlled particle size distribution, such as described by Wu et al. (2013), could be another tool to modify particle residence

time in the spray dryer. Another factor that has to be reviewed is the fines return system. The fines are powder particles that have already passed the spray-drying cycle and that will be exposed again to conditions that provoke lysine loss.

The aim of the drying process should not only be to minimize lysine loss during spray drying but also to produce powders that are stable when stored with a focus on their nutritional quality. The importance of water content was shown in this context.

To sum up, it is possible to improve the nutritional quality of powdered dairy-formulations by considering the results of this study. Moreover, the model of this study can easily be extended to other applications. Other nutrients or valuable compounds can be included in the model via the respective reaction-kinetics models. The CFD simulation of spray drying can be replaced by another process keeping the principal concept of this study. Thus, time-consuming trial-and-error experiments can be replaced by a few targeted experiments to validate the optimal parameter range derived from the simulations.

8 References

- Acevedo NC, Schebor C, Buera P (2008) Non-enzymatic browning kinetics analysed through water-solids interactions and water mobility in dehydrated potato. *Food Chemistry* 108(3):900-906
- Adhikari B, Howes T, Bhandari BR (2007) Use of solute fixed coordinate system and method of lines for prediction of drying kinetics and surface stickiness of single droplet during convective drying. *Chemical Engineering and Processing: Process Intensification* 46(5):405-419
- Adhikari B, Howes T, Bhandari BR, Troung V (2003) Surface stickiness of drops of carbohydrate and organic acid solutions during convective drying: Experiments and modeling. *Drying Technology* 21(5):839
- Aeberhardt K, Bui QD, Normand V (2007) Using low-field NMR to infer the physical properties of glassy oligosaccharide/water mixtures. *Biomacromolecules* 8(3):1038-1046
- Anandharamakrishnan C, Gimbin J, Stapley AGF, Rielly CD (2010) A study of particle histories during spray drying using computational fluid dynamic simulations. *Drying Technology* 28(5):566-576
- Anandharamakrishnan C, Rielly CD, Stapley AGF (2007) Effects of process variables on the denaturation of whey proteins during spray drying. *Drying Technology* 25(4-6):799-807
- Aschenbrenner M, Kulozik U, Foerst P (2012) Evaluation of the relevance of the glassy state as stability criterion for freeze-dried bacteria by application of the Arrhenius and WLF model. *Cryobiology* 65(3):308-318
- Avrami M (1940) Kinetics of phase change. II Transformation-time relations for random distribution of nuclei. *Journal of Chemical Physics* 8(2):212-224
- Belitz H, Grosch W, Schieberle P (2001) *Lehrbuch der Lebensmittelchemie*, 5th rev. and exp. edn. Springer, Berlin
- Bell LN, Touma DE, White KL, Chen YH (1998) Glycine loss and Maillard browning as related to the glass transition in a model food system. *Journal of Food Science* 63(4):625-628
- Biliaderis CG, Lazaridou A, Mavropoulos A, Barbayiannis N (2002) Water plasticization effects on crystallization behavior of lactose in a co-lyophilized amorphous polysaccharide matrix and its relevance to the glass transition. *International Journal of Food Properties* 5(2):463-482
- Birchal V, Passos ML, Wildhagen G, Mujumdar A (2005) Effect of spray-dryer operating variables on the whole milk powder quality. *Drying Technology* 23(3):611-636
- Birchal VS, Huang L, Mujumdar AS, Passos ML (2006) Spray dryers: Modeling and simulation. *Drying Technology* 24(3):359-371
- Birlouez-Aragon I, Pischetsrieder M, Leclere J, Morales FJ, Hasenkopf K, Kientsch-Engel R, Ducauze CJ, Rutledge D (2004) Assessment of protein glycation markers in infant formulas. *Food Chemistry* 87(2):253-259
- Blei S, Sommerfeld M (2011) CFD in drying technology - spray-dryer simulation. In: Tsotsas E, Mujumdar AS (eds) *Modern Drying Technology, Computational Tools at Different Scales*. John Wiley & Sons, Hoboken, pp 155-208
- Bronlund J, Paterson T (2004) Moisture sorption isotherms for crystalline, amorphous and predominantly crystalline lactose powders. *International Dairy Journal* 14(3):247-254
- Büchi Labortechnik AG (2013) Mini Spray Dryer B- 290. Product information, Flawil
- Burin L, Jouppila K, Roos Y, Kansikas J, Buera MdP (2000) Color formation in dehydrated modified whey powder systems as affected by compression and Tg. *Journal of Agriculture and Food Chemistry* 48(11):5263-5268
- CD-adapco (2012) User guide. STAR-CCM+ Version 7.04.011

- Champion D, Le Meste M, Simatos D (2000) Towards an improved understanding of glass transition and relaxations in foods: molecular mobility in the glass transition range. *Trends in Food Science & Technology* 11(2):41-55
- Charissou A, Ait-Ameur L, Birlouez-Aragon I (2007) Kinetics of formation of three indicators of the Maillard reaction in model cookies: influence of baking temperature and type of sugar. *Journal of Agricultural & Food Chemistry* 55(11):4532-4539
- Charlesworth DH, Marshall WR (1960) Evaporation from drops containing dissolved solids. *AIChE Journal* 6(1):9-23
- Chavez-Servin JL, Castellote AI, Lopez-Sabater MC (2008) Evolution of available lysine and lactose contents in supplemented microencapsulated fish oil infant formula powder during storage. *International Journal of Food Science and Technology* 43(6):1121-1128
- Chen XD (2008) The basics of a reaction engineering approach to modeling air-drying of small droplets or thin-layer materials. *Drying Technology* 26(6):627-639
- Chen XD, Lin SXQ (2005) Air drying of milk droplet under constant and time-dependent conditions. *AIChE Journal* 51(6):1790-1799
- Chen XD, Mujumdar AS (2008) *Drying technologies in food processing*. Blackwell Pub., Oxford
- Chen XD, Patel KC (2008) Manufacturing better quality food powders from spray drying and subsequent treatments. *Drying Technology* 26(11):1313-1318
- Chen XD, Xie GZ (1997) Fingerprints of the Drying Behaviour of Particulate or Thin Layer Food Materials Established Using a Reaction Engineering Model. *Food and Bioproducts Processing* 75(4):213-222
- Cheong HW, Jeffreys GV, Mumford CJ (1986) A receding interface model for the drying of slurry droplets. *AIChE Journal* 32(8):1334-1346
- Chiou D, Langrish TAG (2007) Crystallization of amorphous components in spray-dried powders. *Drying Technology* 25:1427-1435
- Chiou D, Langrish TAG, Braham R (2008) Partial crystallization behavior during spray drying: Simulations and experiments. *Drying Technology* 26(1):27-38
- Contreras-Calderon J, Guerra-Hernandez E, Garcia-Villanova B (2008) Indicators of non-enzymatic browning in the evaluation of heat damage of ingredient proteins used in manufactured infant formulas. *European Food Research and Technology* 227(1):117-124
- Contreras-Calderon J, Guerra-Hernandez E, Garcia-Villanova B (2009) Utility of some indicators related to the Maillard browning reaction during processing of infant formulas. *Food Chemistry* 114(4):1265-1270
- Dexter JE, Tkachuk R, Matsuo RR (1984) Amino-acid-composition of spaghetti - effect of drying conditions on total and available lysine. *Journal of Food Science* 49(1):225-228
- Duangkhamchan W, Ronsse F, Depypere F, Dewettinck K, Pieters J (2012) CFD study of droplet atomisation using a binary nozzle in fluidised bed coating. *Chemical Engineering Science* 68(1):555-566
- Elmadfa I, Leitzmann C (1990) *Ernährung des Menschen*, 2nd edn. Ulmer, Stuttgart
- El-Sayed TM, Wallack DA, King CJ (1990) Changes in particle morphology during drying of drops of carbohydrate solutions and food liquids. 1. Effect of composition and drying conditions. *Industrial & Engineering Chemical Research* 29(12):2346-2354
- European Commission (2008) Commission Directive 2006/141/EC of 22 December 2006 on infant formulae and follow-on formulae and amending Directive 1999/21/EC Text with EEA relevance as amended by Commission Regulation (EC) No 1243/2008 of 12 December 2008

- Evangelisti F, Calcagno C, Zunin P (1994) Relationship between blocked lysine and carbohydrate-composition of infant formulas. *Journal of Food Science* 59(2):335-337
- FAO/WHO/UNU (2007) Protein and amino acid requirements in human nutrition. Report of a joint WHO/FAO/UNU expert consultation. WHO technical report series, vol 935. World Health Organization, Geneva
- Fenaille F, Campos-Giménez E, Guy PA, Schmitt C, Morgan F (2003) Monitoring of [beta]-lactoglobulin dry-state glycation using various analytical techniques. *Analytical Biochemistry* 320(1):144-148
- Fenaille F, Parisod V, Tabet JC, Guy PA (2005) Carbonylation of milk powder proteins as a consequence of processing conditions. *Proteomics* 5(12):3097-3104
- Ferrer E, Alegria A, Farre R, Abellan P, Romero F (2000) Effects of thermal processing and storage on available lysine and furfural compounds contents of infant formulas. *Journal of Agricultural and Food Chemistry* 48(5):1817-1822
- Ferrer E, Alegria A, Farre R, Abellan P, Romero F (2003a) Fluorometric determination of chemically available lysine: Adaptation, validation and application to different milk products. *Nahrung-Food* 47(6):403-407
- Ferrer E, Alegria A, Farre R, Abellan P, Romero F, Clemente G (2003b) Evolution of available lysine and furosine contents in milk-based infant formulas throughout the shelf-life storage period. *Journal of the Science of Food and Agriculture* 83(5):465-472
- Ferziger JH, Perić A (2008) *Numerische Strömungsmechanik*. Springer, Berlin
- Filková I, Mujumdar AS (1995) Industrial Spray Drying Systems. In: Mujumdar AS (ed) *Handbook of industrial drying*, 2nd edn. Dekker, New York
- Fink R, Kessler HG (1986a) Erfassung und Berechnung der Lysinverluste gelagerter und erhitzter Milch. *Ernährungs-Umschau* 33(4):121-124
- Fink R, Kessler HG (1986b) Reaction-kinetics evaluation of the oxidative changes in stored UHT milk. *Milchwissenschaft-Milk Science International* 41(2):90-94
- Fink R, Kessler HG (1986c) Recording and calculation of lysine wastings in UHT milk during storage. *Ernährungs-Umschau* 33(4):121-124
- Finot PA (1983) Chemical modifications of the milk-proteins during processing and storage - nutritional, metabolic and physiological consequences. *Kieler Milchwirtschaftliche Forschungsberichte* 35(3):357-369
- Finot PA, Deutsch R, Bujard E (1981) The extent of the maillard reaction during the processing of milk. *Progress in Food and Nutrition Science* 5(1-6):345-355
- Fletcher DF, Guo B, Harvie DJE, Langrish TAG, Nijdam JJ, Williams J (2006) What is important in the simulation of spray dryer performance and how do current CFD models perform? *Applied Mathematical Modelling* 30(11):1281-1292
- Fletcher DF, Langrish TAG (2009) Scale-adaptive simulation (SAS) modelling of a pilot-scale spray dryer. *Chemical Engineering Research & Design* 87(10A):1371-1378
- Foerst P, Kulozik U (2012) Modelling the dynamic inactivation of the probiotic bacterium *L. paracasei* ssp. *paracasei* during a low-temperature drying process based on stationary data in concentrated systems. *Food and Bioprocess Technology* 5(6):2419-2427
- Foerst P, Reitmaier J, Kulozik U (2010) 1H NMR investigation on the role of sorbitol for the survival of *Lactobacillus paracasei* ssp *paracasei* in vacuum-dried preparations. *Journal of Applied Microbiology* 108(3):841-850
- Fries L, Antonyuk S, Heinrich S, Palzer S (2011a) DEM-CFD modeling of a fluidized bed spray granulator. *Chemical Engineering Science* 66(11):2340-2355

- Fries L, Dosta M, Antonyuk S, Heinrich S, Palzer S (2011b) Moisture distribution in fluidized beds with liquid injection. *Chemical Engineering & Technology* 34(7):1076-1084
- Fu N, Chen XD (2011) Towards a maximal cell survival in convective thermal drying processes. *Food Research International* 44(5):1127-1149
- Fu N, Wai Woo M, Qi Lin SX, Zhou Z, Dong Chen X (2011) Reaction engineering approach (REA) to model the drying kinetics of droplets with different initial sizes – experiments and analyses. *Chemical Engineering Science* 66(8):1738-1747
- Fu WY, Suen SY, Etzel MR (1995) Inactivation of *Lactococcus-lactis* ssp *lactis* C2 and alkaline-phosphatase during spray-drying. *Drying Technology* 13(5-7):1463-1476
- Ge Pan G, Melton LD (2007) Nonenzymatic browning of lactose and caseinate during dry heating at different relative humidities. *Journal of Agricultural and Food Chemistry* 55(24):10036-10042
- Gesellschaft Verfahrenstechnik und Chemieingenieurwesen (2006) VDI-Wärmeatlas, 10th edn. Springer, Berlin
- Ghandi A, Powell I, Chen XD, Adhikari B (2012) Drying kinetics and survival studies of dairy fermentation bacteria in convective air drying environment using single droplet drying. *Journal of Food Engineering* 110(3):405–417
- Gianfrancesco A (2009) Spray drying engineering: Particle stickiness in relation with agglomeration. PhD thesis, AgroParisTech, Paris
- Gianfrancesco A, Turchiuli C, Dumoulin E, Palzer S (2009) Prediction of powder stickiness along spray drying process in relation to agglomeration. *Particulate Science and Technology* 27(5):415-427
- Gianfrancesco A, Turchiuli C, Flick D, Dumoulin E (2010) CFD modeling and simulation of maltodextrin solutions spray drying to control stickiness. *Food and Bioprocess Technology* 3(6):946-955
- Goodno CC, Swaisgood HE, Catignani GL (1981) A fluorimetric assay for available lysine in proteins. *Analytical Biochemistry* 115(1):203-211
- Gordon M, Taylor JS (1952) Ideal copolymers and the 2nd-order transitions of synthetic rubbers. 1. non-crystalline copolymers. *Journal of Applied Chemistry* 2(9):493-500
- Greenspan L (1977) Humidity fixed-points of binary saturated aqueous-solutions. *Journal of Research of the National Bureau of Standards Section A-Physics and Chemistry* 81(1):89-96
- Groenewold C, Möser C, Groenewold H, Tsotsas E (2002) Determination of single-particle drying kinetics in an acoustic levitator. *Chemical Engineering Journal* 86(1-2):217-222
- Guerra-Hernandez E, Leon C, Corzo N, Garcia-Villanova B, Romera JM (2002) Chemical changes in powdered infant formulas during storage. *International Journal of Dairy Technology* 55(4):171-176
- Guyomarc'h F, Warin F, Muir DD, Leaver J (2000) Lactosylation of milk proteins during the manufacture and storage of skim milk powders. *International Dairy Journal* 10(12):863-872
- Haque MK, Roos YH (2004) Water plasticization and crystallization of lactose in spray-dried lactose/protein mixtures. *Journal of Food Science* 69(1):E23
- Hede PD, Bach P, Jensen AD (2008) Two-fluid spray atomisation and pneumatic nozzles for fluid bed coating/agglomeration purposes: A review. *Chemical Engineering Science* 63(14):3821-3842
- Hinrichs R (2004) NMR-Messungen zur Wasserbindung und Struktur in Systemen aus Milchproteinen und Hydrokolloiden, PhD Thesis, TU München, Dr. Hut, München
- Hinrichs R, Gotz J, Noll M, Wolfschoon A, Eibel H, Weisser H (2004) Characterisation of different treated whey protein concentrates by means of low-resolution nuclear magnetic resonance. *International Dairy Journal* 14(9):817-827

- Holsinger VH, Posati LP, Devilbis ED, Pallansc MJ (1973) Variation of total and available lysine in dehydrated products from cheese wheys by different processes. *Journal of Dairy Science* 56(12):1498-1504
- Horak FP, Kessler HG (1981) The influence of UHT heating and sterilization on lysine in milk. *Milchwissenschaft-Milk Science International* 36(9):543-547
- Huang LX, Kumar K, Mujumdar AS (2003) A parametric study of the gas flow patterns and drying performance of co-current spray dryer: Results of a computational fluid dynamics study. *Drying Technology* 21(6):957-978
- Huang LX, Mujumdar AS (2007) Simulation of an industrial spray dryer and prediction of off-design performance. *Drying Technology* 25(4-6):703-714
- Huang LX, Passos ML, Kumar K, Mujumdar AS (2005) A three-dimensional simulation of a spray dryer fitted with a rotary atomizer. *Drying Technology* 23(9-11):1859-1873
- Huss W (1970) Lactosekristallisation und Lysinverfügbarkeit nach Lagerung von Trockenmagermilchpulvern bei verschiedener Luftfeuchtigkeit. *Landwirtschaftliche Forschung* 23:275-289
- Ibach A, Kind M (2007) Crystallization kinetics of amorphous lactose, whey-permeate and whey powders. *Carbohydrate Research* 342(10):1357-1365
- Ilo S, Berghofer E (2003) Kinetics of lysine and other amino acids loss during extrusion cooking of maize grits. *Journal of Food Science* 68(2):496-502
- Incropera FP, Dewitt DP, Bergmann TL, Lavine AS (2013) *Principles of heat and mass transfer*, 7th edn. John Wiley, Singapore
- Jeantet R, Ducept F, Dolivet A, Mejean S, Schuck P (2008) Residence time distribution: a tool to improve spray-drying control. *Dairy Science & Technology* 88(1):31-43
- Jin Y, Chen XD (2009) Numerical study of the drying process of different sized particles in an industrial-scale spray dryer. *Drying Technology* 27(3):371-381
- Jouppila K, Kansikas J, Roos Y (1998) Crystallization and X-ray diffraction of crystals formed in water-plasticized amorphous lactose. *Biotechnol Progress* 14(2):347-350
- Jouppila K, Kansikas J, Roos YH (1997) Glass transition, water plasticization, and lactose crystallization in skim milk powder. *Journal of Dairy Science* 80(12):3152-3160
- Jouppila K, Roos YH (1994) Glass transitions and crystallization in milk powders. *Journal of Dairy Science* 77(10):2907-2915
- Karmas R, Buera MP, Karel M (1992) Effect of glass-transition on rates of nonenzymatic browning in food systems. *Journal of Agricultural and Food Chemistry* 40(5):873-879
- Kastner O, Brenn G, Rensink D, Tropea C (2001) The acoustic tube levitator – A novel device for determining the drying kinetics of single droplets. *Chemical Engineering & Technology* 24(4):335-339
- Kedward CJ, MacNaughtan W, Mitchell JR (2000) Crystallization kinetics of amorphous lactose as a function of moisture content using isothermal differential scanning calorimetry. *Journal of Food Science* 65(2):324-328
- Kessler HG (1996) *Lebensmittel- und Bioverfahrenstechnik – Molkereitechnologie*, 4th, rev. and ext. edn. Verlag A. Kessler, München
- Kieviet F, Kerkhof PJAM (1995) Measurements of particle residence time distributions in a cocurrent spray dryer. *Drying Technology* 13(5-7):1241-1248
- Kondoh T, Torii K (2011) Brain mechanisms involved in the detection and adaptation to lysine deficiency. Chapter 154. In: Preedy VR (ed) *Handbook of behavior, food and nutrition*. Springer, New York: 2451-2468

- Kuriakose R, Anandharamakrishnan C (2010) Computational fluid dynamics (CFD) applications in spray drying of food products. *Trends in Food Science & Technology* 21(8):383-398
- Labuza TP, Saltmarch M (1981) Kinetics of browning and protein quality loss in whey powders during steady state and nonsteady state storage conditions. *Journal of Food Science* (47):92-96
- Langrish TAG (2007) New engineered particles from spray dryers: Research needs in spray drying. *Drying Technology* 25(4-6):971-983
- Langrish TAG (2008) Assessing the rate of solid-phase crystallization for lactose: The effect of the difference between material and glass-transition temperatures. *Food Research International* 41(6):630-636
- Langrish TAG (2009) Multi-scale mathematical modelling of spray dryers. *Journal of Food Engineering* 93(2):218-228
- Langrish TAG, Kockel TK (2001) The assessment of a characteristic drying curve for milk powder for use in computational fluid dynamics modelling. *Chemical Engineering Journal* 84(1):69-74
- Langrish TAG, Wang S (2009) Crystallization rates for amorphous sucrose and lactose powders from spray drying: A comparison. *Drying Technology* 27(4):606-614
- Langrish TAG, Zbicinski I (1994) The effects of air inlet geometry and spray cone angle on the wall deposition rate in spray dryers. *Chemical Engineering Research & Design* 72(A3):420-430
- Lehto V, Tenho M, Vahaheikkila K, Harjunen P, Paallysaho M, Valisaari J, Niemela P, Jarvinen K (2006) The comparison of seven different methods to quantify the amorphous content of spray dried lactose. *Powder Technology* 167(2):85-93
- Lievense LC, Verbeek MAM, Taekema T, Meerdink G, Vantriet K (1992) Modeling the inactivation of *Lactobacillus-plantarum* during a drying process. *Chemical Engineering Science* 47(1):87-97
- Lin SX, Chen XD (2002) Improving the glass-filament method for accurate measurement of drying kinetics of liquid droplets. *Chemical Engineering Research & Design* 80(A4):401-410
- Lin SXQ, Chen XD (2006) A model for drying of an aqueous lactose droplet using the reaction engineering approach. *Drying Technology* 24(11):1329-1334
- Lin SXQ, Chen XD (2007) The reaction engineering approach to modelling the cream and whey protein concentrate droplet drying. *Chemical Engineering and Processing* 46(5):437-443
- Lin XY, Ruan R, Chen P, Chung MS, Ye XF, Yang T, Doona C, Wagner T (2006) NMR state diagram concept. *Journal of Food Science* 71(9):R136
- Li XM, Lin SXQ, Chen XD, Chen LZ, Pearce D (2006) Inactivation kinetics of probiotic bacteria during the drying of single milk droplets. *Drying Technology* 24(6):695-701
- Li XY, Zbicinski I, Jing W (2010a) A scaling-up approach from experimental tunnel to spray dryer. *International Journal of Food Engineering* 6(1)
- Li Z, Kind M, Gruenewald G (2010b) Modeling fluid dynamics and growth kinetics in fluidized bed spray granulation. *The Journal of Computational Multiphase Flows* 2(4):235-248
- Lo S (2005) Application of computational fluid dynamics to spray drying. *Lait* 85(4-5):353-359
- Lubach JW, Xu D, Segmuller BE, Munson EJ (2007) Investigation of the effects of pharmaceutical processing upon solid-state NMR relaxation times and implications to solid-state formulation stability. *Journal of Pharmaceutical Sciences* 96(4):777-787
- Luyben KCAM, Liou JK, Bruin S (1982) Enzyme degradation during drying. *Biotechnology and Bioengineering* 24(3):533-552
- Malec LS, Gonzales ASP, Naranjo GB, Vigo MS (2002) Influence of water activity and storage temperature on lysine availability of a milk like system. *Food Research International* 35(9):849-853

- Mariette F (2009) Investigations of food colloids by NMR and MRI. *Current Opinion in Colloid & Interface Science* 14(3):203-211
- Masters K (1991) *Spray drying handbook*, 5th edn. Longman Scientific & Technical, Harlow
- Mateus ML, Champion D, Liardon R, Voilley A (2007) Characterization of water mobility in dry and wetted roasted coffee using low-field proton nuclear magnetic resonance. *Journal of Food Engineering* 81(3):572-579
- Mazza MGG, Brandao LEB, Wildhagen GS (2003) Characterization of the residence time distribution in spray dryers. *Drying Technology* 21(3):525-538
- Mazzobre MF, Aguilera JM, Buera MP (2003) Microscopy and calorimetry as complementary techniques to analyze sugar crystallization from amorphous systems. *Carbohydrate Research* 338(6):541-548
- Mazzobre MF, Soto G, Aguilera JM, Buera MP (2001) Crystallization kinetics of lactose in systems co-lyophilized with trehalose. Analysis by differential scanning calorimetry. *Food Research International* 34(10):903-911
- Meade SJ, Reid EA, Gerrard JA (2005) The impact of processing on the nutritional quality of food proteins. *Journal of AOAC International* 88(3):904-922
- Menshutina NV, Gordienko MG, Voinovskiy AA, Zbicinski I (2010) Spray drying of probiotics: Process development and scale-up. *Drying Technology* 28(10):1170-1177
- Mestry AP, Mujumdar AS, Thorat BN (2011) Optimization of spray drying of an innovative functional food: Fermented mixed juice of carrot and watermelon. *Drying Technology* 29(10):1121-1131
- Mezhericher M, Levy A, Borde I (2009) Modeling of droplet drying in spray chambers using 2D and 3D computational fluid dynamics. *Drying Technology* 27(3):359-370
- Mezhericher M, Levy A, Borde I (2010a) Spray drying modelling based on advanced droplet drying kinetics 49(11):1205-1213
- Mezhericher M, Levy A, Borde I (2010b) Theoretical models of single droplet drying kinetics: A Review. *Drying Technology* 28(2):278-293
- Miao S, Roos YH (2004) Nonenzymatic browning kinetics of a carbohydrate-based low-moisture food system at temperatures applicable to spray drying. *Journal of Agricultural and Food Chemistry* 52(16):5250-5257
- Miao S, Roos YH (2005) Nonenzymatic browning kinetics in low-moisture food system as affected by matrix composition and crystallization. *Journal of Food Science* 70(2):E69-E77
- Morales FJ, Romero C, Jimenez-Perez S (1995) New methodologies for kinetic study of 5-(hydroxymethyl)-furfural formation and reactive lysine blockage in heat-treated milk and model systems. *Journal of Food Protection* 58(3):310-315
- Morgan F, Leonil J, Molle D, Bouhallab S (1999) Modification of bovine beta-lactoglobulin by glycation in a powdered state or in an aqueous solution: Effect on association behavior and protein conformation. *Journal of Agricultural and Food Chemistry* 47(1):83-91
- Morgan F, Nouzille CA, Baechler R, Vuataz G, Raemy A (2005) Lactose crystallisation and early Maillard reaction in skim milk powder and whey protein concentrates. *Lait* 85(4-5):315-323
- Moughan PJ, Rutherfurd SM (2008) Available lysine in foods: A brief historical overview. *Journal of AOAC International* 91(4):901-906
- Nijdam J, Ibach A, Eichhorn K, Kind M (2007) An X-ray diffraction analysis of crystallised whey and whey-permeate powders. *Carbohydrate Research* 342(16):2354-2364
- Ozmen L, Langrish TAG (2003) A study of the limitations to spray dryer outlet performance. *Drying Technology* 21(5):895-917

- Patel KC, Chen XD (2005) Prediction of spray-dried product quality using two simple drying kinetics models. *Journal of Food Process Engineering* 28(6):567-594
- Patel KC, Chen XD (2008a) Drying of aqueous lactose solutions in a single stream dryer. *Food and Bioproducts Processing* 86:185-197
- Patel KC, Chen XD (2008b) Sensitivity analysis of the reaction engineering approach to modeling spray drying of whey proteins concentrate. *Drying Technology* 26(11):1334-1343
- Patel KC, Chen XD, Lin SXQ, Adhikari B (2009) A composite reaction engineering approach to drying of aqueous droplets containing sucrose, maltodextrin (DE6) and their mixtures. *AIChE Journal* 55(1):217-231
- Peleg M (1992) On the use of the WLF model in polymers and foods. *Critical Reviews in Food Science and Nutrition* 32(1):59-66
- Perdana J, Fox MB, Schutyser MAI, Boom RM (2011) Single-droplet experimentation on spray drying: Evaporation of a sessile droplet. *Chemical Engineering Technology* 34(7):1151-1158
- Pereyra Gonzales AS, Naranjo GB, Leiva GE, Malec LS (2010) Maillard reaction kinetics in milk powder: Effect of water activity at mild temperatures. *International Dairy Journal* 20(1):40-45
- Pereyra Gonzales AS, Naranjo GB, Malec LS, Vigo MS (2003) Available lysine, protein digestibility and lactulose in commercial infant formulas. *International Dairy Journal* 13(2-3):95-99
- Písecký J (1997) Handbook of milk powder manufacture. Niro A/S, Copenhagen, Denmark
- Putranto A, Chen XD, Xiao Z, Webley PA (2011) Simple, accurate and robust modeling of various systems of drying of foods and biomaterials: A demonstration of the feasibility of the reaction engineering approach (REA). *Drying Technology* 29(13):1519-1528
- Räderer M (2001) Drying of viscous, shrinking products. Modelling and experimental validation. PhD thesis, TU München, VDI-Verlag, Düsseldorf
- Rahman MS (2009) Food stability beyond water activity and glass transition: Macro-micro region concept in the state diagram. *International Journal of Food Properties* 12(4):726-740
- Rahman MS (2010) Food stability determination by macro-micro region concept in the state diagram and by defining a critical temperature. *Journal of Food Engineering* 99(4):402-416
- Rehner G, Daniel H (2010) *Biochemie der Ernährung*, 3rd edn. Spektrum Akademischer Verlag, Heidelberg, Neckar
- Reinhold M, Horst C, Hoffmann U (2001) Experimental and theoretical investigations of a spray dryer with simultaneous chemical reaction. *Chemical Engineering Science* 56(4):1657-1665
- Rogers S, Fang Y, Sean Xu Qi Lin, Selomulya C, Chen XD (2012) A monodisperse spray dryer for milk powder: Modelling the formation of insoluble material. *Chemical Engineering Science* 71(0):75-84
- Roos YH (1995) *Phase transitions in foods*. Academic Press, San Diego
- Roos YH (2002) Importance of glass transition and water activity to spray drying and stability of dairy powders. *Lait* 82(4):475-484
- Roos YH (2010) Glass Transition Temperature and Its Relevance in Food Processing. *Annual Review of Food Science and Technology* 1:469-496
- Roos YH, Himberg MJ (1994) Nonenzymatic browning behavior as related to glass-transition of a food model at chilling temperatures. *Journal of Agricultural and Food Chemistry* 42(4):893-898
- Roudaut G, Farhat I, Poirier-Brulez F, Champion D (2009) Influence of water, temperature and sucrose on dynamics in glassy starch-based products studied by low field H-1 NMR. *Carbohydrate Polymers* 77(3):489-495

- Roux S, Courel M, it-Ameur L, Birlouez-Aragon I, Pain JP (2009) Kinetics of Maillard reactions in model infant formula during UHT treatment using a static batch ohmic heater. *Dairy Science & Technology* 89(3-4):349-362
- Rufian-Henares JA, Garcia-Villanova B, Guerra-Hernandez E (2002) Furosine content, loss of o-phthaldialdehyde reactivity, fluorescence and colour in stored enteral formulas. *International Journal of Dairy Technology* 55(3):121-126
- Rufian-Henares JA, Guerra-Hernandez E, Garcia-Villanova B (2006) Available lysine and fluorescence in heated milk proteins/dextrinomaltose or lactose solutions. *Food Chemistry* 98(4):685-692
- Rutherfurd SM, Moughan PJ (2005) Digestible reactive lysine in selected milk-based products. *Journal of Dairy Science* 88(1):40-48
- Rutherfurd SM, Moughan PJ (2008) Effect of elevated temperature storage on the digestible reactive lysine content of unhydrolyzed- and hydrolyzed-lactose milk-based products. *Journal of Dairy Science* 91(2):477-482
- Schmidt SJ (2004) Water and solids mobility in foods. *Advances in food and nutrition research* 48:1-101
- Schuck P, Dolivet A, Mejean S, Jeantet R (2008) Relative humidity of outlet air: the key parameter to optimize moisture content and water activity of dairy powders. *Dairy Science & Technology* 88(1):45-52
- Schutyser MAI, Perdana J, Boom RM (2012) Single droplet drying for optimal spray drying of enzymes and probiotics. *Trends in Food Science & Technology* 27(2):73-82
- Sloth J, Bach P, Jensen AD, Kiil S (2008) Evaluation method for the drying performance of enzyme containing formulations. *Biochemical Engineering Journal* 40(1):121-129
- Sloth J, Jørgensen K, Bach P, Jensen AD, Kiil S, Dam-Johansen K (2009) Spray drying of suspensions for pharma and bio products: Drying kinetics and morphology. *Industrial & Engineering Chemical Research* 48(7):3657-3664
- Sloth J, Kiil S, Jensen AD, Andersen SK, Jørgensen K, Schiffter H, Lee G (2006) Model based analysis of the drying of a single solution droplet in an ultrasonic levitator. *Chemical Engineering Science* 61(8):2701-2709
- Stein J (2003) *Praxishandbuch klinische Ernährung und Infusionstherapie*. Springer, Berlin
- Straatsma J, van Houwelingen G, Steenbergen AE, Jong P de (1999) Spray drying of food products: 1. Simulation model. *Journal of Food Engineering* 42(2):67-72
- Thomsen MK, Lauridsen L, Skibsted LH, Risbo J (2005a) Temperature effect on lactose crystallization, Maillard reactions, and lipid oxidation in whole milk powder. *Journal of Agricultural and Food Chemistry* 53(18):7082-7090
- Thomsen MK, Lauridsen L, Skibsted LH, Risbo J (2005b) Two types of radicals in whole milk powder. Effect of lactose crystallization, lipid oxidation, and browning reactions. *Journal of Agricultural and Food Chemistry* 53(5):1805-1811
- Thomsen MK, Lauridsen L, Skibsted LH, Risbo J (2005c) Two types of radicals in whole milk powder. Effect of lactose crystallization, lipid oxidation, and browning reactions. *Journal of Agricultural and Food Chemistry* 53(5):1805-1811
- Thomsen MK, Olsen K, Otte J, Sjøstrøm K, Werner BB, Skibsted LH (2012) Effect of water activity, temperature and pH on solid state lactosylation of β -lactoglobulin. *International Dairy Journal* 23(1):1-8
- Timmermann E, Chirife J, Iglesias H (2001) Water sorption isotherms of foods and foodstuffs: BET or GAB parameters? *Journal of Food Engineering* 48(1):19-31. doi: 10.1016/S0260-8774(00)00139-4

- Tolkach A, Kulozik U (2007) Reaction kinetic pathway of reversible and irreversible thermal denaturation of beta-lactoglobulin. *Lait* 87(4-5):301–315
- Tomé D, Bos C (2007) Lysine requirement through the human life cycle. *Journal of Nutrition* 137(6):1642S
- Ullum T, Sloth J, Brask A, Wahlberg M (2010) Predicting spray dryer deposits by CFD and an empirical drying model. *Drying Technology* 28(5):723-729
- van Boekel MAJS (1998) Effect of heating on Maillard reactions in milk. *Food Chemistry* 62(4):403-414
- van Boekel MAJS (2001) Kinetic aspects of the Maillard reaction: a critical review. *Nahrung-Food* 45(3):150-159
- van Boekel MAJS (2009) *Kinetic Modelling of Reactions in Foods*. CRC Press, Taylor & Francis Group, Boca Raton
- van den Berg C, Bruin S (1981) Water activity and its estimation in food systems: Theoretical aspects. In: Rockland LB, Stewart GF (eds) *Water activity*. Academic Press, New York, pp 1-61
- van Mil PJJM, Jans JA (1991) Storage stability of whole milk powder - Effects of process and storage-conditions on product properties. *Netherlands Milk and Dairy Journal* 45(3):145-167
- Versteeg HK, Malalasekera W (2007) *An introduction to computational fluid dynamics - The finite volume method, second*. Pearson Education Limited, Harlow
- Vuataz G (1988) Preservation of skim-milk powders: role of water activity and temperature in lactose crystallization and lysine loss. In: Seow C (ed) *Food preservation by moisture control*. Elsevier applied science, London, pp 73-101
- Vuataz G (2002) The phase diagram of milk: a new tool for optimising the drying process. *Lait* 82(4):485-500
- Wallack DA, El-Sayed TM, King CJ (1990) Changes in particle morphology during drying of drops of carbohydrate solutions and food liquids. 2. Effects of drying rate. *Industrial & Engineering Chemical Research* 29(12):2354-2357
- Walstra P, Wouters JTM, Geurts TJ (2006) *Dairy science and technology*, 2nd edn. CRC Press, Boca Raton
- Walzel P (1993) Liquid atomisation. *International Chemical Engineering* 33(1):46-60
- Wang S, Langrish T (2009) A review of process simulations and the use of additives in spray drying. *Food Research International* 42(1):13-25
- Williams ML, Landel RF, Ferry JD (1955) Mechanical properties of substances of high molecular weight. 19. The temperature dependence of relaxation mechanisms in amorphous polymers and other glass-forming liquids. *Journal of the American Chemical Society* 77(14):3701-3707
- Woo MW, Daud WRW, Mujumdar AS, Talib MZM, Hua WZ, Tasirin SM (2008a) Comparative study of droplet drying models for CFD modelling. *Chemical Engineering Research & Design* 86(9A):1038-1048
- Woo MW, Daud WRW, Mujumdar AS, Wu ZH, Talib MZM, Tasirin SM (2008b) CFD evaluation of droplet drying models in a spray dryer fitted with a rotary atomizer. *Drying Technology* 26(10):1180-1198
- Wu WD, Liu W, Gengenbach T, Woo MW, Selomulya C, Chen XD, Weeks M (2013) Towards spray drying of high solids dairy liquid: Effects of feed solid content on particle structure and functionality. *Journal of Food Engineering*, doi: 10.1016/j.jfoodeng.2013.05.013
- Yamamoto S, Sano Y (1994) Drying of carbohydrate and protein solutions. *Drying Technology* 12(5):1069-1080

- Yarin AL, Brenn G, Kastner O, Rensink D, Tropea C (1999) Evaporation of acoustically levitated droplets. *Journal of Fluid Mechanics* 399:151-204
- Yarin AL, Brenn G, Kastner O, Tropea C (2002) Drying of acoustically levitated droplets of liquid-solid suspensions: Evaporation and crust formation. *Physics of Fluids* 14(7):2289-2298
- Yazdanpanah N, Langrish TAG (2011) Crystallization and drying of milk powder in a multiple-stage fluidized bed dryer. *Drying Technology* 29(9):1046-1057
- Yoshioka S, Aso Y (2007) Correlations between molecular mobility and chemical stability during storage of amorphous pharmaceuticals. *Journal of Pharmaceutical Sciences* 96(5):960-981
- Zbiciński I, Li X (2006) Conditions for accurate CFD modeling of spray-drying process. *Drying Technology* 24(9):1109-1114
- Zbiciński I, Piatkowski M, Prajs W (2005) Determination of spray-drying kinetics in a small scale. *Drying Technology* 23(8):1751-1759
- Zbiciński I, Strumillo C, Delag A (2002) Drying kinetics and particle residence time in spray drying. *Drying Technology* 20(9):1751-1768